



**SAPIENZA**  
UNIVERSITÀ DI ROMA

# **Thermo-Catalytic Reforming of waste biomass for alternative fuels production in a framework of decarbonisation**

XXXV Ciclo di Dottorato in Energia e Ambiente

Dipartimento di Ingegneria Astronautica, Elettrica ed Energetica (DIAEE)

*PhD Candidate:* **Francesca Di Gruttola**

*Tutor:* **Prof. Domenico Borello**

A.A. 2021/2022





**SAPIENZA**  
UNIVERSITÀ DI ROMA

**Il presente documento è distribuito secondo la licenza  
Tutti i diritti riservati**

This unpublished thesis is copyright of the author

Any use made of information contained in this thesis must be in accordance with that legislation and must be properly acknowledged. Further distribution or reproduction in any format is prohibited without the permission of the copyright holder.



## Abstract

In Europe, the production of alternative biofuels represents a very relevant economic and innovative target, as several European directives and regulations are enacted to secure support for the sustainable development throughout the transport sector. To satisfy the continuity of biofuels production avoiding the risks of technological failures or feedstocks shortage, the use of wastes and second-generation biomass represents a promising solution in terms of availability, economic convenience and environmental impact on overall emissions. In fact, they can be produced worldwide without competing with other industrial uses (e.g. food industry, livestock bedding, horticulture etc.) or having possible negative impacts on environment and biodiversity. The real diversifier for the competitiveness as well as the feasibility of biofuels production is the technology. Among several thermochemical conversion systems, the patented Thermo-Catalytic Reforming (TCR<sup>®</sup>) represents a flexible and reliable technology, capable to convert a wide range of advanced feedstocks in value-added products and fuels (i.e. char, oil and syngas). In this research, waste carbon fibres (CF) and solid grade laminate (SGL) have been investigated in a 2 kg/h lab-scale TCR reactor at the University of Birmingham. They are widely used in the industrial sectors and in many applications such as construction material, furniture, electronics as well as in vehicles, aerospace industry, sporting goods and medical field, thus contributing to high volumes of waste at end of life. Globally, about 130 million of tons of kraft paper is annually produced and partly destined to SGL production and the global demand of carbon fibres in 2022 is equal to 127,000 tons. To evaluate the suitability of TCR technology for SGL and CF, the characterisation of both feedstocks was accomplished, and it was concluded SGL and CF can be processed via TCR. The main energy carriers (char, oil and syngas) were generated under pyrolysis temperatures of 500°C for SGL and 600°C for CF and reforming temperature of 650 °C for SGL and 680°C for CF, respectively. The different temperatures were set according to the preliminary investigation carried out on TGA for both feedstocks. The SGL oil showed good properties and its HHV reached a value of 32.72 MJ/kg. However, a successive upgrading was required to meet specifications for its use as drop in fuels. On the contrary, the CF oil production was negligible, even if its calorific value was 30 MJ/kg. The syngas produced from the treatment of SGL and CF was rich

in hydrogen (about 20-40 vol%). Lastly, char revealed a calorific value of 25.94 MJ/kg and 20 MJ/kg for SGL and CF, respectively, thus exhibiting potential as a fuel as well as a catalyst in the gasification process. Overall, TCR of SGL and CF represents a novelty and it can be a promising route for the valorisation of this type of wastes. Finally, a techno-economic analysis for a commercial TCR3000 plant suggests that the technology is affordable and suitable to be commercialised.

**Key words:** Thermo-Catalytic Reforming, Pyrolysis, Hydrotreatment, Bio-oil, Char, Syngas, Hydrogen, Advanced Biomass, Waste, Carbon Fibres, Laminate.

# Acknowledgements

The author would like to thank the following:

- Her academic Tutor Professor Domenico Borello of Aerospace and Mechanical Engineering Department at the University of Rome La Sapienza, for all his support, supervision, effort and determination during the PhD course;
- Her academic co-supervisor Dr Miloud Ouadi of the Chemical Engineering Department at the University of Birmingham for his guidance and forbearance during all her period as Visiting Postgraduate Researcher;
- Her colleagues at the Aerospace and Mechanical Engineering Department at the University of Rome La Sapienza for their personal and professional assistance;
- Dr Hessam Jahangiri and Dr Artur Majewski for helping with feedstocks characterization and the experimental equipment;
- ATETA – University of Birmingham for its support and funds during the work. A special thanks goes to Frazer Barnes, Chairman and CTO at Gen 2 Carbon and Nat Macaulay, Managing Director at JCM Fine Joinery to provide the material used for the TCR experiments;
- Her family for the unconditional presence and support always and in any case.





# Index

	<i>Pages</i>
<b>1. Introduction</b>	<b>1-9</b>
References	7
<b>2. The availability of wastes and second-generation biomass</b>	<b>11-42</b>
Chapter summary	11
2.1 Feedstocks availability analysis method	12
2.1.1 Databases	12
2.1.2 The Autoregressive Model	14
2.1.3 COVID-19 Related Correction of the Autoregressive Model	17
2.2 Results of the Auto-Regressive Model	19
2.2.1 Chemical Compositions and General Properties	19
2.2.2 Availability in Europe in 2025	22
2.3 Main European Facilities	25
2.3.1 Agricultural Residues	25
2.3.2 Forestry Residues	26
2.3.3 Wastes	28
2.4 Technological Maturity Level for Advanced Biofuels Production	29
2.5 A Proposal for a Technology Ranking	31
2.6 Conclusions	33
References	35
<b>3. The technological background</b>	<b>43-86</b>
Chapter summary	43
3.1 The torrefaction	44
3.2 The hydrothermal liquefaction (HTL)	46
3.3 Hydrothermal Carbonization (HTC)	48
3.4 The gasification	49
3.5 The pyrolysis	53
3.5.1 The influence of key parameters in the pyrolysis	55
3.5.1.1 Size and shape of biomass	55
3.5.1.2 Chemical properties	56
3.5.1.3 Temperature	60
3.5.1.4 Pressure	61
3.5.1.5 Residence time	62
3.5.1.6 Heating rate	63
3.5.1.7 Reactor	64
3.5.1.8 Catalyst	64
3.6 The reforming and cracking processes	65
3.7 The Thermo-Catalytic Reforming (TCR) technology	67
3.8 The hydrotreatment	71
3.9 The technological comparison in terms of TRLs	77
References	79
<b>4. Feedstocks description: Solid Grade Laminate and Carbon Fibres</b>	<b>87-98</b>

Chapter summary	87
4.1 Solid Grade Laminate (SGL)	87
4.2 Carbon Fibres (CF)	91
References	95
<b>5. Methods</b>	<b>99-118</b>
Chapter summary	99
5.1 Solid Grade Laminate	99
5.1.1 Feedstock pretreatment	99
5.1.2 Feedstock characterization	100
5.1.2.1 Proximate analysis	100
5.1.2.2 Ultimate analysis	100
5.1.2.3 HHV	101
5.1.3 TCR experimental procedure	101
5.1.3.1 TCR setup	101
5.1.3.2 TCR methodology	103
5.1.4 TCR products characterization	105
5.1.4.1 Oil and char ultimate and proximate analyses	105
5.1.4.2 HHV	105
5.1.4.3 Water content	105
5.1.4.4 Viscosity	106
5.1.4.5 Density	106
5.1.4.6 Gas Chromatography/Mass Spectrometry (GC-MS)	107
5.1.4.7 Gas analysis	107
5.1.5 Hydrotreatment methodology	108
5.1.5.1 Ultimate and proximate analysis	110
5.1.5.2 HHV	110
5.1.5.3 Water content	111
5.1.5.4 Gas Chromatography/Mass Spectrometry (GC-MS)	111
5.1.5.5 Density	111
5.2 Carbon Fibers	112
5.2.1 Feedstock pretreatment	112
5.2.2 Feedstock characterization	113
5.2.2.1 Proximate analysis	113
5.2.2.2 Ultimate analysis	113
5.2.2.3 HHV	113
5.2.3 TCR experimental procedure	113
5.2.3.1 TCR methodology	113
5.2.4 TCR products characterization	114
5.2.4.1 Oil and char ultimate and proximate analyses	114
5.2.4.2 HHV	115
5.2.4.3 Water content	115
5.2.4.4 Viscosity	115
5.2.4.5 Density	115
5.2.4.6 Gas Chromatography/Mass Spectrometry (GC-MS)	115

5.2.4.7 Gas analysis	115
5.2.4.8 SEM analysis of char from Carbon Fibres	115
References	116
<b>6. Results and Discussions</b>	<b>119-160</b>
Chapter summary	119
6.1 Solid Grade Laminate	119
6.1.1 Feedstock characterization	119
6.1.1.1 Proximate and ultimate analyses of SGL	119
6.1.1.2 Thermal effect analysis	122
6.1.2 Mass and energy balance for SGL	123
6.1.3 Products characterization	126
6.1.3.1 Gas analysis	126
6.1.3.2 Char analysis	129
6.1.3.3 Oil analysis	130
6.1.3.3.1 The GC-MS results	132
6.1.4 The hydrotreatment	134
6.1.4.1 The catalysts	134
6.1.4.2 The mass balance for HDO and HC	135
6.1.4.3 The GC-MS analysis of HDO and HC oil	138
6.2 Carbon fibers	143
6.2.1 Feedstock characterization	143
6.2.1.1 Proximate and ultimate analyses	143
6.2.1.2 Thermal effect analysis	146
6.2.1.3 The mass balances	146
6.2.1.4 The energy balances	151
6.2.1.5 The SEM results	152
6.2.1.6 The GC-MS results	153
References	155
<b>7. Techno-economic assessment</b>	<b>161-178</b>
Chapter summary	161
7.1 TCR3000 setup and process assumptions	162
7.2 Techno-economic evaluation criteria	164
7.3 The plant models	165
7.3.1 Model 1	165
7.3.2 Model 2	165
7.4 Results	167
7.4.1 Solid Grade Laminate	168
7.4.1.1 Total Capital Costs	168
7.4.1.2 Operating Costs	168
7.4.1.3 Revenues	169
7.4.1.4 Profits	170
7.4.1.5 Payback Period	171
7.4.1.6 ROI	172
7.4.2 Carbon Fibers	173

7.4.2.1 Total Capital Costs	173
7.4.2.2 Operating Costs	173
7.4.2.3 Revenues	173
7.4.2.4 Profits	174
7.4.2.5 Payback Period	175
7.4.2.6 ROI	175
Conclusions	176
References	177
<b>Conclusions and future works</b>	<b>179-182</b>
<b>APPENDIX A1</b>	<b>183</b>
(Mass and Energy balance for Solid Grade Laminate – Model 1)	
<b>APPENDIX A2</b>	<b>184</b>
(Mass and Energy balance for Solid Grade Laminate – Model 2)	
<b>APPENDIX B1</b>	<b>185</b>
(Mass and Energy balance for Carbon Fibers – Model 1)	
<b>APPENDIX B2</b>	<b>186</b>
(Mass and Energy balance for Carbon Fibers – Model 2)	
<b>APPENDIX C1</b>	<b>187</b>
(Economic evaluation for Solid Grade Laminate – Model 1)	
<b>APPENDIX C2</b>	<b>188</b>
(Economic evaluation for Solid Grade Laminate – Model 2)	
<b>APPENDIX D1</b>	<b>189</b>
(Economic evaluation for Carbon Fibers – Model 1)	
<b>APPENDIX D2</b>	<b>190</b>
(Economic evaluation for Carbon Fibers – Model 2)	
<b>List of Publications</b>	<b>191-192</b>

## List of Figures

<b>Figure 2.1</b> (a) Residues of sunflower seed and the trend line calculated by the model; (b) Residues of sunflower seed and the sum of the trend with the seasonality calculated by the model; (c) Residues of sunflower seed and the sum of trend, seasonality, and randomness for $k = 1.28$ calculated by the model; (d) Residues of sunflower seed and the sum of trend, seasonality, and randomness for $k = 1.96$ calculated by the model.....	17
<b>Figure 2.2</b> Availability of residues of sunflower without model correction: (a) residues of sunflower without the model correction, $k = 1.96$ ; (b) residues of sunflower the model correction, $k = 1.96$ . ...	19
<b>Figure 2.3</b> Agricultural Residues availability in Europe in 2025 in million tonnes per year. ....	22
<b>Figure 2.4</b> Forestry Residues availability in Europe in 2025 in million tonnes per year. ....	23
<b>Figure 2.5</b> Wastes availability in Europe in 2025 in million tonnes per year. ....	24
<b>Figure 3.1</b> Overview of the main energy conversion processes.....	43
<b>Figure 3.2</b> Scheme of the hydrothermal liquefaction (HTL) process [3.1] .....	47
<b>Figure 3.3</b> C-H-O ternary diagram.....	57
<b>Figure 3.4</b> The van Krevelen diagram [3.41] .....	60
<b>Figure 3.5</b> The effect of pyrolysis temperature on the yield of char, non-condensable gases and bio-oil (i.e., water + organics) [3.29].....	61
<b>Figure 3.6</b> Schematic illustration of devolatilization when the external pressure occurs .....	62
<b>Figure 3.7</b> Schematic illustration of devolatilization .....	63
<b>Figure 3.8</b> Schematic diagram of Thermo-Catalytic Reforming plant.....	67
<b>Figure 3.9</b> Chemical reactions for hydrotreatment [3.63].....	72
<b>Figure 3.10</b> Illustration of the conversion of carboxyl and carbonyl group in Alcohol.....	73
<b>Figure 3.11</b> Reactivity scale of organic compounds according to different temperatures of the hydrotreatment [3.67].....	76
<b>Figure 4.1</b> Solid Grade Laminate used in TCR reactor and its structure [4.3].....	88
<b>Figure 4.2</b> Carbon Fibres used in TCR reactor and their crystal structure [4.20].....	91
<b>Figure 4.3</b> Molecular structure of thermoplastic and thermosetting resins [4.22].....	92
<b>Figure 5.1</b> Blocks of Solid Grade Laminate (SGL).....	99
<b>Figure 5.2</b> Pretreatment of Solid Grade Laminate.....	100
<b>Figure 5.3</b> The Process Flow diagram (PFD) of the TCR-2 (2 kg/h): (1) Feed hopper; (2) Auger reactor; (3) Post reformer; (4) Cyclone, (5) Shell and tube heat exchanger; (6) Scrubber; (7) Oil collection vessel; (8) Ice bath; (9) biodiesel wash bottle; (10) Iso-propanol wash bottle; (11) Acetone wash bottle; (13) Flare [5.6]. ....	102
<b>Figure 5.4</b> Mettler Toledo V20S [5.7] .....	105
<b>Figure 5.5</b> IKA ROTAVISC viscosimeter [5.8] .....	106
<b>Figure 5.6</b> Academy Glass Measuring Cylinder 100 ml $\pm$ 1.0 ml [5.9].....	106
<b>Figure 5.7</b> GC-MS Agilent 8890 [5.10].....	107
<b>Figure 5.8</b> Pollutek GAS 3000P Syngas Analyser [5.11] .....	107
<b>Figure 5.9</b> Series 4560 Mini Reactor on the left [5.12] and its setup diagram on the right: (1) hydrogen tank; (2) manometer; (3) inlet valve; (4) outlet valve; (5) motor; (6) electric heater; (7) reactor; (8) temperature and motor control.....	108
<b>Figure 5.10</b> Catalysts used for HDO (on the left) and for HC (on the right) .....	109
<b>Figure 5.11</b> Experimental methodology for the hydrotreatment of laminate oil.....	110

<b>Figure 5.12</b> Carbon fibres.....	112
<b>Figure 5.13</b> Carbon Fibre resulting from shredding and sieving.....	112
<b>Figure 5.14</b> Carbon Fibres blocked in the hopper .....	114
<b>Figure 5.15</b> Hitachi Tabletop Microscope TM3030 series [5.16] .....	116
<b>Figure 6.1</b> The Van Krevelen [6.2] diagram of Solid Grade Laminate .....	120
<b>Figure 6.2</b> TGA/DTG Pyrolysis Profile Solid Grade Laminate.....	121
<b>Figure 6.3</b> TGA/DTG Ashing Profile Solid Grade Laminate .....	122
<b>Figure 6.4</b> Mass balance of Solid Grade Laminate .....	123
<b>Figure 6.5</b> The energy balance of Solid Grade Laminate.....	125
<b>Figure 6.6</b> The Van Krevelen diagram [6.2] with the H/C and O/C ratios evaluated for conventional fuels, typical fast pyrolysis oil, wood, SGL and its products from TCR (char and laminate oil) ....	126
<b>Figure 6.7</b> Gas analysis over time during TCR experiment.....	126
<b>Figure 6.8</b> Char of Solid Grade Laminate .....	129
<b>Figure 6.9</b> Aqueous phase (on the left) and organic phase (on the right) of SGL.....	131
<b>Figure 6.10</b> 1D representation of GCxGC results of Laminate Oil.....	133
<b>Figure 6.11</b> HDO oil and aqueous phase after the HDO process.....	135
<b>Figure 6.12</b> Mass balance for the hydrodeoxygenation (HDO).....	135
<b>Figure 6.13</b> Mass balance for the hydrocracking (HC) .....	137
<b>Figure 6.14</b> The Van Krevelen diagram for Laminate products.....	138
<b>Figure 6.15</b> Van Krevelen diagram [6.2] of Carbon Fibres.....	144
<b>Figure 6.16</b> TGA/DTG Pyrolysis Profile of Carbon Fibres .....	145
<b>Figure 6.17</b> TGA/DTG Combustion Profile of Carbon Fibres.....	145
<b>Figure 6.18</b> Mass balance .....	147
<b>Figure 6.19</b> Gas analysis during the experiment .....	147
<b>Figure 6.20</b> Char of Carbon Fibres.....	148
<b>Figure 6.21</b> Resin-bonded CF (on the left) and non-bonded CF (on the right) .....	149
<b>Figure 6.22</b> Aqueous phase (on the left) and organics (on the right) of CF.....	150
<b>Figure 6.23</b> Van Krevelen diagram [6.2] for CF and its products deriving from TCR.....	151
<b>Figure 6.24</b> The energy balance of CF .....	152
<b>Figure 6.25</b> 1000x SEM images (a) SE at 5kV of carbon fibres; (b1) SE at 5kV of resin-bonded char – Surface 1; (b2) SE at 5kV of resin-bonded char – Surface 2; (c) SE at 5kV of non-bonded char .....	153
<b>Figure 6.26</b> 1D representation of GCxGC results of carbon fibre oil.....	154
<b>Figure 7.1</b> Process Flow Diagram of TCR-3000 .....	161
<b>Figure 7.2</b> Process Flow Diagram of Model 1 .....	165
<b>Figure 7.3</b> Process Flow Diagram of Model 2 .....	166

## List of Tables

<b>Table 1.1</b> Key properties of biodiesel and fossil diesel [1.24], [1.26] .....	4
<b>Table 1.2</b> Key properties of biojet fuel [1.24] .....	5
<b>Table 2.1.</b> Summary of Categories, Datasets, Time Series and Locations, Provisional horizon implemented by the model.....	12
<b>Table 2.2</b> Residue to production ratio, retention residue for soil, heat and power uses and other uses considered for advanced crops evaluation [2.4][2.5] .....	13
<b>Table 2.3</b> Residue to production ratio (RPR), retained quantity for soil, heat and power uses for advanced forestry residues evaluation .....	13
<b>Table 2.4</b> Type of wastes and disposal operations selected from [2.7]. .....	14
<b>Table 2.5</b> Confidence levels k for the gaussian distribution of probability [2.13]. .....	16
<b>Table 2.6</b> Ultimate analysis of some crop residues .....	19
<b>Table 2.7</b> Cellulose, Hemicellulose and Lignin in the Crop Residues. ....	20
<b>Table 2.8</b> Cellulose, Hemicellulose and Lignin in the Forestry Residues [2.37]. .....	21
<b>Table 2.9</b> Wastes chemical composition. ....	21
<b>Table 2.10</b> Cellulose, Hemicellulose and Lignin content in various wastes [2.20]. .....	21
<b>Table 2.11</b> Summary of feedstocks availability in Europe in 2025 without Covid-19 effects. ....	24
<b>Table 2.12.</b> Operational European facilities for the advanced biofuels production [2.33],[2.52] from agricultural residues. ....	26
<b>Table 2.13</b> Operational European facilities for the advanced biofuels production [2.52] from forestry residues.....	26
<b>Table 2.14</b> Operational European facilities for the advanced biofuels production [2.33],[2.52] from wastes.....	28
<b>Table 2.15</b> Technological Readiness Level (TRL) scale [2.75]. .....	29
<b>Table 2.16</b> Assessment of the technological readiness level (TRL) for each mentioned technology. ....	31
<b>Table 2.17</b> Biofuel quality level for liquid biofuels. ....	32
<b>Table 2.18</b> Feedstocks and production costs for Technologies with the highest TRL according to ref. [2.76]. .....	33
<b>Table 3.1</b> Operating conditions and products yields of different types of pyrolysis [3.36] .....	55
<b>Table 3.2</b> Three types of carbon decomposition in hydrogen production reactions [3.38] .....	58
<b>Table 3.3</b> TCR plants currently in operation.....	68
<b>Table 3.4</b> TCR Product yields of different feedstocks .....	69
<b>Table 3.5</b> Summary of keys parameters in the hydrotreatment process .....	76
<b>Table 3.6</b> Technology readiness level (TRL) of the main thermochemical processes based on biomass .....	78
<b>Table 4.1</b> Chemical composition of Kraft fibres .....	89
<b>Table 4.2</b> Summary of composition and physio-chemical properties for wood and wastepaper bio oil and heavy fuel oil and biodiesel.....	90
<b>Table 4.3</b> Mechanical properties for different classes of carbon fibres [4.23].....	92
<b>Table 4.4</b> Properties and applications of carbon fibres [4.16][4.17] .....	93
<b>Table 6.1</b> Proximate and Ultimate Analysis of Solid Grade Laminate .....	119
<b>Table 6.2</b> The calorific values of SGL and its products and different liquid fuels .....	124
<b>Table 6.3</b> Reactions during pyrolysis.....	127

<b>Table 6.4</b> Example of aliphatic and aromatic hydrocarbons .....	128
<b>Table 6.5</b> Laminate Char characterization .....	130
<b>Table 6.6</b> Laminate oil characterization.....	131
<b>Table 6.7</b> Chemical compounds detected and identified by GC-MS of Laminate oil.....	132
<b>Table 6.8</b> HDO oil (on the left) and aqueous phase (on the right) characterization .....	136
<b>Table 6.9</b> HDO oil (on the left) and HDO+HC oil (on the right) characterization .....	137
<b>Table 6.10</b> GC-MS analysis of HDO oil .....	139
<b>Table 6.11</b> GC-MS analysis of HC oil.....	140
<b>Table 6.12</b> Proximate and Ultimate Analysis of Carbon Fibres .....	143
<b>Table 6.13</b> Syngas composition.....	147
<b>Table 6.14</b> CF char characterization .....	150
<b>Table 6.15</b> Carbon Fibres oil characterization.....	150
<b>Table 6.16</b> Chemical compounds detected and identified by GC-MS of oil from carbon fibre.....	154
<b>Table 7.1</b> List of assumption for TCR3000 process .....	163
<b>Table 7.2</b> Complete list of the total equipment required .....	167
<b>Table 7.3</b> Labour costs assumptions .....	168
<b>Table 7.4</b> Operating costs for Model 1 and Model 2.....	169
<b>Table 7.5</b> Selling prices of products deriving from TCR3000.....	170
<b>Table 7.6</b> Gross Profits for Model 1 and Model 2.....	170
<b>Table 7.7</b> Net Profits for Model 1 and Model 2 .....	171
<b>Table 7.8</b> Payback period for Model 1 and Model 2.....	171
<b>Table 7.9</b> ROI for Model 1 and Model 2 .....	172
<b>Table 7.10</b> Total Capital Costs for Model 1 and Model 2.....	173
<b>Table 7.11</b> Operating costs for Model 1 and Model 2.....	173
<b>Table 7.12</b> Revenues for Model 1 and Model 2 .....	174
<b>Table 7.13</b> Gross Profits for Model 1 and Model 2.....	174
<b>Table 7.14</b> Net Profits for model 1 and model 2.....	174
<b>Table 7.15</b> Payback period for Model 1 and Model 2.....	175
<b>Table 7.16</b> ROI for Model 1 and Model 2 .....	175
<b>Table 7.17</b> Comparison between Model 1 and Model 2 for different feedstocks .....	176



## List of abbreviations

NDCs	Nationally Determined Contributions
GHGs	Greenhouse Gases
EU	European Union
UK	United Kingdom
RED	Renewable Energy Directive
RES	Renewable Energy Sources
ILUC	Indirect Land Use Change
TCR	Thermo-Catalytic Reforming
HDO	Hydrodeoxygenation
HC	Hydrocracking
FAME	Fatty Acid Methyl Ester
HFO	Heavy Fuel Oil
HT	Hydrotreatment
PFD	Process Flow Diagram
TRL	Technology Readiness Level
RPR	Residues To Production Ratio
SPK	Synthetic Paraffinic Kerosene
IBGTL	Integrated Biomass Gasification To Liquids
HVO	Hydrotreated Vegetable Oils
HEFA	Hydroprocessed Esters And Fatty Acids
FTS	Fischer-Tropsch Synthesis
FT-SPK	Fischer-Tropsch Synthetic Paraffinic Kerosene
SNG	Synthetic Natural Gas
AD	Anaerobic Digestion
WtF	Waste-To-Fuels
BtF	Biomass-To-Fuels
HTL	Hydrothermal Liquefaction
HTC	Hydrothermal Carbonization
HHV	Higher Heating Value
PW	Process Water
TGA	Thermo-Gravimetric Analysis
O/C ratio	Oxygen/Carbon Ratio
H/C ratio	Hydrogen/Carbon Ratio
WGS	Water Gas Shift
CD	Carbon Deposition
PAH	Polycyclic Aromatic Hydrocarbon
TAN	Total Acid Number
LHSV	Liquid Hourly Space Velocity
SGL	Solid Grade Laminate
CF	Carbon Fibres
CHPL	Compact High-Pressure Laminate
EPD	Environmental Product Declaration
SOFC	Solid Oxide Fuel Cells
MFC	Microbial Fuel Cells
PAN	Polyacrylonitrile
CFRP	Carbon Fibre Reinforced Polymer

UHM	Ultra-High Modulus
HM	High Modulus
IM	Intermediate Modulus
SM	Standard Modulus
DHM	Dichloromethane
NDIR	Non Dispersive Infrared
TCD	Thermal Conductivity Detector
ECD	Electron Capture Detector
BEIC	Birmingham Energy Innovation Centre
GC-MS	Gas Chromatography/Mass Spectrometry
SEM	Secondary Electron Method
CHP	Combined Heat and Power
MC	Moisture Content
PSA	Pressure Swing Adsorption
TCC	Total Capital Cost
FC	Fixed Capital
WC	Working Capital
PCE	Purchase Cost of Equipment
PPC	Physical Plant Cost
OC	Operating Cost
GP	Gross Profit
NP	Net Profit
ROI	Return on Investment

## 1. Introduction

Since the beginning of the industrial revolution, the world has been consuming ever-increasing amounts of energy from fossil fuels emitting large amounts of CO<sub>2</sub> from their combustion. This is widely believed to be the principal cause of climate change [1.1]. Sustainability and circular economy are the main issues to contrast it and to achieve the net zero target for decarbonizing all sectors by 2050 [1.2].

As of 2015, the Paris Agreement [1.3] heralded a new era of climate actions through actively involving countries around the globe to maintain the increase in the global average temperature to well below 2°C, preferably to 1.5°C, compared to pre-industrial levels.

In the Nationally Determined Contributions (NDCs), each Country must control their own emissions to meet these global climate goals and, thus, to decarbonize the end-use sectors (e.g., buildings, industry and transport). These actions in NDCs are revised every five years to continuously raise climate ambitions all over the world [1.4].

Currently, the energy systems are responsible for more than 75% of greenhouse gases (GHGs) emissions in Europe [1.5] and they must decrease them through new strategic plans which will lay the foundations for a more efficient and interconnected energy sector, oriented towards the dual objective of a cleaner planet and a stronger circular economy.

Furthermore, there are increasing concerns over the price and security in the supply of coal, oil and natural gas, since energy consumption has been increasing even faster with the population growth and the industrial development [1.6].

Therefore, any attempt to decrease the demand on fossil fuels through the use of carbon neutral sources of biomass, leads to a reduction of the emissions and keeps the production levels constant in any industrial sector is now considered environmentally and socially beneficial.

Wastes and second-generation biomass represent one of the most available, cheapest and environmental-friendly resources as they are continuously produced in large quantity without competing with food production or other industrial uses, neither impacting negatively on environment, biodiversity and water use.

However, the large annual amount of wastes makes their disposal more and more challenging and vital to prevent society from the risk of infections, infestations, contaminations, blockage of waterways, accidental fires, and breeding sites for mosquitos and rodents [1.7].

Landfill and incineration are the most common methodologies to get rid of wastes and other bio-residues, but they would emit large amount of GHGs, thus polluting and squandering valuable resources at the same time.

Many technological attempts and revamping methodologies have been investigated so far to enhance their potential to change and decarbonize the industrial sector.

For example, the use of recycled plastic instead of coke in blast furnace and/or the involvement of green hydrogen as reducing agent in the direct reduction-electric arc furnace lines could help to reduce CO<sub>2</sub> emissions in the steel mills as demonstrated in [1.8].

In the power production plants, thermal and mechanical performances of combustor and compressor respectively have also been studied and modelled in such a way that components' deterioration are kept under control and consequently emissions levels are lowered by burning less fossil fuels or hydrogen blended fuels [1.9]-[1.12].

Recently, the valorization of wastes and second-generation biomass through gasification, pyrolysis, and other thermochemical processes have been playing a relevant part in the bioenergy sector as well as in the circular economy. Their conversion in cleaner and/or alternative fuels like hydrogen, syngas and liquid biofuels represents an acceptable and affordable solution especially in the transport sector.

As a matter of fact, many regulations and directives have been introduced aiming at discussing and supporting the most relevant aspects related to energy and environment in terms of alternative fuels as happened in the Fuel Quality Directive aiming at reducing the greenhouse gas intensity by a minimum of 6% by 2020, with monitoring and reporting activities applicable even after that date [1.13].

In this regard, hydrogen and liquid biofuels are expected to play a key role in a future climate-neutral economy, enabling emission-free or low-carbon pathways in the transport, buildings, industrial processes (heat, power or combined heat and power) as well as energy storage.

To mobilize the necessary investments during the pandemic due to Covid-19, the European Commission supported several strategies to boost the EU budget. Among these funds, the Next Generation EU [1.14] will reinforce the long-term budget for 2021-2027 by €750 billion and the Green Deal will unlock investments in clean technologies and strategic value chains through additional funding to Horizon Europe [1.15]. The new European Bauhaus will enrich the European Green Deal including new funds (about €85 billion) and actions [1.16]. These new strategic investment funds will support the development of key technologies for the clean energy transition, including hydrogen systems. In particular, the new "Clean

Hydrogen Alliance" strategy will coordinate and guide the scaling up of the production and the use of clean hydrogen in Europe.

In 2009, the EU issued a mandatory environmental directive, the Renewable Energy Directive (RED) 2009/28/EC [1.17], specifying that 20% of all energy in the EU-27 should be from renewable energy sources (RES) by 2020, with 10% of road transport energy coming from biofuels within the 2020. However, in 2012 an amendment of the directive required that first generation biofuels should be limited to 5%, to avoid that the extensive use of soil for the growth of energy crops could lead to Indirect Land Use Change (ILUC) pushing to eliminate forestry for crop cultivation, eventually leading to a greater rate of GHGs emissions. According to the amendment, the second-generation (or advanced) biofuels production from residues or wastes was reinforced. In 2018, the RED was revised to deliver the EU objective of a minimum 32 % share of RES in final energy consumption by 2030 [1.18]. The EU has adopted even more ambitious climate goals for the European Green Deal, setting a target of -55 % greenhouse gas (GHG) emissions by 2030 and a long-term goal of net zero GHG emissions by 2050. Both targets were enshrined in the new European Climate Law, agreed by the Council and the Parliament in May 2021. To achieve all these climate goals, there will be substantial changes to the existing EU energy legislation. In fact, the European Commission on 14 July 2021 adopted a new climatic package named "fit for 55" to require a much higher share of RES by revising some existing legislative measure like the RED [1.19].

Thus, it is expected that renewable sources (especially wind and photovoltaic energy) will be necessary for the key technologies' development aiming at transforming the surplus electricity produced in certain hours of the day or at certain times of the year into energy. The green hydrogen represents the energy carrier which would effectively support to manage the problem of storing electricity in large quantities and for long periods. In Italy, the Guidelines for a National Strategy for Hydrogen [1.20] stimulates the national growth of the hydrogen market in the main application sectors such as long-haul transport, railways, heavy industries (e.g., chemical and oil refining), blending of hydrogen into the gas network. In 2030, a 2% penetration of hydrogen in the final energy demand, the reduction up to 8 Mt of CO<sub>2</sub> emissions, about 5 GW capacity of electrolysis for the hydrogen production are expected.

In view of the high potential in greenhouse gas emission saving, significant environmental advantages would also derive from wastes, agricultural and forestry residues, thus contributing to liquid biofuels and biogas production for a sustainable development even in decentralized areas.

According to the Italian Hydrogen Action Plan [1.21], Italy ranks among the most virtuous countries in Europe for the share of renewables in the production of electricity (17.8%), but also as a country with the greatest skills in the production of biogas (4th producer of biogas in the world) and bio-methane (2nd producer in Europe) [1.22].

Although the above-mentioned directives and regulations lead all European Countries toward the common goal to decarbonize all industrial sectors, there are also several policies and procedures regarding requirements and specifications for the gaseous and liquid biofuels certifications.

As a matter of fact, alternative biofuels from waste and second-generation biomass are not suitable directly for internal combustion engines because of their physiochemical properties, which vary significantly compared to conventional fossil fuels. Their high viscosity, poor volatility, and low cetane number, resulting from the large molecular mass and chemical structure, can determine incomplete combustion and heavy smoke [1.23], affecting the integrity and the combustion performances of the engine [1.24]. In addition, the structural alteration of the chemical compounds and the presence of hazardous and corrosive elements can be dangerous for human health and the environment [1.25].

In accordance with the purpose of this thesis, based on the thermochemical technologies, particularly thermo-catalytic reforming (TCR) and hydrotreatment, several standards like ASTM D6751, EN 14214, EN590 for biodiesel, ASTM D 7566 and ASTM D1655 for biojet fuel must be checked, respectively. In fact, TCR-derived biooil can be subjected to further processing through zeolite cracking or hydrodeoxygenation (HDO) to produce a deoxygenated bio-oil which after cracking/isomerization produces biojet fuel, petrol, and green diesel [1.24].

In **Table 1.1**, keys properties of biodiesel are reported with their standards and compared to fossil diesel.

**Table 1.1** Key properties of biodiesel and fossil diesel [1.24], [1.26]

Properties	Biodiesel (ASTM D6751)	Biodiesel (EN 14214)	FAME Biodiesel (EN590)	Fossil diesel
Water wt.%			~0	~0
Density 15 °C (kg/m <sup>3</sup> )	880	860–900	820	820–850
Viscosity @ 40 °C (cSt)	1.9–6.0	3.5–5.0	2.0	2.04–3.23
Calorific value (MJ/kg)	-	35	-	42–48
Acidity total (mgKOH/g)	Max. 0.50	Max. 0.5	-	0.02
Cetane number (min)	Min. 47	Min. 51	Min. 51	Min. 40
Iodine number (max)	-	120	-	-
Flash point (°C)	Min. 93	Min. 120	<55	Min. 52

<b>Pour point (°C)</b>	-15 to 10	-	-	-35 to -15
<b>Cloud point (°C)</b>	-3 to 12	-	-	-15 to 5
<b>Cold filter plugging point (°C)</b>	19	Max. 5	-15 (winter) -5 (summer)	5
<b>Copper strip corrosion (3 h-50 °C)</b>	Max. 3	Min. 1	Class 1	Max. 3
<b>Sulphur % (ppm)</b>	Max. 15	Max. 10	Max.10	Max. 15
<b>Sulphated ash % (m/m)</b>	Max. 0.02	Max. 0.02	Max. 0.01	Max. 0.01
<b>Oxidation stability (min, 110 °C)</b>	3	6	20 h	-

**Table 1.2** shows the key properties that the biojet fuel must have to be in accordance with ASTM D1655 fuel.

**Table 1.2** Key properties of biojet fuel [1.24]

<b>Properties</b>	<b>Biojet fuel</b>
	<b>ASTMD7566 / ASTM D1655</b>
<b>Acidity, total (mgKOH/g)</b>	0.1 max
<b>Flash point (°C)</b>	38 min
<b>Density @15 °C (kg/m<sup>3</sup>)</b>	775 to 840
<b>Freezing point (°C), max</b>	-40 (JetA); -47 (JetA1)
<b>Viscosity @ -20 °C (cSt)</b>	8, max
<b>Net heat of comb (MJ/kg)</b>	42.8, min

As previously mentioned, thermo-catalytic reforming was analyzed along with the production of pyrolysis oil, syngas and char, starting from two industrial wastes. These are solid grade laminate (SGL) and carbon fibers (CF), supplied by JCM (UK) and Gen2Carbon (UK) respectively. In UK, the annual sale of laminate destined to the flooring market is approximately 30 million m<sup>2</sup> [1.27] and it could represent an opportunity towards sustainability if reused in large scale biomass. While global demand for carbon fibers is estimated around 117kton in 2022 [1.28].

The thesis includes a general assessment of current and future availability of advanced feedstocks that could be exploited in the thermochemical processes. Afterwards, a general background about the main thermochemical processes is presented in order to understand the key parameters that are involved, also including the thermo-catalytic reforming (TCR) and the hydrotreatment (HT). Then, the experimental methodology follows by describing types and quantities of feedstocks, how they are pretreated, characterized and thermally converted by TCR and HT. Each process is explained with their process flow diagrams (PFD) detailing procedures and equipment used during the experimental tests and for the analysis of the final products after each run.

Feedstocks and products characterization resulting from TCR are critically discussed in terms of their general applications and potential as sustainable fuels.

In conclusion, a techno-economic analysis for a commercial TCR3000 plant based on a real demonstrator is assessed. Results suggest that the technology is affordable and suitable to be commercialized.



## References

- [1.1]. S. Prasad, A. P. Ingle, Chapter 12 - Impacts of sustainable biofuels production from biomass, Sustainable Bioenergy Advances and Impacts, 2019, Pages 327-346;
- [1.2]. Net Zero by 2050: A Roadmap for the Global Energy Sector, International Energy Agency, 2021;
- [1.3]. The Paris Agreement available online at:  
[https://unfccc.int/sites/default/files/english\\_paris\\_agreement.pdf](https://unfccc.int/sites/default/files/english_paris_agreement.pdf) (accessed on 23/09/2021);
- [1.4]. <https://www.irena.org/events/2021/May/Energy-Climate-Dialogue-Southeast-Europe> (accessed on 23/09/2021);
- [1.5]. [https://ec.europa.eu/commission/presscorner/detail/it/ip\\_20\\_1259](https://ec.europa.eu/commission/presscorner/detail/it/ip_20_1259) (in italian) (accessed on 23/09/2021);
- [1.6]. J. Santos, M. Ouadi, He. Jahangiri, A. Hornung, Valorisation of lignocellulosic biomass investigating different pyrolysis temperatures, Journal of the Energy Institute, Volume 93, Issue 5, October 2020, Pages 1960-1969;
- [1.7]. A. Mavukwana, N. Stacey, J. A. Fox, B. C. Sempuga, Thermodynamic comparison of pyrolysis and gasification of waste tyres, Journal of Environmental Chemical Engineering 9 (2021) 105163;
- [1.8]. O. Palone, G. Barberi, F. Di Gruttola, G. G. Gagliardi, L. Cedola, D. Borello, Assessment of a multi-step revamping methodology for cleaner steel production, Journal of Cleaner Production, 2022 (under revision);
- [1.9]. F. Di Gruttola, G. Agati, P. Venturini, D. Borello, F. Rispoli, S. Gabriele, D. Simone, Numerical Study of Erosion due to Online Water Washing in Axial Flow Compressors, Proceedings of the ASME Turbo Expo 2020: Turbomachinery Technical Conference and Exposition. Volume 2B: Turbomachinery. Virtual, Online. September 21–25, 2020. V02BT34A008. ASME;
- [1.10]. G. Agati, F. Di Gruttola, S. Gabriele, D. Simone, P. Venturini, D. Borello, Water washing of axial flow compressors: numerical study on the fate of injected droplets, E3S Web Conf. Volume 197, 2020, 75th National ATI Congress – #7 Clean Energy for all (ATI 2020);
- [1.11]. G. Agati, D. Borello, F. Di Gruttola, D. Simone, F. Rispoli, A. Castorrini, S. Gabriele, P. Venturini, Numerical prediction of long-term droplet erosion and washing efficiency of an axial compressors through the use of a discrete mesh morphing approach, Proceedings of ASME Turbo Expo 2022 Turbomachinery Technical Conference and Exposition, GT2022, June 13-17, 2022, Rotterdam, The Netherlands;

- [1.12]. L. Mazzotta, F. Di Gruttola, O. Palone, D. Borello, Analysis of the nox emissions deriving from hydrogen/air combustion in a swirling non-premixed annular micro-combustor, Proceedings of ASME Turbo Expo 2022, Turbomachinery Technical Conference and Exposition GT2022, June 13 – 17, 2022;
- [1.13]. Available online: [https://ec.europa.eu/clima/eu-action/transport-emissions/fuel-quality\\_en](https://ec.europa.eu/clima/eu-action/transport-emissions/fuel-quality_en) (accessed on 19/08/2022);
- [1.14]. [https://ec.europa.eu/commission/presscorner/detail/en/IP\\_20\\_940](https://ec.europa.eu/commission/presscorner/detail/en/IP_20_940) (accessed on 23/09/2021);
- [1.15]. [https://ec.europa.eu/info/strategy/priorities-2019-2024/european-green-deal/delivering-european-green-deal\\_en](https://ec.europa.eu/info/strategy/priorities-2019-2024/european-green-deal/delivering-european-green-deal_en) (accessed on 23/09/2021);
- [1.16]. [https://ec.europa.eu/commission/presscorner/detail/en/ip\\_21\\_4626](https://ec.europa.eu/commission/presscorner/detail/en/ip_21_4626) (accessed on 23/09/2021);
- [1.17]. <https://eur-lex.europa.eu/LexUriServ/LexUriServ.do?uri=OJ:L:2009:140:0016:0062:en:PDF> (accessed on 28/09/2021);
- [1.18]. <https://eur-lex.europa.eu/legal-content/EN/TXT/PDF/?uri=CELEX:32018L2001&from=EN> (accessed on 05/05/2022);
- [1.19]. <https://www.europarl.europa.eu/legislative-train/api/stages/report/current/theme/a-european-green-deal/file/revision-of-the-renewable-energy-directive> (accessed on 29/09/2021);
- [1.20]. [https://www.mise.gov.it/images/stories/documenti/Strategia Nazionale Idrogeno Linee guida preliminari nov20.pdf](https://www.mise.gov.it/images/stories/documenti/Strategia_Nazionale_Idrogeno_Linee_guida_preliminari_nov20.pdf) (in italian), (accessed on 07/10/2021);
- [1.21]. [https://www.confindustria.it/wcm/connect/552759de-3bb8-472f-a20b-07ab2aa5f21f/Position+Paper\\_Piano+d'azione+per+l'idrogeno\\_ott+2020\\_Confindustria.pdf?MOD=AJPERES&CONVERT\\_TO=url&CACHEID=ROOTWORKSPACE-552759de-3bb8-472f-a20b-07ab2aa5f21f-nuhfm09&\\_cf\\_chl\\_jschl\\_tk\\_=pmd\\_WaUEWkg6z965hEk.VLz0Sd8ypLCcaGz2IwYGYAIf.J0-1633601462-0-gqNtZGzNAXCjcnBszQj9](https://www.confindustria.it/wcm/connect/552759de-3bb8-472f-a20b-07ab2aa5f21f/Position+Paper_Piano+d'azione+per+l'idrogeno_ott+2020_Confindustria.pdf?MOD=AJPERES&CONVERT_TO=url&CACHEID=ROOTWORKSPACE-552759de-3bb8-472f-a20b-07ab2aa5f21f-nuhfm09&_cf_chl_jschl_tk_=pmd_WaUEWkg6z965hEk.VLz0Sd8ypLCcaGz2IwYGYAIf.J0-1633601462-0-gqNtZGzNAXCjcnBszQj9) (in italian), (accessed on 07/10/2021);
- [1.22]. <https://modofluido.hydac.it/idrogeno-in-italia-linee-guida-normative> (in italian), (accessed on 07/10/2021);
- [1.23]. H. Song, K. Sison Quinton, Z. Peng, H. Zhao, N. Ladommatos, Effects of Oxygen Content of Fuels on Combustion and Emissions of Diesel Engines, Energies, 2016, 9, 28;

- [1.24]. A. Fivga, L. G. Speranza, C. M. Branco, M. Ouadi, A. Hornung, A review on the current state of the art for the production of advanced liquid biofuels, *AIMS Energy*, 2019, Volume 7, Issue 1: 46-76;
- [1.25]. Z. Xiaojie, K. Mukherjee, S. Manna, M.Kumar Das, J. Kuk Kim and T. Kumar Sinha, Chapter 24 - Efficient management of oil waste: chemical and physicochemical approaches, *Advances in Oil-Water Separation: A Complete Guide for Physical, Chemical, and Biochemical Processes*, 2022, Pages 439-467;
- [1.26]. Available online: <https://www.ipu.co.uk/en590/> (accessed on 16/08/2022);
- [1.27]. Available online:  
<https://cfa.org.uk/userfiles/files/Zero%20Avoidable%20Waste%20in%20Flooring%20-%20A%20Scoping%20Study.pdf> (accessed on 09/12/2022);
- [1.28]. J. Zhang, V. S. Chevali, H. Wang, C.-H. Wang, Current status of carbon fibre and carbon fibre composites recycling, *Composites Part B: Engineering*, Volume 193, 15 July 2020, 108053.



## **2. The availability of second-generation biomass**

### **Chapter summary**

Nowadays in Europe, the production of advanced biofuels represents a very important objective, given the strong interest in increasing sustainability throughout the transport sector. However, an important aspect to be considered is the prediction of feedstocks availability to produce advanced biofuel. Therefore, the first aim of this thesis is to assess the availability of European agricultural residues, forestry residues, and biogenic wastes by 2025. The data were collected through a deep review on open FAOSTAT and EUROSTAT databases and then elaborated by the author. The analysis focuses on the fraction of feedstocks that can be used for advanced biofuels production, i.e., incorporating specific information on sustainable management practices, competitive uses, and environmental risks to preserve soil quality. An autoregressive model is developed to predict future availability, while also considering corrections due to the current pandemic. The results suggest that several European countries could produce enough sustainable advanced feedstocks to meet the European binding target. To complete the picture, a proper metric is introduced, aiming at generating a technology ranking of the examined alternative fuels, in terms of biomass availability, Technology Readiness Level (TRL), quality of the biofuel, and costs. This analysis allows to compare advanced biofuels and first-generation biofuels, whose utilization can impact the food market, contributing to the increase in the indirect land use change (ILUC). Although the first-generation biofuels remain the most common choice, the renewable (or green) diesel, pyrolysis bio-oil, green jet fuel, and the second-generation bioethanol are promising for different applications in the transport sector. Thus, it seems mandatory that the transport sector will rely more and more on such fuels in future. For such reason, a specific support for advanced biomass collection, as well as specific programs for conversion technologies development, are strongly suggested.

## 2.1 Feedstocks availability analysis method

### 2.1.1 Databases

This section aims at assessing the availability of sustainable feedstocks to produce advanced biofuels in the European Countries by 2025. The feedstocks are divided into three main categories: wastes, crops, and forestry residues, whose data were collected from EUROSTAT and FAOSTAT databases. In **Table 2.1**, each category is summarized indicating the source of dataset with its reference years, data format, location, and 2025 estimate.

**Table 2.1.** Summary of Categories, Datasets, Time Series and Locations, Provisional horizon implemented by the model.

Category	Dataset	Data Format	Past Interval	Location	Provisional Interval
Biogenic wastes	EUROSTAT [2.1]	Excel	2008, 2010, 2012, 2014, 2016	Europe/Europe List	By 2025
Agricultural residues	FAOSTAT [2.2]	Excel	2014–2018	Europe/Europe List	By 2025
Forestry residues	FAOSTAT [2.3]	Excel	2014–2018	Europe/Europe List	By 2025

Crops data were extracted by the FAOSTAT database [2.2] and twelve different crops were analysed: barley, oats, olives, corn, wheat, soybeans, rapeseed, sunflower, sugar beet, rice, rye, and triticale. These crops were chosen among the European most produced crops and mainly used in the bioenergetics sector. To determine their availability for the advanced biofuels production, data were manipulated by deducting the biomass main use (e.g., food) [2.4] i.e., by introducing residues to production ratio (RPR) and the residual part destined for competitive uses such as power, heat, or other (i.e., horticulture, feed or animal bedding). To preserve the soil quality, it is recommended that part of residues should be left on the fields. This percentage varies from country to country as illustrated in ref. [2.5]. **Table 2.2** shows all factors considered to evaluate the sustainable quantity of advanced feedstocks. Note that, the factors for retention for soil, heat & power and other uses are assumed the same for all the twelve crops analysed in this work.

**Table 2.2** Residue to production ratio, retention residue for soil, heat and power uses and other uses considered for advanced crops evaluation [2.4][2.5]

<b>Crop</b>	<b>RPR*</b>	<b>Retention for soil</b>	<b>Heat&amp;Power</b>	<b>Other uses</b>
<b>Barley</b>	0.94			
<b>Maize</b>	0.8			
<b>Oats</b>	1.07			
<b>Olives</b>	0.12			
<b>Rapeseed</b>	1.08			
<b>Rice</b>	1.32	0.62	0.03	0.08
<b>Rye</b>	1.13			
<b>Soybeans</b>	2.5			
<b>Sunflower</b>	1.77			
<b>Triticale</b>	1.04			
<b>Wheat</b>	0.94			
<b>Sugar beet</b>	0.27			

\*Values greater than 1 indicate that more residue is produced compared to the utilized part of the crop, and values less than 1 indicate that less residue is produced than the utilized part of the crop [2.4].

Forestry production was estimated from FAOSTAT database [2.3]. Such products include wood fuels, saw logs and veneer logs, pulpwood (round and split), and other industrial roundwood coming from both coniferous and non-coniferous roundwood. These last categories differ for their density, whose values are shown in [2.6]. To assess the residual part, different residues to production ratios (RPR) are here considered according to the type of roundwood and location (Northern European and all the other European Countries) [2.5] as illustrated in **Table 2.3**. To compute the sustainable fraction of forestry residues, all competitive uses and environmental impacts should be hereby considered, such as the residual part left on soil to prevent ground erosion, and the use of heat and power for the industrial sector.

**Table 2.3** Residue to production ratio (RPR), retained quantity for soil, heat and power uses for advanced forestry residues evaluation

	<b>RPR</b>	<b>RPR</b>	<b>Retained for</b>	<b>Heat &amp; Power</b>
	<b>Northern</b>	<b>Eastern/Southern/Western</b>	<b>soil</b>	<b>[Mton/year]</b>
	<b>Europe</b>	<b>Europe</b>	<b>[Mton/year]</b>	
<b>Coniferous roundwood</b>	0.47	0.17	46.06	14.16

<b>Non-Coniferous roundwood</b>	0.31	0.34	46.06	14.16
-------------------------------------	------	------	-------	-------

Finally, wastes availability data were taken from EUROSTAT [2.1], and they include all hazardous and non-hazardous wastes sent to landfill or disposed as reported in the disposal operations labelled with D1 to D7, D10, and D12 in ref. [2.7] and summarized in **Table 2.4**.

**Table 2.4** Type of wastes and disposal operations selected from [2.7].

<b>Category</b>	<b>Specific Disposal Operations [2.7]</b>
	D 1 Deposit into or on to land (e.g., landfill, etc.)
	D 2 Land treatment (e.g., biodegradation of liquid or sludgy discards in soils, etc.)
Paper and cardboard wastes	D 3 Deep injection (e.g., injection of pumpable discards into wells, salt domes or naturally occurring repositories, etc.)
Household and similar wastes	
Animal and mixed food waste	D 4 Surface impoundment (e.g., placement of liquid or sludgy discards into pits, ponds or lagoons, etc.)
Vegetal wastes	
Animal faeces, urine and manure	D 5 Specially engineered landfill (e.g., placement into lined discrete cells, which are capped and isolated from one another and the environment, etc.)
Wood wastes	
Sorting residues	
Common sludges	D 6 Release into a water body except seas/oceans
	D 7 Release to seas/oceans including sea-bed insertion
	D 10 Incineration on land
	D 12 Permanent storage (e.g., emplacement of containers in a mine, etc.)

### 2.1.2. The Autoregressive Model

In the autoregressive model, future values of feedstocks availability are correlated with real past values and their evolution in time [2.8]. This allows us to predict the availability of feedstocks aiming at meeting the advanced biofuels production needed to fulfil the European binding targets. Feedstocks quantity  $Q(t)$  is described by the additive model [2.9], i.e., through the sum of three components: trend  $T(t)$ , seasonality  $S(t)$ , and randomness  $A(t)$ , as shown below:

$$Q(t) = T(t) + S(t) + A(t) \quad (2.1)$$

The trend  $T$  describes feedstocks increasing or decreasing in the medium-long term. It is related to the systematic events occurred throughout the observation period. Trends can be constant, linear, polynomial, hyperbolic, exponential, or asymptotic [2.10]. In this study, the trend component is assumed to be linear, as illustrated in



Equation (2.2) and in **Figure 2.1.a**, since in the first instance, it is the simplest way to represent the behaviour of the recent data of feedstocks availability (**Table 2.1**):

$$T(t) = a + bt \quad (2.2)$$

The coefficient  $a$  and  $b$  are computed by the least square method [2.11], as reported in Equations (2.3) and (2.4), i.e., the trend line has to minimize the offset between the real values and those represented by the line itself.

$$a = \frac{\sum_i^{Np} Q(t_i)}{Np} = \bar{Q} \quad (2.3)$$

$$b = \frac{\sum_i^{Np} Q(t_i) \cdot t_i}{\sum_i^{Np} t_i^2} \quad (2.4)$$

The  $a$  and  $b$  coefficients are properly obtained by discretizing the time axis in  $Np$  intervals (where  $i$  is the  $i$ -th interval) and positioning the time axis origin at the centre of the data. For completeness, the trend line, computed through the model, is illustrated in Figure 1a, only for the sunflower residues.

The seasonality represents data fluctuations around the trend line due to circumstances periodically appearing in each time interval. In this case, the time series is divided in periods with the same duration. Each period, in turn, is then divided in an equal number of intervals  $j$  with the same behaviour. For the  $j$ -th interval, the corresponding seasonality index  $S_j$  is computed as follows Equation (2.5):

$$S_j = \frac{\sum_1^N \Delta}{N} \quad (\sum S_j = 0) \quad (2.5)$$

where  $\Delta = Q(t_j) - T(t_j)$  and  $N$  is the number of period where there is seasonality.  $S_j$  represents the average of the corresponding offset on the  $j$ -th interval. This process can be called seasonal adjustment of the time series [2.12]. By adding up the trend and the seasonality values, we get for example a behaviour illustrated in Figure 1b for sunflower residues.

Generally, the estimated feedstocks quantity  $\tilde{Q}(t)$ , in terms of trend and seasonality ( $T(t) + S(t)$ ), does not match the actual feedstocks quantity. There is a residual for each  $Np$  (period of observations) computed as follows Equation (2.6):

$$R(t_i) = Q(t_i) - \tilde{Q}(t_i) \quad (2.6)$$

Therefore, the performance indices as bias Equation (2.7) and root means square error Equation (2.8), deriving from the statistics, are introduced in the random component of the predictive model:

$$bias = \sum_{i=1}^{Np} \frac{R(t_i)}{Np} \quad (2.7)$$

$$\sigma_A = \sqrt{\sum_{i=1}^{Np} \frac{R(t_i)^2}{Np}} \quad (2.8)$$

The bias sums all residues with their sign without filtering the compensation effects. Depending on whether the sign of bias is positive or negative, the quantity will be underestimated or overestimated, respectively. If bias has zero value, then the quantity is correctly estimated. The root means square error  $\sigma_A$  measures the spread of data with respect to the average value of feedstocks quantity.

Assuming a Gaussian distribution of probability, the random component will be estimated as in Equation (9) and it is then added to the estimated quantity  $\tilde{Q}(t)$ . By way of illustration, the estimated quantity is reported in **Figure 2.1.c, d** for the sunflower residues according to different values of k.

$$A(t) = bias \pm k\sigma_A \quad (2.9)$$

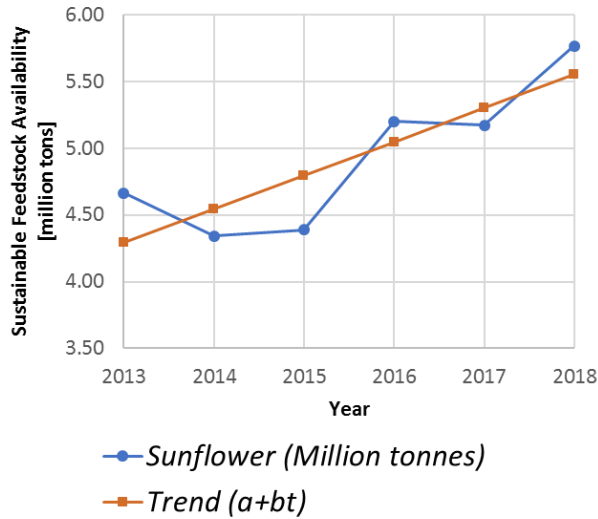
where k is the confidence level of the distribution, whose values are reported in **Table 2.5**.

**Table 2.5** Confidence levels k for the gaussian distribution of probability [2.13].

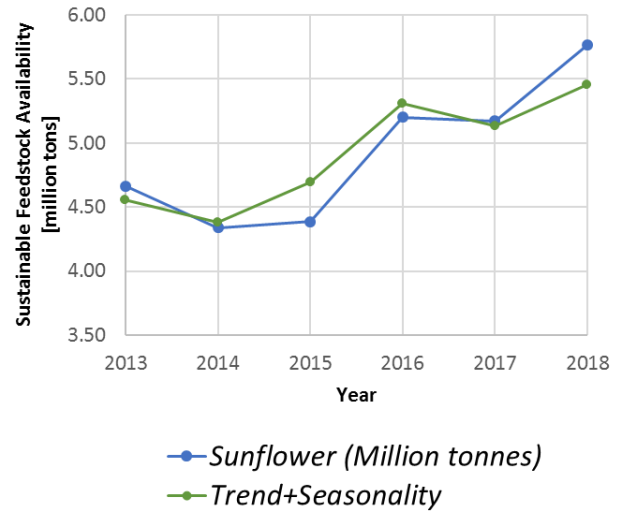
Confidence Level	80.0%	90.0%	95.0%	99.0%	99.9%
k	1.28	1.64	1.96	2.58	3.29

In the present analysis, k is chosen equal to 1.96, i.e., there is a 95% probability that the actual feedstocks availability falls inside the curve whose points represent the feedstocks availability estimated by the model (**Figure 2.1.d**).

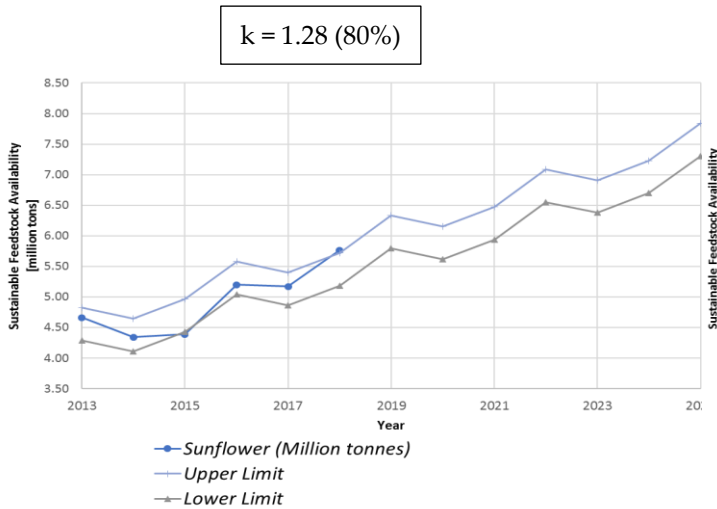
Based on these theoretical considerations, the model was developed, and all the collected data were implemented to assess the availability of advanced feedstocks in 2025.



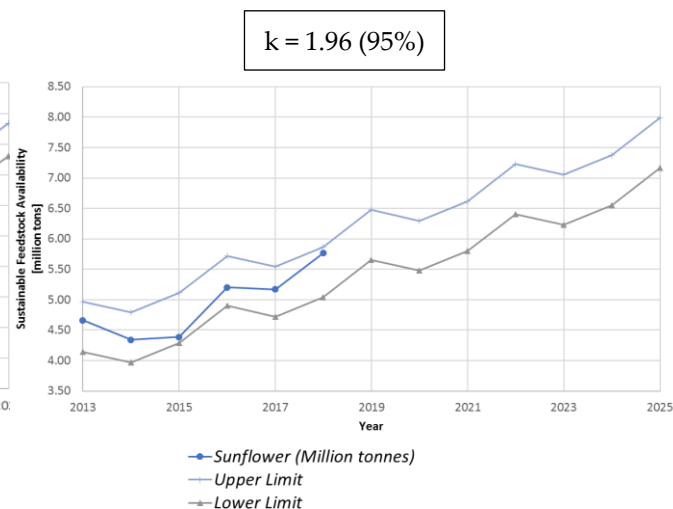
(a)



(b)



(c)



(d)

**Figure 2.1** (a) Residues of sunflower seed and the trend line calculated by the model; (b) Residues of sunflower seed and the sum of the trend with the seasonality calculated by the model; (c) Residues of sunflower seed and the sum of trend, seasonality, and randomness for  $k = 1.28$  calculated by the model; (d) Residues of sunflower seed and the sum of trend, seasonality, and randomness for  $k = 1.96$  calculated by the model.

### 2.1.3. COVID-19 Related Correction of the Autoregressive Model

Lockdowns related to the spreading of COVID-19 pandemic, have altered all aspects of our lives from the basic necessities to the personal and professional interaction. In less than a year, the intensification of smart working led the daily commute to be upended. Thus, the impacts of the COVID-19 have been more readily apparent in the transport than in other energy sector all over the world. This involves the biofuels production for transport too. Indeed, although the global transport biofuels

production reached 162 billion litres in 2019 (17.5 billion litres in Europe), to date the production is expected to be contracted for the next two years by 5% [2.14].

In Europe, IEA forecasts a 13% reduction in biodiesel and Hydrotreated Vegetable Oils (HVO) production and a 12% reduction in ethanol for 2020, due to significant reduction in demand across the continent [2.14]. During the pandemic, a lowering of crude oil prices has been recorded, thus making biofuels less competitive than fossil transport fuels. However, even if biofuel prices fall to a lesser extent, the biofuels production will be an economic challenge for some plants [2.15].

To tackle the revenue losses and continue limiting greenhouse gases (GHG) emissions, local air pollution, noise, safety, and congestion issues, new strategical plans must be redesigned in terms of economic and political solutions. The real challenge will be to provide equitable and affordable access to safe mobility and to restore social inclusion and local economic development. As long as the transport biofuels consumption results are low due to Covid-19 crisis, the lowest affected sector is the transport of goods. Biorefining still remains one of the key strategies in the circular economy, essential to create or preserve jobs, as mentioned in current European facilities, which process residual biomasses.

Since this paper is analysing the sustainable lignocellulosic materials availability, rather than vegetable oils, whose utilization could be unsustainable and in competition with commercial oils production, only the percentage reduction in bioethanol is accounted for with the introduction of a correction in the prediction. Due to the high technological maturity, fermentation is the most used conversion process to produce bioethanol from lignocellulose. To determine the amount of fuel that can be produced from a given mass of biomass via sugar fermentation, mass ratio or biomass-to-fuel efficiency expressed as [kg/kg] is introduced Equation (2.10):

$$\eta_m = \frac{m_{bioethanol}}{m_{lignocellulose}} \quad (2.10)$$

Such value depends on feedstock's type and technological process [2.16]. As reported in [2.17], the theoretical maximum sugar fermentation efficiency from lignocellulosic materials is 325–530 L/dry ton (0.282–0.461 kg/dry kg [2.18]).

Therefore, the amount of corrected lignocellulosic feedstocks can be estimated as equal to:

$$m_{feedstock,corrected} = \frac{m_{bioethanol,old} (1 - 0.12)}{\eta_m} \quad (2.11)$$

where  $m_{bioethanol,old}$  refers to the quantity of bioethanol produced without considering the COVID-19 effects. An example of application of the predictive model with and without correction is reported for sunflower in **Figure 2.2**.

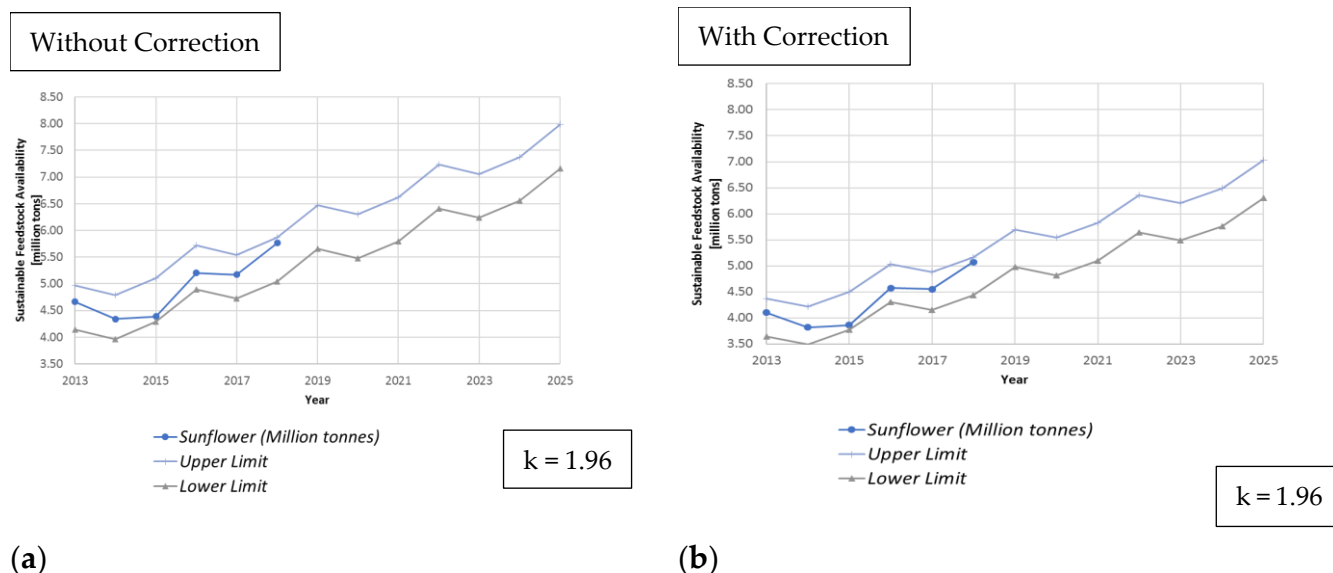


**Figure 2.2** Availability of residues of sunflower without model correction: (a) residues of sunflower without the model correction,  $k = 1.96$ ; (b) residues of sunflower the model correction,  $k = 1.96$ .

## 2.2 Results of the Auto-Regressive Model

### 2.2.1. Chemical Compositions and General Properties

**Table 2.6** and **Table 2.7** show the agricultural residues characteristics relevant for biofuel production when considering biochemical and thermochemical conversion processes. Agricultural residues have high carbon and hydrogen content. This circumstance makes proper feedstocks for the gasification process, to get synthetic gas (e.g., syngas), that can be directly burned for cogeneration or further transformed in biofuels or valuable chemicals (e.g., through Fischer-Tropsch synthetic paraffinic kerosene SPK) [2.17].

**Table 2.6** Ultimate analysis of some crop residues

Crop Residues	Carbon (wt%)	Hydrogen (wt%)	Oxygen (wt%)	Nitrogen (wt%)	Sulphur (wt%)	Chlorine (wt%)
Wheat [2.19],[2.20]	45.5–46.7	5.1–6.3	34.1–41.2	0.4	0.1	-
Rice (husks) [2.20]	37.9–44.6	4.82–5.6	33.7–49.3	0.43	0.17	-
Barley [2.21],[2.22]	45	6.0	-	4.6	1.4	1.1
Maize [2.23]	45.5	6.2	47.0	1.3	-	-
Oats [2.21],[2.22]	48	6.3	-	5.9	1.1	0.06
Rye (husk) [2.24]	75.6	-	18.9	-	1.3	-
Soybeans [2.25]	61.2	9.0	13.1	10.8	<0.1	-

Regarding biochemical processes, agricultural residues are the most interesting resource as they are rich in starch, sugar, and cellulose. Cellulose can be transformed in sugar, by enzymatic or acid hydrolysis, to eventually produce second generation ethanol [2.17]. The crops with higher cellulose share are wheat, barley, maize, and rice (**Table 2.7**). However, many feedstocks are rich of lignin, and they can be involved in further processes to get adhesives as co-product for applications like paper binding, medical tape, surgical glue, and engineered wood panels [2.17]. Finally, hemicellulose of herbaceous plants mainly contains xylan, which can be converted into solubilized monosaccharides (xylose) by hydrothermal liquefaction and upgraded to liquid fuels, platform compounds and valuable chemicals such as furfural, D-xylulose, glyceraldehyde, lactic acid, etc. [2.26].

**Table 2.7** Cellulose, Hemicellulose and Lignin in the Crop Residues.

Crop Residues	Cellulose (%)	Hemicellulose (%)	Lignin (%)
Wheat (Straw) [2.20]	30–39.2	26.1–50.0	15–21.1
Sugar beet [2.27]	20	25	1–8
Barley (straw) [2.28]	31–45	27–38	14–19
Maize (straw) [2.29]	42.6	21.3	8.2
Oats (straw) [2.30],[2.31]	26.6	21.3	24.8
Rice, paddy [2.32]	40.5	29	18.5
Rye [2.24]	26	16	13
Soybeans (hulls) [2.33]	33.49	17.15	9.88
Wheat (bran) [2.31]	32.2	28.0	5.2

The wood is characterized by 49% of Carbon [2.34], which makes it exploitable by both thermal and thermochemical processes to produce heat and power, as well as liquid and gaseous fuels, respectively. Nevertheless, no matter of the type of wood, there are high values of lignin (**Table 2.8**), which is a recalcitrant molecule that impedes polysaccharide accessibility and then its transformation into commercially significant products. For this reason, the removal of lignin is mandatory for biofuels namely lignocellulose-based during the pre-treatment phase [2.35].

These considerations are correct only if wood is sustainable meaning it is harvested correctly. In fact, carbon savings from forest wood is only possible if it is grown over many years. Therefore, effective and efficient forest management is required in conjunction with bioenergy. Lessons must be learned from the recent Drax power station controversy, where Supergen bioenergy hub were assisting Drax power

station to cut down primary/virgin forests in Canada to burn in their power station [2.36].

**Table 2.8** Cellulose, Hemicellulose and Lignin in the Forestry Residues [2.37].

Forestry Residues	Cellulose (%)	Hemicellulose (%)	Lignin (%)
Hardwood	40–44	15–35	18–25
Softwood	40–44	30–32	25–32

The available technologies for wastes belong to the class of the biochemical and thermochemical conversion processes according to wastes properties, recalled in **Table 2.9** and **Table 2.10**. High carbonaceous matter is favourably indicated for thermochemical processes like pyrolysis and gasification whose major products are the pyrolysis bio-oil, syngas, and ethanol, respectively. On the contrary, biological conversion processes, like the anaerobic digestion, produce biogas and biomethane as main fuels. However, high value chemicals are an economically viable and environmentally sustainable solution to recover valuable products from waste resources, since biorefinery platforms are mostly based on biofuels and chemicals too. In this respect, main chemicals are manufacture lubricants, paints, inks, pharmaceuticals, and personal care products [2.17].

Some next-generation biological conversion processes can be applied on wastes to produce biohydrogen. These are dark and photo-fermentation, direct and indirect biophotolysis, microbial electrolysis cells, as well as microbial electro-hydrogenesis cells, as reported in ref. [2.38].

**Table 2.9** Wastes chemical composition.

Waste	Carbon (wt%)	Hydrogen (wt%)	Oxygen (wt%)	Nitrogen (wt%)	Sulphur (wt%)	Chlorine (wt%)
Sewage Sludge (%) [2.39]	31	8.2	19.2	3.9	1.1	-
Paper (%) [2.40]	35.9	4.6	33.1	-	-	-
Garden Waste (%) [2.41]	26.8	3.3	22.5	0.56	0.06	0.10
Wood (%) [2.41]	46.0	5.9	41.3	0.20	0.03	0.04
Manure (%) [2.42]	35.4	4.7	57.5	2.4	-	-

**Table 2.10** Cellulose, Hemicellulose and Lignin content in various wastes [2.20].

Waste	Cellulose (%)	Hemicellulose (%)	Lignin (%)
Paper	85–99	0	0–15
Newspaper	40–55	25–40	18–30

Solid cattle manure	1.6–4.7	1.4–3.3	2.7–5.7
Wastepaper from chemical pulps	60–70	10–20	5–10

### 2.2.2. Availability in Europe in 2025

Future values of agricultural residues for each European country are shown in **Figure 2.3**. The additive model, adopted here, allowed us to identify the upper and the lower limit of the crop residues availability at 2025.

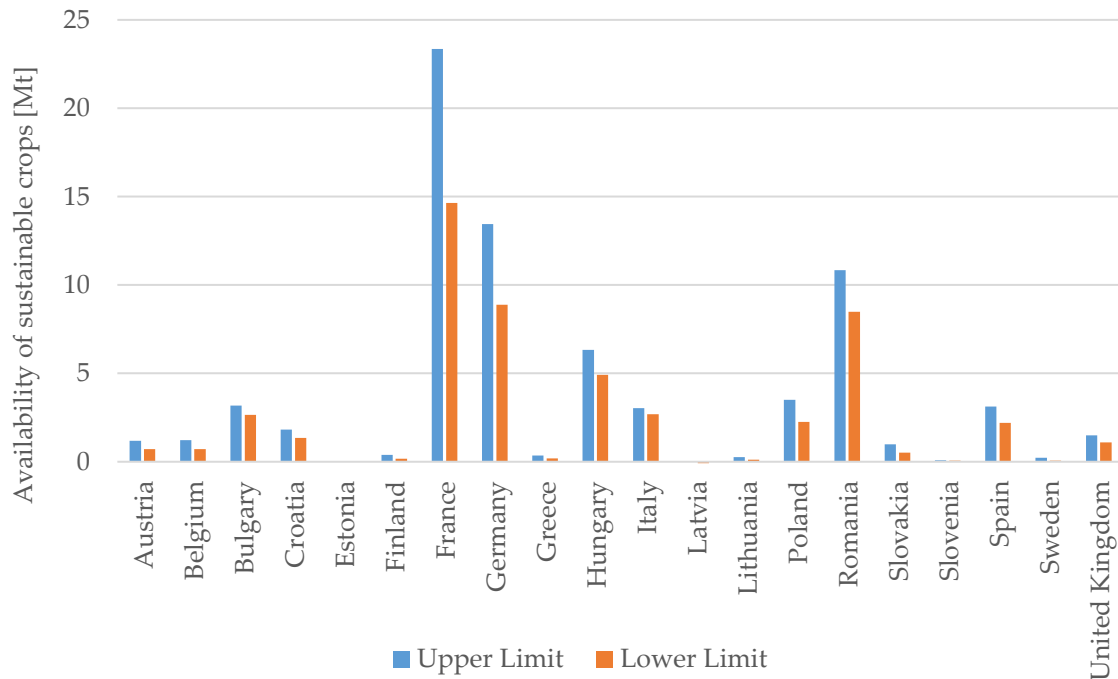


**Figure 2.3** Agricultural Residues availability in Europe in 2025 in million tonnes per year.

France, Germany, and Romania showed the highest production of agricultural residues as they have the largest agricultural sector. Overall, the fraction of residues available for advanced biofuel production ranges between 10 and almost 25 Mt (2025 estimate). In view of the pandemic, the corrected values could be between 8.8 and almost 22 Mt in the same year. In recent years, Romania recorded increasing values of agricultural production, and it is assumed they will just keep increasing by 2038 until they will reach the Germany's level, as illustrated in ref. [2.43]. From this analysis, we can deduce that there are good opportunities to mobilize financial sources, locally or from external countries, intended for the growth of the advanced biofuels sector. The remaining countries, with smaller production of sustainable crops, already use their collectable residues or they have the potential to witness a relevant growth in the



next years, contributing at achieving the Renewable Energy Directive (RED II) targets [2.44] (like Hungary, Poland, Spain, and Italy).

The available forestry residues are very high in Finland, Austria e Sweden. The expected production ranges between 4 and 16 Mt in 2025, as reported in **Figure 2.4**. If we introduce the COVID-19 correction, the estimated availability 3.5 and 14 Mt.

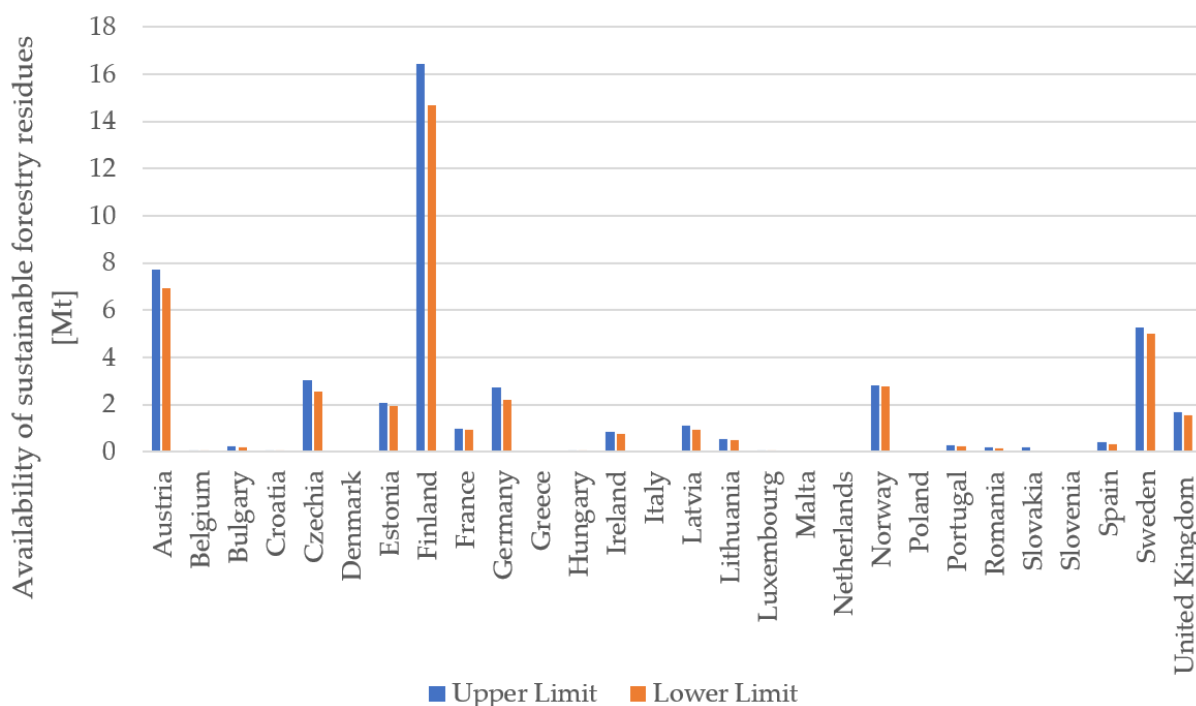


**Figure 2.4** Forestry Residues availability in Europe in 2025 in million tonnes per year.

Austria has a long tradition in the use of forestry residues as well. With a forest coverage of 46% of the country [2.45], it is one of the most densely forested countries in Europe after Sweden, with its 55% productive forest land of the total land area [2.46], and Finland, with its 70% [2.47].

Finland and Sweden have vast forest resources supporting large wood production for industrial uses, energy supply, heat and power. This circumstance leads to an economic growth and social well-being [2.46],[2.47]. However, part of these woody residues is used for the advanced biofuels production. Recent studies on the 2030 EU climate targets concluded that the most cost-efficient way to reduce emissions in Northern Europe is to invest in the production and uptake of advanced drop-in biofuels as they do not require changes to the vehicle fleet or fuel distribution system [2.48].

There are many European countries that will have a high availability of sustainable wastes like Italy, France, and United Kingdom, with values ranging between 2 and 7 Mt in 2025, as shown in **Figure 2.5**.

For that part of wastes, characterized by lignocellulosic material, such as paper and cardboard, vegetal and wood wastes, the corrected model suggests their overall availability will be approximately 1–1.7 Mt in 2025. However, even without any correction, the wastes availability is considerably lower than the crops residues. It is expected that waste generation and landfill will decrease in Europe by 2030, according to the European policies. These include the EU Waste Framework Directive (2008/98/EC) [2.49], the Landfill Directive (1999/31/EC) [2.50], and the Packaging and Packaging Waste Directive (94/62/EC) [2.51].

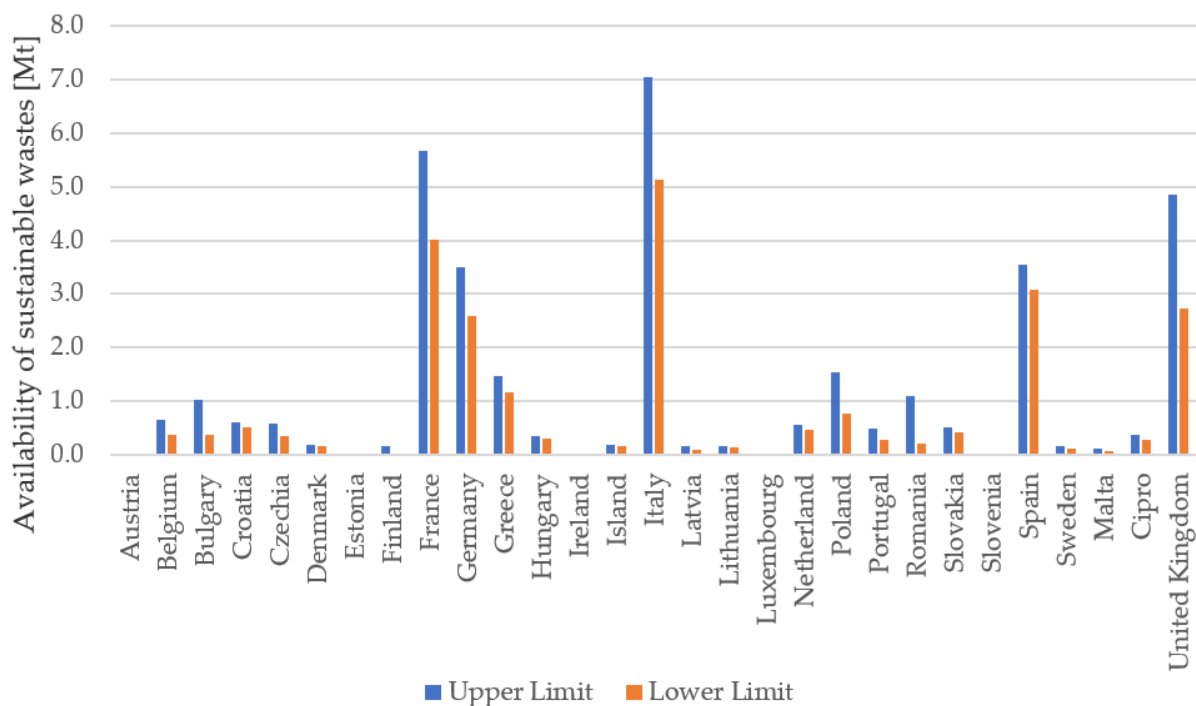


**Figure 2.5** Wastes availability in Europe in 2025 in million tonnes per year.

For the sake of clarity, the results of the maximum and minimum availability of European feedstocks in 2025 are summarized in **Table 2.11** according to the present autoregressive model:

**Table 2.11** Summary of feedstocks availability in Europe in 2025 without Covid-19 effects.

Category	Without COVID-19 Correction		With COVID-19 Correction	
	Max Availability [Mt]	Min Availability [Mt]	Max Availability [Mt]	Min Availability [Mt]
Agricultural residues	74	51	65	49

Forestry residues	46	41	41	36
Wastes	35	24	31	21

## 2.3. Main European Facilities

### 2.3.1. Agricultural Residues

The most relevant technologies able to produce advanced liquid and gaseous biofuels from agricultural residues for the transport sector are described in an open database, available on [2.52], where it is possible to identify the major European industrial plants processing agricultural residues (**Table 2.12**).

As shown in **Figure 2.3**, France, Germany, and Romania have large availability of crop residues. Consequently, in these countries, there are several plants with well-developed technologies. In France, the operational IFP plant (Futurol project), produces second generation ethanol (or cellulosic ethanol) with the support of 11 project partners (ARD, IFP Energies nouvelles, INRA, Lesaffre, Office national des forêts, Tereos, Total, Vivescia, Crédit Agricole Nord Est, CGB, Unigrains) covering the entire process from the plant resource to the fuel tank [2.53]. With a budget of 76.4 million euros, including 29.9 million state funding (Bpifrance), IFP invested in advanced biofuels production, since it creates a solution for the maintenance of agricultural activities exploiting their widely availability of residues at moderate prices.

In Germany, there are already two operational plants: Global Bioenergies and Clariant. In the Global Bioenergies plant, the straw hydrolysates fermentation leads to the production of bio-isobutene [2.54]. The isobutene could eventually be transformed into isooctane fuel, as well as oligomers and polymers, by other chemical processes [2.54]. In the Clariant plant (Sunliquid project), an innovative process to convert agricultural residues in biofuel is employed. The plant uses optimized enzymes to convert cellulose and hemicellulose into ethanol. Since 2012, Clariant has produced up to 1000 metric tonnes of cellulosic ethanol every year [2.55], and in 2018, the same company also broke ground for its first-of-its-kind commercial-scale cellulosic ethanol production plant in Romania with an annual capacity of 50,000 tons of cellulosic ethanol production. Clariant is investing more than EUR 100 million in its first plant, receiving more than EUR 40 million funding from the European Union [2.56].

**Table 2.12.** Operational European facilities for the advanced biofuels production [2.33],[2.52] from agricultural residues.

<b>Owner</b>	<b>Name</b>	<b>Location</b>
IFP	Futurol	France
Clariant	Sunliquid	Germany
Global Bioenergies	Isobutene demo	
Clariant	Clariant Romania	Romania

### 2.3.2. Forestry Residues

According to the database on facilities [2.52], there are many operational facilities of the above-mentioned European Countries able to convert forestry residues and lignocellulosic materials into advanced biofuels. They are summarized in **Table 2.13**.

**Table 2.13** Operational European facilities for the advanced biofuels production [2.52] from forestry residues.

<b>Owner</b>	<b>Name</b>	<b>Location</b>
Chempolis Ltd.	Chempolis Biorefining Plant	Finland
Fortum	Joensuu demo	
Green Fuel Nordic	Green Fuel Nordic	
St1	Cellunolix Kajaani	
VTT Technical Research Centre of Finland Ltd.	Dual fluidized-bed steam gasification pilot plant	
VTT Technical Research Centre of Finland Ltd.	Pressurized FB for synthesis gas production	
AustroCel Hallein	Biorefinery	Austria
RenFuel	RenFuel Backhammer	Sweden
SEKAB	Biorefinery Demo Plant	
Sodra	Sodra biomethanol	
SunPine	SunPine HVO 100 million litres	

In Finland, the country with the highest availability of residues, there are several operational plants. Chempolis Ltd. developed an advanced technology (formico 3G biorefinery [2.57]) for bioethanol production. In 2012, Fortum invested €20 M to build the first industrial-scale integrated bio-oil plant [2.58]. More than 100 tonnes of bio-oil had been produced from sawdust and forest residues, and more than 40 tonnes of bio-oil had been combusted in Fortum’s 1.5 MW district heating plant [2.59]. Green Fuel Nordic based its business on innovative pyrolysis technology in the production of an advanced bio-oil. The annual production capacity of the refinery is 24,000 tons of bio-

oil [2.60]. St1 produces about 10 million litres of advanced bioethanol through its St1 Cellunolix process optimized for softwood with an investment cost of €40 M [2.61]. The VTT Technical Research Centre of Finland Ltd. uses residual biomasses for the combined production of transport fuels, chemicals, and heat through gasification [2.62].

In 2019, the Austrian AustroCel Hallein started the construction of a new plant, able to produce 30 million litres/year of bioethanol. The company also signed a multi-year agreement with integrated oil and gas major OMV AG for the supply of advanced ethanol for blending with gasoline [2.63].

In Sweden, the company RenFuel signed an agreement with the Swedish pulp producer Rottneros and the fuel company Preem to produce advanced biofuel (Lignol) from feedstocks rich of lignin with biological catalysts in a reactor without pressure and at a temperature below the boiling point. The catalytic process is patented and protected by RenFuel [2.64]. The process developed by Sekab E-Technology consists mainly of four steps: pre-treatment with acid and steam at 200 degrees; enzymatic hydrolysis to break down cellulose in sugar; fermentation and reprocessing. The final products are bioethanol, biogas, and chemicals (lignin) [2.65]. Södra produces 5250 tonnes of biomethanol per year from wood raw material. The production begins with the sulphate pulp process at its mill. Wood chips are cooked with chemicals to separate the wood into its constituents, i.e., cellulose, hemicellulose (pulp), and lignin. Methanol is created when the wood and chemicals react. After cooking, the chemicals, lignin, and other residues are washed out of the pulp. They form black liquor, whose water content is then reduced by evaporation. What remains is a condensate of methanol, turpentine, and sulphur compounds. All the process is patented, and the company can produce 10 kg of biomethanol for every ton of pulp [2.66]. Finally, in 2019, SunPine produced 95 million litres of tall diesel, and new investments are being made to achieve a production volume of 150 million litres. Its diesel is then sold to Preem, which refines it into the world's only Nordic Swan eco-labelled diesel [2.67].

### 2.3.3. Wastes

Despite Italy and France being the European countries with the highest availability of wastes, according to [2.52] their facilities are not developed or operational yet. Therefore, in **Table 2.14**, the operational European plants are summarized. The Finnish St1 is focused on ethanol production that is the most used biofuel in the existing distribution networks. In addition, St1 generates fodder, energy, or heat as side products depending on the quality of the feedstock [2.68]. In 2019, St1 invested around 200 M€ in a new biorefinery in Sweden aiming at processing a wide range of feedstocks [2.69] by 2022. The main fuels will be HVO diesel, jet fuel, and naphtha.

**Table 2.14** Operational European facilities for the advanced biofuels production [2.33],[2.52] from wastes.

Owner	Name	Location
St1	Bionolix Hameenlinna	
St1	Etanolix Jokioinen	
St1	Etanolix Vantaa	Finland
St1	Etanolix Lahti	
St1	Etanolix Hamina	
Domsjo Fabriker	Domsjo Fabriker	Sweden
St1	Etanolix Gothenburg	
Advanced Biofuels Solutions Ltd. (ABSL)	Swindon Advanced Biofuels Plant	
Advanced Plasma Power Ltd.	BioSNG pilot plant	UK
Solena Fuels	Solena UK	

Domsjö Fabriker is a biorefinery whose recent businesses are the production of renewable fuels like bioethanol, bioDME, and biomethanol [2.70],[2.71] from forestry wastes. The rest of residual products are used to produce heat, allowing a further energy recovery [2.70]. The production of second-generation bioethanol is delivered to SEKAB, which refines it further into car fuel.

Advanced Biofuels Solutions Ltd. (ABSL) are the licensors of the RadGas technology, which offers reliable, high efficiency conversion of waste and biomass residues into a clean syngas. In particular, the syngas is suitable for the conversion into fuels such as hydrogen, bioSNG, propane, methane, dimethyl ether, kerosene, or diesel [2.72].

Advanced Plasma Power (APP) is a UK-based sustainable energy company that has been operating for eleven years. During this time, it has developed its Gasplasma solution for converting municipal and commercial waste into advanced biofuels and

electricity and has led the project development of several facilities based on its technology [2.73].

Solena Fuels Corporation is one step closer to produce sustainable 100% jet fuel purchased by British Airways at market competitive prices. The goal of the project is providing the gasification process that converts wastes into syngas and then in liquid biofuels (Integrated Biomass Gasification to Liquids (IBGTL)) [2.74].

## 2.4 Technological Maturity Level for Advanced Biofuels Production

Advanced biofuels have been considered a green alternative to fossil fuels for many decades, as clearly indicated in [2.75]. However, industrial technologies are a critical point in the bioeconomic value chain. In fact, there is still a gap between the bench scale and the higher production rates that would help these biofuels to become a commercial reality. To complete the picture, the technology readiness level (TRL) was employed to examine the development of the thermal, thermochemical, biochemical, and chemical conversion processes. The last three are the most widespread and strictly used to produce transport biofuels. For the sake of clarity, the definition of TRL is outlined in the following **Table 2.15**.

**Table 2.15** Technological Readiness Level (TRL) scale [2.75].

TRL	Definition	Description
0	Idea	Unproven concept, no testing has been performed
1	Basic research	Principles postulated and observed but no experimental proof available
2	Technology formulation	Concept and application have been formulated
3	Applied Research	First laboratory tests completed; proof of concept
4	Small scale prototype	Built in a laboratory environment
5	Large scale prototype	Tested in intended environment
6	Prototype system	Tested in intended environment close to expected performance
7	Demonstration system	Operating in operational environment at pre-commercial scale
8	First-of-a-kind commercial system	Manufacturing issues solved
9	Ready for commercialization	Technology available for consumers

Among the chemical conversion processes, we consider Hydrotreated Vegetable Oils (HVO) or Hydroprocessed Esters and Fatty Acids (HEFA), Transesterification, and Bio-Derived synthetic paraffinic kerosene (Bio-SPK). All these can boast of being fully developed technologies, or nearly so, and be able to process vegetable or algal oils and animal fats to get the biodiesel fuel range or synthetic kerosene, used for the transport and aviation sector, respectively. As described in ref. [2.76], HVO is a mature

technology, and it is already integrated in some existing oil refineries to co-process oil crops with fossil streams. For the same reasons, ref. [2.77] assigns TRL of 9 to both HVO and HEFA technologies. Transesterification is a competitive and currently in operation technology too. However, when algal oils are used as feedstocks, ref. [2.78] shows their conversion through transesterification is situated in a range from TRL 2 to 4–5. As a matter of fact, there are not developed industrial plants yet, but just advanced testing labs. Bio-SPK is a promising new solution for the global aviation industry, since its main product, named green jet fuel, has identical properties to jet fuel [2.79]. As appears from ref. [2.17], Bio-SPK is under assessment for commercial production (TRL 8).

In the class of biochemical conversion processes, the most mature technologies are alcohol fermentation, anaerobic digestion, and syngas fermentation. Alcohol fermentation converts sugars and starches from agricultural crops, producing conventional or first-generation ethanol used in gasoline engines. Lignocellulosic residues can also be used to produce advanced (or second-generation or cellulosic) ethanol. According to the different feedstocks, there is a change in the TRL assessment. In fact, ref. [2.77] distinguishes the two biofuels, conventional and cellulosic (or advanced) ethanol, by attributing them TRL 9 and 7, respectively. Generally, TRL 7 technologies, as that for advanced ethanol production, are for demonstration initiatives and not fully commercial. Anaerobic digestion is a widely used process to get mainly biomethane with a TRL 9. Its high technological maturity is due to a demonstrated use on a large variety of available feedstocks, such as organic waste fraction, industrial wastes, sewage and manure sludge, including energy crops, and crop residues [2.76]. Syngas Fermentation is an innovative process to produce ethanol. So, further technological improvements are needed to increase its maturity level. This justifies a TRL value limited to 6–7, as indicated in ref. [2.80]. It is also worth introducing Fischer-Tropsch synthesis (FTS) and Fischer-Tropsch synthetic paraffinic kerosene (FT-SPK). Both these biochemical technologies may be integrated at the thermochemical pathway with the aim to convert syngas in drop-in fuel and green jet fuel, respectively. In recent years, Fischer-Tropsch processes have reached a higher maturity. FTS TRL is ranging from 5–9 [2.17], while TRL of 6–8 is attributed to FT-SPK [2.81].

Finally, in terms of thermochemical conversion, there are two widely used processes, thermal gasification and pyrolysis. During the gasification, both gaseous and liquid



fuels can be produced from all the highlighted categories wastes, forestry, and agricultural residues. The gaseous biomethane and synthetic natural gas (SNG) is obtained via gasification with TRL 7, higher than the liquid fuel from lignocelluloses, whose technology has a TRL equal to 6. Similarly, pyrolysis is also a technology demonstrated in an industrially relevant environment with TRL 6. An overview of the mentioned TRL analysis is reported in **Table 2.16**.

**Table 2.16** Assessment of the technological readiness level (TRL) for each mentioned technology.

Available Technology	TRL	Status
HVO or HEFA [2.77]	9	Commercial
Anaerobic Digestion [2.77]	9	Commercial
Fermentation for conventional ethanol [2.77]	9	Commercial
Fermentation for cellulosic ethanol [2.77]	7	Demonstration
Syngas Fermentation [2.80]	6–7	Demonstration
Thermal gasification for biomethane [2.77]	7	Demonstration
Thermal gasification for biomass to liquid (BTL) [2.77]	6	Demonstration
Pyrolysis [2.77]	6	Demonstration
Transesterification from vegetable oil [2.82]	9	Commercial
Transesterification from algal oil [2.78]	From 2 to 4–5	Research-Pilot
FTS [2.83]	5–9	Pilot-Commercial
FT-SPK [2.81]	6–8	Demonstration—First-of-a-kind commercial
Bio-SPK [2.17]	8	First-of-a-kind commercial

## 2.5 A Proposal for a Technology Ranking

The status and the reliability of the above-mentioned technologies to produce advanced biofuels depend on several factors. Here, some of them are considered to evaluate them and to obtain a comprehensive ranking, aiming at selecting the most promising advanced biofuels. In this study, five items are considered: process maturity, drop-in fuels quality, feedstocks, and biofuel production cost and finally, the feedstocks availability in 2025, according to the current analysis. All these parameters play a significant role in the ranking process, since they are responsible for determining affordability of advanced biofuels in the market development. The rank ranges between 1 and 3 for each of these items, assuming 1 as a poor, 2 as a medium-good, and 3 as a very good qualitative level, as illustrated in **Table 2.17**.

**Table 2.17** Biofuel quality level for liquid biofuels.

Liquid Biofuel	Process Maturity	Drop-in Fuel	Feedstock Cost	Biofuels Production Cost	2025 Feedstocks Availability	Sum
First generation bioethanol	3	1	3	3	1	11
First generation biodiesel	3	2	2	2	2	11
Pyrolysis bio-oil	2	1	3	1	3	10
Second generation biodiesel	2	2	2	1	2	9
Renewable diesel (or green diesel)	3	3	2	1	2	11
Green jet fuel	2	3	1	1	2	9
Second generation bioethanol	2	1	3	1	3	10
Third generation biodiesel	1	2	2	1	1	7
Drop-in biofuel	1	3	2	1	1	8

The process maturity is well represented by the TRL. A lower process maturity requires a higher number of development steps, thus making the technological supply chain complex and expensive. Therefore, if the TRL of the corresponding technologies is 8 or 9, a value of 3 is assigned, if TRL is between 6 and 7 then the rank will be 2, and finally, for all the TRLs lower than 4–5, the rank will be 1.

When a liquid biofuel is drop-in, it is considered as an added value since it is fully compatible with the existing petroleum infrastructures, as reported in ref. [2.84]. In this ranking, if the fuel is drop-in, then the rank will be maximum (i.e., 3). If it is semi drop-in fuel, the rank will be 2, otherwise it will be 1.

Feedstock and production costs strongly influence the final biofuel ranking as they should satisfy the growing demand of the advanced biofuels in the current and future market. When the feedstocks cost is lower than 34 EUR/MWh, the rank is 3, if it is ranging from 34 and 60 EUR/MWh, the value is 2, and for all the feedstocks costs greater than 60 EUR/MWh, the rank is 1. Similarly, if the production cost is lower than 85 EUR/MWh, the rank is 3, if it is included between 85 and 94 EUR/MWh, the rank is 2, and when it is greater than 94 EUR/MWh, the rank is 1. Such division was made based on costs given in ref. [2.76].

Finally, the feedstocks availability could also help to understand and quantify the ecological boundaries of the bioeconomy from wastes, agriculture, and forestry residues. If the fuel comes from crop or forestry residues that are all lignocellulosic sources, the rank will be 3, if it is obtained by oil coming from wastes, the rank will be

2, otherwise all the fuels achieved by vegetable or algae oils (whose availability analysis is not reported in this paper) will be valued with the minimum rank, i.e., 1. Table 15 shows that the second-generation biofuels with the highest scores are the biodiesel fuels.

As previously illustrated in **Table 2.16**, the technologies with the highest TRL are fermentation for conventional ethanol, HVO/HEFA, anaerobic digestion for biogas and transesterification from vegetable oils for biodiesel. However, although all the technologies are mature, only the last four are significant for the advanced biofuels production. With reference to these technologies, feedstock and production costs (as reported in ref. [2.76]), are summarized on average in the following **Table 2.18**, showing the lowest costs for biogas production and comparable values for the alternatives considered biofuels.

**Table 2.18** Feedstocks and production costs for Technologies with the highest TRL according to ref. [2.76].

<b>TRL 9 Technologies</b>	<b>Feedstock Cost [EUR/MWh]</b>	<b>Production Cost [EUR/MWh]</b>	<b>Total [EUR/MWh]</b>
HVO or HEFA	50	78	128
Anaerobic Digestion	18.5	80	98.5
Transesterification from vegetable oil	60	95	155

## 2.6 Conclusions

This study estimated the amount of wastes, agricultural, and forestry residues by 2025 that can be sustainably used to produce advanced biofuels without neglecting aspects related to the environmental impact and other existing competitive uses.

Residues from the agriculture and forestry sector will be the most abundant in 2025 in Europe, since wastes should be limited by European policies, as illustrated previously, as well as they are considered the most promising feedstocks for various types of advanced biofuels used as energy supply in the European transport sector. As suggested by ref. [2.85], the potential of biomass from agricultural sector cannot be considered as a constant value over time because of some changes such as the amount of available agricultural land or the structure of cultivated crops. However, it stands to reason that, by 2025, there will be not large variations in respect of the present

results for both the smallness of the estimated time interval and the considerations of all the aspects related to the biodiversity and the environment.

Despite the pandemic emergency, advanced biofuel demand is expected to continue growing over the next decades and relying heavily on the current and future technologies. According to the present ranking of different technologies, HVO or HEFA are the most used, thanks to their maturity level (TRL equal to 9) and optimized costs. Nevertheless, technological improvements are expected to produce biofuels with even higher efficiencies. In this regard, promising technologies with lower TRL are fermentation for cellulosic ethanol and syngas fermentation, due to high values of agricultural and forestry residues, as emerged in the current paper. Although the first-generation biofuels remain the most common choice from the metric in Table 15, the renewable (or green) diesel is promising for different applications in the transport sector. It is followed by the green jet fuel applied in the aviation sector and the second generation of bioethanol (or cellulosic ethanol), whose technological efforts are still challenging.

By building new biorefineries, the bio-based value chain, based on secondary biomasses, will be established in Europe, providing a tangible example for a successful circular economy approach. These plants lay the foundation for a wide-scale implementation of advanced biofuels production worldwide and for a more sustainable energy supply in the European transport sector.

In this critical financial situation, the support of the biorefineries is essential to preserve and create jobs, and to avoid service degradation. This is indispensable for realizing the true potential of circular economy and to address the concerns of residues and wastes management and alternative energy generation.

## References

- [2.1]. EUROSTAT. Environment and Energy, Environment, Waste, Treatment of Waste—Disposal Landfill and Other (Data Update to 2016). Available online: [https://appsso.eurostat.ec.europa.eu/nui/show.do?dataset=env\\_wastrt&lang=en](https://appsso.eurostat.ec.europa.eu/nui/show.do?dataset=env_wastrt&lang=en) (accessed on 15 October 2020);
- [2.2]. FAOSTAT. CROPS, Production Quantity (Data Calculated on Average between 2014 and 2018). Available online: <http://www.fao.org/faostat/en/#data/QC> (accessed on 6 April 2020);
- [2.3]. FAOSTAT. Forestry Production and Trade, Production Quantity, coniferous, non-coniferous (Data Calculated on Average between 2014 and 2018). Available online: <http://www.fao.org/faostat/en/#data/FO> (accessed on 6 April 2021);
- [2.4]. Searle, S.; Malins, C. *Availability of Cellulosic Residues and Wastes in the EU*; ICCT: Washington, DC, USA, 2013;
- [2.5]. Searle, S.; Malins, C. Waste and residue availability for advanced biofuel production in EU Member States. *Biomass Bioenergy* **2016**, *89*, 2–10;
- [2.6]. UN Economic Commission for Europe (UNECE). *Forest Production Conversion Factors for the UNECE Region*; Gebeva Timber and Forest Discussion Paper 49; UNECE: Geneva, Switzerland, 2009; p. 38. Available online: <http://www.unece.org/fileadmin/DAM/timber/publications/DP-49.pdf> (accessed on 17 November 2020);
- [2.7]. Directive 2008/98/EC of the European Parliament and of the Council of 19 November 2008 on Waste and Repealing Certain Directives. Available online: <https://eur-lex.europa.eu/legal-content/EN/TXT/PDF/?uri=CELEX:32008L0098&from=EN> (accessed on 10 July 2020);
- [2.8]. Autoregressive Model. Available online: <https://it.mathworks.com/help/econ/autoregressive-model.html#References> (accessed on 1 April 2021);
- [2.9]. Time Series Decomposition. Available online: <https://www.mathworks.com/help/econ/detrending.html> (accessed on 1 April 2021);
- [2.10]. Trend, Seasonality, Moving Average, Auto Regressive Model: My Journey to Time Series Data with Interactive Code. Available online: <https://towardsdatascience.com/trend-seasonality-moving-average-auto->

- regressive-model-my-journey-to-time-series-data-with-edc4c0c8284b (accessed on 1 April 2021);
- [2.11]. Least-Squares Fitting. Available online: <https://www.mathworks.com/help/curvefit/least-squares-fitting.html> (accessed on 1 April 2021);
- [2.12]. Seasonal Adjustment. Available online: [https://www.mathworks.com/help/econ/seasonal-adjustment-1.html?searchHighlight=seasonality%20component&s\\_tid=srchtitle](https://www.mathworks.com/help/econ/seasonal-adjustment-1.html?searchHighlight=seasonality%20component&s_tid=srchtitle) (accessed on 1 April 2021);
- [2.13]. Hogan, R. Confidence Intervals and Risk in Measurement, February 12, 2013, Isobudgets. Available online: <https://www.isobudgets.com/confidence-intervals-and-risk-in-measurement/> (accessed on 1 April 2021);
- [2.14]. Report extract Technology summaries. Available online: <https://www.iea.org/reports/renewable-energy-market-update/technology-summaries#transport-biofuels> (accessed on 15 September 2020);
- [2.15]. Transport biofuels. Available online: <https://www.iea.org/reports/renewables-2020/transport-biofuels> (accessed on 15 September 2020);
- [2.16]. McGill University & IATA. The 2nd Generation Biomass Conversion Efficiency. 2009. Available online: <https://www.yumpu.com/en/document/read/322445/2nd-generation-biomass-conversion-efficiency> (accessed on 15 June 2021);
- [2.17]. Guo, M.; Song, W. The growing U.S. bioeconomy: Drivers, development and constraints. *New Biotechnol.* **2019**, *49*, 48–57;
- [2.18]. Badger, P.C. Ethanol from cellulose: A general review. In *Trends in New Crops and New Uses*; Janick, J., Whipkey, A., Eds.; ASHS Press: Alexandria, VA, USA, 2002; pp. 17–21. Available online: <https://hort.purdue.edu/newcrop/ncnu02/v5-017.html> (accessed on 1 June 2020);
- [2.19]. Shah, M.A.; Khan, M.N.S.; Kumar, V. Biomass residue characterization for their potential application as biofuels. *J. Therm. Anal. Calorim.* **2018**, *134*, 2137–2145;
- [2.20]. Chandra, R.; Takeuchi, H.; Hasegawa, T. Methane production from lignocellulosic agricultural crop wastes: A review in context to second generation of biofuel production. *Renew. Sustain. Energy Rev.* **2012**, *16*, 1462–1476;
- [2.21]. Várhegyi, G.; Chen, H.; Godoy, S. Thermal Decomposition of Wheat, Oat, Barley, and Brassica carinata Straws. A Kinetic Study. *Energy Fuels* **2009**, *23*, 646–652;

- [2.22]. Kumar, K.; Goh, K.M. Crop residues and management practices: Effect on soil quality, soil, nitrogen dynamics, crop yield and nitrogen recovery. *Adv. Agron.* **2000**, *68*, 197–319;
- [2.23]. Worasuwanarak, N.; Sonobe, T.; Tanthapanichakoon, W. Pyrolysis behaviors of rice straw, rice husk, and corncob by TG-MS technique. *J. Anal. Appl. Pyrolysis* **2007**, *78*, 265–271;
- [2.24]. Bledzki, A.K.; Mamun, A.A.; Volk, J. Physical, chemical and surface properties of wheat husk, rye husk and soft wood and their polypropylene composites. *Compos. Part A* **2010**, *41*, 480–488;
- [2.25]. Bilgen, S.; Sarıkaya, I.; Ayyıldız, L.M. A new correlation for calculation of the chemical exergy of bio-oils obtained from agricultural residues by using elementary analyses data, *Energy Sources. Part A Recovery Util. Environ. Eff.* **2016**, *38*, 3055–3064;
- [2.26]. Song, C.; Zhang, C.; Zhang, S.; Lin, H.; Kim, Y.; Ramakrishnan, M.; Du, Y.; Zhang, Y.; Zheng, H.; Barceló, D. Thermochemical liquefaction of agricultural and forestry wastes into biofuels and chemicals from circular economy perspectives. *Sci. Total Environ.* **2020**, *749*, 141972;
- [2.27]. Bertin, C.; Rouau, X.; Thibault, J.F. Structure and Properties of Sugar Beet Fibres. *Sci. Food Agric.* **1988**, *44*, 15–29;
- [2.28]. Reddy, N.; Yang, Y. Biofibers from agricultural byproducts for industrial applications. *Trends Biotechnol.* **2005**, *23*, 22–27;
- [2.29]. Sarkar, N.; Ghosh, S.K.; Bannerjee, S.; Aikat, K. Bioethanol production from agricultural wastes: An overview. *Renew. Energy* **2012**, *37*, 19–27;
- [2.30]. Dererie, D.Y.; Trobro, S.; Momeni, M.H.; Hansson, H.; Blomqvist, J.; Passoth, V.; Schnürer, A.; Sandgren, M.; Ståhlberg, J. Improved bio-energy yields via sequential ethanol fermentation and biogas digestion of steam exploded oat straw. *Bioresour. Technol.* **2011**, *102*, 4449–4455;
- [2.31]. Claye, S.S.; Idouraine, A.; Weber, C.W. Extraction and fractionation of insoluble fiber from five fiber sources. *Food Chem.* **1996**, *57*, 305–310;
- [2.32]. Sharma, R.K.; Arora, D.S. Solid state degradation of paddy straw by *Phlebia floridensis* in the presence of different supplements for improving its nutritive status. *Int. Biodeterior. Biodegrad.* **2011**, *65*, 990–996;

- [2.33]. Brijwani, K.; Oberoi, H.S.; Vadlani, P.V. Production of a cellulolytic enzyme system in mixed-culture solid-state fermentation of soybean hulls supplemented with wheat bran. *Process Biochem.* **2010**, *45*, 120–128;
- [2.34]. Friedl, A.; Padouvas, E.; Rotter, H.; Varmuza, K. Prediction of heating values of biomass fuel from elemental composition. *Anal. Chim. Acta* **2005**, *544*, 191–198;
- [2.35]. Machineni, L. Lignocellulosic biofuel production: Review of alternatives, Biomass Conversion and Biorefinery. *Biomass Convers. Biorefinery* **2020**, *10*, 779–791;
- [2.36]. Available online: <https://www.bbc.co.uk/news/science-environment-63089348> (accessed on 10/12/2022);
- [2.37]. Doelle, K.; Bajrami, B. Sodium Hydroxide and Calcium Hydroxide Hybrid Oxygen Bleaching with System. *IOP Conf. Ser. Mater. Sci. Eng.* **2018**, *301*, 012136;
- [2.38]. Nanda, S.; Berruti, F. A technical review of bioenergy and resource recovery from municipal solid waste. *J. Hazard. Mater.* **2021**, *403*, 123970;
- [2.39]. Sommers, L.E. Chemical Composition of Sewage Sludges and Analysis of Their Potential Use as Fertilizers. *J. Environ. Qual.* **1977**, *6*, 225–232;
- [2.40]. Assari, M.R.; Basirat Tabrizi, H.; Najafpour, E.; Ahmadi, A.; Jafari, I. Exergy modeling and performance evaluation of pulp and paper production process of bagasse, a case study. *Therm. Sci.* **2014**, *18*, 1399–1412;
- [2.41]. Boldrin, A.; Christensen, T.H. Seasonal generation and composition of garden waste in Aarhus (Denmark). *Waste Manag.* **2010**, *30*, 551–557;
- [2.42]. Yin, S.; Dolan, R.; Harris, M.; Tan, Z. Subcritical hydrothermal liquefaction of cattle manure to bio-oil: Effects of conversion parameters on bio-oil yield and characterization of bio-oil. *Bioresour. Technol.* **2010**, *101*, 3657–3664;
- [2.43]. Fehera, A.; Goşa, V.; Raicov, M.; Haranguş, D.; Condea, B.V. Convergence of Romanian and Europe Union agriculture—Evolution and prospective assessment. *Land Use Policy* **2017**, *67*, 670–678;
- [2.44]. The Renewable Energy Directive. Available online: <https://eur-lex.europa.eu/legal-content/EN/TXT/?uri=OJ:L:2018:328:TOC> (accessed on 11 March 2020);
- [2.45]. Loibnegger, T. Telling the Story in Austria: Sustainable Wood Energy Supply, WoodHeatSolutions. 2010. Available online: [https://ec.europa.eu/energy/intelligent/projects/sites/iee-projects/files/projects/documents/whs\\_austria\\_sustainable\\_wood\\_energy\\_supply\\_en.pdf](https://ec.europa.eu/energy/intelligent/projects/sites/iee-projects/files/projects/documents/whs_austria_sustainable_wood_energy_supply_en.pdf) (accessed on 17 November 2020);



- [2.46]. Björkman, M.; Börjesson, P. Balancing Different Environmental Effects of Forest Residue Recovery in Sweden: A Stepwise Handling Procedure. *IEA Bioenergy*. 2016. Available online: <https://www.ieabioenergy.com/wp-content/uploads/2018/01/IEA-Bioenergy-Task-43-TR2016-03-ii.pdf> (accessed on 9 July 2021);
- [2.47]. IRENA. *Bioenergy from Finnish Forests: Sustainable, Efficient, Modern Use of Wood*; International Renewable Energy Agency, Abu Dhabi 2018;
- [2.48]. Biofuels in Finland. Available online: [https://www.etipbioenergy.eu/images/EBTP\\_Factsheet\\_Finland\\_250416\\_582afad9527a8.pdf](https://www.etipbioenergy.eu/images/EBTP_Factsheet_Finland_250416_582afad9527a8.pdf) (accessed on 17 November 2021);
- [2.49]. Directive (EU) 2018/851 of the European Parliament and of the Council of 30 May 2018 Amending Directive 2008/98/EC on Waste. Available online: <https://eur-lex.europa.eu/legal-content/en/TXT/PDF/?uri=CELEX:32018L0851&from=EN> (accessed on 9 July 2021);
- [2.50]. The Landfill Directive (1999/31/EC). Available online: <https://eur-lex.europa.eu/legal-content/EN/TXT/PDF/?uri=CELEX:31999L0031&from=EN> (accessed on 9 July 2021);
- [2.51]. European Parliament and Council Directive 94/62/EC of 20 December 1994 on Packaging and Packaging Waste. Available online: <https://eur-lex.europa.eu/legal-content/EN/TXT/PDF/?uri=CELEX:31994L0062&from=en> (accessed on 9 July 2021);
- [2.52]. Database on Facilities for the Production of Advanced Liquid and Gaseous Biofuels for Transport. Available online: <https://demoplants.bioenergy2020.eu/> (accessed on 21 January 2021);
- [2.53]. Futurol Information. Available online: <https://www.ifpenergiesnouvelles.com/article/advanced-bioethanol-futuroltm-technology-set-market-launch> (accessed on 25 February 2021);
- [2.54]. First production of isobutene from wheat straw at demo scale. Available online: <https://www.global-bioenergies.com/first-production-of-isobutene-from-wheat-straw-at-demo-scale/?lang=en> (accessed on 25 February 2021);
- [2.55]. Sunliquid Project. Available online: <https://www.clariant.com/en/Business-Units/New-Businesses/Biotech-and-Biobased-Chemicals/Sunliquid> (accessed on 25 February 2021);

- [2.56]. Sunliquid Project in Romania. Available online: <https://www.clariant.com/en/Company/Contacts-and-Locations/Key-Sites/Romania> (accessed on 25 February 2021);
- [2.57]. Chempolis pure future. Available online: <https://chempolis.com/technologies-solutions/> (accessed on 25 February 2021);
- [2.58]. Fortum. Available online: <https://www.fortum.com/media/2012/03/fortum-invests-eur-20-million-build-worlds-first-industrial-scale-integrated-bio-oil-plant> (accessed on 25 February 2021);
- [2.59]. Välimäki, E.; Autio, J.; Oasmaa, A. Lignocellulosic fuel from wood residues—Industrial demonstration. In Proceedings of the 22nd European Biomass Conference and Exhibition, Hamburg, Germany, 23–26 June 2014;
- [2.60]. Green Fuel Nordic Oy. Available online: <https://www.greenfuelnordic.fi/en/company> (accessed on 25 February 2021);
- [2.61]. St1 Cellunolix process—Lignocellulosic bioethanol production and value chain upgrading. Available online: <https://www.nmbu.no/download/file/fid/34440> (accessed on 12 January 2021);
- [2.62]. VTT develops a new sustainable way to turn forestry waste into transport fuels and chemicals. Available online: <https://www.vttresearch.com/en/news-and-ideas/vtt-develops-new-sustainable-way-turn-forestry-waste-transport-fuels-and-chemicals> (accessed on 12 January 2021);
- [2.63]. AustroCel Hallein begins construction of Austria’s first cellulosic ethanol plant and signs off-take deal with OMV. Available online: <https://bioenergyinternational.com/biofuels-oils/austrocel-hallein-begins-construction-of-austrias-first-cellulosic-ethanol-plant-and-signs-off-take-deal-with-omv> (accessed on 12 January 2021);
- [2.64]. The world’s first lignin plant for biofuels. Available online: <https://www.paperadvance.com/blogs/soeren-back/the-world-s-first-lignin-plant-for-biofuels.html> (accessed on 12 January 2021);
- [2.65]. This is how we make sugar and ethanol from cellulose. Available online: <https://www.sekab.com/en/this-is-how-it-works/biorefinery-demo-plant/our-process/> (accessed on 12 January 2021);
- [2.66]. Refuelling the future. Available online: <https://www.sodra.com/en/global/Bioproducts/biomethanol/> (accessed on 12 January 2021);

- [2.67]. Annual report and sustainability report 2019. Available online: [https://cdn.timelab.se/sunpine/20200831133309/20200824\\_SunPine\\_%C3%85rsred ovisning\\_2019\\_eng.pdf](https://cdn.timelab.se/sunpine/20200831133309/20200824_SunPine_%C3%85rsred ovisning_2019_eng.pdf) (accessed on 12 January 2021);
- [2.68]. Advanced fuels from waste. Available online: <https://www.st1.com/about-st1/company-information/areas-operations/advanced-fuels-waste> (accessed on 12 January 2021);
- [2.69]. St1 invests EUR 200m in new biorefinery for renewable diesel and jet fuel. Available online: <https://bioenergyinternational.com/biofuels-oils/st1-to-invest-eur-200-million-in-new-biorefinery-to-produce-renewable-diesel-and-jet-fuel> (accessed on 12 January 2021);
- [2.70]. Value chain analysis of biofuels: Örnköldsvik in Sweden. Available online: [http://www.topnest.no/attachments/article/12/Value%20Chain%20Analysis\\_Ornskoldsvik.pdf](http://www.topnest.no/attachments/article/12/Value%20Chain%20Analysis_Ornskoldsvik.pdf) (accessed on 20 January 2021);
- [2.71]. Bioenergy Development in Västernorrland, Sweden. Available online: [https://www.nibio.no/en/projects/triborn-triple-bottom-line-outcomes-for-bioenergy-development-and-innovation-in-rural-norway/triborn-background/\\_attachment/inline/873a8b7d-f822-45d6-8327-336aa232279e:d2465c0b240bb6cad10ae6eced5af6d29b20ad70/Anna%20Berlina%20-2017-%20Bioenergy%20development%20in%20V%C3%A4sternorrland%20%20Sweden%20-%20NORDREGIO%20Working%20paper.pdf](https://www.nibio.no/en/projects/triborn-triple-bottom-line-outcomes-for-bioenergy-development-and-innovation-in-rural-norway/triborn-background/_attachment/inline/873a8b7d-f822-45d6-8327-336aa232279e:d2465c0b240bb6cad10ae6eced5af6d29b20ad70/Anna%20Berlina%20-2017-%20Bioenergy%20development%20in%20V%C3%A4sternorrland%20%20Sweden%20-%20NORDREGIO%20Working%20paper.pdf) (accessed on 23 January 2021);
- [2.72]. ABSL—Advanced Biofuel Solution Ltd. Available online: <https://absl.tech/about-us> (accessed on 22 January 2021);
- [2.73]. Bioenergy Review 2018—Call for evidence—Response from Advanced Plasma Power Ltd. Available online: <https://www.theccc.org.uk/wp-content/uploads/2018/12/Biomass-response-to-Call-for-Evidence-Advanced-Plasma-Power.pdf> (accessed on 25 January 2021);
- [2.74]. Sustainable jet fuel is taking off in London with BA. Available online: <https://www.supplychaindigital.com/logistics-1/sustainable-jet-fuel-taking-london-ba> (accessed on 25 January 2021);
- [2.75]. IRENA 2019. Available online: [https://www.irena.org/-/media/Files/IRENA/Agency/Publication/2016/IRENA\\_Innovation\\_Outlook\\_Advanced\\_Liquid\\_Biofuels\\_2016.pdf](https://www.irena.org/-/media/Files/IRENA/Agency/Publication/2016/IRENA_Innovation_Outlook_Advanced_Liquid_Biofuels_2016.pdf) (accessed on 3 June 2020);

- [2.76]. Brown, A.; Waldheim, L.; Landälv, I.; Saddler, J.; Ebadian, M.; McMillan, J.D.; Bonomi, A.; Klein, B. Advanced Biofuels—Potential for Cost Reduction. *IEA Bioenergy* **2020**, *88*, 1–3;
- [2.77]. Müller-Langer, F.; Majer, S.; O’Keeffe, S. Benchmarking biofuels—A comparison of technical, economic and environmental indicators, *Energy. Sustain. Soc.* **2014**, *4*, 1–14;
- [2.78]. Study on Impacts of EU Actions Supporting the Development of Renewable Energy Technologies. Available online: [https://ec.europa.eu/research/energy/pdf/impacts\\_studies/study\\_solar\\_pv.pdf](https://ec.europa.eu/research/energy/pdf/impacts_studies/study_solar_pv.pdf) (accessed on 18 June 2020);
- [2.79]. Jansen, R.S. *Second Generation Biofuels and Biomass: Essential Guide for Investors, Scientists and Decision Makers*; ch. 16; Wiley-VCH Verlag GmbH & Co. KGaA, Weinheim, Germany, 2013;
- [2.80]. Alberts, G.; Ayuso, M.; Bauen, A.; Boshell, F.; Chudziak, C.; Gebauer, J.P.; German, L.; Kaltschmitt, M.; Nattrass, L.; Ripken, R.; et al. *Innovation Outlook Advanced Liquid Biofuels*; IRENA, 2016. Available online: [https://www.irena.org/-/media/Files/IRENA/Agency/Publication/2016/IRENA\\_Innovation\\_Outlook\\_Advanced\\_Liquid\\_Biofuels\\_2016.pdf](https://www.irena.org/-/media/Files/IRENA/Agency/Publication/2016/IRENA_Innovation_Outlook_Advanced_Liquid_Biofuels_2016.pdf) (accessed on 25 January 2021);
- [2.81]. Prussi, M.; O’Connell, A.; Lonzab, L. *Analysis of Current Aviation Biofuel Technical Production Potential in EU28*; Elsevier: Amsterdam, The Netherlands, 2019;
- [2.82]. Catalogue of Bioeconomy Solutions: Finding Key Information of Promising Bioeconomy Solutions. Available online: <https://power4bio.draxis.gr/#/> (accessed on 25 July 2020);
- [2.83]. Jarvis, S.M.; Samsatli, S. *Technologies and Infrastructures Underpinning Future CO<sub>2</sub> Value Chains: A Comprehensive Review and Comparative Analysis*; Elsevier: Amsterdam, The Netherlands, 2018;
- [2.84]. Van Dyk, S.; Su, J.; McMillan, J.D.; Saddler, J.N. ‘Drop-In’ Biofuels: The key role that co-processing will play in its production. *IEA Bioenergy* 2019, Available online: <https://www.ieabioenergy.com/wp-content/uploads/2019/09/Task-39-Drop-in-Biofuels-Full-Report-January-2019.pdf> (accessed on 9 July 2021);
- [2.85]. Knápek, J.; Králík, T.; Vávrová, K., Weger, J. Dynamic biomass potential from agricultural land. *Renew. Sustain. Energy Rev.* **2020**, *134*, 110319.

### 3. Technological background

#### Chapter summary

There are different energy conversion technologies that are waste-to-fuels (WtF) or biomass-to-fuels (BtF) pathways; these are: thermal, thermochemical, biochemical and chemical processes as illustrated in **Figure 3.1**. The scope of this chapter is to analyse the thermochemical processes of torrefaction, gasification, pyrolysis, hydrothermal liquefaction (HTL), hydrothermal carbonization (HTC), thermo-catalytic reforming (TCR) and hydrotreatment. Unlike thermal conversions (e.g. combustion, co-combustion, incineration), thermochemical processes are able to recover the chemical value from waste and biomass rather than only its energetic value in terms of heat, thus producing a wide range of valuable solid, liquid and gaseous fuels with good properties. Moreover, it is also possible to effectively capture carbon and control emissions to lower levels than incineration. In **Figure 3.1**, thermochemical conversion is only reported for lignocellulosic biomass. However, it also includes other biomass wastes such as industrial wastes MSW and some plastics contaminated wastes. Therefore, a review of each thermochemical conversion pathway is deeply investigated by focusing on key parameters basically involved, in order to better understand thermal-catalytic reforming (TCR), proposed to combine intermediate pyrolysis with post-catalytic reforming in complete absence of oxidizing agents (e.g. oxygen, air, steam or carbon dioxide) and convert feedstocks in hydrogen-rich syngas, oil and char.

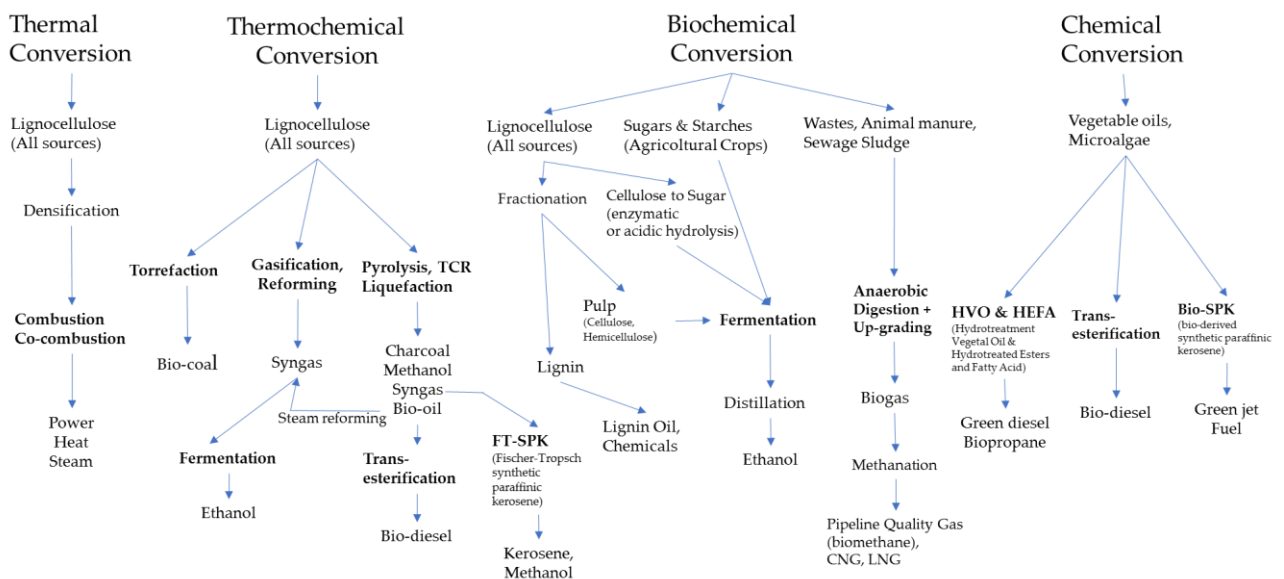


**Figure 3.1** Overview of the main energy conversion processes

### 3.1 The torrefaction

Torrefaction is an endothermic thermochemical process considered like pyrolysis since it operates in absence of oxygen at relatively lower temperatures of 200–300 °C with residence times of 15–60 minutes and similarly producing solid, liquid and gaseous products [3.1] [3.2]. For these reasons, it is sometimes called mild pyrolysis [3.1].

Torrefaction is usually involved in the biomass pre-treatment process to improve the energy quality of solid biomass destined to further conversion processes like combustion, gasification, pyrolysis and liquefaction [3.1], [3.3]. Such improvement is obtained from the removal of oxygen, residual moisture content and low-weight organic volatile components, thereby reducing viscosity, contributing to a higher calorific value and enhancing the grindability and resistance to biodegradation [3.1][3.4].

Torrefaction temperature and duration time are two important key factors for the process performances.

According to temperature, the biomass torrefaction can be classified in severe, mild, and light. The corresponding temperatures are 275–300 °C, 235–275 °C, and 200–235 °C [3.3][3.5]. If the biomass is lignocellulosic, which means it is made of cellulose, hemicellulose and lignin, the torrefaction reactions are depolymerisation, devolatilization and carbonization of cellulose, hemicellulose and lignin [3.4]. Nevertheless, lignin is recalcitrant to be decomposed, unless the torrefaction temperature is high [3.3]. Actually, lignin is a complex aromatic polymer structure that requires more than 500 °C to produce abundant hydrocarbon compounds [3.6].

Severe torrefaction leads to a complete breaking of hemicellulose, a fragmentation of cellulose and a low consumption of lignin, causing a decrease in mass and energy yields, but the torrefied biomass has a higher energy density (MJ/kg). During mild torrefaction, hemicellulose is decomposed in large quantities, and cellulose branches are cracked. When torrefaction is light, hemicellulose is severely degraded. However, cellulose and lignin components are not easily affected because of low temperatures [3.3].

In addition, duration time affects the final products in the torrefaction process. It can vary from several minutes to hours. As the duration time is gradually

prolonged, the energy density and carbon content increases at the expenses of mass and energy yields, which decrease [3.3].

As already mentioned, the collectable products at the end of the process are solid (biochar), liquid (bio-oil) and gaseous. Even though mass and energy vary significantly for different feedstocks, the solid product is presented as a black uniform carbonized material, containing about 70% of the initial mass with the 90% of the initial energy content. The remaining 30% of the mass represents the condensable and non-condensable products [3.4].

The bio oil is the condensable liquid containing mainly acids, ketones, alcohols, phenols, esters, aldehydes, water, and other substances. Water remains the most abundant product (about 50%), but it decreases by increasing the torrefaction temperature, thus upgrading the liquid product as a fuel. [3.5]. It has been demonstrated that bio oil properties are strongly affected by temperature rather than duration time [3.5].

The gaseous fraction is composed of CO<sub>2</sub>, CO, CH<sub>4</sub>, H<sub>2</sub>, and C<sub>2</sub>H<sub>4</sub> (ethylene) [3.7] but its heating value is too low to be reused as a fuel [3.3].

Furthermore, catalysts can be considered a key parameter in the torrefaction process. Indeed, several studies have been carried on and it has been demonstrated that alkali and alkaline earth metals (AAEMs) can improve the bio-char yield and its quality in terms of high energy density, heating value, and grindability, and improved thermal degradation properties [3.1], [3.8], [3.9]. Despite its benefits in terms of pelletization, grindability and resistance to the biodegradation, the torrefaction has the disadvantage to produce biochar as an unstable form of carbon, also containing Volatile Organic Content (VOC), due to the low processing temperatures imposed. Moreover, the volume of torrefied biomass is slightly reduced by 10-20% than dried feedstock and its energy density (GJ/m<sup>3</sup>) does not improve significantly, despite higher calorific values [3.10].

### 3.2 The hydrothermal liquefaction (HTL)

Hydrothermal liquefaction or HTL is the thermochemical conversion of biomass into liquid fuels by a high-temperature pressurized environment for less than 60 minutes [3.11]. The corresponding temperature and pressure are 250–374 °C and 4–22 MPa, respectively [3.1]. In liquefaction, one of the most important factor is the hot compressed water, which acts as catalyst [3.12], which explains why the most suitable feedstocks for HTL are those with high-moisture content contrarily to pyrolysis which requires at least a pre-drying [3.1][3.12]. However, the process also requires the presence of other catalysts (e.g. alkali metal salts) and supplemental CO and H<sub>2</sub> as reactants to facilitate the liquefaction [3.13].

The main products of the reaction are bio-crude, char, water-soluble substances and gas. The water-soluble products can contain C<sub>5</sub>-C<sub>6</sub> sugars and C<sub>4</sub>-C<sub>2</sub> organic acid as reported in [3.14] for the HTL of macro-alga. The bio-crude has good properties, since HTL technology is able to improve the quality of bio-oil in terms of high heating value, bio-oil yield, and oxygen and nitrogen contents [3.1], [3.12]. The addition of various alkaline catalysts can also improve oil yield and quality [3.12] and suppress char e tar formation [3.1]. According to [3.15], HTL of lignocellulosic biomass can be divided in three major steps which are depolymerisation, decomposition, and polymerization (or recombination) [3.1][3.13] [3.15] and shown in **Figure 3.2**.

Firstly, hemicellulose is depolymerized to monomers and oligomers through catalytic hydrolysis, while cellulose and lignin depolymerize based on the liquefaction conditions [3.1] [3.15]. Water at high temperatures and pressure breaks down the hydrogen-bonded structure of cellulose and causes the formation of glucose monomers. Since fructose is more reactive than glucose, it rapidly degrades in plethora of products by different types of reactions [3.15]. These latter include cleavage, dehydration (loss of H<sub>2</sub>O), dehydrogenation (loss of H<sub>2</sub>), deoxygenation (loss of O<sub>2</sub>), decarboxylation (loss of CO<sub>2</sub>) and deamination (removal of amino acid content) reactions [3.1], [3.13]. The dehydration and decarboxylation facilitate the removal of oxygen from the biomass in the form of H<sub>2</sub>O and CO<sub>2</sub>, respectively. Most of the degradation products such as polar organic molecules, furfurals, glycoaldehydes, phenols and organic acids are highly soluble in water. Finally, polycondensation and polymerization occur, thus forming hydro-char-insoluble carbonaceous materials and bio-oil [3.1].



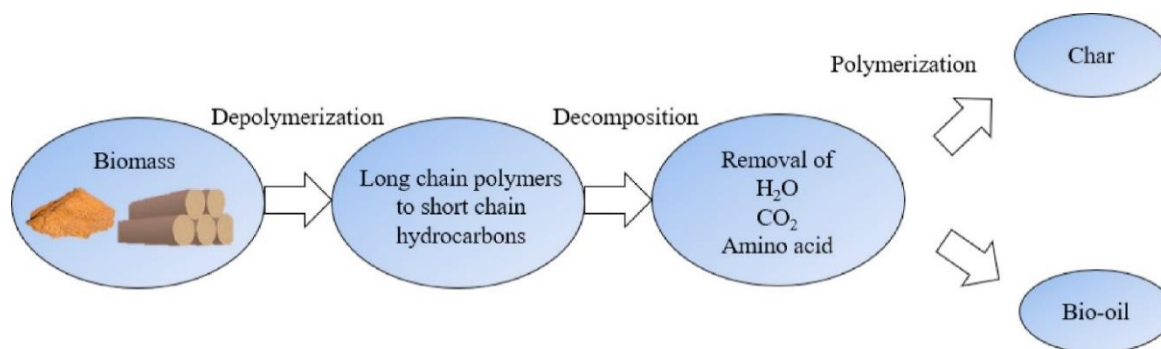


**Figure 3.2** Scheme of the hydrothermal liquefaction (HTL) process [3.1]

The critical parameters of HTL are temperature, residence time, catalysts which influence the process of re-polymerization, condensation and decomposition of the components [3.15], thus contributing to different yields of products.

Catalysts used in HTL are categorized as homogeneous (water-soluble) and heterogeneous (no water-soluble) catalysts [3.1]. Both have shown positive effects on the bio-oil yield and quality.

Alkali salts and acids are homogeneous catalysts. It has been demonstrated that the formers provide better catalyst effect due to the potassium carbonate ( $K_2CO_3$ ), the latter increase the yields and the HHV of the bio-oil [3.1].

Transition metals and zeolites are heterogeneous catalysts able to improve bio-oil quality. Transition metals are selected due to their low cost and high activity for upgrading bio-oil. Since heterogeneous catalysts are insoluble in water, they show the advantage for reuse and recycle after liquefaction [3.1].

The low operating temperature, high energy efficiency, low tar yield, stable oil product and an aqueous reaction environment, which does not require energy consuming drying of the biomass are the key parameters that drive the attention of researchers on the liquefaction process [3.12] [3.15]. However, HTL cannot still compete with pyrolysis in terms of yields due to the severe process conditions such as high pressures which require more energy and put tough requirements on process components (e.g. feed pumps). Furthermore, corrosion requires the use of expensive alloys and the external catalysts need constant replacement or regeneration [3.12].

### 3.3 Hydrothermal Carbonization (HTC)

The HTC is a thermochemical process where the biomass is heated up at 160-250°C (lower than pyrolysis temperatures) in a closed system with the presence of water under saturation pressure around (2-10 MPa) which is expected to increase accordingly with temperature during the process [3.16].

Typically, the biomass used in HTC is rich in water allowing to act as a reaction medium, which explains why HTC uses digestate, sewage sludge, wastewater. This characteristic makes the preliminary drying treatment unnecessary in HTC with respect to gasification or pyrolysis, thus saving energy in the overall process. HTC can convert this type of biomass into slurry and gases (mainly CO<sub>2</sub> and CH<sub>4</sub>, H<sub>2</sub>, CO). The slurry is in turn separated in its solid fraction named hydro-char and liquid fraction (oil and water) called aqueous HTC liquid or process water (PW). Optionally, the process water could be redirected toward the digester to increment the biogas production in the overall water waste treatment process. However, if the water contains phenols as well as ammonia, it must be fed only in small quantities. In fact, phenol is a well-known disinfectant, and it would inhibit all enzymes in AD if in large quantities [3.17].

Generally, the mass balance of the HTC process is composed of 45-70wt% of hydro-char, 5-30wt% of process water and 5-25wt% of gas [3.16].

It has been estimated that hydro-char has higher content of carbon than that obtained from pyrolysis and gasification [3.18].

Frequently HTC is integrated with an anaerobic digestion (AD) plant, since it can improve the sludge dewatering, its sanitization and stabilization and consequently reduce the sludge volume.

The HTC reactions are hydrolysis, dehydration, decarboxylation, condensation, polymerization and aromatization, occurring both in sequence and parallel [3.19]. Due to its lower activation energy, hydrolysis is the first reaction and it degrades the biomass in monomers and oligomers [3.20]. The dehydration implies the release of water in the reaction medium, thus reducing the hydroxyl groups (-OH) and its H/C and O/C ratios. The decarboxylation means the removal of carboxyl (COOH) and carbonyl groups (C = O), producing more gases from release of CO<sub>2</sub> and CO [3.21]. During the condensation and polymerization, small molecules combine, thus forming larger molecules and releasing water. Finally,

aromatization determines aromatic polymeric structures which lead to hydro-char formation [3.22].

Since hydro-char is the major product from HTC, several studies have been reported in literature regarding its physicochemical properties as function of temperature, residence time, type of feedstock.

Regarding the feedstock type, HTC can process a wide range of digestate whose properties can affect char properties. For example, higher inorganics content in digestate leads to a lower H/C molar ratio than other biomasses, while O/C ratio depends on volatiles content present in the feedstock as reported in [3.16].

By increasing the temperature, hydro-char yield decreases as occurs for char in pyrolysis. In fact, the higher temperature leads to a major thermal decomposition, allowing volatiles to leave the matter. If mild temperatures and short residence time are adopted, the hydrochar yield increases [3.16].

Phosphorus, nitrogen are strongly concentrated in char from digestate rather than from biomasses, this result suggests strategies to recover them and create a high quality N/P fertilizer [3.16]. However, ash concentration in the hydro-char can lead to slagging and fouling issues, limiting its application in combustion [3.23],[3.24].

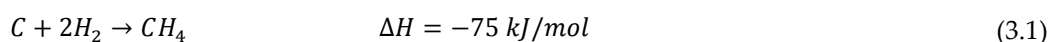
### **3.4 The gasification**

Gasification is the conversion of a solid or a liquid biomass to a gaseous energy carrier named syngas or synthetic gas composed of H<sub>2</sub>, CO, CO<sub>2</sub>, and CH<sub>4</sub>, whose heating value can be useable in many applications. In fact, gas products deriving from gasification have greater versatility than thermal processes. Syngas can be burned in kilns and furnaces in place of conventional fuels, or in a prime mover, or in a gas turbine for power generation, or even used for biofuels production. Other by-products from gasification are composed by a solid phase known as char and a condensable phase named tar [3.25]. This conversion requires a source of heat from an external source, meaning that the conversion is endothermic, but self-sustaining once started. Furthermore, the addition of an oxidant is needed. This latter can be oxygen, air, steam or CO<sub>2</sub>, at levels below the stoichiometric amount required for full conversion of the carbon contained in the feedstock as typically occurs in combustion, thus limiting the NO<sub>x</sub> formation and other emissions [3.25]. The composition and yield of syngas is highly dependent on the type of material, gasifying agent, and temperature [3.26].

Gasification can be described through several stages: (i) drying; (ii) pyrolysis; (iii) combustion/oxidation and gasification; and finally, (iv) char reduction and secondary reactions like water gas shift, steam/CO<sub>2</sub> reforming of hydrocarbons [3.26], [3.27], [3.28]. An energy change characterizes each of these stages, which are mainly endothermic, yet there is data demonstrating pyrolysis can also be exothermic under certain conditions [3.23], [3.1].

In the gasification, the operating temperatures vary from 700 to 1700°C [3.28] according to the stage, the type of biomass and the oxidising agent.

The drying stage (T < 150-200°C [3.25]) consists of the evaporation of the residual moisture contained in the initial feedstock. As drying is an endothermic process, the heat required for evaporation is proportional to the moisture content of the feedstock. Therefore, the more moisture content and the higher heat is required, contributing at decreasing the gasifier's temperature and shifting the reaction equilibrium toward higher methane concentration and lower hydrogen content in the product gas [3.25] as illustrated in the following exothermic hydrogen gasification (or hydrogasification) equation:



This is the reason why drying is considered beneficial and sometimes imperative in order to design smaller reactors, and to enable a higher temperature to be achieved more readily.

Anyway, drying is also considered resource-intensive because a drier equipment, adjacent to the gasifier is required, thus increasing the power consumption. In this regard, possible solutions could be the heat recovery from other processes or even a reasonable choice of the initial feedstock with a low moisture content.

The pyrolysis (T= 150-700°C [3.25]) represents the second stage of the gasification and it is the endothermic decomposition of the solid organic matter into gaseous compounds (syngas) and solid residues mainly composed of carbon (char).

During the pyrolysis stage, the fuel particle is locally reducing, and certain elements volatilize to the gas phase. As temperature increases, a further devolatilization of inorganics may also occur and the chemical environment changes during char oxidation [3.27].

Afterwards, part of volatiles released during pyrolysis may condense on colder surfaces and form liquid products called tars (which must be cracked either by

thermal or catalytic cracking), whereas the permanent gaseous species remain in gas phase as CO<sub>2</sub>, H<sub>2</sub>, CO, CH<sub>4</sub>, and light hydrocarbons.

The condensation occurs in the gas phase, when some elements precipitate homogeneously from the gas and form very fine particles, especially during gas cooling. These solid particles, more commonly ash or bed material, may serve as condensation nuclei having high hygroscopic properties able to absorb a sufficiently high number of molecules, thus leading to the condensation. Many inorganics, like alkalis, can interact chemically with the condensation nuclei on the surface and form a layer of sticky, low melting, “glassy” material that causes agglomeration of the particles, particle fouling of surfaces and even sintering or melting. These phenomena have impacts on the effectiveness of the gasifier, in terms of generation of pressure drop, channelling of gas and oxidant, temperature deviations, defluidization, corrosion of metals and refractories, fouling and plugging of gas coolers [3.27].

At temperatures below 350°C, the main reactions are depolymerisation as well as dehydration, decarbonylation, and decarboxylation releasing water, carbon monoxide, and carbon dioxide, respectively [3.30]. At temperatures above 350°C, more products that are aromatic are released [3.25].

Theoretically, pyrolysis is a complex process consisting of primary and secondary reactions involving both endothermic and exothermic energy changes.

During the primary endothermic reactions, chemical bonds of biomass break releasing volatiles made of permanent and condensable gases (tars) and forming the solid carbonaceous residue (char). During the secondary reactions, a portion of the tar decomposes to form secondary tars and gas and polymerizes to secondary char. Secondary tar decomposition could occur homogeneously in the vapour phase or heterogeneously on the surface of the solid [3.30]. The secondary tar cracking reactions depend on residence time of volatiles at temperatures between 300°C and 700°C. Increasing the residence time of tar within the solid–gas interface leads to tar cracking, release in hydrogen, methane and forming of solid carbon [3.31]. An example of relevant secondary reactions is the formation of aromatic radicals [3.32]. These latter can easily react with aromatic molecules leading to the formation and growth of polycyclic aromatic hydrocarbons (PAHs) [3.33].

The char oxidation and the partial oxidation reactions follow the pyrolysis stage and they are represented as follows:

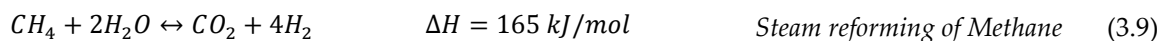
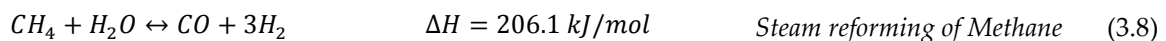
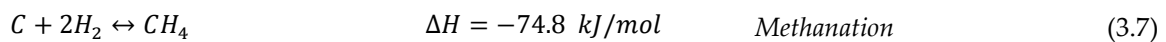
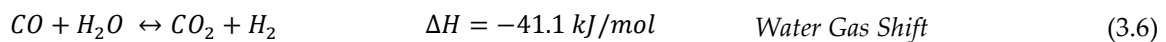
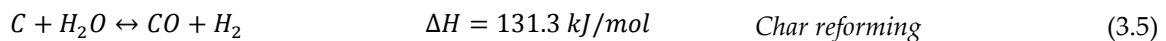
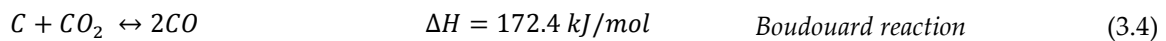


The reactions are exothermic, slow at low temperatures, and provide the energy for further reactions.

When air is used as oxidizing agent, the oxygen is consumed, while the concentration of CO<sub>2</sub> increases proportionally. In fact, oxygen burns a portion of the carbon in the feedstock until all free carbon is exhausted and penetrates the material surface only to a small extent, because O<sub>2</sub> more easily reacts at the surface with the formed carbon monoxide and hydrogen gases [3.25].

The last stage involves several reactions that form the final syngas and the char.

The main reactions are reported below:



In these reactions, water gas shift and methanation are exothermic and occur at low temperatures forming further hydrogen and methane, while the Boudouard reaction and the reforming ones are endothermic, and they take place at higher temperatures. Therefore, the syngas characteristics and char formation can be influenced by varying temperature. In particular, higher temperatures reduce the formation of tars and solid residue at the end of the process, but increase ash sintering and decrease the energy content syngas [3.34].

As temperature increases, methane concentration decreases because endothermic steam reforming reactions take place, thus increasing hydrogen and CO concentration. However, that endothermic steam reforming of methane, which produces CO<sub>2</sub>, is penalised by the increase of temperature since Boudouard reaction is more dominant, changing the equilibrium toward the right and producing more CO as temperature increases [3.25]. Although gasification is a well-experienced and commercialised technology, it has a considerable number of technical issues due to the quality of syngas (which can contain tars), the lack of feedstock flexibility and the type of gasifier as reported in [3.35].

### 3.5 The pyrolysis

Pyrolysis represents the thermochemical decomposition of the biomass under oxygen-free atmosphere. The process is also endothermic between 180 and 270 °C, meaning that it requires a certain amount of heat for the reactions to occur. However, at higher temperatures, pyrolytic reactions result controversial in terms of endothermicity as reported in [3.29]. In fact, decomposition and devolatilization in pyrolysis do not occur in a single step and primary and secondary reactions can occur.

Primary decomposition reactions are highly endothermic, whereas secondary reactions are exothermic and consist of cracking and/or re-polymerization of primary volatile compounds, if sufficient vapour residence times are allowed. This results in the production of additional char (i.e. secondary char) and non-condensable gases (syngas) at the expense of volatiles in the vapour phase. Furthermore, it is likely that primary char (the solid carbonaceous product resulting from primary reactions) catalyzes the secondary cracking reactions, yielding secondary char [3.29].

The temperature of pyrolysis is typically ranging between 300°C and 800°C, significantly lower than that of the gasification process (i.e. 800-1000°C), where oxygen, steam or air are used as a gasifying agents to enhance the combustion reactions. These temperature values can change accordingly with the physio-chemical properties of biomass to pyrolyze or gasify, since temperature of different volatiles can change.

The pyrolysis can take place singularly or in combination with other processes or even as a consequent step of another process. For example, in this latter case, pyrolysis follows the drying phase of biomass (100-200°C) and precedes the combustion and the gasification reactions during the gasification process.

During the pyrolysis, the degree of decomposition of the biomass depends on the following key parameters:

- Size and shape of the biomass;
- Chemical properties;
- Temperature;
- Pressure;
- Residence time;
- Heating rate;

- Reactor;
- Catalysts

Depending on heating rate, temperature and residence time above-mentioned, pyrolysis is mainly categorised into slow, intermediate, fast and flash. All three categories produce oil, char and syngas as final products, but with different yields. The oil is a liquid fraction containing tar, water and organic low-molecular-weight compounds (aldehydes, acids, ketones, alcohols). The biochar is a carbonaceous high-molecular-weight residue with ash, inert material and metals. Finally, the syngas represents the gaseous fraction with low-medium calorific value, containing CO, CO<sub>2</sub>, H<sub>2</sub>, H<sub>2</sub>O and light hydrocarbons (typically consisting of C1-C4 e.g. CH<sub>4</sub>). The different yields depend on the operating conditions as well as the initial biomass.

In fact, high temperatures lead to an increase of the gaseous phase because of the devolatilization reactions, which mainly occur at the expense of charring reactions at low thermal regimes.

When high temperatures are combined with very short residence time (fast and flash pyrolysis), the pyrolysis enhances the conversion of the biomass mainly in an oil-water mixture which does not phase separate and is viscous like tar. This is due to the rapid heating of the biomass and rapid removal of the condensable vapors (primary volatiles). In this way, further secondary reactions into cracking and re-polymerization are prevented resulting in a low char yield, as only primary char is being formed, and the overall pyrolysis reaction is highly endothermic [3.29].

On the contrary, low temperature and high residence (slow pyrolysis) time encourage the char formation, thereby favoring secondary cracking into additional char and non-condensable gases. Slow pyrolysis is overall an exothermic reaction [3.29]. When both mild temperatures and moderate solids residence time (intermediate pyrolysis) characterize the process, the oil is produced with lower yields and the char yields can increase depending on the feedstock. All fuels produced during the intermediate pyrolysis are usable at the end unlike fast pyrolysis.

For the sake of clarity, **Table 3.1** indicates conditions and yields for each type of pyrolytic process.



**Table 3.1** Operating conditions and products yields of different types of pyrolysis [3.36]

Type	Conditions	Char	Oil	Syngas
Slow	~300 °C, long solid residence time (hrs.-days)	35%	30%	35%
Intermediate	~400 °C, moderate solid residence time (min)	25%	50%	25%
Fast	~500 °C, short solid residence time (< 2s)	12%	75%	13%
Flash	~600 °C, short solid residence time (< 1s)	7%	83%	10%

### 3.5.1 The influence of key parameters in the pyrolysis

Several studies on pyrolysis using different biomasses and operating conditions demonstrated their influence on the conversion process. In this paragraph, each key parameter, already mentioned in section 3.5, is discussed in order to understand how the pyrolytic process occurs and the biomass decomposes.

#### 3.5.1.1 Size and shape of biomass

Size and shape of feedstocks affects the process in terms of heat- and mass-transfer, and consequently they influence the properties of the products.

The bigger the feed particle, the more difficult the diffusion will be in the volatilization process. During this phase, the volatile matter goes through a longer path to come out and it could react with the biomass, thus contributing to the re-polymerization and forming more char (mass-transfer effect [m/s]). In this case, more heat should be required to reach the activation energy for larger particles due to poor heat-transfer coefficient [W/m<sup>2</sup>K], which causes lower liquid yield [3.37]. Therefore, smaller size of particles is preferred in order to achieve an easier and more uniform heating. The pyrolysis of large pieces of biomass requires longer conversion times compared to the pyrolysis of a feedstock in the form of a powder [3.29]. Particle sizes also influence the choice of the type of reactor used. Fluidized bed favours powders and fine particles whereas auger reactors require compact uniform pellets/chips or granular.

Finally, size and shape have also a practical meaning when they are used in a conversion process. In fact, blockages due to coarser materials could occur in

the feeding systems, especially if these latter work by gravity without any support of electromechanical devices.

### 3.5.1.2 Chemical properties

Chemical properties are associated with characterization parameters of the biomass and computed in the proximate and ultimate analyses.

The proximate analysis consists of moisture content, ash content, volatile matter, fixed carbon and the higher heating value, while the ultimate analysis defines the carbon, hydrogen, nitrogen, sulphur, and oxygen contents.

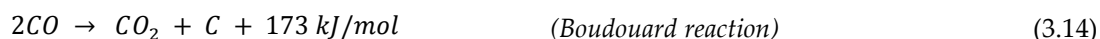
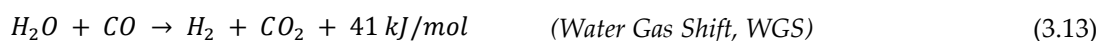
The proximate analysis suggests if the feedstocks is usable as fuel in the conversion process.

The moisture content is typically present in the biomass, and it is required to be removed using drying temperatures of 105 °C, preferably using waste heat, if available at the pyrolysis site. In this way, the heat of volatilization (latent heat) has not to be considered in the energy balance of the pyrolysis. Furthermore, the higher moisture content, the more diluted the pyrolysis vapors and gases will be with water vapour, hence diminishing the calorific value of these pyrolysis gases and vapors [3.29]. Water in the feedstock may also affect the chemical reactions and their kinetics during carbonization. It has been claimed that water could act as a catalyst in slow pyrolysis resulting in higher char yields. Indeed, steam can act as an oxidizing agent, similar to the use of steam in gasification or in the production of activated carbon, although the reaction rates are significantly lower given the lower temperatures used in carbonization (~400-500 °C) versus gasification/activation (900 °C and above). Consequently, the mild oxidizing action of water aids in the internal surface development of the char [3.29].

To some extent, the process becomes like a steam reforming occurring when steam is added to produce more hydrogen in the reactor. The following reactions can take place, assuming methane as main hydrocarbon present in the reactor:



Further reactions can also occur as reported below:



The WGS reaction allows carbon monoxide to react with water in order to get more hydrogen, the reaction is enhanced at lower temperatures (exothermic reaction with a reaction enthalpy of -41 kJ/mol).

The Boudouard reaction can lead to Carbon Deposition (CD) in the catalyst layer. Two moles of carbon monoxide splitted in one mole of CO<sub>2</sub> and one mole of atomic C. Both the reactions are strongly dependent on both the operating temperature and the steam-carbon ratio. Lower values of steam-carbon ratio or temperature can lead to carbon deposition phenomena.

The C-H-O ternary diagram, shown in **Figure 3.3**, can potentially foresee the carbon deposition phenomenon.

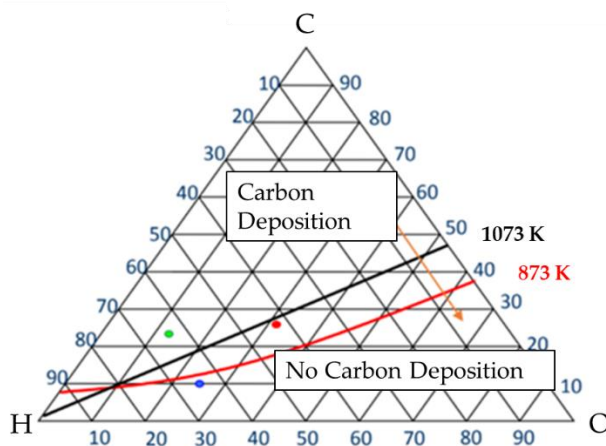


**Figure 3.3** C-H-O ternary diagram

In the diagram, there are three different feedstocks compositions characterized by three different points (red, blue and green) and two possible temperatures. Although the blue and green composition are not strongly influenced by temperatures since both of them belong to a specific area of the diagram, the temperature for the red composition is strongly decisive for the carbon deposition. Therefore, when the biomass loses its water content during the process, its composition changes in the ternary diagram moving toward the carbon deposition area.

Precipitated carbon can be classified into three types as illustrated in **Table 3.2**. The whisker carbons are very common at relatively lower temperature and

they deposit on the surface of the Ni catalyst due to the increase of diffusion of C in the fuel.

Encapsulating polymers form at temperatures lower or equal to 500°C but this formation gradually deactivates.

In fact, as temperature increases pyrolytic carbon occurs. This is generated by thermal decomposition of hydrocarbons as a feedstock. For this reason, this phenomenon occurs in a temperature range of 600°C or more.

Precipitated carbon can be classified into three types as illustrated in **Table 3.2**.

**Table 3.2** Three types of carbon decomposition in hydrogen production reactions [3.38]

	<b>Whisker Carbon</b>	<b>Encapsulating Polymers</b>	<b>Pyrolytic Carbon</b>
<b>Formation</b>	Diffusion of C through Ni-crystal: nucleation and whisker growth with Ni crystal at top	Slow polymerization of hydrocarbon radicals on Ni-surface into encapsulating film	Thermal cracking of hydrocarbon: deposition of C-precursors on catalysts
<b>Temperature</b>	>300°C	<500°C	>600°C
<b>Phenomenon</b>	Deactivation breakdown of catalyst and increasing DP	Gradual deactivation	Encapsulation of catalyst particle: deactivation and increasing DP
<b>Critical parameters</b>	Low steam/carbon Low activity Aromatic feed in feedstock Abrupt temperature change	Low temperature Low steam/carbon Low H <sub>2</sub> /carbon in feedstock Aromatic reed in feedstock	High temperature High void fraction Low steam/carbon high-pressure deactivation

When the biomass is heated up, the chemical bonds start breaking down, and some compounds are released in gaseous form from the solid matrix. This phase is called volatilization and the gaseous compounds are volatiles.

Volatiles are the main component of biomass, hence representing about the 70-90% in weight. The volatilization temperatures depend on the type of biomass, but they can start forming rapidly at about 200-250 °C.

Volatiles are mainly composed by combustible gases e.g. CO, H<sub>2</sub>, C<sub>x</sub>H<sub>y</sub>, CO<sub>2</sub>, H<sub>2</sub>O (g), and condensable organic fraction named tar. Tar are bigger molecules which are gaseous at high temperatures, but they can condensate and stick to the colder parts of the plant thus blocking pipes, heat exchangers, etc.

The concentration of the various species depends on the temperature in the reactor. In the gasification process, the high content of volatiles leads to the combustion, developing a long flame. The reactor's volume must be properly designed in order to accommodate it. Therefore, this aspect must be considered in the design of the reactor. The volatile matter is the weight difference between the dry and ash-free material and the fixed carbon.

The fixed carbon is defined as the amount of organic (ash-free) material that remains after pyrolysis up to a certain threshold temperature [3.29]. It gives information of the amount of char formation in the thermochemical process after the volatiles matter drives off. The objective of using such carbonaceous substance is to exploit its appreciable influence in terms of catalytic action capacity.

Biomass feedstocks contain varying amounts of inorganic material, including alkali and heavy metals as well as chlorine, phosphorus, and sulphur that form collectively ash. Its content in biomass is determined through proximate analysis by weighing the residue after heating a feedstock sample in an oxidative environment (i.e., air) in a muffle furnace or in the Thermogravimetric analysis (TGA). The ash content value depends on both the feedstock type and the concentration of inorganics due to the heterogeneous distribution within the biomass. Although chlorine and sulphur lead to increased corrosion, potentially limiting the use of the char, high level of ash in the feedstocks positively affects properties of char. In fact, most noticeably alkaline and earth alkaline metals, exhibit catalytic activity in pyrolysis favoring higher yields of non-condensable gases and char [3.29].

Finally, the HHV is determined using the unified correlation for fuels developed by Channiwala et al. [3.39], starting from carbon, hydrogen, sulphur, oxygen, nitrogen and ash weight fraction, respectively:

$$HHV \left[ \frac{MJ}{kg} \right] = 0.341 (C) + 1.1783 (H) + 0.1005 (S) - 0.1034 (O) - 0.0151 (N) - 0.0211 (A) \quad (3.15)$$

Channiwala equation calculates a good estimation of HHV. However, the best way is by actual determination through the use of bomb calorimetry.

The amount of carbon, hydrogen, sulphur, oxygen, nitrogen derived from the ultimate analysis. They give information about the heating value of feedstocks. As a matter of fact, carbon and hydrogen increase the heating value. Then part of the carbon will be in the volatile matter and part will form the char, while most of the hydrogen will be in the volatile matter. On the contrary, the oxygen reduces the heating value. The presence of both the nitrogen and sulphur is significant in terms of NO<sub>x</sub> and SO<sub>x</sub> pollutants emissions. Finally, the water content can lead to the formation of HCl rather than Cl<sub>2</sub>. If any chlorine was in the biomass, it may cause accelerated corrosion [3.40].

Typically, for fuel applications H/C and O/C ratios are used to measure the degree of aromaticity and maturation [3.29] and are often plotted against each other in a so-called van Krevelen diagram as illustrated in **Figure 3.4**.

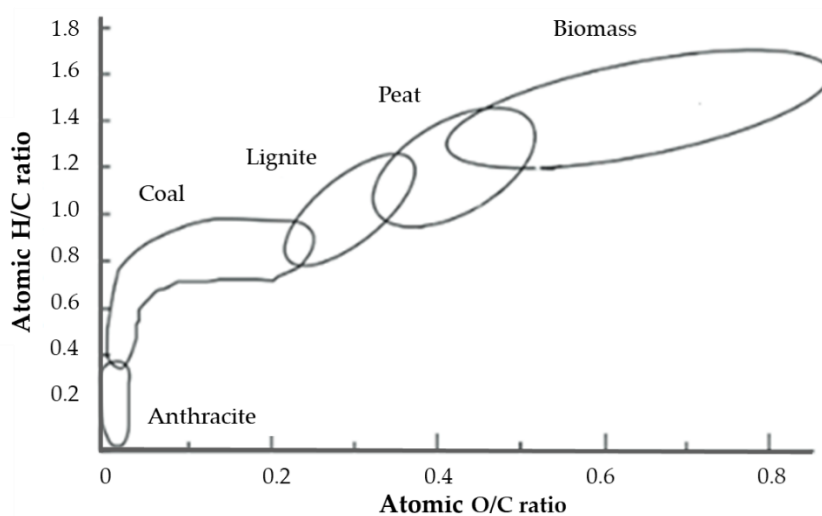


**Figure 3.4** The van Krevelen diagram [3.41]

The higher H/C and O/C ratios, the higher oxygen and hydrogen content will be in the feedstocks, hence increasing both the reactivity of the material and the volatiles released during the pyrolysis.

### 3.5.1.3 Temperature

The pyrolysis takes place over different temperature ranges, as widely mentioned above. At temperature below 300 °C, decomposition results mainly in vapors and non-condensable gases (syngas) including CO, CO<sub>2</sub>, H<sub>2</sub>, CH<sub>4</sub>,

water and low molecular weight oxygenated organic compounds (mainly acetic acid, formic acid, methanol, acetone, and furfural according to the type of biomass) [3.29]. As slow pyrolysis (carbonization) involves temperatures higher than 300 °C, extensive devolatilization happens. At temperatures around 500 °C, peak devolatilization occurs. When temperatures are greater than 500°C, secondary vapor-phase cracking reactions are dominant, hence yielding additional non-condensable gases and secondary char.

If high bio-oil yields are required from the pyrolysis, temperatures are set around 500°C as happens in the fast pyrolysis in order to strike a balance between devolatilization and minimal secondary cracking of vapors. This reasoning is reported in **Figure 3.5**, where char does not have a minimum in yield, perhaps because additional secondary char occurs at higher temperatures is offset by the further devolatilization of primary char.

The net effect is a diminishing char yield versus carbonization temperature [3.29].

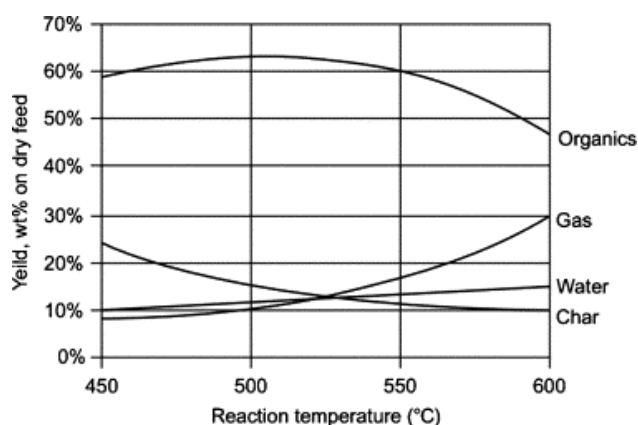


**Figure 3.5** The effect of pyrolysis temperature on the yield of char, non-condensable gases and bio-oil (i.e., water + organics) [3.29].

#### 3.5.1.4 Pressure

Typically, pyrolysis occurs at atmospheric pressure because the increase of pressure would lead the reaction rate of secondary char from vapor-phase reactions to increase accordingly, thus lowering the release of volatiles.

This behaviour is due to the reduction of the pressure gradient across the reacting biomass particle as illustrated in **Figure 3.6**. In fact, the internal pressure generated by devolatilization and responsible for internal mass transport (vapors) would be contrasted by the increasing external pressure,

slowing the internal mass transport [3.29]. Consequently, the residence time of vapors in the particle increases, favouring the secondary char formation.

On the contrary, the char yield decreases while a higher condensable vapours (oil) yield is expected by reducing pressure.

In conclusion, low pressures are typically used in fast pyrolysis but the reduced convective heat transfer (external to particle) should be considered.

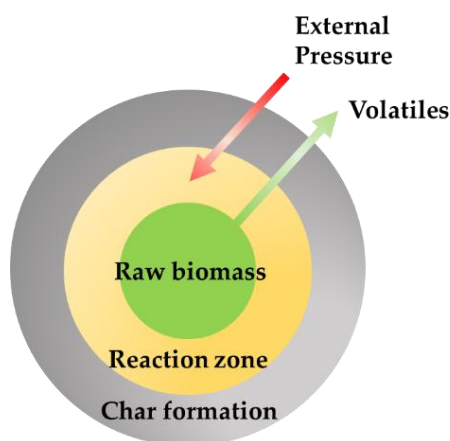


**Figure 3.6** Schematic illustration of devolatilization when the external pressure occurs

#### 3.5.1.5 Residence time

Residence time is considered another key parameter during the pyrolysis. Low vapor residence time is selected together with high heating rate to maximize the yield of bio-oil fraction (e.g. in the fast pyrolysis). As pyrolysis bio-oil is considered a crude liquid biofuel that can be used in stationary heat and power applications or further upgraded to a drop-in transportation biofuel, most biomass pyrolysis research efforts have focused on fast pyrolysis and bio-oil utilization. Temperature as well as residence time during pyrolysis are also determining factors in bio char stability. Bio char stability is correlated to its fixed carbon content: the higher the pyrolysis temperature and the residence time, the higher the fixed carbon content. As already mentioned, pyrolysis is characterized by primary and secondary reactions. These latter comprise cracking and re-polymerization of primary volatiles and they can be predominant if only vapor residence time is sufficient, thereby favoring secondary cracking into additional char and non-condensable gases. Therefore, it influences the extent to which additional secondary vapor-phase reactions



take place. Additionally, as a result of limited heat-transfer, large particles have a slower rate of carbonization and, if the residence time in the reactor is limited, a lower extent of pyrolysis (decomposition and devolatilization) compared to smaller particles. This poses a problem regarding the homogeneity of the char obtained from feedstocks characterized by a wide particle distribution.

### 3.5.1.6 Heating rate

According to heating rate, there are different distributions and yields of the pyrolysis product fractions, being directly linked to the heat transfer process during the pyrolysis. Additionally, heating rate influences the properties of activated carbon together with the temperature [3.29].

Low heating rates, typically involved in the slow pyrolysis, result in the biomass conversion being rate limited by the heat transfer. Furthermore, the slow devolatilization resulting from a slow heating trajectory ensures maximum secondary char formation. Heat transfer has to be effective to avoid that high heat losses cause reduced char yields in the carbonization process where limited amounts of air (or oxygen) are used for partial combustion of the feedstock.

On the contrary, high heating rate allows a fast devolatilization as volatile particles move rapidly from the particle's centre outward, through the pores within the biomass (**Figure 3.7**). In this case, particles have not enough time to make a reactive front within the charred layer, thus evacuating without cracking. This results in a reducing char yield.

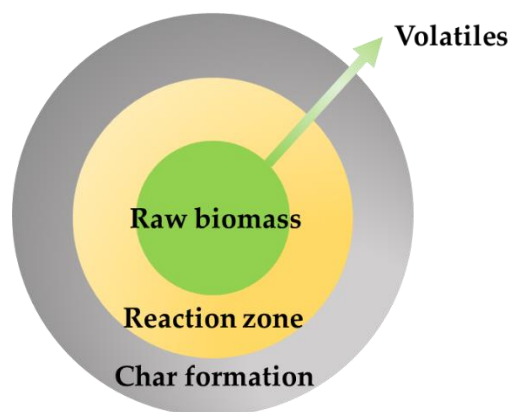


**Figure 3.7** Schematic illustration of devolatilization

### 3.5.1.7 Reactor

The reactor is essential for the success of the feedstock's conversion. Generally, the preferred feedstocks are those with low ash content and homogeneity, which leads to simplified process requirements [3.29].

The criteria to choose the reactor for pyrolysis depend on the following:

- Integration with the heat and energy source;
- Ease to recover valuable by products that can be consumed on-site;
- Flexibility with respect to the feedstocks type and its seasonal variability;
- Allow fine-tuning of process conditions with respect to the desired properties of the char product;
- Compactness to be moved through transportable units where feedstocks are more available.

Technologies that meet the above criteria are pyrolysis reactors based on screw (auger) technology, as well as rotary kilns/retorts.

The biomass, pelleted or chipped or compact chunks, goes through the feeding system, transported in the heated reactor zone by a rotating, helical screw and then, discharged at the opposite end.

The screw reactor is particularly interesting for its use on a small scale. Rotating screw reactors allow the proper control of biomass residence time in the reactor by manipulating the rotational frequency of the electrical engines plugged to the screw in the reactor.

The feeding system can be mechanical or under gravity. In the first case the use of mechanical force can easily move several particles dimensions, while in the second case particles could be cohesive, causing the blockage of the reactor. The morphological characteristics of feedstocks are extremely important for the proper functioning of the reactor. As a matter of fact, reactor must accommodate as many feedstocks as possible from fine powder to lumpy, sticky and fibrous material avoiding to process materials that could foul the inner barrel of the screw reactor [3.29].

### 3.5.1.8 Catalyst

Pyrolysis can be performed in both the absence and the presence of catalysts. Typically, the catalysts improve several parameters such as re-polymerisation

of bio-oil components, high total acid number, high corrosivity, and compatibility with petroleum products and others.

There are different types of catalysts involved in the pyrolysis process. However, it has been demonstrated that char itself acts as a heterogeneous catalyst in pyrolysis, promoting secondary cracking reactions and the formation of secondary char [3.29][3.42].

### **3.6 The reforming and cracking processes**

The reforming process is an endothermic conversion used for the improvement of products. In fact, the molecular structure of the feedstock can be reorganized without significant effects on the molecular weight [3.43]. In the bioenergy sector, the process is commonly used to produce gaseous mixture (syngas) with a higher content of hydrogen from other combustible gases (e.g. methane, ethane and propane or biogas from anaerobic digestion) at higher temperature than pyrolysis. Typical values of reforming temperatures are around 500-800°C. The reforming reactions can be thermal or catalytic.

The thermal reforming occurs at high temperatures and pressures, 500-800°C and 1-70 atm, respectively. It also implies a cracking process of long paraffins to get methane, ethane, propane and olefins and the dehydrogenation and cracking of cycloparaffins to get cyclo-olefins without producing any aromatic compound.

The products of thermal reforming are gases, reformat, and residual oil or small amount of non-volatile residuum, where reformat is meant as a fuel (e.g. gasoline) with a higher-octane number after the reforming process.

The yield and quality of the reformat product is dependent on the temperature. Generally, the higher the reforming temperature, the higher the octane number, but the lower the yield of reformat [3.43].

The catalytic reforming not only converts feedstock in fuel with higher octane numbers, but it also produces aromatics (benzene, toluene, xylene), which are typically presented in the conventional fuels, thus contributing to get better properties from bio-oil [3.43] [3.44]. During the catalytic reforming, the following isomerization, dehydrogenation, dehydrocyclization and hydrocracking can occur [3.43]. Depending on the catalyst, a definite sequence of reactions takes place, involving structural changes in the feedstock. This more modern concept rendered thermal reforming obsolescent [3.43].

The reforming usually follows the gasification and pyrolysis processes to maximize syngas production and reduce the tar rich stream generally produced during the gasification. Tar can be classified as primary, secondary and tertiary. Primary tar compounds are mostly oxygenated compounds deriving from the decomposition of biomass. Then, primary tars react further and form secondary and tertiary tar compounds, which were not in the initial biomass. The secondary tar typically consists of alkylated one-ring and two-ring aromatic compounds (including heterocyclic compounds), whereas tertiary tar consists of aromatic hydrocarbon derivatives such as benzene, naphthalene, and various polycyclic aromatic hydrocarbon derivatives (PAHs, also called polynuclear aromatic compounds, PNAs). Tar constituents are typically classified according to the number of rings in the constituents or by boiling point distribution or physical properties. More generally, tar is defined as aromatic compounds that are higher boiling than benzene, and in addition, an operational definition for tar depending on the end-use application has been used [3.43].

It is expected that catalytic reforming can be a potential future option to remove tars and adjust the H<sub>2</sub>/CO ratio of syngas produced from the gasification and pyrolysis [3.45]. Moreover, the catalytic reforming can remove contaminants in the syngas like phenolic compounds and heavy metals [3.46]. Recently, the development of the pyrolytic route with in-line catalytic reforming is considered promising, since pyrolysis vapours are immediately reformed without any need for syngas conditioning (e.g. TCR) and can be carried out at milder conditions when compared to that required in gasification [3.47].

Generally, fluidised and fixed bed reactors are used during the catalytic pyrolysis.

The reforming processes can vary according to the desired gas exiting the reactor and the operating conditions. Some of them are: (i) steam reforming; (ii) methane reforming, (iii) liquid reforming; (iv) dry reforming; (v) partial oxidation reforming; (vi) autothermal reforming; (vii) hydrogen reforming.

As already mentioned, cracking endothermic reactions can take place during the reforming. This allows larger saturated hydrocarbons (alkanes) to be broken in smaller hydrocarbons (alkanes and alkenes), some of which are unsaturated (alkenes). The reason why such conversion is typically achieved is that smaller hydrocarbons are more useful as fuels than larger ones. Actually, alkenes are more reactive than alkanes because they are unsaturated, meaning that they have a double bond between

carbons (C=C), while alkanes have a single bond (C-C), thus allowing alkenes to take part in reactions that alkanes cannot.

This result also influences the physiochemical properties of the fuel like its density, viscosity, composition, HHV, octane number, cetane number, boiling point, freezing point, cloud point, pour point, flash point, auto ignition temperature etc.

As in reforming, there are two methods that can be used for cracking: the catalytic cracking with temperature around 550°C and a catalyst (e.g. zeolite) and the thermal cracking which uses higher temperature (over 800°C) without catalyst [3.48].

### 3.7 The Thermo-Catalytic Reforming (TCR) technology

The thermo-catalytic reforming (TCR®) is a patented thermochemical conversion technology [3.49], that combines the intermediate pyrolysis and the catalytic cracking/reforming. The process can convert second-generation biomass into hydrogen-rich syngas, high-quality oil and char without volatiles with yields based on the type of biomass and operating conditions. A schematic diagram of TCR is illustrated in **Figure 3.8**. It shows the feeding system in (1), a rotary kiln including a multi-zone screw reactor in (2) to enable the material transport and to control the residence time for the intermediate pyrolysis [3.50] and finally a fixed bed post-reformer in (3) where solids are stored as soon as they leave the pyrolysis reactor.

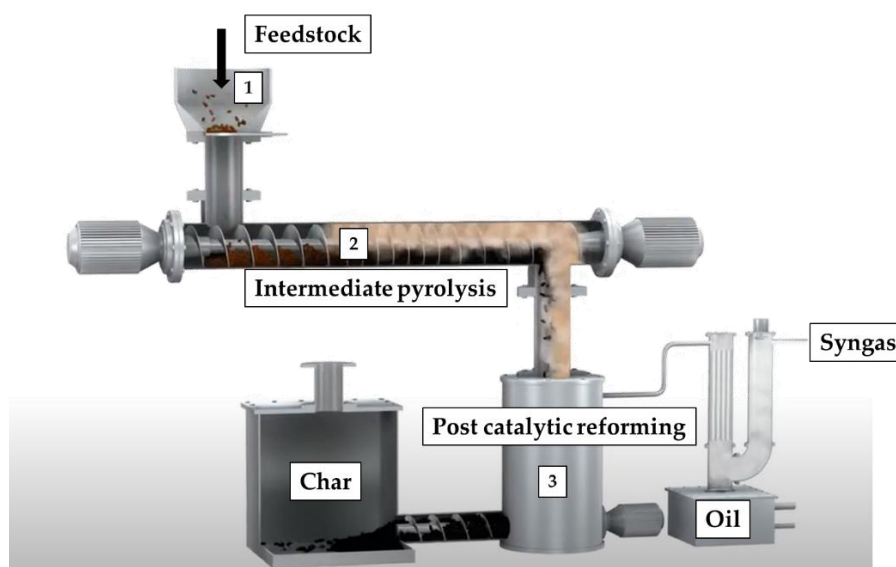


**Figure 3.8** Schematic diagram of Thermo-Catalytic Reforming plant

The residence time is controlled through the feeding rate of the inlet screw. Higher feeding rates lead to shorter residence times in order to process a constant mass flow

rate, while the intermediate pyrolysis operates at a standard pressure and temperatures up to 450-500°C. The cracking/reforming takes place at higher temperatures than pyrolysis. The most promising reforming temperatures range between 500–800 °C. Before each experiment, the plant is flushed with nitrogen for inertization and external heating bands or heating jackets to ensure steadily increasing temperatures during the process [3.50]. Unlike pure pyrolysis, TCR advantage is that the design of the reactor is of such that it is possible to carefully control solid and vapor residence times to achieve desired outputs.

It was proved that the reforming step is essential for high product quality [3.50], [3.51]. For example, in the case of anaerobic digestion waste, sugarcane bagasse and oat hulls [3.51], higher reforming temperatures led carbon content to increase and oxygen to decrease, thus showing a higher rate of carbonization and a good removal of oxygenated compounds. Moreover, due to further reactions during the post-reforming, the total acid number (TAN) was also found reduced [3.51][3.52].

High quality bio-oil is not the only product deriving from TCR, the char is another one and it acts either as heat carrier for the upgrading pyrolysis oil or as a promoter for hydrogen formation. In this way, larger amounts of H<sub>2</sub>, CH<sub>4</sub>, and CO are also produced and less tar is generated thanks to lower temperatures than those used in the steam gasification, which would cause high tar content, and further more energy intensive tar removal steps [3.50]. This latter aspect and the advantage to optimize separately the operating conditions for both pyrolysis and reforming represents a novelty in the general overview of thermochemical technologies, thus allowing high feedstock flexibility, high scalability, and high fuel quality in the TCR.

The reforming temperature affects not only the quality of bio-oil but also the yield of both gas and liquid products. The higher reforming temperatures, the higher gas yield and the lower liquid yield [3.50] [3.52].

There exist several TCR plants according to their size due to the capacity of processing feedstocks. These plants are presented in **Table 3.3**:

**Table 3.3** TCR plants currently in operation

Name	Capacity [kg/h]	Status	Location
TCR2	2	Lab-scale	Birmingham, FHNW (Switzerland) [3.53]
TCR30	30	Demo-scale	Birmingham, Sulzbach-Rosenberg [3.54]
TCR300	300	Large Demo-scale	Sulzbach-Rosenberg [3.55]

TCR500	500	Large Demo-scale	Hohenburg [3.54], Berkley
TCR3000	3000	Design & Engineering phase	-

The first recommendation could be the use of Lab-scale TCR2 or Demo-scale TCR30 to test the suitability of new feedstocks and later process them in higher capacity plants (i.e. TCR300 or TCR500).

One of the main differences between the above-mentioned plants is how to supply heat during the process. While TCR2 and TCR30 use external electrical heating mantles to increase and keep temperature constant, TCR300 and TCR500 are thermally heated by combustion chambers, as it is the most energy efficient way to bring in the heat. For this reason, a second recommendation would be the use of lower size plants to process feedstock with moisture content up to 30 wt%. On the contrary, when combustion systems are present in situ, feedstocks can have moisture content over 50 wt% as the plant provides heat to dry them [3.53].

The heat supply via combustion chambers makes the plant structure bigger and more complex, therefore more expensive and with longer heating time. Consequently, the third recommendation would be that only continuous mode experiments are reasonable from the economic point of view.

Over 50 different feedstocks have been tested so far, including digestate, paper sludge, sewage sludge, wood chips, pre-conditioned agriculture olive residues, evergreen oak and vine shoots, or even de-inking sludge and municipal solid waste, sugarcane bagasse, oat hulls, wheat husks [3.50], [3.52], [3.56] and many of new feedstocks could be tested in future. The goal is to produce sufficient amount of oil that can be upgraded later through hydrotreatment to get drop-in fuel or even hydrogen that can be used as either chemical or fuel in the transport sector. These potential products make TCR technology very interesting.

According to the mass balances of several feedstocks (i.e. digestate, sewage sludge, sugarcane bagasse and oat hulls), the ranges of product yields are illustrated in the following **Table 3.4**:

**Table 3.4** TCR Product yields of different feedstocks

	Char	Aqueous phase	Bio-oil	Syngas
<b>Product yield wt%</b>	20.9 - 50	19.5 - 34.4	2.7 - 11	25.4 - 50.4

From the energy point of view, it was found that sewage sludge gives the best oil in terms of high calorific value (HHV), lower oxygenated compounds and lower TAN. One of the reasons could be that sewage sludge is free of lignocellulosic compounds, thus exhibiting a lower density than oil from digestate or woody material [3.50]. Furthermore, ash in sewage sludge is also active as a reforming catalyst, thus cracking the heavy organic compounds.

Even though bio-oil from sewage sludge has a very high HHV (35.6 MJ/kg [3.50]) compared to other bio-oils deriving from TCR, the mass balance accounts it only for 6 wt%, while syngas and char are 25.4 and 48.5 wt% of the initial feedstock, respectively [3.57].

As expected, high char yields were observed for feedstock with a high ash content like sewage sludge and paper sludge [3.58]. In fact, the ash content of the feedstock was demonstrated to be correlated with the char yield according to other studies [3.58][3.59][3.60].

Regarding syngas yields, lignocellulosic materials like wood chips and laminate (which is analysed in the present thesis) were found to be the highest laminate with value greater than 50% [3.58].

In conclusion, what makes TCR preferable to conventional thermochemical technology are the following:

- Lower formation of tar;
- High quality oil and high yield of syngas;
- Higher flexibility in feedstocks;
- Modularity;
- Ability to optimize each reactor singularly.

The novelty of TCR technology is the utilisation of char formed during its process as catalyst for the upgrading pyrolysis liquids and the advantage to optimize separately the operating conditions for both pyrolysis and reforming. This allows having high feedstock flexibility, high scalability, and high fuel quality in the TCR.

As will be shown next, the temperatures used in the process are lower than those used in the steam gasification, which leads to high tar content, and more energy intensive tar removal steps.



### 3.8 The hydrotreatment upgrading

The oil deriving from thermochemical processing (pyrolysis, TCR and HTL) of wastes and second-generation biomass is recommended as suitable for internal combustion engines only as blends with other fuels, because of its physiochemical properties, which varies significantly from conventional fossil fuels. Actually, its higher viscosity, poor volatility, and low cetane number, resulting from the large molecular mass and chemical structure, can determine incomplete combustion and smoke [3.61].

To comply with product specifications in fuels (e.g. density, viscosity, stability, cetane number, colour, freeze point, TAN, water, oxygen, sulphur content, HHV) and to meet environmental legislations, the hydrotreatment of bio-oil is required.

The hydrotreatment takes place in a reactor under proper conditions of temperature and pressure and it consists of the dual effect of the activated catalyst together with the hydrogen source, necessary to achieve the removal of specific heteroatoms or contaminants and to produce oil as a drop-in fuel. Typically, temperatures and pressures range between 200-500 °C and 3-30 MPa, respectively and the catalyst is made of metal or metal/support [3.62].

According to the heteroatom or contaminant, there are different processes for the hydrotreatment:

- (i) *Hydrodeoxygenation (removal of oxygen and oxygenated compounds);*
- (ii) *Hydrodesulfurization (removal of sulphur);*
- (iii) *Hydrodenitrogenation (removal of nitrogen);*
- (iv) *Hydrodemetalation (removal of metal e.g., Ni and V);*
- (v) *Hydrogenation (removal of hydrogen);*
- (vi) *Hydrogenolysis (removal of C-C and C-O);*
- (vii) *Hydrocracking (removal of contaminants and heavy hydrocarbons C<sub>x</sub>H<sub>y</sub>);*
- (viii) *Dehydration (removal of water);*
- (ix) *Decarboxylation (removal of carboxyl group -COOH)*
- (x) *Decarbonylation (removal of carbonyl group C=O)*

For sake of clarity, some of them are also illustrated in **Figure 3.9**.

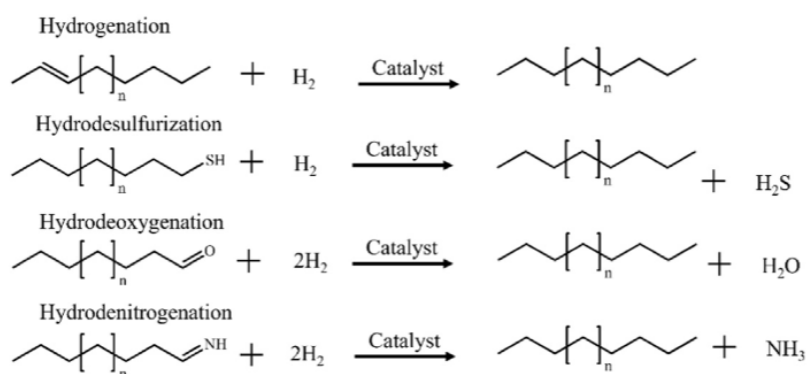


**Figure 3.9** Chemical reactions for hydrotreatment [3.63]

There are different parameters that influence the bio-oil upgrading process and its resulting composition as a fuel. They are listed as follows:

- Initial feedstock;
- Operating conditions (temperature, pressure, reaction time, LHSV (Liquid Hourly Space Velocity), H<sub>2</sub>/oil ratio);
- Type of catalyst;

The physical and chemical structure of the initial feedstock is strongly interrelated with the quality of bio-oil produced downstream of the thermochemical process.

If the biomass had high level of oxygen upstream, typically due to the water content or to organic compounds, it is expected that the resulting bio-oil should be deoxygenated by removing oxygen which limits the calorific value of the final biofuel (**Channiwala equation 3.15**) [3.64]. In this case, the proper process would be the hydrodeoxygenation or HDO. On the contrary, other materials, for example waste tyres could be rich in sulphur, as it is used as an additive during the process of vulcanisation, thus leading to the hydrodesulfurization process to remove it from the raw bio-oil deriving from the previous thermochemical processes.

The upgrading reactions proceed simultaneously through both thermal and catalytic pathways, therefore, the optimal setting of the operating conditions as well as the choice of the catalyst for a specific feedstock, are crucial parameters to get oil without undesired compounds and/or contaminants. As illustrated in [3.64] and [3.65], according to the raw material, different conditions of temperature, pressure, residence time, LHSV, H<sub>2</sub>/oil and catalysts were used in literature aiming at optimizing the biofuels yield as well as their quality as fuels. These results show how the hydrotreatment does not imply a unique method, but it is the achievement of different

tests, by varying multiple parameters. Therefore, the hydrotreatment can follow several experimental methodologies. A typical procedure could be:

1. Activation of the catalysts;
2. Stabilization of the oil;
3. Hydrodeoxygenation.

Before the removal of heteroatoms, the sulfiding of the catalyst is necessary to make it active and stable. This stage is typically accomplished in a reactor by letting the metal oxides of the catalyst react with hydrogen sulfide (H<sub>2</sub>S) in the presence of hydrogen under certain conditions of pressure, temperature and reaction time. In this way, the sulphur binds to metal, while hydrogen and oxygen form water as illustrated approximately in the following equation (1):



A typical method, used to provide the optimum H<sub>2</sub>S concentration in the sulfiding stage, is to utilize liquid sulfiding agents. Common examples are carbon disulfide, dimethyl sulfide, and dimethyl disulphide [3.64]. Sometimes, the catalyst can be already presulfided [3.64]. In this case, the sulfiding phase is skipped and consecutively upgrading time will be saved. This is considered an advantage, especially in the refining industry where time savings improve the plants productivity.

The temperature plays an important role in both the stabilization step and the HDO as it converts oxygenated compound into hydrocarbons, thus decreasing oxygen and increasing carbon and hydrogen contents in the oil.

In the stabilization step, the optimal values of temperature and pressure are demonstrated to be around 100-300°C and 29-290 bar, respectively with time intervals between 30 minutes up to 4 hours in the presence of a catalyst. This step is necessary to convert carboxyl and carbonyl functional groups to alcohol and to get good oil yields (17-92%) [3.62].

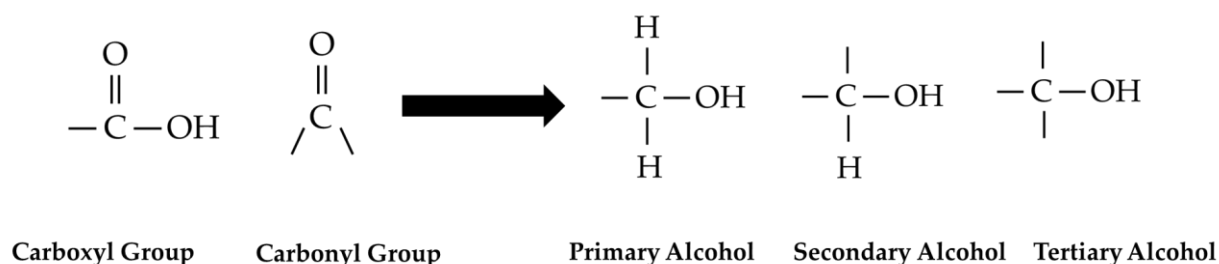


**Figure 3.10** Illustration of the conversion of carboxyl and carbonyl group in Alcohol

After the stabilisation, the oil still has high oxygen content, that is the reason why HDO is required later. During the hydrodeoxygenation, temperatures are higher. They are around 350-400°C to allow the cracking of the larger molecules [3.62].

It was observed that the higher temperature (between 240-360°C), the better oil in terms of lower acid number (TAN) and O/C ratio, and higher heating value (HHV) and H/C ratio [3.62]. However, the increase of temperature also enhances the coke formation on the catalyst's surface during the hydrotreatment, due to aromatization and polymerization reactions, thus deactivating the active sites of the catalyst and blocking the reactor. If the temperature is even more increasing (between 375-400°C), the lowest oxygen and the highest carbon contents can be obtained, but for temperature greater than 450°C, oxygen content can increase while carbon content decreases again, because the catalyst is less active for the coke deposition.

The hydrogen pressure is another important operating parameter in the hydrotreatment process. In the HDO, high pressure leads to higher solubility of hydrogen in the bio-oil and its higher proximity to the catalyst surface, thus increasing the reaction rate and reducing the coke formation of the catalyst [3.64]. Indeed, the higher pressure (around 8 MPa) and the stronger deoxygenation activity (or hydrogenation of the organic compounds) that converts organic compounds of the raw bio-oil to gasoline. On the contrary, a lower hydrogen pressure (around 2 MPa) could lead to a major condensation, thus increasing the heavy products in the oil.

The hydrogen pressure has also effects on different bio-oil properties. As reported in [3.66], the higher hydrogen pressure and the lower density, TAN (acidity), water content and viscosity. In line with effects of temperature on the hydrotreatment process, the pressure can also enhance condensation reactions with production of heavy compounds when it is lower. Finally, high pressures are also essential to avoid evaporation of water that can be separated later [3.63].

Regarding LHSV, it represents the rate at which the bio-oil is fed into continuous batch reactor where the hydrotreatment takes place and it is typically around 0.2-8 h<sup>-1</sup> [3.67]. It is considered an important parameter for the regulation of the catalyst effectiveness and catalyst life expectancy [3.68]. Furthermore, according to [3.62], low LHSV produces less coke and increases the hydrogen active sites, thus favouring hydrogenation and hydrocracking reactions that, in turn, produce less heavy products.

The H<sub>2</sub>/oil ratio is another operating parameter in the hydrotreatment that has a proper effect on hydrogenation and cracking reaction efficiency, even if the optimal ratio is different according to the heteroatom to be removed [3.68]. If the hydrotreatment was combined downstream with TCR, then the hydrogen would be green, as it would be derived from the process itself and not from external sources such as methane reforming or electrolysis of water.

The choice of the catalysts is critical to avoid the hydrogenation of aromatics in the bio-oil, which would lead to higher hydrogen consumption and even lower octane number of the fuel [3.64].

The catalysts used for HDO can be:

- Metal sulphides (e.g. MoS<sub>2</sub>, Ni–MoS<sub>2</sub>, and Co–MoS<sub>2</sub>) with support;
- Noble metals-based catalyst (e.g. Ru, Rh, Pd, Pt, Re) with support;
- Transition metal-based catalysts (e.g. Cu, Fe, Mo, Co and Ni) with or without support [3.62].

The most used supports for these catalysts are alumina-silica, activated carbon, titania (rutile), and zirconia (monoclinic form) [3.67].

The choice of the catalyst is made on its capacity to improve the conversion of the bio-oil compounds and enhance the selectivity on desired products.

Eventually, noble metals are particularly suitable for HDO, but they are too expensive and consume more hydrogen than transition metal-based catalyst [3.62].

Instead, metal sulphide with the support of alumina (Al<sub>2</sub>O<sub>3</sub>) are widely used, as the presence of sulphur keeps the catalyst active and enhance the deoxygenation reactions, while the alumina catalyses deoxygenation reactions like dehydration, decarboxylation, decarbonylation and convert acids, aldehydes, ketones into hydrocarbons with lower acidity [3.69]. In this regard, the oil stabilization phase could also be overridden, since alumina can convert carbonyl and carboxyl group into hydrocarbons,

Molybdenum (Mo) and tungsten (W) in the catalysts are usually involved in the oxygen removal due to their resistance to the deactivation by oxygen, acids and alkali [3.67]. Furthermore, hydrogen is reactive on Co, Ni, Ru, Rh, Pd, Os, Ir, Pt, Sc, Ti, V, Y, Zr, Nb, Mo, La, Hf, Ta, W, Cr, Mn, Fe, Tc, Re, and, in order to promote an efficient adsorption of hydrogen at lower temperature, the catalyst can have a second metal [3.67]. For example, when CoMo and NiMo sulphided catalysts are used, the

hydrogenation reactions of different organic compounds occur at different temperatures as illustrated in **Figure 3.11**.

Generally, Co and Ni work as promoter in the catalyst and they are supported by alumina for conventional hydrotreatment (HDS, HDO and HDN) and silica-alumina and zeolite for hydrocracking [3.70]. Silica-alumina is preferred to maximize the middle distillates (jet fuel, kerosene, diesel fuel, light fuel oil) and zeolite also to produce gasoline [3.70].

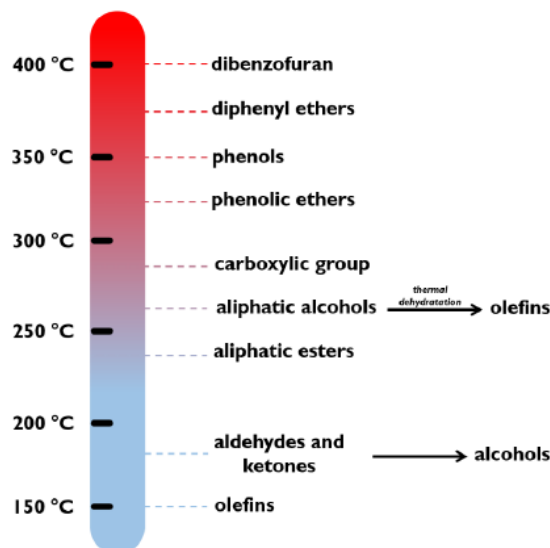


**Figure 3.11** Reactivity scale of organic compounds according to different temperatures of the hydrotreatment [3.67]

For sake of clarity, the summary of the main keys parameters for hydrotreatment of pyrolysis oil are reported in **Table 3.5**:

**Table 3.5** Summary of keys parameters in the hydrotreatment process

Keys parameters	Optimal values	Description
Temperature	240-400°C	High values of temperature are required but not higher than 450°C to avoid coke formation and the deactivation of the catalyst.
Pressure	8 MPa (80bar)	Higher value of pressure improves bio-oil properties by enhancing deoxygenation reactions.
Reaction time	0.5-4 h	It has been proven this time interval is ideal to obtain good bio-oil yield and low oxygen content [3.62].
LHSV	0.2-8 h <sup>-1</sup>	In a continuous batch reactor, it is better to have lower LHSV to produce less coke and more the hydrogen active sites, thus favouring hydrogenation and hydrocracking reactions.

H <sub>2</sub> /oil	-	The H <sub>2</sub> /oil ratio has a proper effect on hydrogenation and cracking reaction efficiency, even if the optimal ratio is different according to the heteroatom to be removed. Anyway, high values of ratio lead to higher hydrogen consumption.
Catalyst	-	It depends on the heteroatom to be removed and the cost of the catalyst itself.

---

### 3.9 The technological comparison in terms of TRLs

The level of technological maturity of waste biomass valorisation via thermochemical processes can be assessed with the metrics of technology readiness level (TRL), that is already described in **Chapter 2**.

In this case, TRL helps to evaluate and compare all the alternatives described in this chapter and illustrated with their TRLs in **Table 3.6**. The TCR, which represents the scope of this thesis, has a TRL equal to 7 meaning that its prototype has been tested and validated in an operational environment (integrated pilot system level). From literature, many trials pointed out pelletised sewage sludge as the best commercial feedstock to produce and sell biodiesel deriving from TCR oil after a further hydrotreatment.

Hence, even though the maturity is at TRL 7, it is necessary to keep in mind that TCR is now almost a commercial ready technology and it is a combination of pyrolysis and catalytic reforming/cracking which have the highest values in terms of TRLs.

This result shows how potential is its growth compared to torrefaction and gasification, since there are not great tar-related issues as TCR temperatures are not as high as gasification ones and it is possible to collect not only gas and char but also a liquid fraction to produce advanced and alternative biofuels for the transport sector. Unlike gasification, the TCR also has the ability to process feedstocks with lower ash melting points such as straw. Because excessive temperatures are not used by the process. Surely, there are still some challenges in TCR of biomass due to thermal requirements for drying the biomass or difficulties in handling and feeding of specific materials, but once overcome, the process has been validated to be very flexible, modular, and with a good footprint for future commercial plants as demonstrated in the TO-SYN-FUEL project founded by Horizon 2020 [3.71].

**Table 3.6** Technology readiness level (TRL) of the main thermochemical processes based on biomass

<b>Technologies</b>	<b>TRL</b>	<b>Ref.s</b>
Torrefaction	6-7	[3.72]
HTL	6-8	[3.73]
HTC	8	[3.74]
Gasification	6-7	[3.72]
Pyrolysis	7-9	[3.72]
Reforming/cracking	5-7/7-9	[3.75][3.76]
TCR	6	[3.77]
Hydrotreatment	5	[3.78]



## References

- [3.1] H. C. Ong, W. Chen, A. Farooq, Y.-Y. Gan, K. T. Lee, V. Ashokkumar, Catalytic thermochemical conversion of biomass for biofuel production: A comprehensive review, *Renewable and Sustainable Energy Reviews* 113 (2019) 109266;
- [3.2] J.A. Okolie, E. I. Epelle, M. E. Tabat, U. Orivri, A. Nosakhare Amenaghawon, P. U. Okoye, B. Gunes, Waste biomass valorization for the production of biofuels and value-added products: A comprehensive review of thermochemical, biological and integrated processes, *Process Safety and Environmental Protection* 159 (2022) 323–344;
- [3.3] L. Dai, Y. Wang, Y. Liu, R. Ruan, C. He, Z. Yu, Integrated process of lignocellulosic biomass torrefaction and pyrolysis for upgrading bio-oil production: a state-of-the-art review, *Renew Sustain Energy Rev*, 107 (2019), pp. 20-36;
- [3.4] M. Klaas, C. Greenhalf, M. Ouadi, H. Jahangiri, A. Hornung, C. Briens, F. Berruti, The effect of torrefaction pre-treatment on the pyrolysis of corn cobs, *Results in Engineering*, Volume 7, September 2020, 100165;
- [3.5] W.-H. Chen, S.-H. Liu, T.-T. Juang, C.-M. Tsai, Y.-Q. Zhuang, Characterization of solid and liquid products from bamboo torrefaction, *Appl Energy*, 160 (2015), pp. 829-835;
- [3.6] M. Zabeti, J. Baltrusaitis, K. Seshan, Chemical routes to hydrocarbons from pyrolysis of lignocellulose using Cs promoted amorphous silica alumina catalyst, *Catalysis Today*, 269 (2016), pp. 156-165;
- [3.7] D. Chen, A. Gao, Z. Ma, D. Fei, Y. Chang, C. Shen, In-depth study of rice husk torrefaction: characterization of solid, liquid and gaseous products, oxygen migration and energy yield, *Bioresource Technology*, 253 (2018), pp. 148-153;
- [3.8] S.B. Saleh, B.B. Hansen, P.A. Jensen, K. Dam-Johansen, Influence of biomass chemical properties on torrefaction characteristics, *Energy Fuel*, 27 (2013), pp. 7541-7548;
- [3.9] H. Chen, X. Chen, Z. Qiao, H. Liu, Release and transformation characteristics of K and Cl during straw torrefaction and mild pyrolysis, *Fuel*, 167 (2016), pp. 31-39;

- [3.10] Available online:  
[https://www.agrireseau.net/references/32/presentations\\_guelph/2Torrefaction%20-%20Pros%20and%20Cons%20By%20Mathias%20Leon%20UoG.pdf](https://www.agrireseau.net/references/32/presentations_guelph/2Torrefaction%20-%20Pros%20and%20Cons%20By%20Mathias%20Leon%20UoG.pdf)  
(accessed on 11/12/2022);
- [3.11] J. Yang, Q. He, L. Yang, A review on hydrothermal co-liquefaction of biomass, *Applied Energy*, 250 (2019), pp. 926-945;
- [3.12] S.S. Toor, L. Rosendahl, A. Rudolf, Hydrothermal liquefaction of biomass: a review of subcritical water technologies, *Energy*, 36 (2011), pp. 2328-2342;
- [3.13] M. Verma, S. Godbout, S. K. Brar, O. Solomatnikova, S. P. Lemay, J. P. Larouche, Biofuels Production from Biomass by Thermochemical Conversion Technologies, *International Journal of Chemical Engineering*, 2012;
- [3.14] Q.-V. Bach, K.-Q. Tran, K. Q. Lystad, Fast Hydrothermal Liquefaction of Macro-Alga: Characterization of Products, *Chemical Engineering Transactions*, Vol. 50, 2016;
- [3.15] A.R.K. Gollakota, N. Kishore, S. Gu, A review on hydrothermal liquefaction of biomass, *Renewable Sustainable Energy Reviews*, 81 (2018), pp. 1378-1392;
- [3.16] A. Catenacci, G. Boniardi, M. Mainardis, F. Gievers, G. Farru, F. Asunis, F. Malpei, D. Goi, G. Cappai, R. Canziani, Processes, applications and legislative framework for carbonized anaerobic digestate: Opportunities and bottlenecks. A critical review. *Energy Conversion and Management*, 263, 2022, 115691;
- [3.17] S. Poirier, O. Chapleur, Inhibition of anaerobic digestion by phenol and ammonia: Effect on degradation performances and microbial dynamics, *Data in Brief*, Volume 19, 2018, Pages 2235-2239;
- [3.18] J. Wang, S. Wang, Preparation, modification and environmental application of biochar: a review, *Journal of Cleaner Production*, 227, 2019, pp. 1002-1022;
- [3.19] M. Ahmed, G. Andreottola, S. Elagroudy, M. S. Negm, L. Fiori, Coupling hydrothermal carbonization and anaerobic digestion for sewage digestate management: Influence of hydrothermal treatment time on dewaterability and bio-methane production, *Journal of Environmental Management*, 2021, 281, 111910;

- [3.20] M. Heidari, A. Dutta, B. Acharya, S. Mahmud, A review of the current knowledge and challenges of hydrothermal carbonization for biomass conversion, *J Energy Inst*, 92, 2019, pp. 1779-1799;
- [3.21] A. Funke, F. Ziegler, Hydrothermal carbonization of biomass: A summary and discussion of chemical mechanisms for process engineering, *Biofuels, Bioprod Bioref*, 4, 2010, pp. 160-177;
- [3.22] Gupta D, Mahajani SM, Garg A. Hydrothermal carbonization of household wet waste – characterization of hydrochar and process wastewater stream, *Bioresour Technol*, 2021; 342, 125972;
- [3.23] A.E. Brown, J. M. Hammerton, M. A. Camargo-Valero, A. B. Ross, Integration of Hydrothermal Carbonisation and Anaerobic Digestion for the Energy Valorisation of Grass, *Energies* 2022, 15, 3495;
- [3.24] M. Niinipuu, K.G. Latham, JF. Boily, M. Bergknut, S. Jansson, The impact of hydrothermal carbonization on the surface functionalities of wet waste materials for water treatment applications. *Environ Sci Pollut Res* 27, 24369–24379 (2020);
- [3.25] S. Ciuta, D. Tsiamis, M. J. Castaldi, Chapter Two - Fundamentals of Gasification and Pyrolysis, *Gasification of Waste Materials Technologies for Generating Energy, Gas, and Chemicals from Municipal Solid Waste, Biomass, Nonrecycled Plastics, Sludges, and Wet Solid Wastes* 2018, Pages 13-36;
- [3.26] M. Shahbaz, T. Al-Ansari, M. Inayat, S. A. Sulaiman, P. Parthasarathy, G. McKay, A critical review on the influence of process parameters in catalytic co-gasification: Current performance and challenges for a future prospectus, *Renewable and Sustainable Energy Reviews*, Volume 134, December 2020, 110382;
- [3.27] L. Waldheim, Gasification of waste for energy carriers A review, *IEA Bioenergy*, 2018;
- [3.28] P. Basu, Chapter 8 - Design of Biomass Gasifiers, *Biomass Gasification, Pyrolysis and Torrefaction (Third Edition), Practical Design and Theory*, 2018, Pages 263-329;
- [3.29] F. Ronsse, R. W. Nachenius, W. Prins, Chapter 11 - Carbonization of Biomass, *Recent Advances in Thermo-Chemical Conversion of Biomass*, Elsevier, 2015, 293-324;

- [3.30] A. Pollex, A. Ortwein, M. Kaltschmitt, Thermo-chemical conversion of solid biofuels, *Biomass Convers. Biorefin.*, 2 (1) (2012), pp. 21-39;
- [3.31] J. LeBlanc, J.F. Quanci, M.J. Castaldi, Investigating secondary pyrolysis reactions of coal tar via mass spectrometry techniques, *Energy & Fuels* (2016);
- [3.32] J. LeBlanc, J. Quanci, M.J. Castaldi, Experimental investigation of reaction confinement effects on coke yield in coal pyrolysis, *Energy Fuels*, 30 (8) (2016), pp. 6249-6256;
- [3.33] A. Comandini, T. Malewicki, and K. Brezinsky, Chemistry of Polycyclic Aromatic Hydrocarbons Formation from Phenyl Radical Pyrolysis and Reaction of Phenyl and Acetylene, *J. Phys. Chem. A* 2012, 116, 10, 2409–2434;
- [3.34] A. Molino, S. Chianese, D. Musmarra, Biomass gasification technology: the state-of-the-art overview, *J. Energy Chem.*, 25 (1) (2016), pp. 10-25;
- [3.35] A. Mohammadi, and A. Anukam, The Technical Challenges of the Gasification Technologies Currently in Use and Ways of Optimizing Them: A Review, *Latest Research on Energy Recovery [Working Title]*. London, United Kingdom: IntechOpen, 2022. Available online: <https://www.intechopen.com/online-first/80419> (accessed on 11/12/2022);
- [3.36] A.V. Bridgwater, Review of fast pyrolysis of biomass and product upgrading, *Biomass and Bioenergy* 38 (2012), 68-94;
- [3.37] R. Kaur, P. Gera, M. K. Jha, Study on Effects of Different Operating Parameters on the Pyrolysis of Biomass: A Review, *Journal of Biofuels and Bioenergy* (December 2015) 1(2): 135-147;
- [3.38] Hi. Uchida, M. R. Harada, Chapter 5 - Hydrogen Energy Engineering Applications and Products, *Science and Engineering of Hydrogen-Based Energy Technologies, Hydrogen Production and Practical Applications in Energy Generation*, 2019, 201-220;
- [3.39] S.A. Channiwala, P.P. Parikh, A unified correlation for estimating HHV of solid, liquid and gaseous fuels, *Fuel* 81 (2002) 1051-1063;
- [3.40] S. Caillat, E. Vakkilainen, 9 - Large-scale biomass combustion plants: an overview, *Biomass Combustion Science, Technology and Engineering*, Woodhead Publishing, 2013, Pages 189-224;
- [3.41] G. Trif-Tordai, I. Ionel, Waste Biomass as Alternative Bio-Fuel - Co-Firing versus Direct Combustion, *Alternative Fuel*, 2011, Available Online: <https://www.intechopen.com/chapters/17594> (accessed on 08/09/2022);

- [3.42] F. Ronsse, X. Bai, W. Prins, R.C. Brown, Secondary reactions of levoglucosan and char in the fast pyrolysis of cellulose, *Environ. Prog. Sustainable Energy* 31 (2012) 256–260;
- [3.43] J. G. Speight, 2 - Introduction to refining processes, *The Refinery of the Future* (Second Edition), 2020, Pages 43-84;
- [3.44] Y. Zheng, J. Wang, D. Wang, Z. Zheng, Advanced catalytic upgrading of biomass pyrolysis vapor to bio-aromatics hydrocarbon: A review. *Applications in Energy and Combustion Science*, 2022, 100061;
- [3.45] Lu Zhanga, Wei Wu, Nyima Siqua, Tenzin Dekyia, Yongjie Zhang, Thermochemical catalytic-reforming conversion of municipal solid waste to hydrogen-rich synthesis gas via carbon supported catalysts, *Chemical Engineering Journal* 361 (2019) 1617–1629;
- [3.46] L. Zhang, W. Wu, Y. Zhang, X. Zhou, Clean synthesis gas production from municipal solid waste via catalytic gasification and reforming technology, *Catalysis Today* 318 (2018) 39–45;
- [3.47] M. Shahabuddin, B.B. Krishna, T. Bhaskar, G. Perkins, Advances in the thermos chemical production of hydrogen from biomass and residual wastes: Summary of recent techno-economic analyses, *Bioresource Technology* 299 (2020) 122557;
- [3.48] Available online:  
<https://www.bbc.co.uk/bitesize/guides/zshvw6f/revision/5> (accessed on 30/06/2022);
- [3.49] Pyrolysis Oil and Method and System For The Production Thereof, Publication number: 20220081620, Type: Application, Filed: June 24, 2021, Publication date: March 17, 2022, Applicant: Fraunhofer-Gesellschaft zur Förderung der angewandten Forschung e.V., Inventors: Andreas Hornung, Andreas Apfelbacher, Miloud Ouadi, Johannes Neumann. Online: <https://patents.justia.com/inventor/andreas-afelbacher> (accessed on 12/12/2022);
- [3.50] N. Schmitt, A. Apfelbacher, N. Jäger, R. Daschner, F. Stenzel, A. Hornung, Thermo-chemical conversion of biomass and upgrading to biofuel: The Thermo-Catalytic Reforming process – A review, *Biofuels, Bioproducts and Biorefining*, John Wiley & Sons, Ltd, Volume 13, 822-837, 2019;

- [3.51] J. Neumann, J. Meyer, M. Ouadi, A. Apfelbacher, A. Binder, A. Hornung, The conversion of anaerobic digestion waste into biofuels via a novel Thermo-Catalytic Reforming process, *J Waste Manage* 47:141–148 (2016);
- [3.52] J. Santos, M. Ouadi, H. Jahangiri, A. Hornung, Thermochemical conversion of agricultural wastes applying different reforming temperatures, *Fuel Processing Technology*, Volume 203, 15 June 2020, 106402;
- [3.53] Available online:  
[https://ec.europa.eu/energy/sites/ener/files/documents/20\\_andreas\\_hornung-fraunhofer.pdf](https://ec.europa.eu/energy/sites/ener/files/documents/20_andreas_hornung-fraunhofer.pdf) (accessed on 03/10/2022);
- [3.54] Available online: [https://www.umsicht-suro.fraunhofer.de/en/Our\\_Solution/tcr-technology.html](https://www.umsicht-suro.fraunhofer.de/en/Our_Solution/tcr-technology.html) (accessed on 22/06/2022);
- [3.55] Available online: <https://bioenergyinternational.com/fraunhofer-umsicht-supply-laboratory-tcr-plant-to-italy/> (accessed on 22/06/2022);
- [3.56] J. Santos, M. Ouadi, H. Jahangiri, A. Hornung, Valorisation of lignocellulosic biomass investigating different pyrolysis temperatures, *Journal of the Energy Institute*, Volume 93, Issue 5, October 2020, Pages 1960-1969;
- [3.57] M. A. Bashir, S. Lima, H. Jahangiri, A. J. Majewski, M. Hofmann, A. Hornung, M. Ouadi, A step change towards sustainable aviation fuel from sewage sludge, *Journal of Analytical and Applied Pyrolysis*, Volume 163, 2022, 105498;
- [3.58] R. Conti, N. Jäger, J. Neumann, A. Apfelbacher, R. Daschner, A. Hornung, Thermocatalytic reforming of biomass waste streams. *Energy Technol (Weinheim, Germany)* 5:104–110 (2017);
- [3.59] K. B. Cantrell, P. G. Hunt, M. Uchimiya, J. M. Novak, K. S. Ro, *Bioresour. Technol.* 2012, 107, 419–428;
- [3.60] R. Conti, A. G. Rombol/, A. Modelli, C. Torri, D. Fabbri, *J. Anal. Appl. Pyrolysis* 2014, 110, 239–247;
- [3.61] H. Song, K. Sison Quinton, Z. Peng, H. Zhao, N. Ladommatos, Effects of Oxygen Content of Fuels on Combustion and Emissions of Diesel Engines, *Energies* 2016, 9, 28;
- [3.62] R. Kumar, V. Strezov, Thermochemical production of bio-oil: A review of downstream processing technologies for bio-oil upgrading, production of hydrogen and high value-added products, *Renewable and Sustainable Energy Reviews*, Volume 135, January 2021, 110152;

- [3.63] Z. Xiaojie, K. Mukherjee, S. Manna, M. K. Das, J. K. Kim, T. K. Sinha, Chapter 24 - Efficient management of oil waste: chemical and physicochemical approaches, *Advances in Oil-Water Separation A Complete Guide for Physical, Chemical, and Biochemical Processes* 2022, Pages 439-467;
- [3.64] R. Lødeng, L. Hannevold, H. Bergem, M. Stöcker, Chapter 11 - Catalytic Hydrotreatment of Bio-Oils for High-Quality Fuel Production, Elsevier, 2013, Pages 351-396;
- [3.65] M. C. Vasquez, E. E. Silva, E. F. Castillo, Hydrotreatment of vegetable oils: A review of the technologies and its developments for jet biofuel production, *Biomass and Bioenergy* 105 (2017) 197-206;
- [3.66] M. Auersvald, B. Shumeiko, D. Vrtiška, P. Straka, M. Staš, P. Šimáček, et al, Hydrotreatment of straw bio-oil from ablative fast pyrolysis to produce suitable refinery intermediates, *Fuel*, 238 (2019), pp. 98-110;
- [3.67] G. Bagnato, A. Sanna, E. Paone, E. Catizzzone, Recent Catalytic Advances in Hydrotreatment Processes of Pyrolysis Bio-Oil, *Catalysts* 2021, 11, 157;
- [3.68] S. Bezergianni, A. Dimitriadis, A. Kalogianni, K. G. Knudsen, Toward Hydrotreating of Waste Cooking Oil for Biodiesel Production. Effect of Pressure, H<sub>2</sub>/Oil Ratio, and Liquid Hourly Space Velocity, *Ind. Eng. Chem. Res.* 2011, 50, 3874–3879;
- [3.69] A. Eschenbacher, A. Saraeian, P.A. Jensen, B.H. Shanks, C. Li, J.Ø. Duus, et al., Deoxygenation of wheat straw fast pyrolysis vapors over Na-Al<sub>2</sub>O<sub>3</sub> catalyst for production of bio-oil with low acidity, *Chem Eng J*, 394 (2020), p. 124878;
- [3.70] L. D. Sharma, M. Kumar, J. K. Gupta, M. S. Rana, V. S. Dangwal, G Murali Dhar, Characterization and catalytic activity of Ni-W/SiO<sub>2</sub>-Al<sub>2</sub>O<sub>3</sub> hydrocracking catalysts, *Indian Journal of Chemical Technology* Vol. 8, May 2001, pp. 169-175;
- [3.71] Available online: <https://www.tosynfuel.eu/> (accessed on 16/12/2022);
- [3.72] Available online: [https://www.izes.de/sites/default/files/publikationen/ARBOR\\_8\\_R\\_Dowdall\\_Uni\\_College\\_Dublin.pdf](https://www.izes.de/sites/default/files/publikationen/ARBOR_8_R_Dowdall_Uni_College_Dublin.pdf) (accessed on 03/10/2022);
- [3.73] S. Wijeyekoon, K. Torr, H. Corkran, P. Bennett, Commercial status of direct thermochemical liquefaction technologies, *IEA Bioenergy: Task 34*, August 2020, available online: <https://www.ieabioenergy.com/wp->

[content/uploads/2020/09/Direct-Thermochemical-Liquefaction Commercialization Overview.pdf](https://ec.europa.eu/research/participants/documents/downloadPublic?documentIds=080166e5c630ff84&appId=PPGMS) (accessed on 03/10/2022);

- [3.74] Available online: <https://ec.europa.eu/research/participants/documents/downloadPublic?documentIds=080166e5c630ff84&appId=PPGMS> (accessed on 03/10/2022);
- [3.75] M. Draxler, A. Sormann (K1-MET), T. Kempken, T. Hauck (BFI), J.-C. Pierret, J. Borlee (CRM), A. Di Donato, M. De Santis (CSM), C. Wang (Swerim), Technology Assessment and Roadmapping, Green Steel for Europe Consortium, June 2021. Available online: <https://www.estep.eu/assets/Uploads/Technology-Assessment-and-Roadmapping.pdf> (accessed on 03/10/2022);
- [3.76] M. Solis, S. Silveira, Technologies for chemical recycling of household plastics – A technical review and TRL assessment, Waste Management, Volume 105, 15 March 2020, Pages 128-138;
- [3.77] Available online: <https://www.retealtatecnologia.it/technology-report/reforming-termocatalitico-valorizzazione-di-biomasse-residuali-e-scarti-mediante> (in italian) (accessed on 03/10/2022);
- [3.78] Available online: <https://energiforskmedia.blob.core.windows.net/media/25751/pyros-energiforskrapport-2018-550.pdf> (accessed on 03/10/2022).



## 4. Feedstocks description

### Chapter summary

This chapter gives a general overview of two wastes that were investigated via thermal catalytic reforming (TCR) technology in the present work. These are solid grade laminate (SGL) and carbon fibres (CF).

Their properties as raw material as well as their production process, availability and applications are reviewed. However, since both feedstocks have never been processed by TCR and TCR is a combination of intermediate pyrolysis and reforming technologies, other thermochemical processes (e.g. pyrolysis and/or gasification) are studied to understand their suitability in TCR.

Moreover, the final gaseous, liquid and solid products, that are syngas, oil and char, respectively, are analysed according to their properties.

This analysis is strategic from the industrial, environmental and economical point of view, since it is possible to get supplementary sales revenues and create new valorisation pathways from wastes. Moreover, their reuse can also direct the industrial sectors towards a virtuous, environmental-friendly and sustainable management of wastes.

### 4.1 Solid Grade Laminate (SGL)

Feedstocks, as received from JCM Fine Joinery (UK), was dry solid grade laminate (SGL) blocks (**Figure 4.1**) composed of more than 60% of compressed Kraft paper layers and the remaining 30-40% of phenolic resin for core layers and melamine resin for the surface layer. It is estimated that approximately 130 million of tons of Kraft paper are produced annually via Kraft process [4.1], even if it is not easy to determine the amount of Kraft paper destined to SGL production.

According to the Environmental Product Declaration (EPD), SGL or Compact High-Pressure Laminate (CHPL) is produced in a high-pressure process. Papers are impregnated with thermosetting resins and pressed together under simultaneous application of heat (temperature > 120°C) and high specific pressure ( $\geq 5$  MPa). This method produces a homogeneous, nonporous material with a density equal to 1350 kg/m<sup>3</sup>. The applications of solid grade laminate are wide thanks to its compactness, resistance to moisture, impacts, scratches and stains and its easy maintenance. It is

suitable as counter, worktop, wall panelling, door, cubicles, furniture as well as all types of surfaces [4.2]. Therefore, it would not be surprising to find high volumes of SGL in the waste streams, especially in the manufacturing companies. Such abundance of waste SGL could be potentially used to produce value-added products by thermochemical processes.

To date, waste SGLs are only subjected to: (i) a collection process meaning that they could be collected separately or with mixed construction waste; (ii) a recovery system to be reused, recycled or for further energy recovery; (iii) a disposal to be incinerated in waste-to-energy (WtE) applications or stored in landfill [4.2].

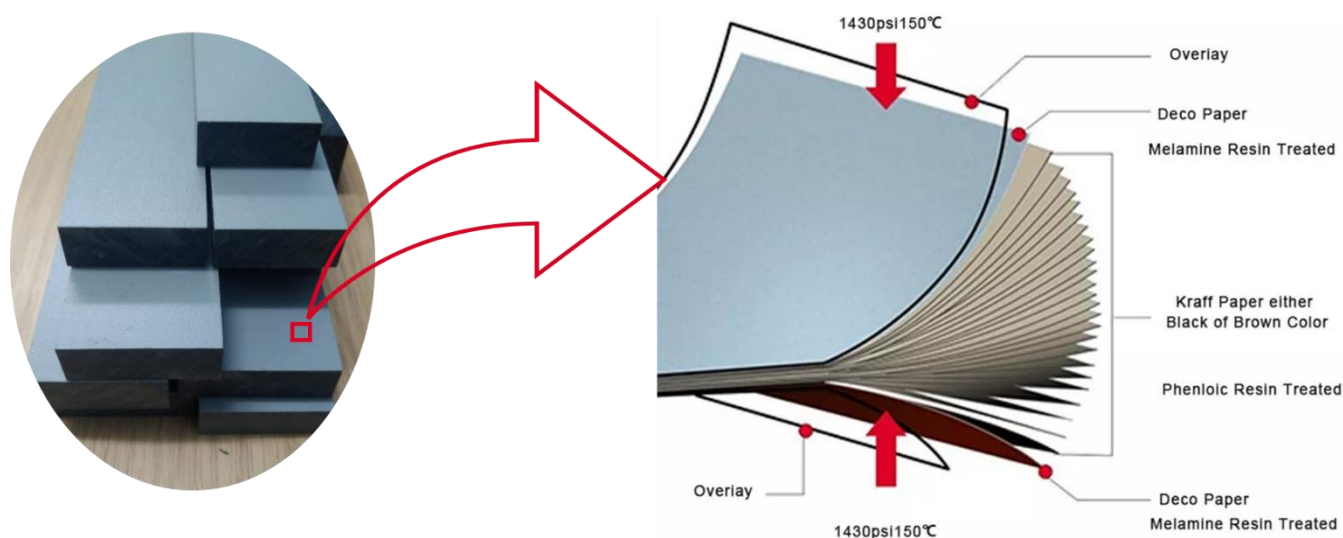


**Figure 4.1** Solid Grade Laminate used in TCR reactor and its structure [4.3]

Next step is to focus on (ii) and to understand if SGLs may have a potential to produce value-added products like alternative fuels through thermo-chemical processes or it must be classified as wastes and destined to landfill.

The thermochemical conversion of SGL, either gasification or pyrolysis, is still an unexplored field as demonstrated by the lack of specific information in literature.

However, being SGL mainly composed of Kraft paper, also named paper, paperboard or cardboard, there would seem possible to extend some results deriving from gasification and/or pyrolysis of wood, paper or other lignocellulosic materials under proper considerations. In fact, Kraft paper is characterized by cellulose, hemicellulose and lignin whose values are compared with wood and other lignocellulosic residues and shown in **Table 4.1**.

**Table 4.1** Chemical composition of Kraft fibres

	Unit	Lignin	Cellulose	Hemicellulose
<b>Kraft fibres</b> [4.4]	wt.%	7.6	76.2	16.2
<b>Paper</b> [4.5]	wt.%	0-15	85-99	0
<b>Newspaper</b> [4.5]	wt.%	18-30	40-55	25-40
<b>Wastepaper from chemical pulps</b> [4.5]	wt.%	5-10	60-70	10-20
<b>Wood</b> [4.5]	wt.%	18-32	40-44	15-35

As Kraft paper is produced from wood pulp in a dedicated process, their compositions are quite comparable. However, Kraft fibres have higher content of cellulose and lower content of both lignin and hemicellulose than wood, since they are subjected to the delignification treatment.

The Kraft process consists of a particular mechanical and chemical treatment of wood chips with a mixture of water, sodium hydroxide (NaOH), and sodium sulfide (Na<sub>2</sub>S), known as white liquor, that breaks the bonds that link lignin, hemicellulose, and cellulose under pressure and high temperatures [4.6], [4.7] until the delignification of wood into cellulose fibres occurs in this chemical pulping process.

Afterwards, the Kraft papers are supposed to be impregnated with phenolic and melamine resins and compressed together to build blocks of SGL

The low lignin content in Kraft paper is low constitutes a benefit in terms of biofuel production. Indeed, although lignin showed a great potential in producing fuels, value-added chemicals, and functional materials thanks to its high-energy density and intrinsic aromatic-based structure [4.7], [4.8], it is also a recalcitrant molecule that impedes accessibility to polysaccharide and then their transformation into commercially significant products. That is why the upstream removal of lignin is often mandatory in the feedstocks pre-treatment to produce biofuels [4.9].

Pyrolysis and gasification are often employed for the conversion of lignocellulosic material thanks to their high temperatures. Different products are obtained from them: a solid (char and ash), a liquid/condensed fraction (tars and oil) and a non-condensable gas (syngas).

**Table 4.2** reports the main physiochemical properties and composition of wood and wastepaper bio-oil deriving from both pyrolysis and TCR in comparison with heavy fuel oil (HFO) and biodiesel.

**Table 4.2** Summary of composition and physio-chemical properties for wood and wastepaper bio oil and heavy fuel oil and biodiesel

Physio-chemical properties	Typical Wood bio-oil from pyrolysis [4.10]	Wastepaper bio-oil [4.11]	Wood chips bio-oil from TCR [4.12]	Heavy Fuel Oil [4.10]	Biodiesel [4.12]
Moisture (wt%)	15-30	-	9.5	0.1	<0.1
C (wt%)	54-58	40.8	73.2	85	77.2
H (wt%)	5.5-7.0	6.29	8.0	11	13.2
O (wt%)	35-40	52.91	17.0	1.0	9.4
N (wt%)	0-0.2	0	1.5	0.3	0.1
S (wt%)	-	-	0.3	-	<0.1
Ash (wt%)	0-0.2	0.35	0.4	0.1	<0.1
HHV (MJ/kg)	16-19	13.19	35.3	40	39.3
Dynamic viscosity (kg/m s)	40-100 (at 50°C)	-	-	180	-
Density (kg/m <sup>3</sup> )	1100-1300 (at 15°C)	1205	-	-	-
Flash point (°C)	40-110	200	-	-	-

On the basis of previous considerations, it is expected that the SGL oil has properties similar to the pyrolysis oil reported in **Table 4.2** with calorific value between 13 and 35 MJ/kg, lower than HFO and biodiesel.

The calorific value of syngas derived from the valorisation of paper by thermochemical processes is lower than 10 MJ/kg, thus allowing to use it as a gaseous fuel for boilers, internal combustion engines and if purified from poisoning components solid oxide fuel cells (SOFC) to produce thermal and electrical power [4.13].

The wood-based char is found to be useful for multiple applications such as thermal energy recovery through combustion or gasification. This circumstance allows to satisfy the heat demand of pyrolysis or other conversion processes. Possible, interesting applications are the use as a soil fertilizer or either as a solid absorbent substance for microbial fuel cells (MFCs) electrodes to facilitate the simultaneous treatment of wastewater and electricity generation as shown in [4.14] [4.15].

## 4.2 Carbon Fibres (CF)

Carbon fibres (**Figure 4.2**) used in TCR experiments were supplied by Gen2Carbon (UK) and are typically made of fibres about 5-10 $\mu\text{m}$  in diameter and mainly composed of carbon ( $\sim 90\%$ ) [4.16][4.17]. The raw material used to obtain carbon fibres is called precursor and it can be a different material depending on the mechanical, electrical or thermal property that is expected from CFs. Typical precursors are polyacrylonitrile (PAN), pitch and cellulose [4.18]. Generally, carbon fibres are long strings of organic polymers bound together by carbon atoms and they are typically made of 90% polyacrylonitrile (PAN) and 10% rayon or petroleum pitch [4.16]. The reason why PAN is widely used as a precursor is due to the achievement of the highest carbon yields as reported in [4.18]. More recently, interest has been shifted to lignin as a renewable resource to produce CF because of its relative abundance and capacity to be processed through melt spinning, thus negating the expense of costly solvents [4.19].

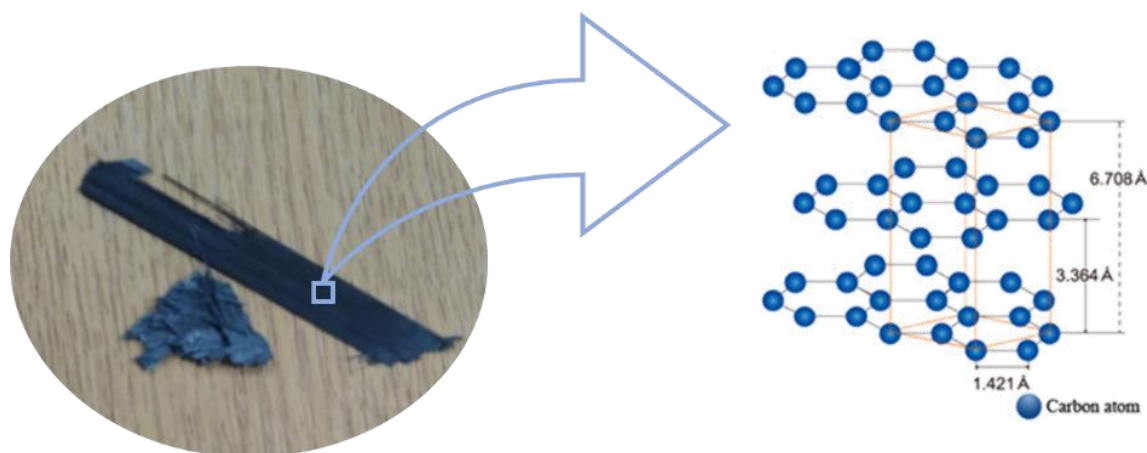
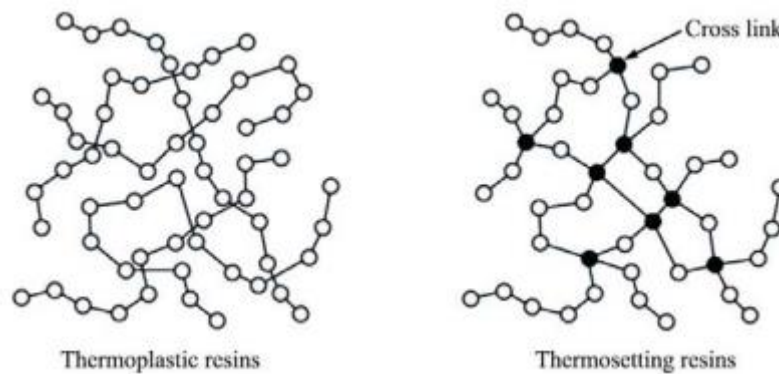


**Figure 4.2** Carbon Fibres used in TCR reactor and their crystal structure [4.20]

Briefly, PAN-derived carbon fibres are manufactured through a multi-stage process involving polymerisation of acrylonitrile  $\text{C}_3\text{H}_3\text{N}$  (deriving from the reaction between propylene and ammonia), fibres spinning and stabilization, carbonization ( $T=1000\text{-}3000^\circ\text{C}$ , solvents) and surface treatment (with the addition of resins) according to the properties required for the specific application [4.16][4.19][4.21]. Generally, carbon fibres are reinforced with a polymer resin forming an advanced non-metallic composite material named Carbon Fibre Reinforced Polymer (CFRP) with superior performances, such as high strength, lightweight, no corrosion and high fatigue

resistance [4.22]. The polymer resins for CFRPs can be thermoplastic or thermosetting resins as illustrated in **Figure 4.3**. Their difference is due to the specific molecular structure. In fact, thermoplastic resins are polymers with a linear or branched molecular structure linked by intermolecular interactions (Van der Waals forces) providing a restriction in their motion, making them remeltable and tractable through heat and pressure. On the contrary, thermosetting resins are polymers linked by chemical bonds (cross-link) conferring a rigid molecular structure in terms of motion, making them unmeltable and untreatable [4.22]. Among thermosetting polymers, epoxy is widely used, since it positively influences the tensile strength by 0.115GPa versus 0.086GPa on average for thermoplastic resins at the same density [4.22].

**Figure 4.3** Molecular structure of thermoplastic and thermosetting resins [4.22]



Carbon fibres can be grouped on modulus, strength and final heat treatment, as defined in [4.16][4.23]:

- i. Ultra-high modulus UHM (modulus > 450GPa);
- ii. High modulus HM ((modulus between 350-450GPa);
- iii. Intermediate-modulus IM (modulus between 200-350Gpa);
- iv. Standard modulus SM or High strength/high strain (modulus < 250GPa)

After the manufacturing process, the material appears with a very low-density and with excellent mechanical properties as reported in **Table 4.3**.

**Table 4.3** Mechanical properties for different classes of carbon fibres [4.23]

	Unit	HS	HM	UHM	Steel
Density	kg/m <sup>3</sup>	1800	1850	2100	7850
Tensile Modulus E	GPa	230	400	700	210

<b>Tensile strength</b>	MPa	5000	3000	1500	540
<b>Ultimate Strain (elongation)</b>	%	2.0	0.9	0.3	20
<b>Specific resistance</b>	MPa/kg	2.78	1.62	0.71	0.07

Furthermore, CFs have not only good mechanical properties but also good electrical and thermal qualities. In **Table 4.4**, the main CFs properties and their corresponding applications are reported:

**Table 4.4** Properties and applications of carbon fibres [4.16][4.17]

<b>Properties</b>	<b>Applications</b>
<b>Physical strength, specific toughness, light weight</b>	Aerospace, road and marine transport, sporting goods
<b>High dimensional stability, low coefficient of thermal expansion, and low abrasion</b>	Missiles, aircraft brakes, aerospace antenna and support structure, large telescopes, optical benches, waveguides for stable high-frequency (GHz) precision measurement frames
<b>Good vibration damping, strength, and toughness</b>	Audio equipment, loudspeakers for Hi-fi equipment, pickup arms, robot arms
<b>Electrical conductivity</b>	Automobile hoods, novel tooling, casings and bases for electronic equipments, EMI and RF shielding, brushes
<b>Biological inertness and x-ray permeability</b>	Medical applications in prostheses, surgery and x-ray equipment, implants, tendon/ligament repair
<b>Fatigue resistance, self-lubrication, high damping</b>	Textile machinery, genera engineering
<b>Chemical inertness, high corrosion resistance</b>	Chemical industry; nuclear field; valves, seals, and pump components in process plants
<b>Electromagnetic properties</b>	Large generator retaining rings, radiological equipment
<b>Microporosity</b>	Adsorbent material, molecular sieve, electrodes, catalyst (oxidation of SO <sub>2</sub> and NO [4.17])

The wide field of applications of carbon fibers suggests a challenge in the waste recycling. It is estimated that the global demand for CF is 117kton in 2022. Therefore, the recovery of used carbon fibers could significantly reduce their environmental impact in the waste management. Moreover, it is reported that the overall production process of carbon fibers is energy-intensive, consuming around 195-595 MJ/kg [4.24]. There is hence a clear and exigent demand for recycling and managing carbon fibers waste through the development of economically viable and sustainable technologies.

Recently, carbon fibres have been investigated in the thermochemical conversion processes (e.g. pyrolysis and gasification). Indeed, it is possible to recover fibres from the composite material, by removing the polymeric resin, where CF are embedded. For this purpose, temperatures used in the pyrolysis process are usually between 400 and 600°C (typical values of pyrolysis temperatures) to allow resins to be broken down, thus producing gases, vapours and a light layer of carbonaceous product (char) that cover the CF [4.21]. This layer must be removed later to enhance a proper adhesion of reclaimed CF and the new resins in further reuses [4.21].

Reclaimed carbon fibres are not the only value-added products obtained from the pyrolysis route. The synthesis gases, especially hydrogen, could be used as an alternative fuel and the material used as fillers in the solid bed of the reformer can have an appreciable influence in terms of catalytic for producing hydrogen. In this regard, it has been demonstrated that the best results are obtained using highly refractory material, whose presence of alkali metal oxides and iron oxide can determine the production of 17wt% of syngas, whose 57% in volume is hydrogen.

On the contrary, when no filler is used in the conventional slow pyrolysis, the main products are char, as expected, and bio-oil suitable to produce alternative fuels [4.21]. Pyrolysis has been identified as the most viable and sustainable process to recover and recycle CFs and CFRPs [4.24]. Frequently, pyro-gasification is also used to recover CFRPs. In fact, firstly pyrolysis enables the separation between resin and carbon fibres, while gasification removes char deposited on the CFs surface [4.25]. It is proved that 1300 °C represents the optimal temperature to remove char layer and thus to clean the surface of fibres. In this way, fibres can be recovered, despite their strength is significantly reduced [4.26].



## References

- [4.1]. K. M. Anil, A. Amith, K. M. Kiran, K. S. Rajeev, Chapter 9 - Lignocellulosic Biorefinery Wastes, or Resources? Waste Biorefinery Potential and Perspectives 2018, Pages 267-297;
- [4.2]. <https://en.polyrey.com/sites/polyrey/files/docs/resources/ENV-EN-REYSIPUR-20160922.pdf> (accessed on 04/05/2022);
- [4.3]. Available online: [https://www.alibaba.com/product-detail/Wholesale-phenolic-hpl-12mm-compact-laminate\\_1995837116.html](https://www.alibaba.com/product-detail/Wholesale-phenolic-hpl-12mm-compact-laminate_1995837116.html) (accessed on 05/09/2022);
- [4.4]. X. Yang, F. Berthold, L. A. Berglund, Preserving Cellulose Structure: Delignified Wood Fibers for Paper Structures of High Strength and Transparency, *Biomacromolecules* 2018, 19, 3020–3029;
- [4.5]. F. Di Gruttola, D. Borello, Analysis of the EU Secondary Biomass Availability and Conversion Processes to Produce Advanced Biofuels: Use of Existing Databases for Assessing a Metric Evaluation for the 2025 Perspective, *Sustainability* 2021, 13, 7882;
- [4.6]. N. Bijok, J. Fiskari, R. R. Gustafson, V. Alopaeus, Modelling the Kraft pulping process on a fibre scale by considering the intrinsic heterogeneous nature of the lignocellulosic feedstock, *Chemical Engineering Journal* Volume 438, 15 June 2022, 135548;
- [4.7]. J. M. Jardim, P. W. Hart, L. A. Lucia, H. Jameel, H. Chang, The Effect of the Kraft Pulping Process, Wood Species, and pH on Lignin Recovery from Black Liquor, *Fibers* 2022, 10-16;
- [4.8]. L. Hao, M. A-O. Mahdi, Chemicals from Lignin, *Encyclopedia of Sustainable Technologies*, 2017, Pages 573-585;
- [4.9]. L. Machineni, Lignocellulosic biofuel production: Review of alternatives, *Biomass Conversion and Biorefinery*. *Biomass Convers. Biorefinery* 2020, 10, 779–791;
- [4.10]. S. Czernik, A.V. Bridgwater, Overview of Applications of Biomass Fast Pyrolysis Oil, *Energy Fuel* 18 (2) (2004) 590–598;
- [4.11]. A.T. Hoang, H.C. Ong, I.M.R. Fattah, C. T. Chong, C. K. Cheng, R. Sakthivel, R., Y.S. Ok, Progress on the lignocellulosic biomass pyrolysis for biofuel

- production toward environmental sustainability, *Fuel Processing Technology* 223 (2021) 10699;
- [4.12]. N. Schmitt, A. Apfelbacher, N. Jäger, R. Daschner, F. Stenzel, A. Hornung, Thermo-chemical conversion of biomass and upgrading to biofuel: The Thermo-Catalytic Reforming process – A review, *Biofuels, Bioproducts and Biorefining*, John Wiley & Sons, Ltd, Volume 13, 822-837, 2019;
- [4.13]. M. Ouadi, A. Fivga, H. Jahangiri, M. Saghir, A. Hornung, A Review of the Valorization of Paper Industry Wastes by Thermochemical Conversion, *Industrial & Engineering Chemistry Research*, 2019, 58, 15914–15929;
- [4.14]. S. B. Patwardhan, S. Pandit, P. Kumar Gupta, N. Kumar Jha, J. Rawat, H. C. Joshi, K. Priya, M. Gupta, D. Lahiri, M. Nag, V. Kumar Thakur, K. Kumar Kesari, Recent advances in the application of biochar in microbial electrochemical cells, *Fuel*, Volume 311, 2022, 122501;
- [4.15]. Y. Zhou, S. Qin, S. Verma, T. Sar, S. Sarsaiya, B. Ravindran, T. Liu, R. Sindhu, A. Kumar Patel, P. Binod, S. Varjani, R. Rani Singhnia, Z. Zhang, M. Kumar Awasthi, Production and beneficial impact of biochar for environmental application: A comprehensive review, *Bioresource Technology*, Volume 337, October 2021, 125451;
- [4.16]. P. Bhatt, A. Goel, Carbon Fibres: Production, Properties and Potential Use, *Material Science Research India*, 2017, Vol. 14(1), 52-57, Available online: <https://www.materialsciencejournal.org/vol14no1/carbon-fibres-production-properties-and-potential-use/> (accessed 05/09/2022);
- [4.17]. S.-J. Park, Recent uses of carbon fibers, *Springer Series in Materials Science*, 2018, Volume 210, Pages 241 – 277;
- [4.18]. M. Limburg, J. Stockscläder, P. Quicker, Thermal treatment of carbon fibre reinforced polymers (Part 1: Recycling), *Waste Management & Research*, 2019, Vol. 37(1), 73–82;
- [4.19]. B. A. Newcomb, Processing, structure, and properties of carbon fibers, *Composites Part A: Applied Science and Manufacturing*, Volume 91, Part 1, December 2016, Pages 262-282;
- [4.20]. V.K. Srivastava, Pramod Kumar Jain, Parshant Kumar, Alessandro Pegoretti, Chris R. Bowen, Smart Manufacturing Process of Carbon-Based Low-Dimensional Structures and Fiber-Reinforced Polymer Composites for

- Engineering Applications, *Journal of Materials Engineering and Performance*, 2020, 29.7: 4162-4186;
- [4.21]. Lopez-Uriónabarrenechea, N. Gastelu, E. Acha, B.M. Caballero, A. Orue, A. Jimenez-Suarez, S.G. Prolongo, I. de Marco, Reclamation of carbon fibers and added-value gases in a pyrolysis based composites recycling process, *Journal of Cleaner Production* 273 (2020) 123173;
- [4.22]. Y. Liu, B. Zwingmann, M. Schlaich, Carbon Fiber Reinforced Polymer for Cable Structures—A Review, *Polymers*, 2015, 7, 2078–2099;
- [4.23]. Prof. Mauro Pasquali, Lezione 13 Fibre di Carbonio, Sapienza University of Rome available on: <http://www.sbai.uniroma1.it/~mauro.pasquali/page2/page9/page10/files/05-00.pdf> (accessed on 07/09/2022) (in italian);
- [4.24]. J. Zhang, V. S. Chevali, H. Wang, C.-H. Wang, Current status of carbon fibre and carbon fibre composites recycling, *Composites Part B: Engineering*, Volume 193, 15 July 2020, 108053;
- [4.25]. A. Fernández, C. S. Lopes, C. González, F. A. López, Characterization of Carbon Fibers Recovered by Pyrolysis of Cured Prepregs and Their Reuse in New Composites, in *Recent Developments in the Field of Carbon Fibers*. London, United Kingdom: IntechOpen, 2018, Available online: <https://www.intechopen.com/chapters/59532> (accessed on 07/09/2022);
- [4.26]. G. Oliveux, L. O. Dandy, G. A. Leeke, Current status of recycling of fibre reinforced polymers: Review of technologies, reuse and resulting properties, *Progress in Materials Science*, Volume 72, 2015, Pages 61-99.



## 5. Methods

### Chapter summary

This chapter describes the experimental methods applied for Thermo-catalytic reforming (TCR) of solid grade laminate (SGL) and carbon fibres (CF). Types and quantity of feedstocks received from the industrial suppliers are preliminary described. Afterwards, pre-treatment and feedstocks characterisation were analysed in order to simulate the same thermal condition experienced in TCR. Finally, the thermal conversion via TCR of the feedstocks is presented, detailing the plant setup and the experimental procedure to be used. Finally, the characterisation of each product deriving from TCR and experimental methods and equipment used for further analyses is described.

### 5.1 Solid Grade Laminate

#### 5.1.1 Feedstock pretreatment

For the present analysis, we used approximately 10 kg of dry SGL blocks (**Figure 5.1**) received from JCM Fine Joinery (UK). The feedstock was composed for more than 60% of compressed Kraft paper layers and for the remaining 30-40% of (a) phenolic resin for core layers and (b) melamine resin for the surface layer. The material contained an initial moisture content of 1.5wt%.



**Figure 5.1** Blocks of Solid Grade Laminate (SGL)

Before TCR, the laminate was firstly pre-treated. The dry solid grade laminate blocks were shredded down by the HECHT 6420 and further sieved with a VWR test sieve, having a mesh size of 5.6 mm and a sieve diameter of 200 mm (according to ISO 3310-1). The procedure is shown in **Figure 5.2**.

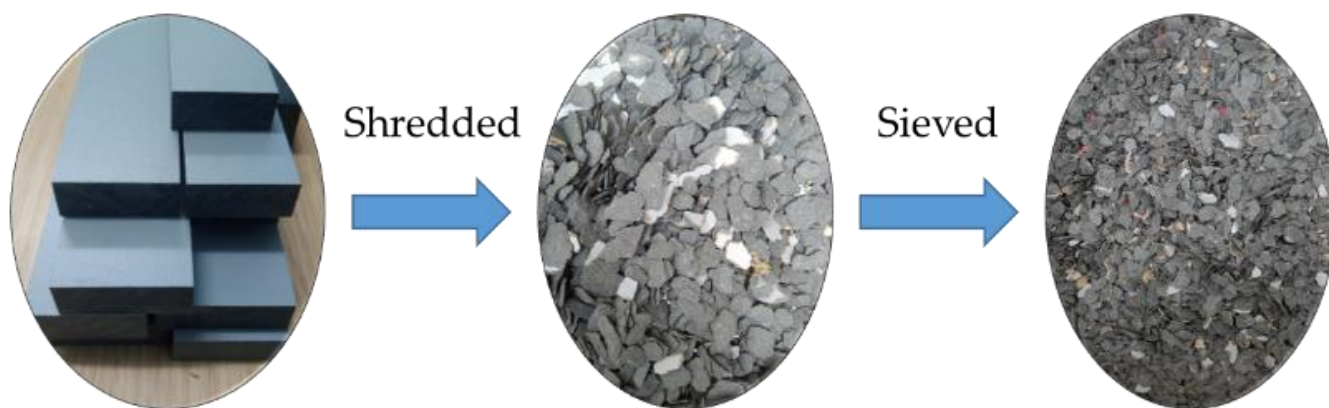


**Figure 5.2** Pretreatment of Solid Grade Laminate

## 5.1.2 Feedstock characterization

### 5.1.2.1 Proximate analysis

A small sample size of approximately 20 mg was subjected to pyrolysis via Thermogravimetric Analysis (TGA) under a  $N_2$  atmosphere to determine its proximate composition in terms of moisture, volatiles and fixed carbon content. The sample was also tested under TGA combustion to determine its total ash content. The instrument used for TGA was a NETZSCH TG 209 F1 heating up to a maximum temperature of  $900 \pm 10$  °C for both TGA pyrolysis and combustion, with heating rate of 10 K/min, and a total flowrate of purge gas of 50 ml/min (according to BS EN 15148:2009).

### 5.1.2.2 Ultimate analysis

The SGL was sent to an external accredited laboratory, Medac Ltd, where the elemental content was quantified. Carbon, Hydrogen, Nitrogen, Sulphur and Oxygen (CHNSO) content was analysed using the CHN and Eltra Helios (S) analysers following the ISO 16948:2015 and ISO 16994:2016 standards. The oxygen was then determined by difference, once computed the ash content deriving from TGA.

### 5.1.2.3 HHV

The HHV is determined using the unified correlation for fuels (**equation 5.1**) developed by Channiwala et al. [5.1], starting from carbon, hydrogen, sulphur, oxygen, nitrogen and ash weight fraction, respectively:

$$HHV [MJ/kg] = 0.341 (C) + 1.1783 (H) + 0.1005 (S) - 0.1034 (O) - 0.0151 (N) - 0.0211 (A) \quad (5.1)$$

### 5.1.3 TCR experimental procedure

This section explains how the TCR experiments were performed, specifying both the type of equipment used and the experimental procedure.

#### 5.1.3.1 TCR setup

The TCR-2 bench scale reactor (**Figure 5.3**) is located at the University of Birmingham and it has a capacity to process up to 2 kg/h of feedstock. The plant works in an oxygen free environment through applying a nitrogen purge at around 100 mbar gauge inside both the feed hopper (1) and the pyrolysis auger reactor (2), where the temperature can range between 500-700°C. The biomass is manually fed in the reactor. The auger reactor or screw reactor represents a very reliable and affordable solution for pyrolysis thanks to its simplicity of construction and operation [5.2]. It comprises two co-axial rotating screws plugged to two different electrical engines, thus allowing to regulate the rotating speeds independently. Its main function is to improve heat transfer within the reactor and good mixing of char and fresh feedstock inside which improves catalytic cracking. This can also represent an advantage in terms of modularity and avoiding risk of reactor blockage always possible in case there was a single screw. The inner screw conveys the biomass through 1 m in length of the reactor, while the outer screw connects the reactor with the fixed-bed post reformer (3). In the post reformer, the catalytic cracking of vapours and reforming reactions occurs at high temperatures (650-800 °C) between char and pyrolysis vapours to form condensable organic vapours and synthesis gas (or syngas). The solid char is then separated in the cyclone (4), thanks to the combined effect of inertial and gravity forces; while the gas comes through the impinger tube for gas extraction to reach the condensation system. This latter consists of a shell and a tube condenser operating at -5°C (5) and an ice bath cooler (8) where part of condensable gases (oil and water) is collected in a proper

vessel (7). The remaining part of non-condensable gas (syngas) is destined to the filtration system: a scrubber (6) and a series of washing bottles containing biodiesel (9), isopropanol (10) and acetone (11), respectively.

Generally, dust, tars, corrosive compounds (sulphur, chlorine and nitrogen), alkali and heavy metals deriving from wastes or second-generation biomass contaminate syngas produced during the TCR [5.3]. Consequently, liquids in washing bottles act as solvents to clean such contaminants, thus allowing a good accuracy during the gas analysis. Biodiesel is usually used as a trap for heavy hydrocarbons and tars [5.4], while isopropanol and acetone easily dissolve tars [5.5]. Then, the gas runs through the wool bottle (12) that captures further solid particles like particulate and tars. Finally, a gas analyser detects the clean gas before permanent gases are flared with propane (13). The gas analyzer was fitted with an upstream carbon bag filter to protect against harmful contaminants and particulates. To heat up the TCR system, external electrical heating tapes are used. The operating temperature is measured and controlled through several K type thermocouples installed all along the unit. The process control is performed using a Siemens SIMATIC WinCC software developed by Fraunhofer UMSICHT, where the parameters of the unit can be changed offering a wide range of options.

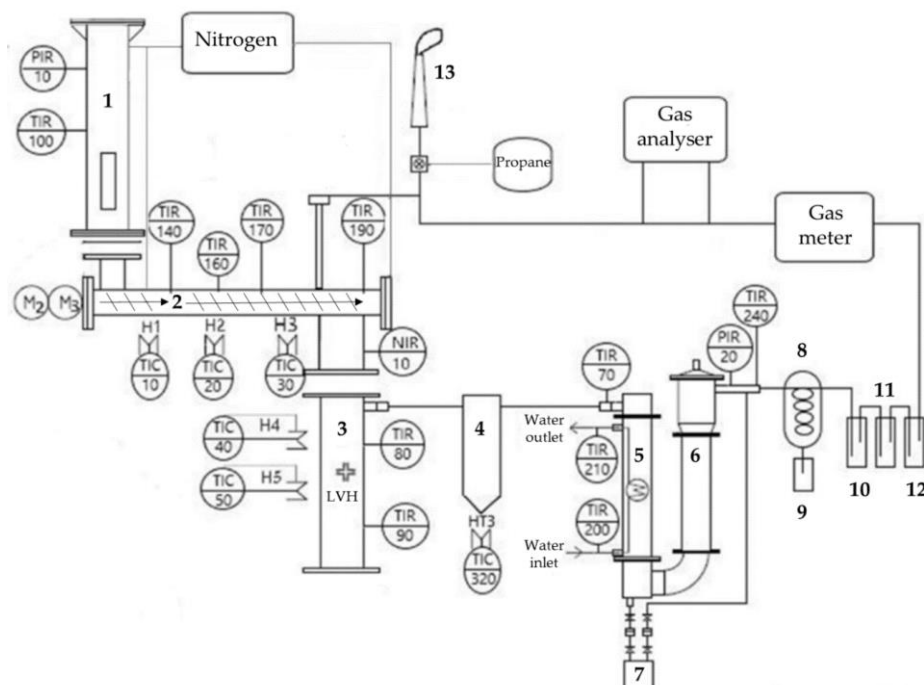


**Figure 5.3** The Process Flow diagram (PFD) of the TCR-2 (2 kg/h): (1) Feed hopper; (2) Auger reactor; (3) Post reformer; (4) Cyclone, (5) Shell and tube heat exchanger; (6) Scrubber; (7) Oil collection vessel; (8) Ice bath; (9) biodiesel wash bottle; (10) Iso-propanol wash bottle; (11) Acetone wash bottle; (13) Flare [5.6].



### 5.1.3.2 TCR methodology

Before running the experiment, the TCR-2 plant was cleaned, closed and flushed with N<sub>2</sub> at 80-100 mbar gauge to remove the oxygen for the pyrolysis process and to test if there was any leakage from the system. Once the gas analyser detected an oxygen content below 0.5% in the plant, the N<sub>2</sub> flow was stopped. During the experiment, the temperature in the auger screw reactor was gradually increased up to 500°C until it reaches the intermediate pyrolysis conditions before the introduction of SGL. In the post reformer stage, the temperature was set to 650 °C. During the heating process, the rotating screws was turned on and the speeds of the inner and outer screws were calibrated to have a residence time of about 40 minutes corresponding to the intermediate pyrolysis condition. Once the TCR reached steady state temperatures, the screw in the auger reactor was stopped and the sealed hopper was opened to feed the plant with 4.6 kg of SGL. Afterwards, the feed hopper was closed, and the unit was flushed again with N<sub>2</sub> to decrease the oxygen below to 0.5%. When the N<sub>2</sub> flow was stopped, the first screw in the auger reactor was turned on to push the biomass along the TCR-2. The formation of the carbonized biomass produced as char in the auger screw reactor promoted an internal catalytic effect improving the quality of the TCR-2 products and avoiding the exit of fine particles and dust from the post reformer. The char formed in the auger reactor was then transported to the post-reformer through the screw. There, the residence time was regulated through the screws speed of the auger reactor. The post reformer had the double function of collecting the char produced from the previous step and enable the conversion of permanent gases into a syngas rich of H<sub>2</sub>, due to the catalytic effect caused by the reactions between the char (with high porosity) and the pyrolysis vapours. During the reforming process, the condensable organic vapours were also catalytically upgraded enhancing their chemical and physical fuel properties. The char rich in carbon and with low hydrogen and oxygen contents remained in the post reformer until the end of the experiment. Subsequently, upgraded organic vapours were quenched at -5°C in the condensing unit to guarantee a complete separation between the pyrolysis liquid and the gas fraction. The pyrolysis oil was collected and stored in an external vessel. Then, the remaining non-condensable vapours passed through the filtration unit for the removal of aerosols, fine particles and other contaminants. The cleaned gas was directly measured and analysed via an online gas analyser.

TCR-2 experiments took around 4 h to be completed and stabilized. The plant worked in a semi-continuous mode with an overpressure of approximately 70-100 mbar controlled by a pressure indicator and the TCR software. The volume of synthetic gases was registered every 10-15 minutes. When no gas production was observed, the experiment was considered concluded and consequently, the heaters and auger reactor screws were switched off. The plant was left to cool down for at least 24 hours. Afterwards the auger pyrolysis reactor was cleaned from unconverted residues via vacuum cleaner. The post reformer was emptied by extracting the solid char produced from the bottom. The dust and fine particles, deriving from char, in the gas tube of the reforming unit were removed manually to prevent blockages in the following trials. Lastly, the condensing unit was cleaned to avoid the contamination between different oils produced in different experiments with different operating conditions. All the products obtained from the cleaning was weighed and included in the mass balance. The washing bottle connected to the ice bath after the condensing unit were refilled with 600-700 ml of biodiesel, isopropanol and acetone. In the filtration unit, activated carbon, candle and glass wool filters were weighed, replaced and connected to the plant again. For the mass balance, all the liquids collection vessels, filters and wash bottles were weighed. Additionally, the char from the post reformer was collected, separated, weighed and a sample was sent for analysis to an external lab. The organics and the aqueous phases of the pyrolysis liquid were separated using a separating funnel. Because of the different densities, the organics remained at the bottom, while the aqueous phase at the top and after 24 h, the organic and aqueous phases were then stored separately, measured and sent for their characterization to an external lab. The permanent gas data were further analysed.

#### **5.1.4 TCR products characterization**

The main products from TCR were char, permanent gas (or syngas) and condensable gas. This latter was a liquid fraction composed of water and organic fractions. In order to separate them, it was left to settle down by gravity for 24 hours using a separating funnel. Because of the different densities, the organic oil remains at the top, while the aqueous phase at the bottom. Then, the pyrolysis liquid was analysed to determine the chemical and physical properties. Char and syngas were also characterized.

#### 5.1.4.1 Oil and char ultimate and proximate analyses

Pyrolysis oil and char samples were analysed externally at MEDAC Ltd, applying the same method as in **section 5.1.2.1** for the determination of the elemental compositions (C, H, N, S and O). Regarding oil, the oxygen was determined by difference as described in the following **equation 5.2**, assuming ash content approximately lower than 0.001 wt%:

$$O \text{ [wt\%]} = 100 - \sum (CHNS + ash) - water \quad (5.2)$$

The water content is computed as it will be illustrated in **section 5.1.4.3**.

Furthermore, Medac Ltd also made a complete CHNSO analysis for char, while the ash content was computed by difference, by reversing **equation 5.2** and neglecting the water content.

#### 5.1.4.2 HHV

The HHV of the bio-oil and char was determined using the unified correlation for fuels as described in **equation 5.1**.

#### 5.1.4.3 Water content

The water content of the raw laminate oil was determined using a Mettler Toledo V20S (**Figure 5.4**) compact volumetric Karl Fischer titration in accordance with ASTM E203.



**Figure 5.4** Mettler Toledo V20S [5.7]

#### 5.1.4.4 Viscosity

The dynamic viscosity of oil was tested by IKA ROTAVISC (according to DIN 53019) at temperature of 23.2°C and with a rotational speed of 100 rpm. The instrument, illustrated in **Figure 5.5**, measured the resistance of the oil to flow when an external (rotational) force was applied, without considering the fluid density (or the inertial force).



**Figure 5.5** IKA ROTAVISC viscosimeter [5.8]

#### 5.1.4.5 Density

The pyrolysis oil density was measured by Academy Glass Measuring Cylinder (Figure 5.6) at 20 °C having a total volume of 100 ml and a tolerance of  $\pm 1.0$  ml.



**Figure 5.6** Academy Glass Measuring Cylinder 100 ml $\pm$ 1.0 ml [5.9]

#### 5.1.4.6 Gas Chromatography/Mass Spectrometry (GC-MS)

The chemical compounds of the oil were detected by GC-MS Agilent 8890 (**Figure 5.7**) using H<sub>2</sub> as a carrier gas. The oil sample was dissolved in dichloromethane (DHM) solution. The concentration of oil was 1% in the total solution. Afterwards, the compounds were identified by library searches (NIST libraries).



**Figure 5.7** GC-MS Agilent 8890 [5.10]

#### 5.1.4.7 Gas analysis

The produced pyrolysis gas was frequently measured and analysed using a Pollutek GAS 3000P Syngas Analyser (**Figure 5.8**). The measurement principle of the gas analyser is based on Non dispersive Infrared (NDIR) sensor (CO, CO<sub>2</sub>, CH<sub>4</sub>, CnHm), a thermal conductivity sensor TCD (H<sub>2</sub>) and an electron capture (ECD) detector (O<sub>2</sub>) [5.11].



**Figure 5.8** Pollutek GAS 3000P Syngas Analyser [5.11]

### 5.1.5 Hydrotreatment methodology

The experimental methodology for hydrotreatment of raw laminate oil comprised four steps as follows:

1. Activation of catalysts TK-341
2. Hydrodeoxygenation (HDO)
3. Activation of catalysts TK-932
4. Hydrocracking (HC)

Both HDO and HC occurred in the presence of catalysts in the Parr stirred series 4560 reactor (or autoclave) [5.12] represented in **Figure 5.9** and installed at the Birmingham Energy Innovation Centre (BEIC). The system was connected to the external tank (1) and hydrogen was used as carrier gas to pressurise the reactor (7) by setting pressure through manometer (2) and inlet valve (3). The outlet valve (4) was used to purge out the remaining oxygen from the reactor. The motor (5) and the electric heater (6) were required to put in motion and heat the reactor, respectively. The controller (8) monitored both speed and temperature.

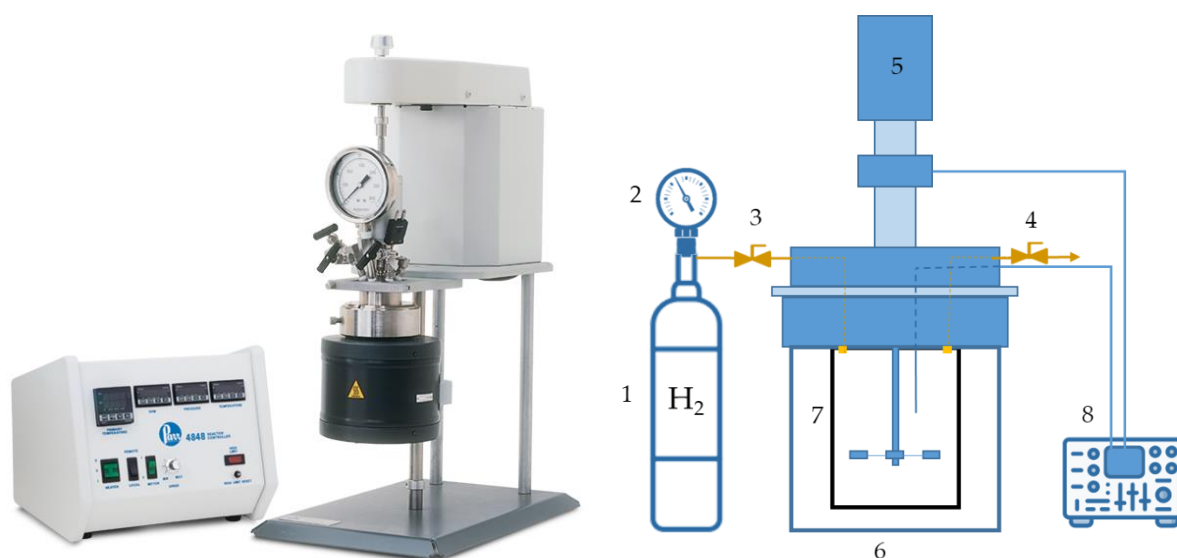


**Figure 5.9** Series 4560 Mini Reactor on the left [5.12] and its setup diagram on the right: (1) hydrogen tank; (2) manometer; (3) inlet valve; (4) outlet valve; (5) motor; (6) electric heater; (7) reactor; (8) temperature and motor control

The choice of the catalysts is crucial to avoid the hydrogenation of aromatics in the bio-oil, which would lead to higher hydrogen consumption and even lower octane

number of the fuel [5.13]. Moreover, high pressures are essential to avoid evaporation of water [5.14] and remove the liquid product more easily.

In this research, the catalysts used for HDO and HC were TK-341 and TK-932 (**Figure 5.10**), respectively, both supplied by Haldor Topsoe Green Fuels Research.

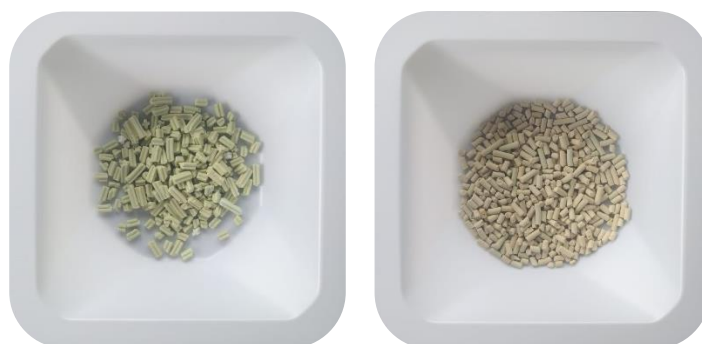


**Figure 5.10** Catalysts used for HDO (on the left) and for HC (on the right)

For the first activation phase, TK-341 HDO catalyst was dried at 105 °C by Sartorius MA 160 until all moisture (1.33%) was removed after 4 minutes and 30 seconds.

10 g of the dried catalyst was weighed and then added to the reactor along with 10 ml of DMDS measured using a Sartorius pipette.

Afterwards, the reactor was pressurised up to 30 bar using hydrogen after all oxygen was purged from the reactor and heated up to 350 °C, which represents the upper limit of temperature for the autoclave [5.12].

It was also found that the stabilization step before HDO shows good characteristics of temperature and pressure equal to 350°C and 100 bar, respectively [5.15].

The reactor reached 350°C after approximately 40 minutes showing a pressure of 77 bar. From now on, the catalyst was maintained for 4 hours under these conditions, which corresponds well to the recommendation for catalyst activation from the manufacturer. Once complete, the autoclave's motor and heater were stopped, the reactor was cooled, and eventually the remaining gases in the reactor were purged out.

After the activation, 100 ml of raw oil derived from TCR and measured using a cylinder, was added to 10 g of the activated and stable catalyst in the reactor and the HDO reaction conditions were set. The reactor was pressurised up to 50 bar using hydrogen after all oxygen was purged from the reactor and heated up to 350 °C. It reached 350°C after 30 minutes showing a pressure of 121 bar. Under these conditions, HDO took place for 4 hours.

The second activation involved 10 mg of TK-932 catalyst, which was dried at 105°C by Sartorius MA 160 until all moisture (0.89%) had been removed after 4 minutes and 12 seconds.

Akin to what occurred in the first activation, the catalyst was mixed with 10 ml of DMDS in the reactor, pressurized at 30 bar and heated at 350°C maximum.

After 30 minutes, the reactor reached the desired temperature with pressure of about 80 bar, thus enabling the activation reactions for 4 hours.

The final step of hydrotreatment is the hydrocracking obtained by mixing 50 ml of HDO oil reacting with 5g of activated HC catalyst.

The reactor was pressurized at 50 bar and heated up at 350°C. After 30 minutes, the reactor reached the desired temperature with pressure of about 98 bar, thus enabling the activation reactions for 4 hours.

For sake of clarity, **Figure 5.11** illustrates the experimental methodology for the hydrotreatment of laminate oil.

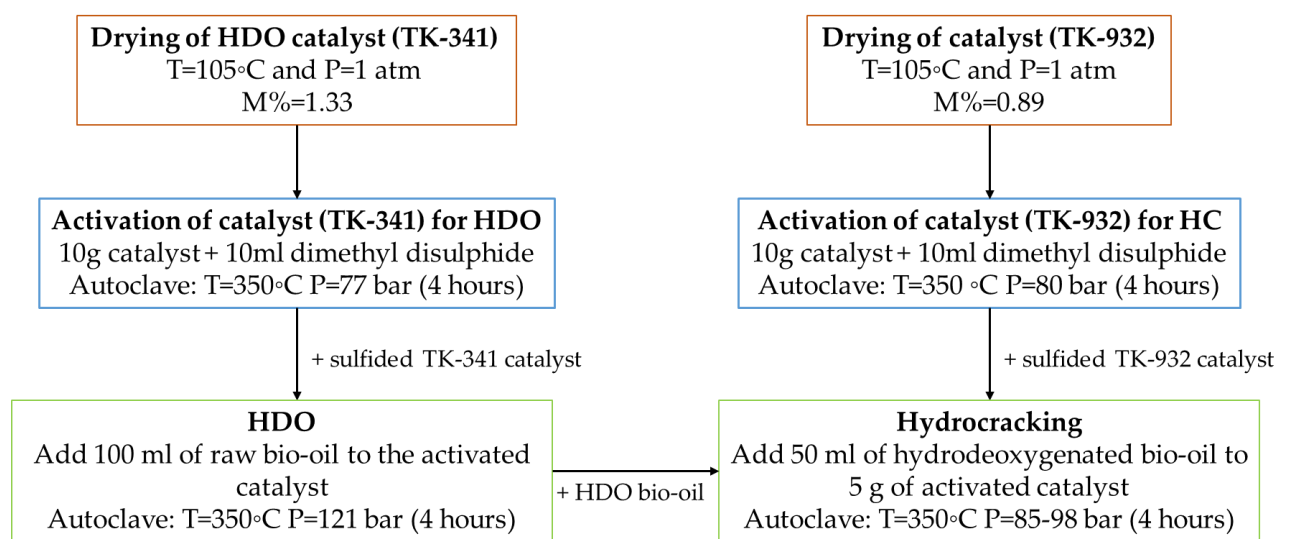


**Figure 5.11** Experimental methodology for the hydrotreatment of laminate oil

#### 5.1.5.1 Ultimate and proximate analysis

The oils (1.5ml) deriving from both the HDO and HDO and HC were analysed as described in **section 5.1.2.1 and 5.1.2.2**.

#### 5.1.5.2 HHV

The HHV of the bio-oil and char was determined using the unified correlation for fuels as described in **section 5.1.2.3**.



#### *5.1.5.3 Water content*

The water content presents in the hydrotreated oil was measured by difference, neglecting ash content, as a first approximation.

#### *5.1.5.4 Gas Chromatography/Mass Spectrometry (GC-MS)*

The GC-MS of the hydrodeoxygenated and hydrocracked oil were determined using the same methodology described in **section 5.1.4.6**.

#### *5.1.5.5 Density*

The hydrotreated oil density was measured as described in **section 5.1.4.5**.

## 5.2 Carbon Fibres

### 5.2.1 Feedstock pretreatment

The feedstocks received from Gen2Carbon (about 10 kg) was dry carbon fibers (**Figure 5.12**) containing an initial moisture content of 0.49wt% and reinforced with epoxy resin.



**Figure 5.12** Carbon fibres

Due to the low density and sizes greater than the optimal values of 20-30 mm in length and 5-20 mm in width requested for TCR, it was first necessary to pre-treat carbon fibres by further shredding and sieving them. Carbon fibres were shredded down by the HECHT 6420 device and further sieved with a sieve, having a mesh size of around 10 mm, in order to properly feed TCR-2 bench-scale reactor. The shredded and sieved material is shown in **Figure 5.13**.



**Figure 5.13** Carbon Fibre resulting from shredding and sieving

## 5.2.2 Feedstock characterization

### 5.2.2.1 Proximate analysis

A small sample size of approximately 10 mg was subjected to Thermo Gravimetric Analysis (TGA) pyrolysis under a N<sub>2</sub> atmosphere to determine its proximate composition in terms of moisture, volatiles and fixed carbon content. The sample was also subjected to TGA combustion to determine its total ash content.

The instrument used for TGA was a NETZSCH TG 209 F1 device heating up to a maximum temperature of  $900 \pm 10$  °C for both TGA pyrolysis and ashing, with heating rate of 10 K/min, total flowrate of purge gas of 50 ml/min (according to BS EN 15148:2009).

### 5.2.2.2 Ultimate analysis

The sample was sent to an external accredited laboratory, Medac Ltd, where the elemental content was quantified. Carbon, Hydrogen, Nitrogen, Sulphur and Oxygen (CHNSO) content was analysed using the CHN and Eltra Helios (S) analysers following the ISO 16948:2015 and ISO 16994:2016 standards. Then, oxygen content was calculated by difference.

### 5.2.2.3 HHV

The HHV of carbon fibres was determined using the unified correlation for fuels as described in **section 5.1.2.3** for solid grade laminate.

## 5.2.3 TCR experimental procedure

The following section only illustrates details about the TCR methodology for carbon fibres, as the TCR setup was already described in **section 5.1.3.1**.

### 5.2.3.1 TCR methodology

As already known, TCR technology is the combination of intermediate pyrolysis and catalytic reforming. The former occurred in the auger screw reactor by heating gradually the carbon fibers in the absence of oxygen at pyrolytic temperature of 600°C. The catalytic cracking of pyrolysis vapours, using char as catalyst, took place in a fixed-bed post reformer at higher reforming temperature equal to 680°C, to promote the formation of syngas and further cracking of volatile organic compounds. In order

to decrease the oxygen content in the reactor during the pyrolysis, the unit was flushed with N<sub>2</sub> at around 100 mbar.

About 1 kg of carbon fibres was tested for 6 hours and the plant subsequently was left to cool down due to the blockage of the reactor hopper shown in **Figure 5.14**. This result implies the necessary to gradually feed the system with small quantities of pelletized material, in order to reduce the risk of blockages, alternatively significant modifications to the reactor feeding system would be required to fully process this type of low-density feedstock.



**Figure 5.14** Carbon Fibres blocked in the hopper

The reactor was then cleaned by removing the carbon fibers from the hopper. Afterwards, the final products were collected from the plant for their final characterization.

#### **5.2.4 TCR products characterization**

The collectable products were syngas, oil and char. This latter was obtained as non-homogeneous material made of resin-bonded and non-bonded char. All of them were characterized as described in the following sections.

##### *5.2.4.1 Oil and char ultimate and proximate analyses*

The elemental composition in terms of carbon, hydrogen, nitrogen, sulphur and oxygen content in pyrolysis oil and both types of char were analysed by Medac Ltd. Regarding proximate analysis, only ash and HHV were computed. For both resin-bonded and non-bonded chars, ash content was derived by difference considering

water content negligible. For pyrolysis oil, ash content was neglected, while water content was computed by difference as described in **section 5.2.4.3**.

The HHV of both oil and char was described in **section 5.2.4.2**.

#### *5.2.4.2 HHV*

The HHV of carbon fibres oil and chars was determined using the unified correlation for fuels as described in **section 5.1.2.3**, assuming neglectable the ash content for oil and water content for char.

#### *5.2.4.3 Water content*

The water content of pyrolysis oil was computed by difference by reversing **equation 2** and neglecting the ash content.

#### *5.2.4.4 Viscosity*

Unfortunately, the amount of oil deriving from TCR was not sufficient to be further analysed in terms of viscosity.

#### *5.2.4.5 Density*

Because of the scarcity of oil, it was not possible to measure its density.

#### *5.2.4.6 Gas Chromatography/Mass Spectrometry (GC-MS)*

The GC-MS of the pyrolysis oil was determined using the same methodology described in **section 4.2.4.6**.

#### *5.2.4.7 Gas analysis*

Even if the volume of synthetic gases were registered every 10-15 minutes by using a Pollutek GAS 3000P Syngas Analyser, it was difficult to consistently represent the distribution of syngas during the entire experiment.

#### *5.2.4.8 SEM analysis of char from Carbon Fibres*

The original feedstock and the two types of chars obtained from TCR were analysed by Hitachi Tabletop Microscope TM3030 series (**Figure 5.15**) to get topographical information (Secondary Electron or SE signal) of their surface. All samples were

magnified by 1000x with accelerating voltage of 5kV, which allowed a good observation of these specimens.



**Figure 5.15** Hitachi Tabletop Microscope TM3030 series [5.16]

## References

- [5.1] S.A. Channiwala, P.P. Parikh, A unified correlation for estimating HHV of solid, liquid and gaseous fuels, *Fuel* 81 (2002) 1051-1063;
- [5.2] F. L. P. Resende, Chapter 1 - Reactor configurations and design parameters for thermochemical conversion of biomass into fuels, energy, and chemicals, *Reactor and Process Design in Sustainable Energy Technology*, 2014, Pages 1-25;
- [5.3] Gas analysis in gasification of biomass and waste, *IEA Bioenergy*, 2018;
- [5.4] J.P.A. Neeft, H.A.M. Knoef, G.J. Buffinga, U. Zielke, K. Sjöström, C. Brage, P. Hasler, P.A. Smell, M. Suomalainen, M.A. Dorrington, C. Greil A.V. Bridgwater (Ed.), *Progress in Thermochemical Biomass Conversion* (2008);
- [5.5] A. Paethanom, S. Nakahara, M. Kobayashi, P. Prawisudha, K. Yoshikawa, Performance of tar removal by absorption and adsorption for biomass gasification, *Fuel Processing Technology*, Volume 104, December 2012, Pages 144-154;
- [5.6] A. Fivga, H. Jahangiri, M.A. Bashir, A.J. Majewski, A. Hornung, M. Ouadi, *Journal of Analytical and Applied Pyrolysis*, 146 (2020), 104773;
- [5.7] Available online: [https://www.mt.com/ch/it/home/products/Laboratory\\_Analytics\\_Browse/Product\\_Family\\_Browse\\_titrators\\_main/Karl\\_Fischer\\_Titration/V20S\\_Volumetric\\_KF\\_Titrator.html](https://www.mt.com/ch/it/home/products/Laboratory_Analytics_Browse/Product_Family_Browse_titrators_main/Karl_Fischer_Titration/V20S_Volumetric_KF_Titrator.html) (accessed on 26/10/2022);
- [5.8] Available online: <https://www.ika.com/en/Products-Lab-Eq/Viscometers-csp-279/> (accessed on 26/10/2022);
- [5.9] Available online: <https://www.betterequipped.co.uk/academy-measuring-cylinder-round-base-100ml-8078> (accessed on 26/10/2022);
- [5.10] Available online: <https://www.agilent.com/cs/library/brochures/brochure-gc-8890-5994-0476en-agilent.pdf> (accessed on 26/10/2022);
- [5.11] Available online: <http://www.pollutek-gasanalysis.com/files/Portable-GAS-3100P-Syngas-Analyser---EN17v3.pdf> (accessed on 14/06/2022);

- [5.12] Available online: <https://www.parrinst.com/products/stirred-reactors/series-4560-100-600-ml-mini-reactors/> (accessed on 23/05/2022);
- [5.13] R. Lødeng, L. Hannevold, H. Bergem, M. Stöcker, Chapter 11 - Catalytic Hydrotreatment of Bio-Oils for High-Quality Fuel Production, Elsevier, 2013, Pages 351-396;
- [5.14] Z. Xiaojie, K. Mukherjee, S. Manna, M. K. Das, J. K. Kim, T. K. Sinha, Chapter 24 - Efficient management of oil waste: chemical and physicochemical approaches, Advances in Oil-Water Separation A Complete Guide for Physical, Chemical, and Biochemical Processes 2022, Pages 439-467;
- [5.15] Available online: <https://www.topsoe.com/our-resources/knowledge/our-products/catalysts/tk-341?hsLang=en> (accessed on 23/05/2022);
- [5.16] Available online: [https://www.hitachi-hightech.com/file/us/pdf/library/literature/TM3030\\_brochure\\_letter.pdf](https://www.hitachi-hightech.com/file/us/pdf/library/literature/TM3030_brochure_letter.pdf) (accessed on 26/10/2022).



## 6. Results and discussions

### Chapter summary

This chapter describes the characterization of the original feedstocks and the products obtained from the conversion of solid grade laminate (SGL) and carbon fibres (CF). Their preliminary characterization was necessary in order to determine their feasibility to be processed in the thermo-catalytic reformer (TCR). As previously mentioned, the feasibility of feedstocks depends on several key parameters including both the physiochemical properties and the operating conditions. All the analyses demonstrate the TCR efficiency in producing both solid, gaseous and liquid fuels from SGL and CF at the end-of-life.

### 6.1 Solid Grade Laminate

#### 6.1.1 Feedstock characterization

##### 6.1.1.1 Proximate and ultimate analyses of SGL

Chemical properties of SGL can be analysed through proximate and ultimate analyses. As already mentioned, the proximate analysis consists of the evaluation of moisture content, ash content, volatile matter, fixed carbon and the higher heating value (HHV); while the ultimate analysis is defined as the determination of carbon, hydrogen, nitrogen, sulphur and oxygen contents. Both analyses allow to determine if feedstock can be used as a fuel in the energy conversion processes (i.e. combustion, co-combustion, incineration) or if it can be used to get value-added by-products like gaseous or liquid fuels. The results of proximate and ultimate analyses of SGL are presented in **Table 6.1**.

**Table 6.1** Proximate and Ultimate Analysis of Solid Grade Laminate

	Units	Result
<b>Proximate Analysis</b>		
Moisture	wt%	1.5
Volatiles	wt%	63.2
Fixed Carbon	wt%	31
Ash	wt%	4.3
HHV	MJ/kg	18.6
<b>Ultimate Analysis</b>		
C	wt%	44.4
H	wt%	5.9

N	wt%	7.8
S	wt%	0.48
O*	wt%	35.62

\*calculated by difference

Both the nitrogen and sulphur contents give information about the possible formation of SO<sub>x</sub> and NO<sub>x</sub> emissions during the thermochemical process (e.g. pyrolysis and gasification). Lower values of sulphur and nitrogen correspond to lower emissions. Nitrogen is an inert element, meaning that it does not react during the conversion process and it can create a free-oxygen environment during the pyrolysis. Furthermore, NO<sub>x</sub> deriving from TCR are not expected, as temperatures are under the threshold required for their formation. Eventually at large scales, SO<sub>x</sub> and NO<sub>x</sub> emissions are easily removed in the downstream gas cleaning system by using scrubbers. If compared with wood biomass, Nitrogen and Sulphur were found to be high for this feedstock; it is approximately 4x higher for Nitrogen and 5x higher in terms of Sulphur content [6.1]. The ultimate analysis shows that the initial atomic O/C and H/C ratios of SGL are 0.6 and 1.59, respectively. These values are reported in the Van Krevelen diagram illustrated in **Figure 6.1**. This shows the degree of stability of the feedstock in terms of char decomposition, in comparison with other biomasses. It is noted that SGL belongs to the biomass area with values of O/C ratio comparable with those of wood, but with higher values of H/C ratio.

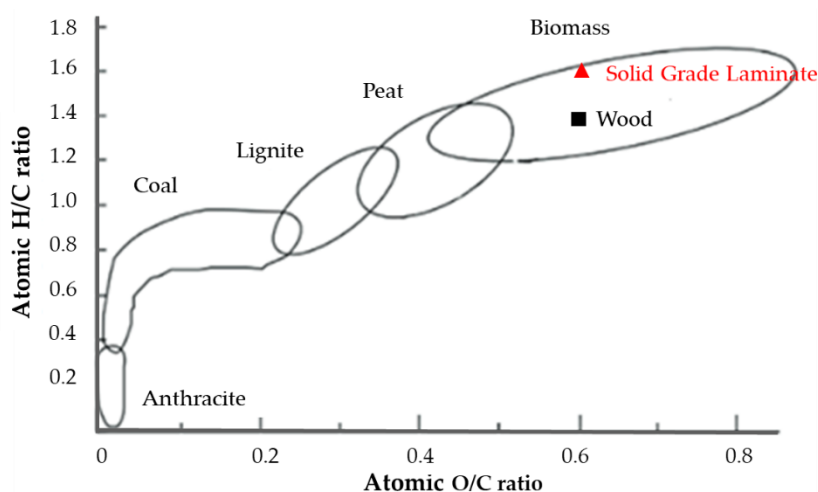


**Figure 6.1** The Van Krevelen [6.2] diagram of Solid Grade Laminate

The thermal behaviour of a small SGL sample size of approximately 20 mg was investigated in the Thermo-Gravimetric Analysis (TGA) of pyrolysis under a N<sub>2</sub> atmosphere to determine its proximate composition in terms of moisture, volatiles and

fixed carbon content. The sample was also subjected to TGA of combustion under air conditions to determine its total ash content.

The TGA profiles for both the pyrolysis and combustion as a function of temperature are shown in **Figure 6.2** and **Figure 6.3**, respectively.

The results in **Figure 6.2** show a weight loss of 1.5% in moisture from ambient temperature (25°C) to 105°C. In the range between 150°C and 210°C, there is another mass change of 7.41%, attributed to the volatilization of Kraft paper. This value fits well with literature which also suggests that Kraft paper releases volatiles starting from 150 °C [6.3]. Most volatiles are released between 240°C up to 390°C, which contributes to approximately 36.36% in weight loss. This result also matches the degradation temperature of melamine resin whose values are around 250°C and 400°C [6.4]. The peak is between 400°C up to 470°C which corresponds well with the release of phenol resin and cellulose [6.5], [6.6] accounting for 11.42%. The total amount of volatiles released from the biomass is 63.2%.

The fixed carbon is obtained as difference between the total mass and the moisture and volatiles fractions in percentage. It gives information about the amount of char formation in the thermochemical process after the volatiles matter drives off. The value is equal to 31 wt%, meaning that one third of the initial feedstock can be used as char in the post reformer. The objective of using such carbonaceous substance is to exploit its appreciable influence in terms of catalytic action capacity to reform the syngas and produce more hydrogen.

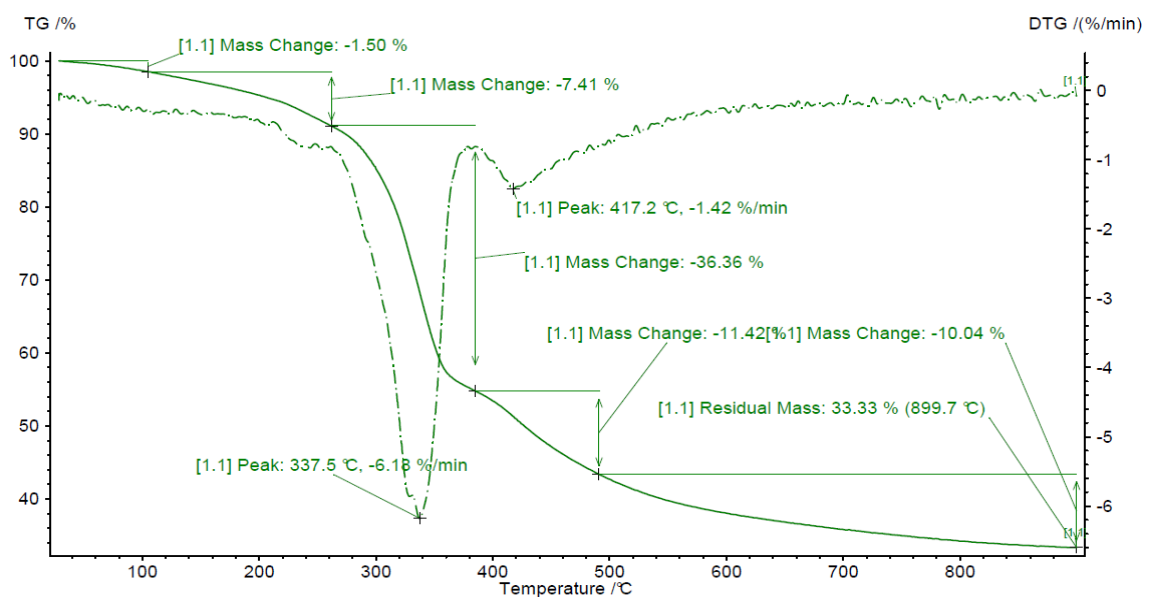


**Figure 6.2** TGA/DTG Pyrolysis Profile Solid Grade Laminate

The results in **Figure 6.3** show a weight loss of 1.62% in moisture from ambient temperature (25°C) to 105°C. In the range between 150°C and 250°C, there is a little drop, corresponding to a mass change of 9.72%, which is attributed to the volatilization of Kraft paper [6.3]. Then, cellulose fibres and volatiles are released between 270°C and 390°C and then again between 400°C and 450°C due to resins content [6.4], [6.5], [6.6] with an overall weight loss of about 51.5%. As soon as the laminate is burnt between 500°C and 600°C under air conditions, fixed carbon is released much faster than that obtained from the pyrolysis trial in the same temperatures range. In this regard, weight loss accounts for 31.32%.

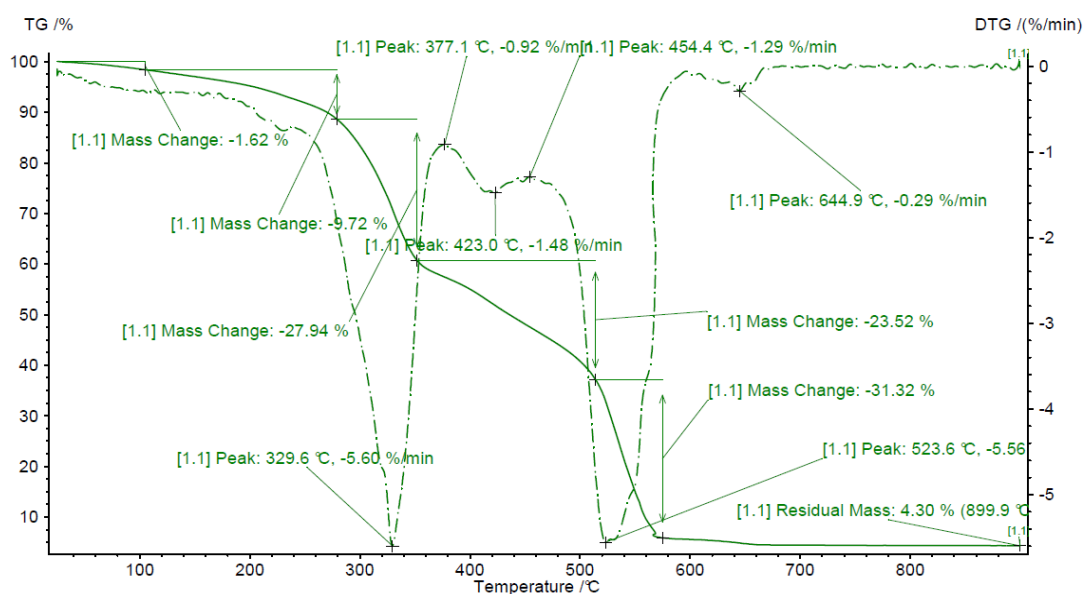


**Figure 6.3** TGA/DTG Ashing Profile Solid Grade Laminate

#### 6.1.1.2 Thermal effect analysis

A qualitative analysis was also investigated in order to determine any melting and heating effects of samples. The solid grade laminate was heated up in the CARBOLITE GERO AAF 1100 furnace. The objective was to carry on six heating ramps (17-250°C, 250-350°C, 350-450°C, 450-550°C, 550-650°C, 650-700°C) with a heating rate of 10°C/min and dwelling time of 15 minutes. The results show a gradual release of both volatiles in air and resins around the crucible's surface. At 700°C, the residual samples appear to be ash.

### 6.1.2 Mass and energy balances for SGL

In order to account for the material conversion during TCR, a mass balance was conducted. It consisted of weighting the initial material and its resulting products deriving downstream from TCR. The final products were char, oil and syngas.

The mass balance for laminate experiments is reported in **Figure 6.4** without considering any mass loss due to errors in measuring weights, non-detectable gases by the gas analyser and the remained oil in the cleaning section. The initial weight of the SGL was 4.6 kg. About 50% of the initial feedstock was comprehensively converted to syngas, 28% to char and 22% to a liquid fraction containing both water and organics.

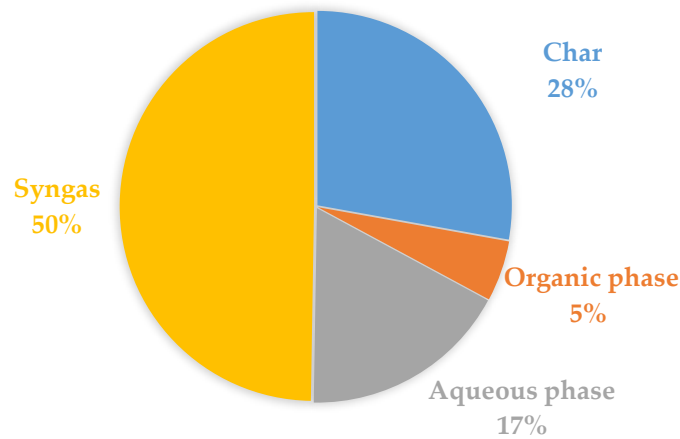


**Figure 6.4** Mass balance of Solid Grade Laminate

The energy balance showed how the energy of the initial feedstock was distributed in time unit among its products during the TCR conversion process and it was computed through the following **equation 6.1**:

$$Q_i [MW] = \sum_i \dot{M}_i \left[ \frac{kg}{s} \right] \cdot HHV_i \left[ \frac{MJ}{kg} \right] \quad (6.1)$$

Where  $Q$  is the output energy power of each  $i$ -th final product (i.e. char, oil and syngas) according to its mass flow rate  $\dot{M}$  and higher heating value (HHV).

For the sake of clarity, the HHV values of the all above-mentioned fuels are reported in **Table 6.2**.

For instance, by comparing laminate oil from TCR with a typical fast pyrolysis oil, the laminate oil has a higher HHV. This is due to the operating conditions used in the different processes. The fast pyrolysis has the same temperature range as the

intermediate pyrolysis as illustrated in **Table 3.1 (Chapter 3)**, but faster heating rates which does not allow sufficient gas residence times for cracking to occur, thus permitting to obtain higher yields of oil. However, TCR includes not only the intermediate pyrolysis but also a further reforming of the gaseous phase. This step helps to improve the quality of products, including the increase of aromatics in the oil. On the contrary, the HHV of laminate oil is lower than that of conventional fuels like heavy oil, gasoline and diesel which have higher aromatics as derived from fossil source.

**Table 6.2** The calorific values of SGL and its products and different liquid fuels

Fuels	HHV [MJ/kg]	Ref.s
Solid Grade Laminate	18.6	TCR results
Char	25.94	TCR results
Syngas	20.07	TCR results
Laminate oil	32.72	TCR results
Typical fast pyrolysis oil	17.0 – 22.5	[6.7]
Heavy oil	41.8	[6.8]
Gasoline	46.4	[6.8]
Diesel	45.6	[6.8]

The mass flow rate  $\dot{M}$  was computed by dividing the mass of each *i*-th product for the experiment time (around 4 hours) as described in **equation 6.2**:

$$\dot{M} = \frac{\text{mass}}{\text{exp time}} \left[ \frac{\text{kg}}{\text{s}} \right] \quad (6.2)$$

According to the energy balance illustrated in **Figure 6.5**, the majority of the energy moves from feedstock to syngas and char with percentage of 56% and 39% respectively. The remaining 5% is characterised by pyrolysis oil. Heat losses and heat input are not considered here, but only the transfer of chemical energy. However, heat input is approximately 16% of total energy from feedstock required for TCR heat demand. These results will be discussed in detail in the following sections.

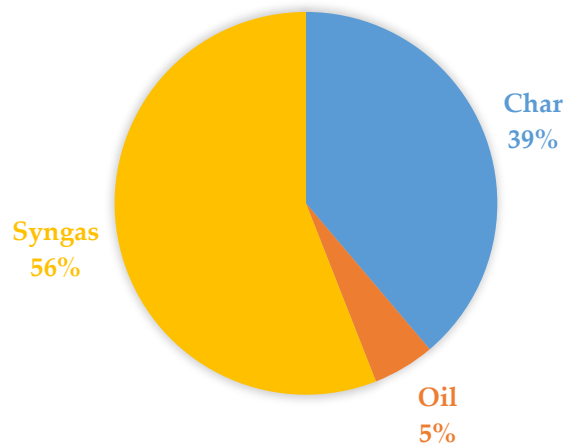


**Figure 6.5** The energy balance of Solid Grade Laminate

In **Figure 6.6**, the Van Krevelen diagram is shown in order to highlight the H/C and O/C ratios of laminate and its products obtained from TCR. Although, both laminate oil and char have approximately the same O/C ratio, meaning that they lost many oxygenated compounds in favour of a major carbonization, the oil shows a greater H/C ratio, due to the presence of a high amount of hydrogen, thus contributing to a better value of its HHV. This is 32.72 MJ/kg, which is almost double that of the original solid grade laminate. The increase of the calorific value is due to the catalytic reforming and cracking occurring in the post reformer. As demonstrated in the literature, the reforming process converts feedstocks in fuel with higher octane numbers, lower oxygen content and tar and more aromatics, thus contributing to get the best properties out of pyrolysis oil [6.9][6.10]. As a matter of fact, a higher-octane number of a fuel leads a less volatility and a major compression [6.11] and the lower oxygen content increases the HHV [6.12].

However, when the laminate oil is compared with conventional heavy fuel oil and fossil fuels, it shows a lower H/C ratio and higher O/C ratio. The presence of oxygen in the laminate oil, which is basically zero in the conventional fuels, influences negatively its HHV. Eventually, the heavy oil, gasoline and diesel have a higher HHV than laminate oil. Their corresponding values are equal to 41.8, 46.4 and 45.6 MJ/kg, respectively [6.8] and are reported in **Table 6.2**. Overall, the laminate oil shows excellent results if compared with typical fast pyrolysis oil from lignocellulosic material, whose O/C and H/C ratio are much higher as reported in **Table 6.2** and illustrated in **Figure 6.6** [6.24].

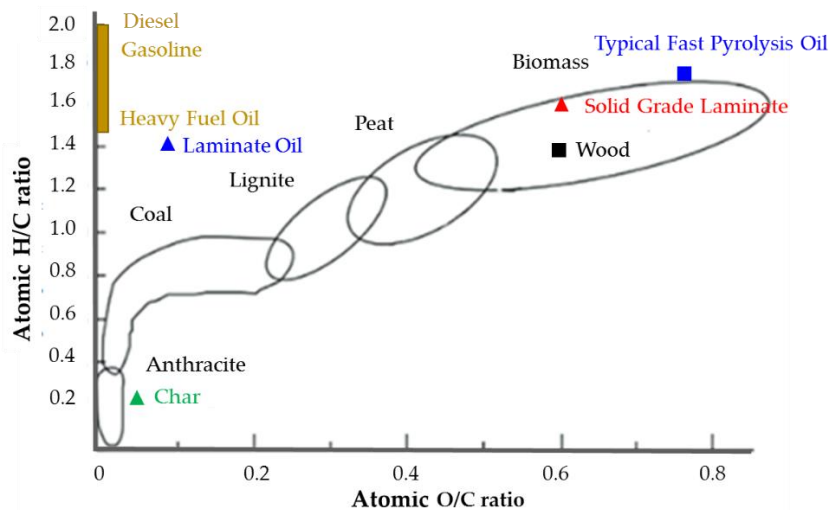


**Figure 6.6** The Van Krevelen diagram [6.2] with the H/C and O/C ratios evaluated for conventional fuels, typical fast pyrolysis oil, wood, SGL and its products from TCR (char and laminate oil)

### 6.1.3 Products characterization

#### 6.1.3.1 Gas analysis

The syngas represents the gaseous fraction made of CO, CO<sub>2</sub>, H<sub>2</sub>, CH<sub>4</sub> and light hydrocarbons (typically consisting of C<sub>1</sub>-C<sub>4</sub>), whose volumes were recorded during the TCR process and then normalised with respect to the volume of oxygen and nitrogen, as shown in **Figure 6.7**. Hydrogen represents almost 50% in volume of the syngas, while carbon monoxide, carbon dioxide, methane stands between 15 and 25% in volume and the light hydrocarbons fraction was considered negligible (**Figure 6.7**).

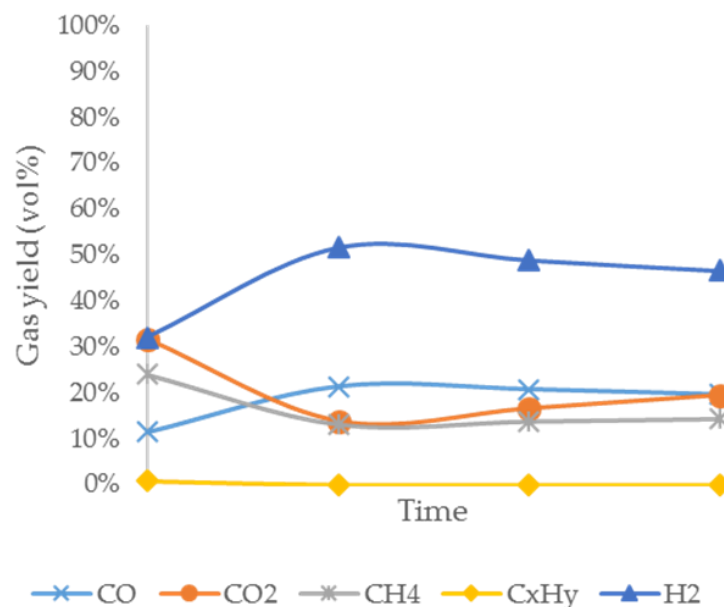


**Figure 6.7** Gas analysis over time during TCR experiment



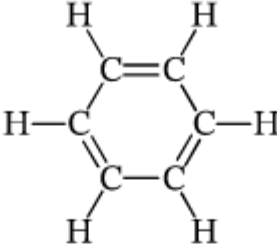
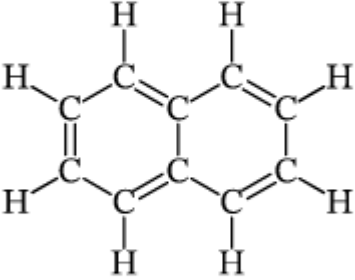
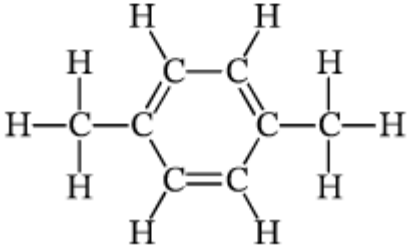
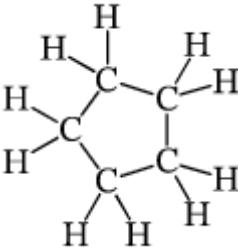
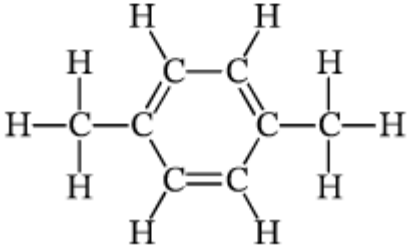
However, the behaviour of gases does not look like the same over the time. Indeed, there is a time interval where H<sub>2</sub> and CO reach the maximum, whilst CO<sub>2</sub> and CH<sub>4</sub> have a minimum. The reason of such a pattern might be related to the pyrolysis temperature. Although it was set on 500°C, the volatiles that are released during the exothermic phase of pyrolysis increase the temperature. It is believed that the increase of temperature is due on that range as it is experimentally expected the volumes of CO<sub>2</sub> and CH<sub>4</sub> decrease, allowing H<sub>2</sub> and CO to increase. Additionally, the higher pyrolysis temperature inhibits the degradation of hemicellulose and cellulose, thus reducing the formation of CO<sub>2</sub> that could be released by the cracking of carboxyl and carbonyl compounds. On the contrary, the lignin could be easily decomposed at higher temperature, thus releasing much more hydrogen deriving from its aromatic ring and methyl group [6.13][6.14]. Finally, the increase of CO could be also related to all endothermic reactions occurring at higher temperatures and reported in the following **Table 6.3**:

**Table 6.3** Reactions during pyrolysis

Reaction	Equation	$\Delta H^\circ$ [KJ mol <sup>-1</sup> ]
Steam reforming: CH <sub>4</sub>	$CH_4 + H_2O \leftrightarrow 3H_2 + CO$	206.2
Water gas (primary reaction) shift	$C + H_2O \leftrightarrow H_2 + CO$	131.3
	$C + 2H_2O \leftrightarrow 2H_2 + CO_2$	90.1
Boudouard	$C + CO_2 \leftrightarrow 2CO$	172.5

Phenolic resin could also play a role during such a process. As demonstrated in [6.15], the pyrolysis of phenolic resin occurs in three major stages. The first stage (T=300-500°C) is characterised by both the formation of additional crosslinks between aromatic rings and the production of similar yields of water and low molecular weight substances (i.e. phenol and cresol). During the second stage (400-800°C), crosslinks begin to break and disappear. Especially, aliphatic carbon-hydrogen bonds concentration decreases in favour of a major ring-related aromatic carbon-hydrogen bonds. Example of aliphatic and aromatic hydrocarbons are shown in **Table 6.4**. As a result, the amount of water decreases, whilst hydrogen production increases. Also, methane, carbon monoxide and small amounts of carbon dioxide and ethane are formed. Finally, the third stage (T=560-900°C), the products evolve predominantly in hydrogen with some carbon monoxide and water, and a small amount of carbon dioxide.

**Table 6.4** Example of aliphatic and aromatic hydrocarbons

Aliphatic hydrocarbons	Aromatic hydrocarbons
$  \begin{array}{cccc}  & \text{H} & \text{H} & \text{H} & \text{H} \\  &   &   &   &   \\  \text{H} & -\text{C} & -\text{C} & -\text{C} & -\text{C}-\text{H} \\  &   &   &   &   \\  & \text{H} & \text{H} & \text{H} & \text{H}  \end{array}  $ <p style="text-align: center;">Alkane</p>	
$  \begin{array}{ccc}  & \text{H} & \text{H} & \text{H} \\  &   &   &   \\  & \text{C} & =\text{C} & -\text{C}-\text{H} \\  &   & &   \\  & \text{H} & & \text{H}  \end{array}  $ <p style="text-align: center;">Alkene</p>	
$  \begin{array}{cccccc}  & \text{H} & \text{H} & & \text{H} & \text{H} \\  &   &   & &   &   \\  \text{H} & -\text{C} & -\text{C} & -\text{C}\equiv\text{C} & -\text{C} & -\text{C}-\text{H} \\  &   &   & &   &   \\  & \text{H} & \text{H} & & \text{H} & \text{H}  \end{array}  $ <p style="text-align: center;">Alkyne</p>	
 <p style="text-align: center;">Cycloalkane</p>	

Another possible explanation for such a behaviour of gases could be due to the stabilisation time of TCR reactor. In fact, the post-reformer needed time to collect char and reformat the gas during the whole process. Consequently, more oil and less syngas were expected at the beginning because of the low char content in the post-reformer. Later, the increase of char led to H<sub>2</sub> and CO formation resulting from

reforming reactions. Once the char was stabilised in the post-reformer, catalytic reactions occurred, thus increasing CH<sub>4</sub> and CO<sub>2</sub> yields [6.16] [6.17].

Afterwards, the behaviour appears stationary, with values constant until the end of the experiment.

Regarding HHV of the syngas, since CO, H<sub>2</sub>, CH<sub>4</sub> are combustible gases, its value is 20.11 MJ/kg computed by difference after the energy balance through the reversed **equation 6.3**:

$$HHV_{syngas} \left[ \frac{MJ}{kg} \right] = \frac{Q_{syngas} [MW]}{Mass\ flow\ rate_{syngas} \left[ \frac{kg}{s} \right]} \quad (6.3)$$

Where Q is the energy per time unit deriving from syngas formed in the post reactor.

#### 6.1.3.2 Char analysis

The char (**Figure 6.8**) intended as a residual mass (ash included) represents the 28% of the initial feedstock. The amount of solid carbon formed during TCR process was lower than during pure pyrolysis as shown in **Figure 6.1**. This was due to both the longer residence time in TCR and the continuous contact with syngas and vapours where carbon was gasified, thus reacting with H<sub>2</sub>O and CO<sub>2</sub> accordingly to reactions in **Figure 6.3**. Char is a carbonaceous high-molecular-weight residue with ash, inert material and metals and it can be used as a catalyst, as it exhibits catalytic activity favouring higher yields of non-condensable gases [6.18]. The catalytic effect of char is used not only for tar cracking, but also to de-oxygenate volatile compounds. This is especially true when using high ash-containing feedstocks such as sewage sludge and de-inking sludge [6.19][6.20]. These results were investigated in a patented Pyroformer whose patents are reported in [6.21][6.22].



**Figure 6.8** Char of Solid Grade Laminate

The characteristics of the produced char are reported in **Table 6.5**. As expected, only carbon and ash contents increased with respect of the initial feedstock, by 1.6 and 4.7 respectively, while the remaining elements decreased. From the energy point of view, the calorific value of char is equal to 25.94 MJ/kg, which is about 30% more than the initial HHV of laminate (18.6 MJ/kg). This result suggests its potential use as a fuel in other thermal and thermochemical process like combustion, co-combustion or gasification to produce a tar-free syngas.

Other potential purposes are its application as a soil amendment or as an adsorbent material. Indeed, char can remain in the soil for years due to its high stability, thus improving the soil quality. However, its composition should be analysed in order to avoid the release of toxic compounds or other negative impacts in terms of soil properties variations, even though char from TCR experiment is stable.

Finally, char can be used as adsorbent to remove pollutants, heavy metals or contaminant gases [6.23].

**Table 6.5** Laminate Char characterization

	Units	Result
<b>Ultimate Analysis</b>		
C	wt%	71.83
H	wt%	1.56
N	wt%	1.49
S	wt%	<0.10
O	wt%	5.09
Ash*	wt%	20.03
HHV	MJ/kg	25.94

\*Calculated by difference

#### 6.1.3.3 Oil analysis

The liquid products (oil and water) accounting for 22% of the weight and deriving from TCR, were left to settle for 24 hours to separate water from the organics and a clear phase separation was observed. Afterwards, both were weighted, and the percentages of oil and aqueous phase were 5% and 17%, respectively, as shown in **Figure 6.9**. The oil yield from laminate was slightly lower than that obtained from TCR trials with sugarcane bagasse, oat hulls, sewage sludge at the same pyrolysis temperatures [6.24], [6.25]. However the oil yield is expected to decrease, as the reforming temperature increases for sugarcane bagasse and oat hulls, since other

volatiles are released during the reforming step, thus enhancing the syngas yield as demonstrated in [6.26]. To target increased yields of oil formation as opposed to syngas the TCR process would implement a lower reforming temperature and use of externally sourced catalysts such as steel slag [6.16][6.25] which has been found to lower reforming temperatures whilst retaining high yields of hydrogen production.



**Figure 6.9** Aqueous phase (on the left) and organic phase (on the right) of SGL

After the separation, the 5wt% of oil from laminate was analysed in the lab of the Birmingham Energy Innovation Centre (BEIC). Its water content was equal to 7.21% on average resulting about 2-4 times lower than common fast pyrolysis bio-oils [6.27]. This result remarks that heating value is significantly higher than other bio-oils, even though, it is still lower than the heavy fuel oil (~0.10%). This difference suggests the presence of oxygenated compounds in the pyrolysis oil, which leads to detrimental physical and chemical properties. The resulting heating value is 32.72 MJ/kg, that fits well with values in [6.27]. As regulated in standard ASTM D 7544 for pyrolysis liquid biofuel, the maximum permissible water content is 25–30% to use it as a fuel in the turbine and boiler. For this type of application, the laminate oil results suitable [6.28]. The dynamic viscosity of oil was 31 mPa·s at temperature of 23.2°C, resulting lower than heavy fuel oil, whose value is about 230 mPa·s at 30°C [6.27]. Proximate and ultimate analysis of SGL oil are shown in **Table 6.6**.

**Table 6.6** Laminate oil characterization

	Units	TCR Result	Heavy Fuel Oil (from Table 4.2)
<b>Proximate Analysis</b>			
Water	wt%	7.21	0.1

Ash	wt%	<0.001	0.1
HHV	MJ/kg	31.97	40
Viscosity	mPa·s	31 (@23.2°C)	230 (@ 30°C) [6.27]
Density	kg/m <sup>3</sup>	856	-
<b>Ultimate Analysis</b>			
C	wt%	69.12	85
H	wt%	8.27	11
N	wt%	3.46	0.3
S	wt%	0.65	-
O	wt%	11.29*	1.0

\*Calculated by difference

#### 6.1.3.3.1 The GC-MS results

In order to detect and identify the organic compounds in the pyrolysis oil deriving from TCR, two-dimensional gas chromatography and mass spectrogram were computed.

In **Table 6.7**, the chemical compounds of the SGL oil are reported with their molecular formula, peak value and retention time detected by GC-MS Agilent 8890.

GC-MS analysis of the oil revealed that it was composed mainly of aromatics, phenols and furans as suggested by peak values. However, phenols' peak is not as high as hydrocarbons in the oil, meaning that was partly cracked during reforming.

**Table 6.7** Chemical compounds detected and identified by GC-MS of Laminate oil

Chemical compound	Molecular Formula [6.29]	Retention I (min)	Peak Value
1,3,5-Cycloheptatriene	C <sub>7</sub> H <sub>8</sub>	4.66	85663.73
p-Xylene	C <sub>8</sub> H <sub>10</sub>	6.34	68358.30
Benzene, 1-ethyl-2-methyl-	C <sub>9</sub> H <sub>12</sub>	8.25	24007.01
Benzene	C <sub>6</sub> H <sub>6</sub>	3.46	22506.99
Ethylbenzene	C <sub>8</sub> H <sub>10</sub>	6.18	16815.06
Benzofuran	<u>C<sub>8</sub>H<sub>6</sub>O</u>	8.85	13618.73
Chromium, tricarbonyl[(1,2,3,4,5,6- <sup>n</sup> )-1,3,5,7-cyclooctatetraene]-	-	6.78	11139.36
1H-Pyrrolo[2,3-b]pyridine, 2-methyl-	<u>C<sub>8</sub>H<sub>8</sub>N<sub>2</sub></u>	10.83	9764.16
Benzyl alcohol	<u>C<sub>7</sub>H<sub>8</sub>O</u>	10.08	9065.15

1H-Benzimidazole, 5,6-dimethyl-	<u>C<sub>9</sub>H<sub>10</sub>N<sub>2</sub></u>	13.07	8566.90
Phenol, 4-ethyl-	<u>C<sub>8</sub>H<sub>10</sub>O</u>	11.04	7636.60
Cinnamaldehyde, (E)-	<u>C<sub>9</sub>H<sub>8</sub>O</u>	10.99	7102.42
2,4,5-Trihydroxypyrimidine	<u>C<sub>4</sub>H<sub>4</sub>N<sub>2</sub>O<sub>3</sub></u>	12.59	6083.76
2-Propenal, 2-methyl-3-phenyl-	<u>C<sub>10</sub>H<sub>10</sub>O</u>	12.88	5569.08
o-Xylene	C <sub>8</sub> H <sub>10</sub>	6.78	5331.62
1,3,5-Cycloheptatriene, 1-methoxy-	<u>C<sub>8</sub>H<sub>10</sub>O</u>	11.85	5157.36
p-Cresol	<u>C<sub>7</sub>H<sub>8</sub>O</u>	10.54	5018.91
1,2-Dimethylindol-4-amine	<u>C<sub>10</sub>H<sub>12</sub>N<sub>2</sub></u>	14.71	4582.31
Cyclohexene, 1-(1-propynyl)-	C <sub>9</sub> H <sub>12</sub>	8.07	4546.32
1,5-Heptadien-3-yne	C <sub>7</sub> H <sub>8</sub>	3.57	3779.06

The aromatics and cycloaromatic hydrocarbons are the most common in the oil as also represented in **Figure 6.10**, thus suggesting promising results for its usage as a fuel, since these chemical compounds are basically present in conventional ones.

On the contrary, phenols and furans deriving from resins, hemicellulose and lignin are not interesting as they contain oxygenated compounds that minimize the calorific value of the fuel. It would be possible to remove the oxygenated substances after a further hydrotreatment process.

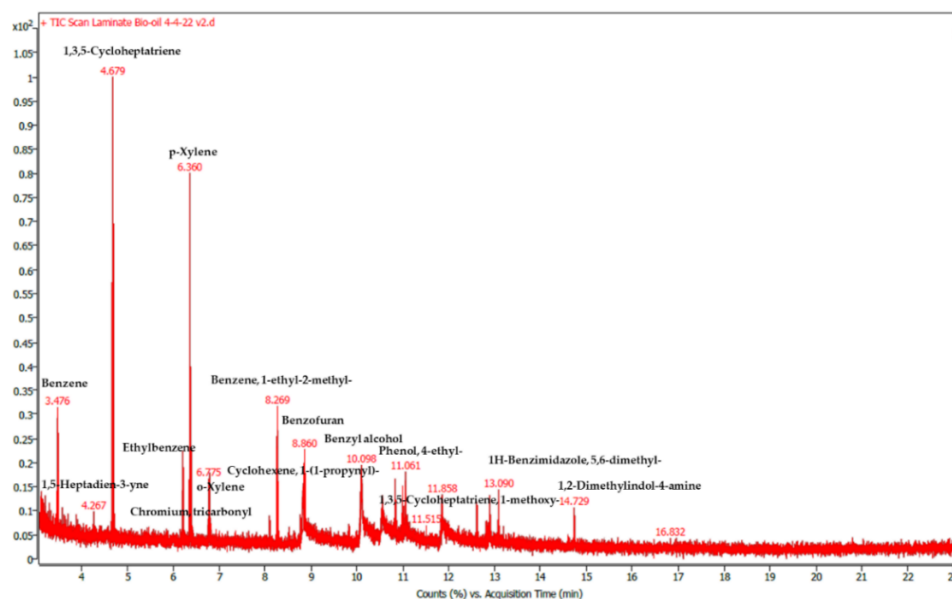


**Figure 6.10** 1D representation of GCxGC results of Laminar Oil

## 6.1.4 The hydrotreatment

### 6.1.4.1 The catalysts

The hydrotreatment consisted of removal of sulphur, nitrogen and oxygen that were noticed in the laminate oil as shown in **Table 6.6** and **Table 6.7**, as it was not expected other contaminants to be in the laminate oil.

As already mentioned in **Chapter 5**, hydrodeoxygenation (HDO) and hydrocracking (HC) were realized with catalysts TK-341 and TK-932, respectively.

TK-341 is a nickel-molybdenum supported on alumina ( $\text{NiMo}/\gamma\text{-Al}_2\text{O}_3$ ) catalyst and developed for fixed-bed HDO service [6.30]. This type of catalyst in its sulfide form is being commercially used for hydrodesulphurization over the past two decades [6.31]. Furthermore, sulfide  $\text{NiMo}/\text{Al}_2\text{O}_3$  catalysts are efficient to eliminate the nitrogen heteroatom compounds ahead of further upgradation [6.32]. Normally, Mo is used as the main active metal and either Ni or Co as the promoter, supported on  $\text{SiO}_2$ , or  $\text{Al}_2\text{O}_3$ . It has been demonstrated that the binary Ni-Mo catalyst are more reactive than the single Mo or Ni [6.33].  $\text{NiMo}/\gamma\text{-Al}_2\text{O}_3$  was used in HDO for not only spirulina, aspen wood, cornstalk bio-oils deriving from fast pyrolysis and HTL, but also for carbohydrates-derived oxygenates (e.g. methyl heptanoate and methyl hexanoate) according to [6.33]. All these feedstocks have in common high oxygen content around 40 wt% for spirulina [6.34], aspen wood [6.35], cornstalk [6.36], and around 20 wt% for methyl heptanoate ( $\text{C}_8\text{H}_{16}\text{O}_2$ ) and methyl hexanoate ( $\text{C}_7\text{H}_{14}\text{O}_2$ ) [6.37], [6.38]. This means that this type of catalyst should have high efficiency in removing oxygenated compounds, nitrogen and sulphur from the oil, whose contents are strictly regulated in some applications. There are some binding regulations about the sulphur content in the oil. For example, the sulphur content for diesel fuel must be 10 mg/kg (i.e. 1 wt%) according to BS EN590 [6.39]. While the sulphur content for ships' fuel oil has recently been reduced from 3.5% to 0.5% according to International Maritime Organization (IMO) 2020 [6.40]. In this case, the sulphur content of raw SGL oil is 0.65%, which was already a good result even prior to hydrotreatment and therefore it is expected oil with better properties afterwards.

TK-932 is a commercial nickel wolfram catalyst supported on silica-alumina ( $\text{NiW}/\text{SiO}_2\text{-Al}_2\text{O}_3$ ), designed for dewaxing renewable diesel as reported in [6.30]. Typically, decarboxylation and decarbonylation are favoured over NiW catalysts [6.41], but the support material ( $\text{SiO}_2\text{-Al}_2\text{O}_3$ ) shows the highest yield of monocyclics [6.42]. Compared to other catalysts,  $\text{NiW}/\text{SiO}_2\text{-Al}_2\text{O}_3$  supports both hydrogenation and



cracking activities [6.42] and it has found to have high selectivity for cracking to middle distillates such as kerosene, jet fuel and diesel fuel [6.43]. By using this catalyst, it is expected to improve the catalytic performance and the physicochemical properties of the liquid product (e.g. dynamic viscosity, density, distillation range and hydrocarbon content) [6.44].

#### 6.1.4.2 The mass balance for HDO and HC

For the hydrodeoxygenation 100 ml of raw oil was processed in the autoclave reactor as specified in **Chapter 5**. The resulting HDO oil was separated from the aqueous phase through a separating funnel shown in **Figure 6.11**.

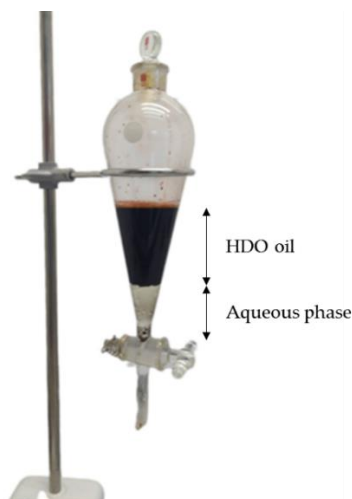


**Figure 6.11** HDO oil and aqueous phase after the HDO process

According to **Figure 6.12**, 78% in volume of the initial oil was converted in hydrodeoxygenated oil and water, while the remaining 22% was lost during the conversion. After the separation, the aqueous phase accounted for the 10% in volume.

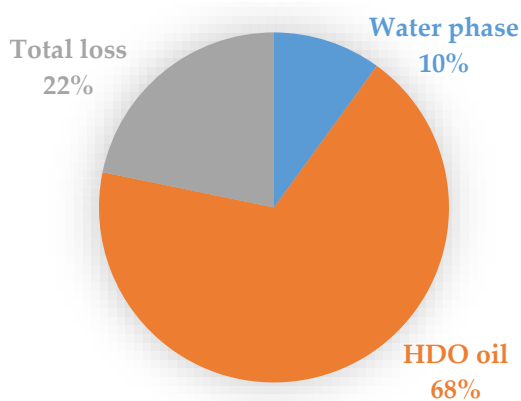


**Figure 6.12** Mass balance for the hydrodeoxygenation (HDO)

**Table 6.8** reports the analyses over HDO oil and the aqueous phase. HDO positively affects the content of Carbon and Hydrogen in the oil, thus allowing the formation of more hydrocarbons and reducing the presence of oxygenated compounds, nitrogen and sulphur. The reduction percentages were about 60wt%, 21wt%, 40wt%, 85wt% for water, oxygen, nitrogen and sulphur, respectively, while the increase of carbon was around 11wt%. Finally, the hydrogen content could be basically considered unchanged. However, HDO must be optimized by using a continuous flow reactor as to constantly replenish the H<sub>2</sub> consumed by reactions and pressures implemented were low due to reactor limitations usually we should go up to 130 bar.

**Table 6.8** HDO oil (on the left) and aqueous phase (on the right) characterization

HDO oil	Units	Result			
<b>Proximate Analysis</b>			<b>Aqueous Phase from HDO</b>		
Water*	wt%	2.875		<b>Units</b>	<b>Result</b>
Ash	wt%	-			
HHV	MJ/kg	35.61	<b>Ultimate Analysis</b>		
<b>Ultimate Analysis</b>			C	wt%	5.11
C	wt%	77.535	H	wt%	11.22
H	wt%	8.075	N	wt%	5.7
N	wt%	2.535	S	wt%	<0.10
S	wt%	<0.10	O, H <sub>2</sub> O*	wt%	~ 77.87
O	wt%	8.98	*calculated by difference		

\*calculated by difference

Regarding the aqueous phase which accounts for 10% in volume after HDO, its significant amount of water and oxygen could receive more attention in its reuse as a medium in the HDO of biomass. Indeed, water would have several effects such as regulating the mass transfer, stabilizing the transition states, promoting the ring-opening, participating at the catalytic reaction, occupying active site and changing catalyst structure, although it could cause problem of the catalyst stability, thus leading to deactivated phenomena of catalyst (e.g. leaching, sintering, collapse of catalyst support) [6.45].

Furthermore, the oil's aqueous phase can be applied in a wide range of applications such as composting, crop pest control, crop growth promotion, feed additives, deodorising, coagulating and antifungal agents [6.46][6.47].

For the hydrocracking, 50 ml of HDO oil were processed and after the process the hydrocracked oil was the 82%, while the 18% was not converted as illustrated in **Figure 6.13**.

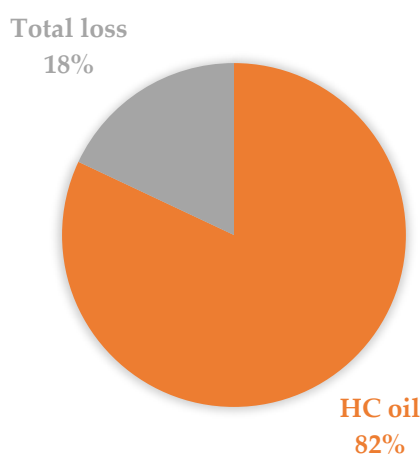


**Figure 6.13** Mass balance for the hydrocracking (HC)

The results deriving from the hydrotreatment tests, in terms of proximate and ultimate analyses are illustrated in **Table 6.9**.

**Table 6.9** HDO oil (on the left) and HDO+HC oil (on the right) characterization

HDO oil	Units	Result	HDO+HC oil	Units	Result
<b>Proximate Analysis</b>			<b>Proximate Analysis</b>		
Water*	wt%	2.875	Water*	wt%	1.6
Ash	wt%	-	Ash	wt%	-
HHV	MJ/kg	35.61	HHV	MJ/kg	37.05
<b>Ultimate Analysis</b>			<b>Ultimate Analysis</b>		
C	wt%	77.535	C	wt%	78.9
H	wt%	8.075	H	wt%	8.86
N	wt%	2.535	N	wt%	1.945
S	wt%	<0.10	S	wt%	<0.10
O	wt%	8.98	O	wt%	8.695

\*calculated by difference

\*calculated by difference

Although the sulphur content was practically eliminated from raw oil, the oxygen content was still too high in both HDO and HDO+HC oil, showing a poor selectivity of catalysts with oxygen compounds. This result suggests or TK-341 catalyst was good for desulphurisation but not for deoxygenation or the operating conditions (temperature and pressure) adopted for the hydrotreatment should be set differently. Eventually, considerations over HDO must be repeated for HC in terms of continuous injection of hydrogen at higher pressure. The reason why the reactor was not continuously replenished with hydrogen is due to the fact it was a batch reactor.

After hydrocracking, the oil has a HHV of 37.05 MJ/kg, almost matching with heavy fuel oil (HFO), even if the hydrogen content decreased compared with the raw laminate oil, thus reducing the H/C ratio as illustrated in the Van Krevelen diagram in **Figure 6.14**.

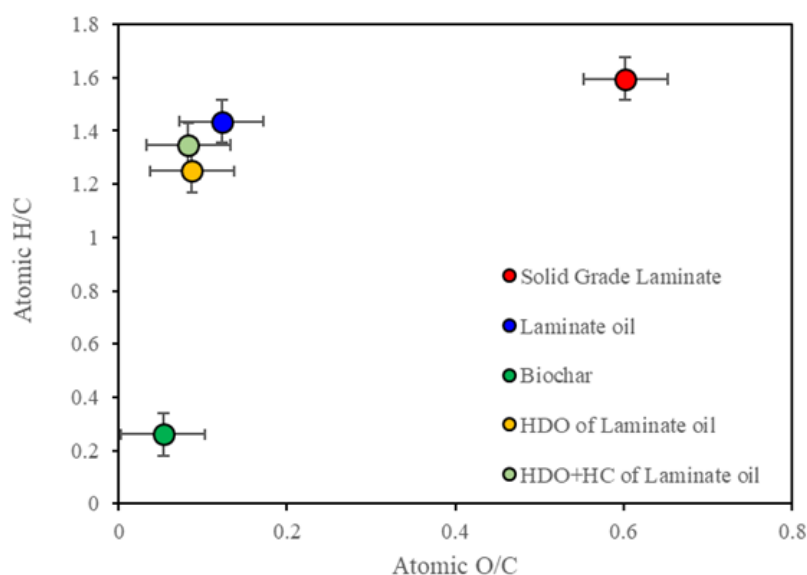


**Figure 6.14** The Van Krevelen diagram for Laminate products

#### 6.1.4.3 The GC-MS analysis of HDO and HC oil

The GC-MS analysis of HDO oil, reported in **Table 6.10**, suggests there are still undesired heteroatoms in the oil like oxygen, chlorine and nitrogen. Chlorine was not present in the initial raw oil, meaning that part of dichloromethane used as solvent in the GC-MS analysis created new bonds with the hydrocarbons.

**Table 6.10** GC-MS analysis of HDO oil

#	Compound Name	Molecular Formula [6.48]	Retention I (min)	Peak Value
1	Toluene	C <sub>7</sub> H <sub>8</sub>	4.68	146984.97
2	o-Xylene	C <sub>8</sub> H <sub>10</sub>	6.37	62875.63
3	Benzene	C <sub>6</sub> H <sub>6</sub>	3.48	38039.02
4	Ethylbenzene	C <sub>8</sub> H <sub>10</sub>	6.22	36697.57
5	Benzene, (1-methylethyl)-	C <sub>9</sub> H <sub>12</sub>	8.26	20042.61
6	Cyclopentane, methyl-	C <sub>6</sub> H <sub>12</sub>	3.21	18939.55
7	Cyclohexane	C <sub>6</sub> H <sub>12</sub>	3.49	7880.87
8	Benzene, 1-ethyl-4-methyl-	C <sub>9</sub> H <sub>12</sub>	8.11	7747.54
9	Cyclohexane, methyl-	C <sub>7</sub> H <sub>14</sub>	4.15	7461.47
10	Deltacyclene	C <sub>9</sub> H <sub>10</sub>	9.63	7031.66
11	1,7-Dichloroheptane	<u>C<sub>7</sub>H<sub>14</sub>Cl<sub>2</sub></u>	4.25	6918.62
12	Furaneol	<u>C<sub>6</sub>H<sub>8</sub>O<sub>3</sub></u>	12.65	6888.45
13	Ethylbenzene	C <sub>8</sub> H <sub>10</sub>	6.82	6844.23
14	Benzene, (1-methylethyl)-	C <sub>9</sub> H <sub>12</sub>	7.36	6034.38
15	Benzyl isopentyl ether	<u>C<sub>12</sub>H<sub>18</sub>O</u>	10.76	5112.99
16	Hexanoyl chloride	<u>C<sub>6</sub>H<sub>11</sub>ClO</u>	17.72	4827.16
17	Methylene chloride	<u>CH<sub>2</sub>Cl<sub>2</sub></u>	3.11	4513.29
18	cis-Bicyclo[4.2.0]octa-3,7- diene	C <sub>8</sub> H <sub>10</sub>	14.43	4376.10
19	Oxalic acid, monoamide monohydrazide, N-benzyl- N''-(1-oxo-3-phenylprop-2- enyl)-	<u>C<sub>18</sub>H<sub>17</sub>N<sub>3</sub>O<sub>3</sub></u>	11.07	4157.59
20	2H-Pyran-2,6(3H)-dione, dihydro-4,4-dimethyl-	<u>C<sub>7</sub>H<sub>10</sub>O<sub>3</sub></u>	3.71	3748.57
21	Benzene, (2-methyloctyl)-	C <sub>15</sub> H <sub>24</sub>	16.11	3685.45

22	Benzene, [(2-propenyloxy)methyl]-	<u>C<sub>10</sub>H<sub>12</sub>O</u>	10.10	3602.60
23	1,3,5-Cycloheptatriene, 7-ethyl-	C <sub>9</sub> H <sub>12</sub>	7.96	3467.78
24	Cyclohexene, 1-(1-propynyl)-	C <sub>9</sub> H <sub>12</sub>	8.79	3324.77
25	Tricyclo[5.2.1.0(2,5)]dec-5(6)-ene	C <sub>10</sub> H <sub>14</sub>	10.00	2797.63
26	Pyridine, 2-nitro-	<u>C<sub>5</sub>H<sub>4</sub>N<sub>2</sub>O<sub>2</sub></u>	8.79	2793.51
27	(3E,5Z)-3,5-Undecadien-1-yne	C <sub>11</sub> H <sub>16</sub>	3.67	2743.23
28	cis-Bicyclo[4.2.0]octa-3,7-diene	C <sub>8</sub> H <sub>10</sub>	12.89	2731.16
29	Propanal dibenzyl acetal	<u>C<sub>17</sub>H<sub>20</sub>O<sub>2</sub></u>	10.58	2616.32
30	(E,E)-3,5-Undecadien-1-yne	C <sub>11</sub> H <sub>16</sub>	8.85	2265.75
31	N-Benzyloxy-2-carbomethoxyaziridine	<u>C<sub>11</sub>H<sub>13</sub>NO<sub>3</sub></u>	11.06	2233.12

The GC-MS analysis of HC oil, reported in **Table 6.11**, also suggests the presence of undesired heteroatoms in the oil like oxygen, chlorine and nitrogen. Iodine and phosphorous could be or contaminations or approximations from the GC-MS library.

**Table 6.11** GC-MS analysis of HC oil

#	Compound Name	Molecular Formula [6.48]	Retention I (min)	Peak Value
1	Toluene	C <sub>7</sub> H <sub>8</sub>	4.68	192682.58
2	2,4-Azetidinedione, 3,3-diethyl-1-methyl-	<u>C<sub>8</sub>H<sub>13</sub>NO<sub>2</sub></u>	4.15	142814.44
3	Cyclohexane	C <sub>6</sub> H <sub>12</sub>	3.49	113231.98
4	Benzene, 1,3-dimethyl-	C <sub>8</sub> H <sub>10</sub>	6.37	68393.01
5	Cyclohexane, 1,3-dimethyl-, cis-	C <sub>8</sub> H <sub>16</sub>	4.89	51091.36
6	Ethylbenzene	C <sub>8</sub> H <sub>10</sub>	6.22	47857.07

7	Benzene, 1,2,3-trimethyl-	C <sub>9</sub> H <sub>12</sub>	8.26	25614.86
8	Cyclohexane, 1,3-dimethyl-, cis-	C <sub>8</sub> H <sub>16</sub>	5.30	25248.18
9	1-Pentanol, 4-methyl-	<u>C<sub>6</sub>H<sub>14</sub>O</u>	3.21	19125.28
10	Formic acid, cis-4-methylcyclohexyl ester	-	4.73	18017.82
11	Cyclohexane, ethyl-	C <sub>8</sub> H <sub>16</sub>	5.77	17327.66
12	Heptane	C <sub>7</sub> H <sub>16</sub>	3.79	13366.07
13	Indane	C <sub>9</sub> H <sub>10</sub>	9.62	11814.75
14	Benzene, 1-ethyl-4-methyl-	C <sub>9</sub> H <sub>12</sub>	8.12	11694.80
15	Ethylbenzene	C <sub>8</sub> H <sub>10</sub>	6.82	11475.06
16	Hexane, 3-methyl-	C <sub>7</sub> H <sub>16</sub>	3.57	9074.27
17	Dodecane, 1-iodo-	<u>C<sub>12</sub>H<sub>25</sub>I</u>	14.43	8567.31
18	3-Hexanone, 2,4-dimethyl-	<u>C<sub>8</sub>H<sub>16</sub>O</u>	12.65	7818.14
19	1-Pentanone, 1-phenyl-	<u>C<sub>11</sub>H<sub>14</sub>O</u>	7.38	6890.40
20	Heptane, 2,4-dimethyl-	C <sub>9</sub> H <sub>20</sub>	5.10	6483.26
21	trans-2-Hexenyl phenylacetate	<u>C<sub>14</sub>H<sub>18</sub>O<sub>2</sub></u>	7.56	6448.87
22	3-Hexanone, 2,4-dimethyl-	<u>C<sub>8</sub>H<sub>16</sub>O</u>	17.72	6075.45
23	1-Ethyl-3-methylcyclohexane (c,t)	C <sub>9</sub> H <sub>18</sub>	6.75	6072.99
24	Benzene, propyl-	C <sub>9</sub> H <sub>12</sub>	7.96	5970.67
25	Benzene, 1,2,3-trimethyl-	C <sub>9</sub> H <sub>12</sub>	8.78	5452.92
26	N-Cyano-3-methylbut-2-enamine	<u>C<sub>6</sub>H<sub>10</sub>N<sub>2</sub></u>	4.25	5366.71
27	2,2,4-Trimethyl-3-pentanone	<u>C<sub>8</sub>H<sub>16</sub>O</u>	16.11	5255.88
28	trans-2-Hexenyl phenylacetate	<u>C<sub>14</sub>H<sub>18</sub>O<sub>2</sub></u>	5.03	4827.50
29	4-Penten-1-ol, 3-methyl-	<u>C<sub>6</sub>H<sub>12</sub>O</u>	3.71	4809.37
30	Benzyl oxy tridecanoic acid	<u>C<sub>20</sub>H<sub>32</sub>O<sub>3</sub></u>	5.70	4379.26
31	2(3H)-Furanone, 3-(5-bromo-1H-1,2,4-triazol-1-yl)dihydro-	-	4.34	4281.66
32	(E,E)-3,5-Undecadien-1-yne	C <sub>11</sub> H <sub>16</sub>	8.81	4208.03

33	Nonane, 1-chloro-	<u>C<sub>9</sub>H<sub>19</sub>Cl</u>	6.85	4156.56
34	Cyclopropylphenylmethane	C <sub>10</sub> H <sub>12</sub>	12.12	4131.16
35	4-Octen-3-one	<u>C<sub>8</sub>H<sub>14</sub>O</u>	7.12	3887.44
36	Ethanone, 1-(4-methylphenyl)-	<u>C<sub>9</sub>H<sub>10</sub>O</u>	9.98	3856.69
37	Pyridine, 2-(1H-tetrazol-5-yl)-	<u>C<sub>6</sub>H<sub>5</sub>N<sub>5</sub></u>	3.18	3694.20
38	1,4-Decadiyne	C <sub>10</sub> H <sub>14</sub>	5.56	3667.32
39	Methylene chloride	<u>CH<sub>2</sub>Cl<sub>2</sub></u>	3.14	3446.58
40	Benzeneacetic acid, 2-tridecyl ester	<u>C<sub>21</sub>H<sub>34</sub>O<sub>2</sub></u>	19.24	3425.19
41	Benzyl phosphine	<u>C<sub>7</sub>H<sub>9</sub>P</u>	5.61	2812.87
42	4-Benzyloxy-3-hydroxy-2-methyl-1-butene	<u>C<sub>12</sub>H<sub>16</sub>O<sub>2</sub></u>	10.77	2740.86
43	Benzoyl benzyl disulfide	<u>C<sub>14</sub>H<sub>12</sub>OS<sub>2</sub></u>	8.18	2735.28
44	Cyclopropanebutanoic acid, 2,4-dioxo-, methyl ester	<u>C<sub>8</sub>H<sub>10</sub>O<sub>4</sub></u>	6.14	2721.77
45	D-Ribo-Hex-5-enofuranose, 3-O-benzyl-5,6-dideoxy-1,2-O-isopropylidene-, α-	-	10.10	2633.46
46	1-Methylene-2-benzyloxy-cyclopropane	<u>C<sub>11</sub>H<sub>12</sub>O</u>	11.87	2482.67
47	Hexane, 2,5-dimethyl-	C <sub>8</sub> H <sub>18</sub>	4.59	2466.79

---



## 6.2 Carbon fibres

### 6.2.1 Feedstock characterization

#### 6.2.1.1 Proximate and ultimate analyses

Similarly to **section 6.1.1.1**, carbon fibres, received from Gen2Carbon (UK), was characterized through proximate and ultimate analyses. As already mentioned in the Methods (**Chapter 5**), prepared samples were analysed by TGA under pyrolysis and combustion conditions and some of them were sent to an external accredited laboratory (MEDAC Ltd) for CHNS analysis. The oxygen was then determined by difference, considering the ash content equal to 1.52wt% resulting from TGA (**Figure 6.17**). The overall characterisation results are presented in **Table 6.12**.

**Table 6.12** Proximate and Ultimate Analysis of Carbon Fibres

	Units	Result
<b>Proximate Analysis</b>		
Moisture	wt%	0.49
Volatiles	wt%	32.25
Fixed Carbon	wt%	65.74
Ash	wt%	1.52
HHV	MJ/kg	30.78
<b>Ultimate Analysis</b>		
C	wt%	80.47
H	wt%	2.93
N	wt%	4.22
S	wt%	2.25
O*	wt%	8.61

\*calculated by difference

From the TGA graph under pyrolysis conditions, the weight loss of moisture and volatiles can be computed. They are 0.49 and 32.25wt%, respectively. The fixed carbon is obtained as difference between the total mass, the moisture and volatiles fractions in percentage. Fixed carbon gave information of the amount of char formation in the thermochemical process after the volatile matter drives off. The value is equal to 65.74wt%, meaning that two third of the initial feedstock can be used as char in the post reformer. The objective of using such carbonaceous substance in this research is to investigate its influence in terms of catalytic action capacity for TCR oil production.

The HHV is determined using the unified Channiwala correlation for fuels starting from carbon, hydrogen, sulphur, oxygen, nitrogen and ash weight fraction, respectively. The resulting value is equal to almost 31 MJ/kg similar to coal. The ash content was evaluated as the residual mass after combustion as illustrated in **Figure 6.17**.

The nitrogen and sulphur content from ultimate analysis gave information about the possible formation of SO<sub>x</sub> and NO<sub>x</sub> emissions during the thermochemical process (pyrolysis and gasification). Therefore, lower values correspond to lower emissions. Nitrogen is also an inert element, meaning that it does not react during the conversion process. Nitrogen and Sulphur were found to be high for this feedstock in comparison to wood biomass, it was approximately 35 x higher for Nitrogen and 16 x higher in terms of Sulphur content [6.49]. The reason of such high content of nitrogen and sulphur could be related to the improvement of electrical conductivity, thus making carbon fibres suitable as supercapacitors. Indeed, carbon fibre has some defects in terms of electrochemical performance due to lack of electrochemical active site and low specific surface area [6.50].

The initial atomic O/C and H/C ratios of carbon fibres were 0.08 and 0.43, respectively. The low O/C ratio suggests a limited release of organic compounds that can be collected in the oil. In fact, carbon fibres are very close to coal/anthracite rather than biomass as illustrated in Van Krevelen diagram in **Figure 6.15**. Which indicates that the feedstock itself is already a very stable form of carbon. This corresponds well with the findings of TGA that showed a high FC content.

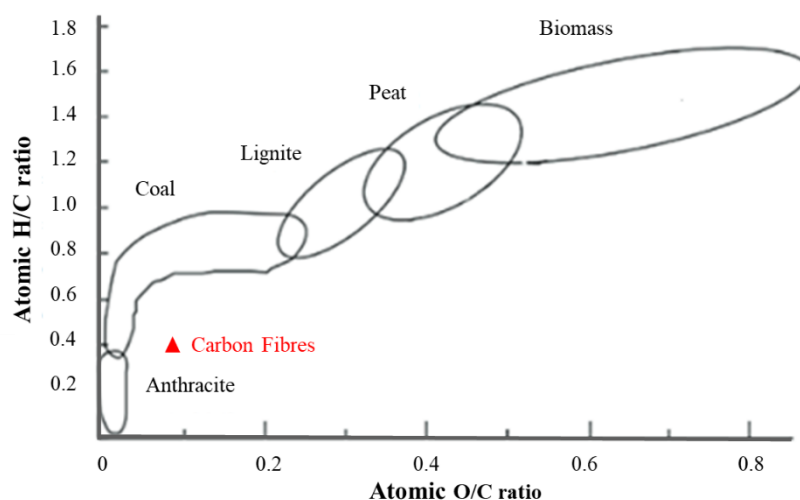


**Figure 6.15** Van Krevelen diagram [6.2] of Carbon Fibres

The TGA profiles for both TGA pyrolysis and TGA combustion are also presented as shown by **Figure 6.16** and **Figure 6.17**, respectively.

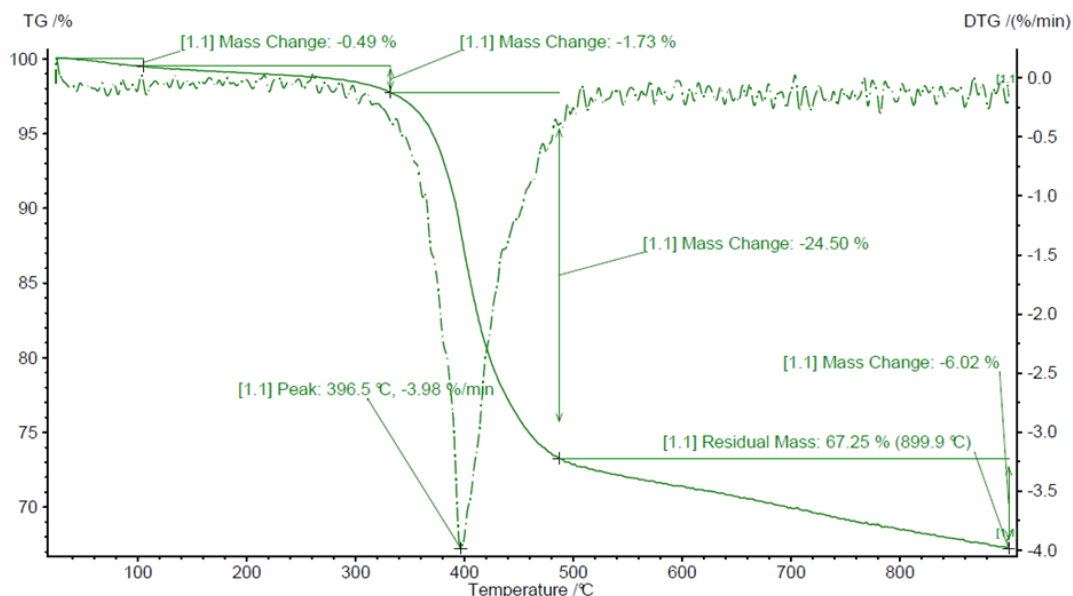


**Figure 6.16** TGA/DTG Pyrolysis Profile of Carbon Fibres

The results in **Figure 6.16** (TGA pyrolysis) show a weight loss moisture of 0.49% from ambient temperature (25°C) to 105°C. Then, the weight decreases of 1.73% before reaching the maximum value of volatilization temperature between 350°C and 500°C as illustrated in the DTG, where the mass change is estimated to be 24.50%. This sharp loss in the mass can be attributed to the conversion of the epoxy matrix into volatiles [6.51]. Finally, the fixed carbon is released slowly from 500 up to 900°C.

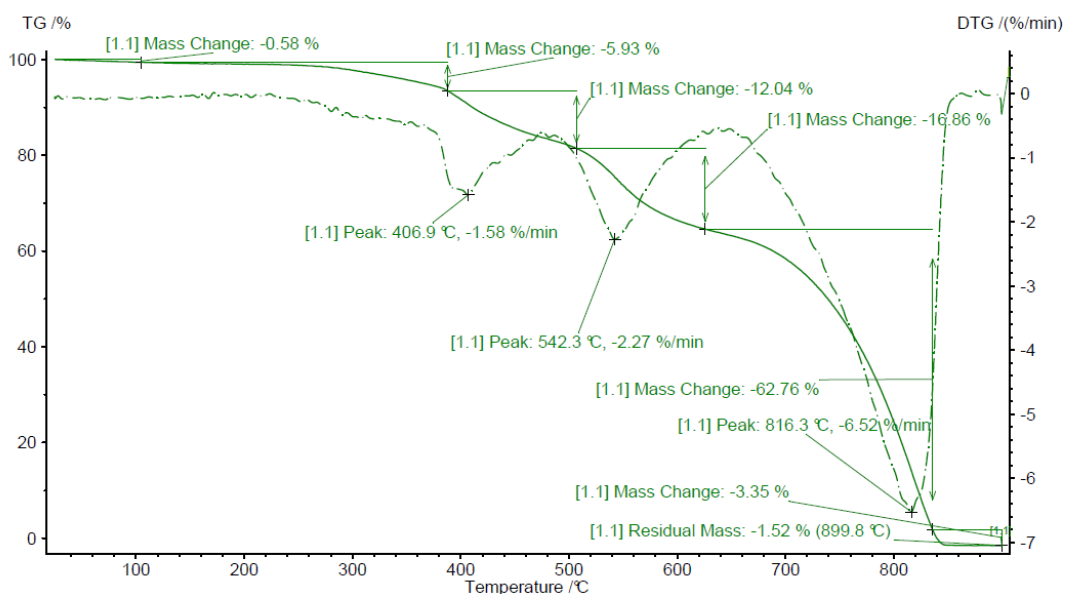


**Figure 6.17** TGA/DTG Combustion Profile of Carbon Fibres

The results in **Figure 6.17** (TGA combustion) show a weight loss moisture of 0.58% from ambient temperature (25°C) to 105°C. Then, the mass starts gradually decreasing. The first peak corresponds to the degradation of the epoxy resin, whose decomposition starts at 230°C [6.52], reaching the maximum value of 12.04% in mass loss at 400°C. The second peak is related to the oxidation of the volatile carbon occurring at about 550°C, where the mass change is 16.86 wt%. Finally, the third peak represents the oxidation of fixed carbon, which is expected to be at temperature of 820°C, and here, the mass loss is considerably high and equal to 62.76 wt%. This result fits well with literature, where the same behaviour is met [6.52].

#### *6.2.1.2 Thermal effect analysis*

A qualitative analysis was also investigated in order to determine any melting and heating effects of samples. The carbon fibre was heated up in the CARBOLITE GERO AAF 1100 furnace. The objective was to carry on six heating ramps (17-250°C, 250-350°C, 350-450°C, 450-550°C, 550-650°C, 650-700°C) with a heating rate of 10°C/min and a dwelling time of 15 minutes. The results showed a gradual release of both volatiles in air and epoxy resin around the crucible's surface. At 700°C, the residual samples appeared to have a high fixed carbon content and the samples did not melt in the crucible indicating that it is suitable to be processed via TCR thermal treatment.

#### *6.2.1.3 The mass balance*

The mass balance for carbon fibres experiments is shown in **Figure 6.18**. However, this could not be accurately determined during the run as significant quantities of unprocessed carbon fibre remained in the hopper and some oxygen may have entered the system during the run, which caused oxidation reactions of the fixed carbon to occur. However, 35 wt% of char was recovered and 2 wt% of a liquid fraction containing both water and organics was recovered. Syngas fraction was then determined by difference and was found to be 63 wt%. The mass balance analysis concluded that products obtained under TCR conditions were predominantly syngas and char.

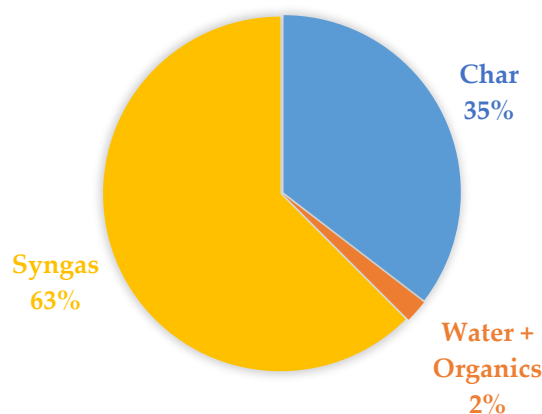


Figure 6.18 Mass balance

The syngas represents the gaseous fraction made of CO, CO<sub>2</sub>, H<sub>2</sub>, CH<sub>4</sub> and light hydrocarbons (typically consisting of C1-C4). It was difficult to consistently represent the distribution of syngas during the entire experiment due to the reactor blockage related to the size and shape of carbon fibres. However, a snapshot of the syngas produced during the run is presented in **Figure 6.19**.

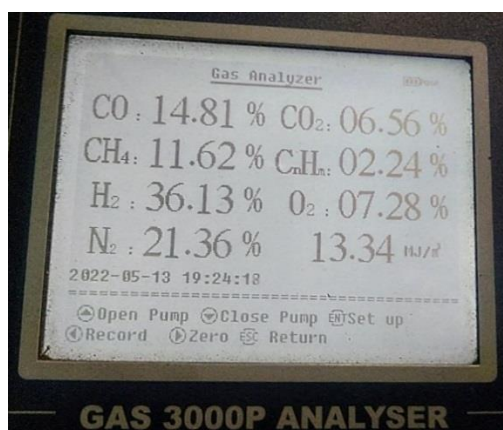


Figure 6.19 Gas analysis during the experiment

Assuming gas volumes in **Figure 6.19** as representative, the normalized values, discounting N<sub>2</sub> and O<sub>2</sub> from purge gas, are shown in **Table 6.13**, in comparison with values obtained from experimental tests on pyrolysis of carbon fibres in [6.53].

Table 6.13 Syngas composition

	Measured Syngas [vol%]	Normalised Syngas [vol%]	Normalised Syngas from ref. [6.53] on average
H <sub>2</sub>	36.13	50.63	50.6
N <sub>2</sub>	21.36	-	-

O <sub>2</sub>	7.28	-	-
C <sub>x</sub> H <sub>y</sub>	2.24	3.14	9.44*
CO <sub>2</sub>	6.56	9.2	5.13
CO	14.81	20.75	11.93
CH <sub>4</sub>	11.62	16.28	22.9

\*calculated by the difference

As shown above, hydrogen represents about 50 vol% of the syngas, while methane equates to 16 vol% and gradually decreased during the run. Carbon monoxide and light hydrocarbons were 20 vol% and 3 vol%, respectively, while carbon dioxide reached approximately 9 vol%. Hence, despite the limitations imposed by size and shape of carbon fibres, the composition of TCR syngas is comparable with values deriving from pyrolysis of carbon fibres in [6.53].

According to values in **Figure 6.19**, the HHV of combustible gases (CO, H<sub>2</sub>, CH<sub>4</sub> and C<sub>x</sub>H<sub>y</sub>) was 18 MJ/kg.

The char (**Figure 6.20**) equated to 35 wt% of the initial feedstock. This was the maximum amount that could be recovered from the initial feedstock, as most was lost during the run due to continuous removal of sample, which may have caused some oxidation reactions to occur. Under stable pyrolysis conditions it is expected that at least 70 wt% of the char can be recovered.



**Figure 6.20** Char of Carbon Fibres

The collected char was not homogenous showing both resin-bonded and non-bonded carbon as illustrated in **Figure 6.21**. It was found that disposal of this type of degraded materials by landfill is harmful to the environment and not economical [6.54]. Additionally, it was demonstrated in literature that during the process, a layer of pyrolytic carbon can form onto the reclaimed fibres. This could hamper a good

adhesion when carbon fibres are infused with new resin. However, this product can be considered highly valuable after an upgrading process based on oxidative treatment, which returns fibres back to their original form, and they could be recycled [6.55].



**Figure 6.21** Resin-bonded CF (on the left) and non-bonded CF (on the right)

The characteristics of both types of char were analysed by Medac Ltd and reported in **Table 6.14**. The ash content was computed by difference and HHV by Channiwalla equation.

Regarding resin-bonded CF, their carbon and ash content increased with respect of the initial feedstock, by 1.1 and 3.3 respectively, while the remaining elements decreased. On the contrary, the non-bonded CF showed a reduction in carbon content of approximately 25% compared with the original sample as well as hydrogen, nitrogen, sulphur and oxygen. Only the ash content consistently increased by 22.9%. The loss of carbon and hydrogen and the increase in ash presents further evidence that the samples were partially oxidised under combustion conditions during the run.

From the energy point of view, the calorific value of resin-bonded and non-bonded CF is equal to 33.08 and 20.17 MJ/kg, respectively. The first slightly increased compared with the initial carbon fibres, while the second decreased due to the reduction of carbon, hydrogen and sulphur. The char deriving from carbon fibres can be broadly used as filter [6.56], electrode material in batteries [6.57] or remanufacture of new carbon fibre [6.53]. Though in general recycled fibres cannot be reused for the same original applications due to possible lack in performance as well as owing to a form factor which cannot be controlled during the process (i.e. short fibres does not perform as well as long fibres to reinforce the material) [6.55]. Other possible applications of recycled carbon fibres after pyrolysis can be as conductive concrete for self-heating and de-icing in urban furniture as described in [6.58].

**Table 6.14** CF char characterization

Resin-bonded Carbon Fibers			Non bonded Carbon Fibres		
	Units	Result		Units	Result
<b>Ultimate Analysis</b>			<b>Ultimate Analysis</b>		
C	wt%	89.58	C	wt%	55.04
H	wt%	1.62	H	wt%	1.70
N	wt%	2.91	N	wt%	1.69
S	wt%	0.76	S	wt%	2.06
O	wt%	0.20	O	wt%	4.72
Ash*	wt%	4.94	Ash*	wt%	34.76
HHV	MJ/kg	33.08	HHV	MJ/kg	20.17

\*calculated by difference

The 2% of liquid fraction was left to settle for 24 hours in order to separate the aqueous and organic phases (**Figure 6.22**). The percentage of bio-oil and aqueous phase was 18% and 82%, respectively.

**Figure 6.22** Aqueous phase (on the left) and organics (on the right) of CF

The amount of oil derived from TCR was not enough to evaluate proximate analysis due to unstable reaction conditions as the feedstock should be pelletised before reactions. Oil yields are expected to be around 10% even for this feedstock. The ultimate analysis is shown in **Table 6.15**. Overall, the 96.43% is composed of carbon, hydrogen, nitrogen sulphur and oxygen, while the remaining 3.57% accounts for both water and ash. Approximately, the HHV of carbon fibres oil is around 30 MJ/kg.

**Table 6.15** Carbon Fibres oil characterization

	Units	Result
<b>Ultimate Analysis</b>		
C	wt%	64.73
H	wt%	7.77



N	wt%	5.66
S	wt%	1.46
O	wt%	16.81
<b>Proximate Analysis</b>		
Ash + Water	wt%	3.57*
HHV	MJ/kg	30

\*calculated by difference

In **Figure 6.23**, the Van Krevelen diagram highlights the H/C and O/C ratios of CF and its products obtained from TCR. Non-bonded CF and especially resin-bonded CF showed a great carbonization, getting even closer to the anthracite zone. This suggests a complete removal of oxygenated compounds. On the contrary, the oil had a greater H/C and O/C ratios, due to the presence of hydrogen and oxygen. However, the oil is still far from the conventional fuels, whose oxygen content is basically zero, thus positively affecting their HHVs equal to 41.8, 46.4 and 45.6 MJ/kg, for heavy oil, gasoline and diesel, respectively [6.8]. For this reason, it would require the right set of HDO/HC upgrading techniques.

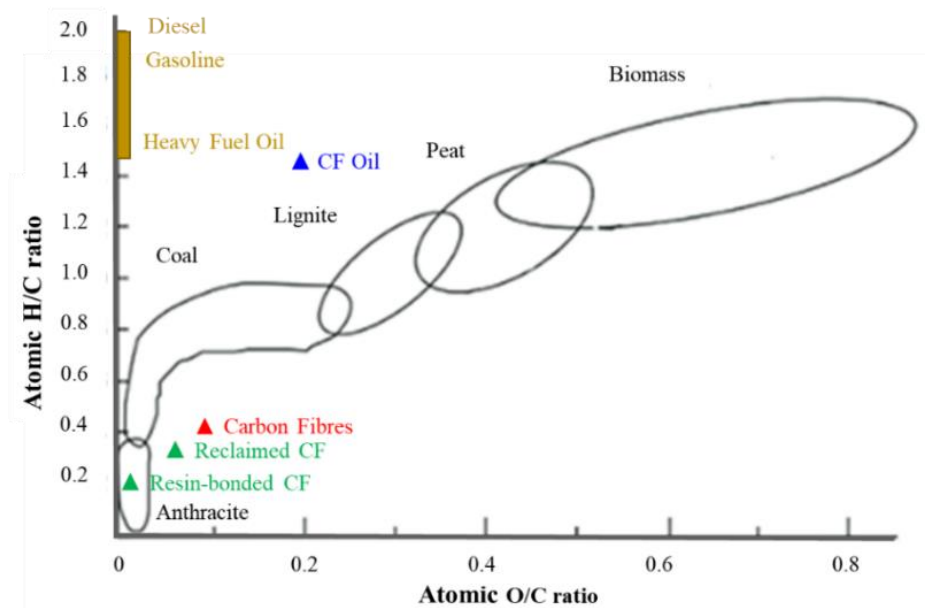


**Figure 6.23** Van Krevelen diagram [6.2] for CF and its products deriving from TCR

#### 6.2.1.4 The energy balance

According to the energy balance illustrated in **Figure 6.24**, the majority of the energy moves from the initial feedstock to syngas and char, 68% and 31% respectively.

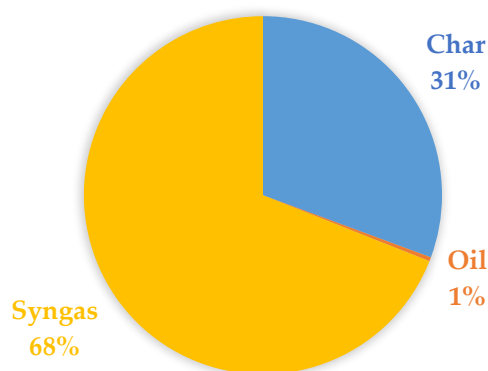


**Figure 6.24** The energy balance of CF

Only 1% of the energy is transformed in oil. For this reason, it is strongly advised to repeat experiments for further analysis especially with respect to achieving steady state stable conditions within the reactor. The oil could also be further investigated for its use as a fuel blend or upgrading via hydrotreatment. Before such experiments can be performed it is first necessary to adequately pre-treat the feedstock. Pellets are recommended to avoid any blockages occurring within the reactor.

#### 6.2.1.5 The SEM results

The original feedstock and the two types of chars were analysed by Hitachi Tabletop Microscope TM3030 series to get topographical information (Secondary Electron or SE signal) of their surface. All samples were magnified by 1000x with accelerating voltage of 5kV, which allowed a good observation of these specimens as illustrated in **Figure 6.25**. The original carbon fibres in **Figure 6.25,a** is well distributed along the same axis without any appreciable damage other than those due to the shredding. After the TCR, the resin-bonded char appears disomogeneous: part of fibres is partially damaged but still ordinated, with the intrusion of smaller particles deriving from the fibres' breaking and spread all along the surface (**Figure 6.25,b1**); part of fibres is completely broken and misaligned (**Figure 6.25,b2**). Finally, the non-bonded char is shown in **Figure 6.25,c** with chaotically distributed fibres, which caused loss of stiffness and high porosity. This aspect sounds beneficial as non-bonded char can be used as adsorbent material. This means it works well like a molecular sieve letting the gases with lower molecular sizes pass and separating them from the other gaseous species. For example, this type of material can find its application in the pollutants removal or

hydrogen filtration from the gas mixture in case it would show any selectivity like zeolites or activated carbon in the pressure swing adsorption (PSA) method. At first glance, the pores diameter ranges from 20 to 100  $\mu\text{m}$  (**Figure 6.25,c**) which are still too large as molecular sieves have diameter in the range of 3-10 $\text{\AA}$  (e.g. 1  $\text{\AA}$  = $10^{-4}$   $\mu\text{m}$ ).

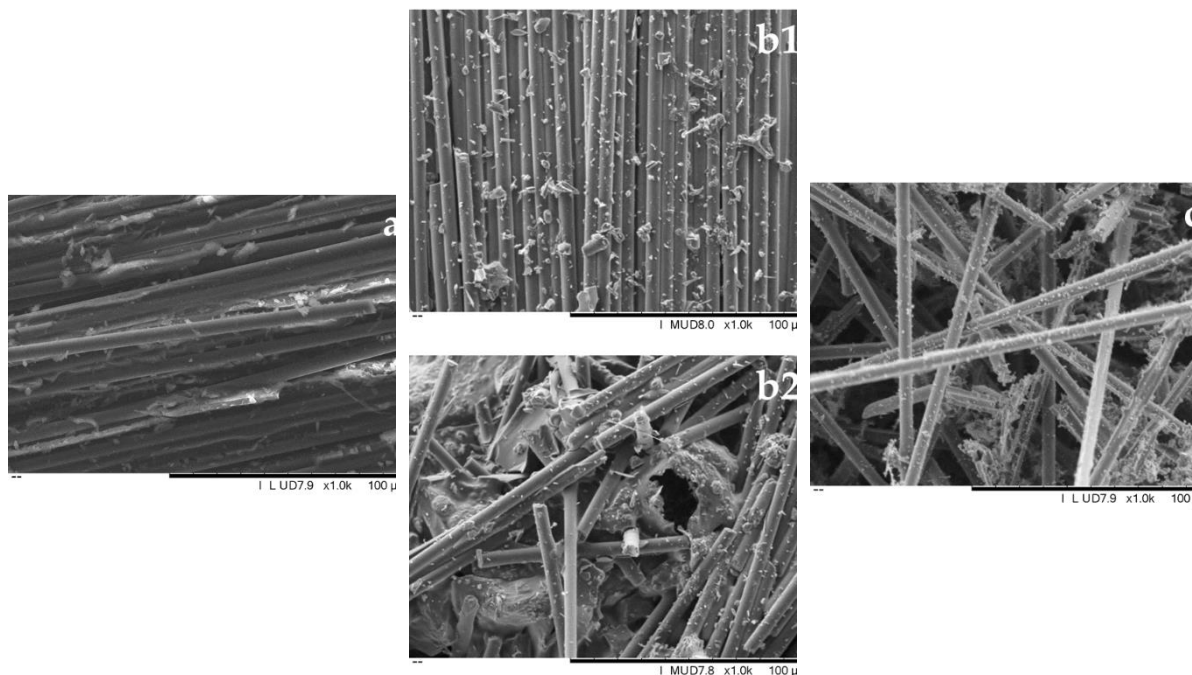


**Figure 6.25** 1000x SEM images (a) SE at 5kV of carbon fibres; (b1) SE at 5kV of resin-bonded char – Surface 1; (b2) SE at 5kV of resin-bonded char – Surface 2; (c) SE at 5kV of non-bonded char

#### 6.2.1.6 The GC-MS results

In **Table 6.16**, the chemical compounds of the oil are reported with their molecular formula, peak value and retention time detected by GC-MS Agilent 8890. GC-MS analysis of the oil revealed that it was composed mainly of aromatic hydrocarbons like toluene, benzene, ethylbenzene, cis-Bicyclo[4.2.0]octa-3,7-diene, thus suggesting promising results in terms of fuels as some of these chemical compounds are basically present in conventional ones (e.g. gasoline, fuel oil [6.59]).

However, there are also some other compounds with nitrogen, sulphur and chlorine as heteroatoms, meaning that the oil requires a further hydrotreatment to be improved as a fuel. Unfortunately, the amount of oil deriving from TCR was not enough to be hydrotreated due to insufficient time to repeat experiments and optimize conditions to obtain best results.

**Table 6.16** Chemical compounds detected and identified by GC-MS of oil from carbon fibre

Compound Name	Molecular formula [6.29]	Retention I (min)	Peak Value
Toluene	C <sub>7</sub> H <sub>8</sub>	4.68	108511.68
Benzene	C <sub>6</sub> H <sub>6</sub>	3.48	97486.56
Ethylbenzene	C <sub>8</sub> H <sub>10</sub>	6.37	7935.34
2-methyl-Pyridine	<u>C<sub>6</sub>H<sub>7</sub>N</u>	8.55	6332.33
2-Pyridylacetonitrile	<u>C<sub>7</sub>H<sub>6</sub>N<sub>2</sub></u>	8.87	5463.23
Benzene, (ethylsulfonyl)-	<u>C<sub>8</sub>H<sub>10</sub>O<sub>2</sub>S</u>	16.36	3854.50
5-Chlorovaleryl amide, N-(2-phenylethyl)-N-heptyl-	-	12.63	3775.31
cis-Bicyclo[4.2.0]octa-3,7-diene	C <sub>8</sub> H <sub>10</sub>	6.80	3038.19
(3E,5Z)-3,5-Undecadien-1-yne	C <sub>11</sub> H <sub>16</sub>	22.79	2224.80
Dichloroacetaldehyde	<u>C<sub>2</sub>H<sub>2</sub>Cl<sub>2</sub>O</u>	3.28	1890.57
cis-Bicyclo[4.2.0]octa-3,7-diene	C <sub>8</sub> H <sub>10</sub>	9.54	1883.97
Spiro[bicyclo[3.1.0]hexane-2,1'-cyclopropan]-3-ene	-	8.65	1855.22
Clofexamide	<u>C<sub>14</sub>H<sub>21</sub>ClN<sub>2</sub>O<sub>2</sub></u>	3.11	1822.32

Compounds with higher peaks are also reported in the following chromatogram in **Figure 6.26**.

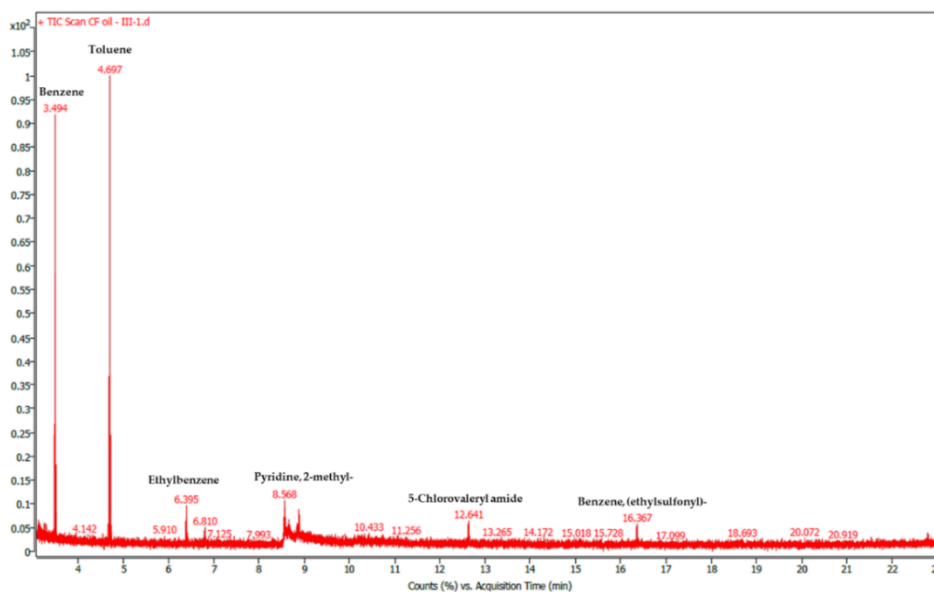


**Figure 6.26** 1D representation of GCxGC results of carbon fibre oil

## References

- [6.1] A. Sattara, G. A. Leeke, A. Hornung, J. Wood, Steam gasification of rapeseed, wood, sewage sludge and miscanthus biochars for the production of a hydrogen-rich syngas, *Biomass and Bioenergy*, Volume 69, October 2014, Pages 276-286;
- [6.2] G. Trif-Tordai, I. Ionel, Waste Biomass as Alternative Bio-Fuel - Co-Firing versus Direct Combustion, *Alternative Fuel*, 2011, Available Online: <https://www.intechopen.com/chapters/17594> (accessed on 08/09/2022);
- [6.3] A. Batuer, D. Chen, L. Yin, Y. Feng, Correlation between mechanical properties and thermochemical behaviours of waste papers in their early devolatilization stage, *Journal of Analytical and Applied Pyrolysis*, 137 (2019) 128–137;
- [6.4] P. Girods, A. Dufour, Y. Rogaume, C. Rogaume, A. Zoulalian, Thermal removal of nitrogen species from wood waste containing urea formaldehyde and melamine formaldehyde resins, *Journal of Hazardous Materials* 159 (2008) 210–221, available online: [https://www.academia.edu/29694004/Thermal\\_removal\\_of\\_nitrogen\\_species\\_from\\_wood\\_waste\\_containing\\_urea\\_formaldehyde\\_and\\_melamine\\_formaldehyde\\_resins](https://www.academia.edu/29694004/Thermal_removal_of_nitrogen_species_from_wood_waste_containing_urea_formaldehyde_and_melamine_formaldehyde_resins) (accessed on 15/03/2022);
- [6.5] F. Torres-Herrador, A. Eschenbacher, J. Coheur, J. Blondeau, T. E. Magin, K. M. Van Geem, Decomposition of carbon/phenolic composites for aerospace heatshields: Detailed speciation of phenolic resin pyrolysis products, *Aerospace Science and Technology* 119 (2021) 107079;
- [6.6] T. Shoji, H. Kawamoto, S. Saka, Boiling point of levoglucosan and devolatilization temperatures in cellulose pyrolysis measured at different heating area temperatures, *Journal of Analytical and Applied Pyrolysis* 109 (2014) 185–195;
- [6.7] A.V. Bridgwater, D. Meier, D. Radlein, An overview of fast pyrolysis of biomass, *Organic Geochemistry* Volume 30, Issue 12, 1999, Pages 1479-1493;
- [6.8] Available online: [https://www.engineeringtoolbox.com/fuels-higher-calorific-values-d\\_169.html](https://www.engineeringtoolbox.com/fuels-higher-calorific-values-d_169.html) (accessed on 03/05/2022);

- [6.9] J. G. Speight, 2 - Introduction to refining processes, *The Refinery of the Future* (Second Edition), 2020, Pages 43-84;
- [6.10] Y. Zheng, J. Wang, D. Wang, Z. Zheng, Advanced catalytic upgrading of biomass pyrolysis vapor to bio-aromatics hydrocarbon: A review. *Applications in Energy and Combustion Science*, 2022, 100061;
- [6.11] H. Xiang, R. Xin, N. Prasongthum, P. Natewong, T. Sooknoi, J. Wang, P. Reubroycharoen, X. Fan, Catalytic conversion of bioethanol to value-added chemicals and fuels: A review, *Resources Chemicals and Materials*, 1(1), 2022, 47-68;
- [6.12] S.A. Channiwala, P.P.Parikh, A unified correlation for estimating HHV of solid, liquid and gaseous fuels, *Fuel* 81 (2002) 1051-1063;
- [6.13] H.P. Yang, R. Yan, H.P. Chen, D.H. Lee, C.G. Zheng, Characteristics of hemicellulose, cellulose and lignin pyrolysis, *Fuel* 86 (2007) 1781-1788;
- [6.14] M.N. Uddin, W.M.A.W. Daud, H.F. Abbas, Effects of pyrolysis parameters on hydrogen formations from biomass: a review, *RSC Adv.* 4 (2014), 10467-10490;
- [6.15] K. A. Trick, T.E. Saliba, Mechanisms of the pyrolysis of phenolic resin in a carbon/phenolic composite, *Carbon* Vol. 33, No. 11, pp. 1509-1515,1995;
- [6.16] J. Santos, H. Jahangiri, M. Asif Bashir, A. Hornung, M. Ouadi, The Upgrading of Bio-Oil from the Intermediate Pyrolysis of Waste Biomass Using Steel Slag as a Catalyst, *ACS Sustainable Chem. Eng.* 2020, 8, 50, 18420–18432;
- [6.17] M. Asif Bashir, H. Jahangiri, A. Hornung, M. Ouadi, Deoxygenation of Bio-oil from Calcium-Rich Paper-Mill Waste, *Chemical Engineering & Technology* 44(1):194-202;
- [6.18] F. Ronsse, R. W. Nachenius, W. Prins, Chapter 11 - Carbonization of Biomass, *Recent Advances in Thermo-Chemical Conversion of Biomass*, Elsevier, 2015, 293-324;
- [6.19] M. Ouadi, J. G. Brammer, Y. Yang, A. Hornung, M. Kay, The intermediate pyrolysis of de-inking sludge to produce a sustainable liquid fuel, *J Anal Appl Pyrol*, 102 (2013), pp. 24-32;
- [6.20] A. Hornung, H. Jahangiri, M. Ouadi, C. Kick, L. Deinert, B. Meyer, J. Grunwald, R. Daschner, A. Apfelbacher, M. Meiller, S. Eder, Thermo-Catalytic Reforming (TCR)–An important link between waste management and

renewable fuels as part of the energy transition, Applications in Energy and Combustion Science, Volume 12, 2022;

- [6.21] A. Hornung, et al., The Thermal Treatment of Biomass, Great Britain Patent Application Number: GB 0808739.7: Application submitted: May 15, 2009, World Patent Applied for (WO 2009/138757; November 19, 2009), 2009;
- [6.22] A Hornung, A. Apfelbacher Thermal treatment of biomass (2009) UK patent application GB2460156A [http://worldwide.espacenet.com/publicationDetails/biblio?FT=D&date=20110330&DB=EPODOC&locale=en\\_EP&CC=EP&NR=2300560A2&KC=A2&ND=4;](http://worldwide.espacenet.com/publicationDetails/biblio?FT=D&date=20110330&DB=EPODOC&locale=en_EP&CC=EP&NR=2300560A2&KC=A2&ND=4;)
- [6.23] J. Argudo-Santamaria, H. Ortiz, B. Cano, I. Auclair, M. Silva, J. Palomino, F. Fernández, S. Garcia, T. Pham, A. Ramírez, Production and Applications of Pyrolytic Oil and Char from Lignocellulosic Residual Biomass, Valorization of Biomass to Value-Added Commodities 2020, pp.261-284;
- [6.24] J. Santos, M. Ouadi, H. Jahangiri, A. Hornung, Valorisation of lignocellulosic biomass investigating different pyrolysis temperatures, Journal of the Energy Institute 93 (2020) 1960-1969;
- [6.25] M. A. Bashira, S. Lima, H. Jahangiri, A. J. Majewski, M. Hofmann, A. Hornung, M. Ouadi, A step change towards sustainable aviation fuel from sewage sludge, Journal of Analytical and Applied Pyrolysis, Volume 163, 2022, 105498;
- [6.26] J J. Santos, M. Ouadi, H. Jahangiri, A. Hornung, Thermochemical conversion of agricultural wastes applying different reforming temperatures, Fuel Processing Technology, Volume 203, 15 June 2020, 106402;
- [6.27] S. Cheng, L. Wei, X. Zhao, J. Julson, Application, Deactivation, and Regeneration of Heterogeneous Catalysts in Bio-Oil Upgrading, Catalysts 2016, 6, 195;
- [6.28] Available online: <https://www.eeer.org/journal/view.php?number=1217> (accessed on 25/05/2022);
- [6.29] Available online: <https://pubchem.ncbi.nlm.nih.gov/> (accessed on 14/06/2022);

- [6.30] Available online: <https://www.topsoe.com/our-resources/knowledge/our-products/catalysts/tk-341?hsLang=en> (accessed on 23/05/2022);
- [6.31] S. Vedachalam, A.K. Dalai, Hydrotreating and oxidative desulfurization of heavy fuel oil into low sulfur marine fuel over dual function NiMo/ $\gamma$ -Al<sub>2</sub>O<sub>3</sub> catalyst, *Catalysis Today*, 2022;
- [6.32] S. Rudra, M. Jayathilake, 5.08 - Hydrothermal Liquefaction of Biomass for Biofuel Production, *Comprehensive Renewable Energy (Second Edition)*, Volume 5, 2022, Pages 165-186;
- [6.33] M. Zhang, Y. Hu, H. Wang, H. Li, X. Han, Y. Zeng, C. C. Xu, A review of bio-oil upgrading by catalytic hydrotreatment: Advances, challenges, and prospects, *Molecular Catalysis*, Volume 504, March 2021, 111438;
- [6.34] K. Chaiwong, T. Kiatsiriroat, N. Vorayos, C. Thararax, Study of bio-oil and bio-char production from algae by slow pyrolysis, *biomass and bioenergy* 56 (2013), 600-606;
- [6.35] T. H. Pedersen, N. H. Hansen, O. M.s Pérez, D. E. V. Cabezas, L. A. Rosendahl, Renewable hydrocarbon fuels from hydrothermal liquefaction: A techno-economic analysis, *Biofuels, Bioproducts and Biorefining*, 2017;
- [6.36] L. Wang, W. Yi, A. Zhang, Z. Li, Ho. Cai, Y. Li, Catalytic Fast Pyrolysis of Corn Stalk for Phenols Production With Solid Catalysts, *Frontiers in Energy Research*, 7, 2019;
- [6.37] Available online: <https://mccordresearch.com.au/library/volatiles/esters/methyl-heptanoate/> (accessed on 17/06/2022);
- [6.38] Available online: <https://mccordresearch.com.au/library/volatiles/esters/methyl%20hexanoate/> (accessed on 17/06/2022);
- [6.39] Available online: <https://www.ipu.co.uk/en590/> (accessed on 24/05/2022);
- [6.40] Available online: <https://www.imo.org/en/MediaCentre/PressBriefings/pages/02-IMO-2020.aspx> (accessed on 24/05/2022);



- [6.41] R. Kumar, B. S. Rana, R. Tiwari, D. Verma, R. Kumar, R. K. Joshi, M. O. Garga, A. K. Sinha, Hydroprocessing of jatropha oil and its mixtures with gas oil, *Green Chem.*, 2010,12, 2232-2239;
- [6.42] B. Demirel, W. H. Wiser, Production of high octane gasoline components by hydroprocessing, of coal-derived aromatic hydrocarbons, *Studies in Surface Science and Catalysis*, Volume 106, 1997, Pages 469-478;
- [6.43] I. S. Golubev, P. P. Dik, M. O. Kazakov, V. Y. Pereyema, O. V. Klimov, M. Y. Smirnova, I. P. Prosvirin, E. Y. Gerasimov, D. O. Kondrashev, V. A. Golavachev, O. S. Vedernikov, A. V. Kleimenov and A. S. Noskov, "The effect of Si/Al ratio of zeolite Y in NiW catalyst for second," *Catalysis Today*, vol. 378, pp. 65-74, 2021;
- [6.44] W. Cui, W. Li, R. Gao, H. Ma, D. Li, M. Niu, X. Lei, Hydroprocessing of Low-Temperature Coal Tar for the Production of Clean Fuel over Fluorinated NiW/Al<sub>2</sub>O<sub>3</sub>-SiO<sub>2</sub> Catalyst, *Energy Fuels* 2017, 31, 4, 3768–3783;
- [6.45] Z. Zhang, H. Li, Water-mediated catalytic hydrodeoxygenation of biomass, *Fuel*, Volume 310, Part A, 15 February 2022, 122242;
- [6.46] Z. Rui, D. Wei, Y. Zhibin, Z. Chao, A. Xiaojuan, Effects of wood vinegar on the soil microbial characteristics, *Chem. Pharmaceut. Res.* 6 (2014) 1254-1260;
- [6.47] Y. Baimark, N. Niamsa, Study on wood vinegars for use as coagulating and antifungal agents on the production of natural rubber sheets, *Biomass Bioenergy*, 33 (2009) 994-998;
- [6.48] Available online: <https://pubchem.ncbi.nlm.nih.gov/> (accessed on 14/06/2022);
- [6.49] H. Shi, W. Si, X. Li, The Concept, Design and Performance of a Novel Rotary Kiln Type Air-Staged Biomass Gasifier, *Energies* 2016, 9, 67;
- [6.50] C. Ruan, Y. Xie, Electrochemical performance of activated carbon fiber with hydrogen bond-induced high sulfur/nitrogen doping, *RSC Adv.*, 2020, 10, 37631;
- [6.51] S. Q. Hao, K. H. Wong, X. L. Liu, C. D. Rudd, Influence of chemical treatment on the recycling of composites before pyrolysis, *J. Phys.: Conf. Ser.* 1765 012019;

- [6.52] J. Deng, L. Xu, L. Zhang, J. Peng, S. Guo, J. Liu, S. Koppala, Recycling of Carbon Fibers from CFRP Waste by Microwave Thermolysis, *Processes* 2019, 7, 207;
- [6.53] A. Lopez-Urionabarrenechea, N. Gastelu, E. Acha, B.M. Caballero, A. Orue, A. Jimenez-Suarez, S.G. Prolongo, I. de Marco, Reclamation of carbon fibers and added-value gases in a pyrolysisbased composites recycling process, *Journal of Cleaner Production* 273 (2020) 123173;
- [6.54] O. I. Arowosafe, M. I. Okoroh, A. M. Dean, Application of Iso14001 for Composites Waste Management, *Sustainable Building Conference* 2013;
- [6.55] L. Mazzocchetti, T. Benelli, E. D'Angelo, C. Leonardi, G. Zattini, L. Giorgini, Validation of carbon fibers recycling by pyro-gasification: The influence of oxidation conditions to obtain clean fibers and promote fiber/matrix adhesion in epoxy composites, *Composites Part A* 112 (2018) 504–514;
- [6.56] F. Baker, N. Gallego, C. Contescu, T. Burchell, Use of carbon fiber composite molecular sieves for air separation, Metals and Ceramics Division, Prepared for Fossil Energy AR&TD Materials Office, ORNL/TM-2005/527. Available online: <https://info.ornl.gov/sites/publications/Files/Pub522.pdf> (accessed on 19/12/2022);
- [6.57] H. Sukanto, W. Wisnu Raharjo, D. Ariawan, J. Triyono, Carbon fibers recovery from CFRP recycling process and their usage: A review, *IOP Conf. Ser.: Mater. Sci. Eng.* 1034 012087, 2021;
- [6.58] G. Faneca, T. Ikumib, J. M. Torrents, A. Aguado, I. Segura, Conductive concrete made from recycled carbon fibres for self-heating and de-icing applications in urban furniture, *Materiales de Construcción* Vol. 70, Issue 339, July–September 2020, e223;
- [6.59] P.K. Gupta, Chapter 8 - Solvents, vapors, and gases, *Illustrated Toxicology with Study Questions*, 2018, Pages 247-263. Available online: <https://www.sciencedirect.com/topics/neuroscience/ethylbenzene> (accessed on 19/12/2022).

## 7. Techno-economic assessment

### Chapter summary

The chapter assesses a detailed techno-economical estimation for a commercial TCR3000 plant based on a real demonstrator. In this case study, the plant is supposed to process 3000 ton/h of dried feedstocks (i.e. solid grade laminate and carbon fibres, respectively) and its overall process flow diagram (PFD) is presented in **Figure 7.1**.

In particular, the analysis was carried out according to two plant models. The first model (Model 1) determined revenues deriving from the thermal and electrical energy produced by CHP, the sale of kerosene, gasoline, diesel and the excess of hydrogen; while the second one (Model 2) computed the income from the thermal and electrical energy produced by CHP and the sale of the entire green hydrogen production.

Both the models are described in detail, and each step of the process was characterized in Excel assuming values deriving from the mass and energy balances obtained from TGA or during the experimental trials in the lab scale TCR2 and hence scaled up in the commercial plant. On the contrary, the electrical and thermal energy consumptions are assumed those typical for a commercial plant.

The techno-economic assessment does not consider any subsidies, incentives or other variable costs which could include interests from the government or the financial institutions. The analysis is based on steady state computations assuming a private investment.

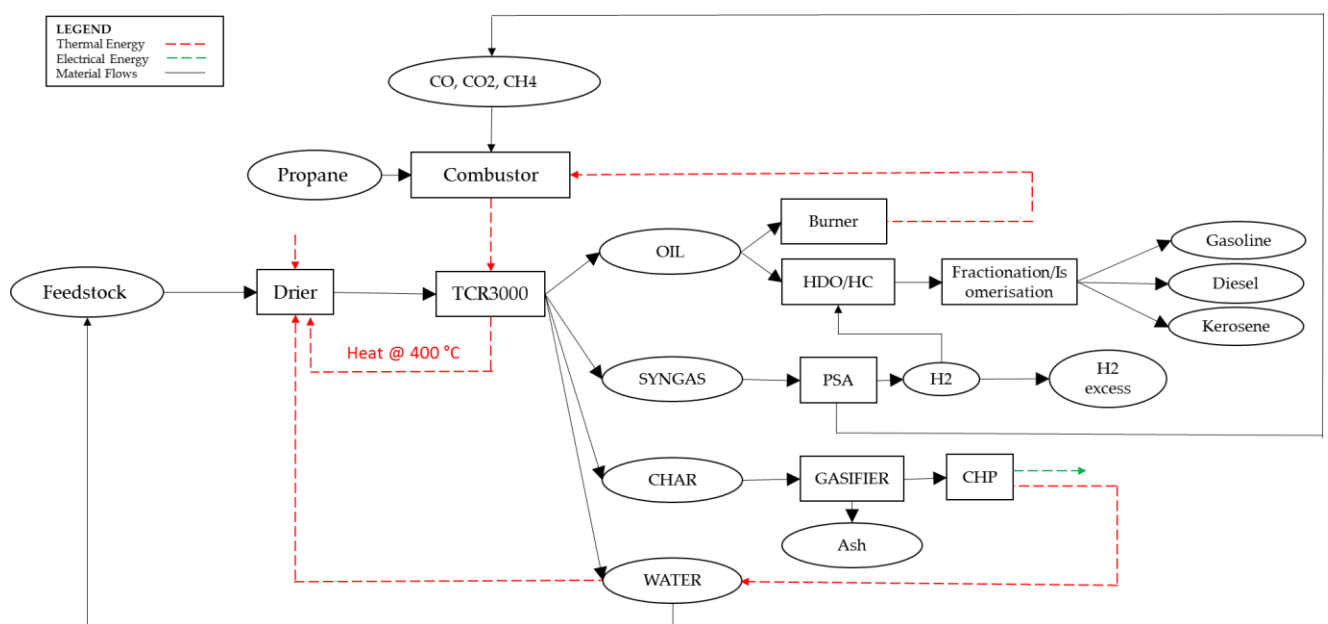


Figure 7.1 Process Flow Diagram of TCR-3000

## 7.1 TCR3000 setup and process assumptions

The TCR3000 can process 3000 ton/h of dried feedstock, more than 24,000 tons per year (according to the moisture content of the feedstock) assuming 8000 operating hours per year. The commercial plant scheme was designed within “To-Syn-Fuel” and “Green-FlexJET” projects to work with sewage sludge. However, sewage sludge is not the only type of feedstock that can be processed in TCR, as the technology showed a high potential in the utilization of many other second-generation biomasses.

Indeed, the aim of this chapter was to assess the techno-economic feasibility of TCR3000 technology in case solid grade laminate (SGL) and carbon fibres (CF) were used separately as feedstocks.

In this commercial configuration (**Figure 7.1**), the dryer supplies the thermal energy necessary to dry the biomass, before it enters the TCR reactor. Moreover, the drier is considered out of this scope, since both SGL and CF were already dry, but the equipment could be destined for all other applications where feedstock has high moisture content (e.g. sewage sludge with MC > 70wt%) and requires to be dried. The specific thermal energy to evaporate waste water is around 2.6 MJ/kg (i.e. 1 kW of thermal power is required for 1 kg of water) and it can be supplied externally (e.g. a natural gas burner [7.1]), either through the waste heat recovered from TCR, by supplying a temperature around 400°C (high enough for water evaporation), or using thermal energy deriving from CHP plant. The plant also includes a combustion chamber which burns propane and supplies the thermal energy necessary to heat up the auger reactor of the TCR plant and the post reformer. Afterwards, the thermo-catalytic reforming occurs, and it produces oil, syngas, char and water, as described in the previous chapters.

In turn, TCR can receive 20% of thermal input from hydrogen-free syngas (the resulting tail gas at  $T \sim 900^{\circ}\text{C}$  [7.2]) exiting the PSA, thus reducing the propane consumption as the process is self-reliant.

The hydrogen coming from PSA can serve to hydrotreat the pyrolysis oil or be sold as a green hydrogen fuel. The oil deriving from TCR has high carbon content, low water content, low oxygen content and high heating value, which make it a high-quality fuel. Consequently, this latter would be applicable not only as feed in boilers/burners or as blend with other fuels, but also as a biofuel for internal combustion engines and vehicles after a successive upgrading. It has been estimated an HDO efficiency around

75% and a hydrogen consumption of about 10% (i.e. each ton of hydrotreated oil requires around 100 kg of hydrogen) [7.3]. This percentage was obtained by doubling it in order to have enough hydrogen and guarantee the continuity of the hydrotreatment process. In fact, excess hydrogen is recycled back into the reactor at full scale.

Potentially, it is feasible to achieve good fractions of gasoline, kerosene and diesel after the distillation process, with assumed efficiency percentages of 30wt%, 35wt% and 35wt%, respectively. These percentage mass yields are collected from previous experimental trials of distillation at the University of Birmingham.

The char collected in the post reformer has still enough calorific value (e.g. HHV > 12 MJ/kg) to be used directly as a fuel, hence a gasifier is installed and connected to a cogeneration (CHP) plant for the combined production of thermal energy and electricity. The gasifier thermal efficiency is considered equal to 80% [7.4], while the thermal and electrical engine efficiencies are estimated 35% [7.5] and 30% [7.6], respectively.

The residual mass exiting the gasifier is ash and fixed carbon. The amount of fixed carbon is assumed to be half of that obtained from TGA results as not all fixed carbon can be collected at the end of the process. For the sake of clarity, all the assumptions are reported in **Table 7.1**.

**Table 7.1** List of assumption for TCR3000 process

<b>Assumptions</b>	
Mass flow rate (kg/h)	3000
Operation hours (h)	8000
Thermal input energy (%)	20
HDO efficiency (%)	75
H <sub>2</sub> consumption (kg <sub>H2</sub> /kg <sub>oil</sub> )	0.1
Gasoline conversion efficiency (%)	30
Kerosene conversion efficiency (%)	35
Diesel conversion efficiency (%)	35
Gasifier thermal efficiency (%)	80
Thermal engine efficiency (%)	35
Electrical engine efficiency (%)	35

## 7.2 Techno-economic evaluation criteria

The techno-economic analysis was broken down in the following parts:

- a. *Total Capital Cost (TCC)*: the total capital investment required to install all necessary equipment so that the plant is operational under steady state conditions;

TCC is the sum of Fixed Capital (FC) and Working Capital (WC). FC includes the Total Equipment Purchase (PCE) and the auxiliary equipment purchases computed as incrementals of PCE (e.g. equipment erection, piping, instrumentation, electrical wiring, building and utilities infrastructures, storage and site development). Their sum represents the Total Physical Plant Cost (PPC) to which other fees (e.g. design and engineering, contracts and fee, contingency) are added. Finally, WC is estimated on average to be 3% of FC.

For sake of clarity, the evaluation of TCC is reported below:

$$TCC = FC + WC = PCE + Aux + Other\ fees + 3\%FC = PPC + Other\ fees + 3\%FC$$

- b. *Operating Cost (OC)*: all costs incurred during operation of the plant (e.g. labour costs, disposal costs, maintenance and repair costs, administration and insurance, site rent, transport cost);
- c. *Gross Profit (GP)*: total yearly income received from sales of products (heat, electricity, hydrogen and/or biofuels) by the plant after operating costs but before tax deductions;
- d. *Net Profit (NP)*: total yearly net revenue made by the plant after all costs and tax deductions estimated;
- e. *Payback period*: total time required to recover the Total Capital Cost (TCC) of the plant;
- f. *Return on Investment (ROI)*: the ratio of after-tax operating income to the net depreciated value of assets computed in the Total Capital Cost.

For the purpose of this study, all the costs are expressed in EURO and depreciation is not considered. The percentages used for Total Capital Costs and Operating Costs are reported in [7.7]. A more precise economic appraisal would require a thorough analysis and critique into the specific aspects of the plant design which is beyond the scope of this study.

### 7.3 The plant models

The techno-economic analysis is based on two different plant models: Model 1 and Model 2. Both plants are applied for solid grade laminate and carbon fibres and require different equipment which influence greatly the Total Capital Costs (TCC) evaluation and hence the Net Profit (NP) deriving from such investment. Their configurations are described in detail in the following sections.

#### 7.3.1 Model 1

The Model 1 is reported in **Figure 7.2** and it encompasses the hydrotreatment section to produce biofuels from the pyrolysis oil deriving from TCR. The hydrogen required for the upgrading is taken from the PSA of syngas. Its consumption is studied with the aim of meeting the whole demand required for HDO/HC and understanding if the process needs extra amount of H<sub>2</sub> or not. The resulting biofuels (gasoline, kerosene and diesel) are assumed to be sold together with the excess of hydrogen, if possible, and thermal and electrical power from CHP plant.

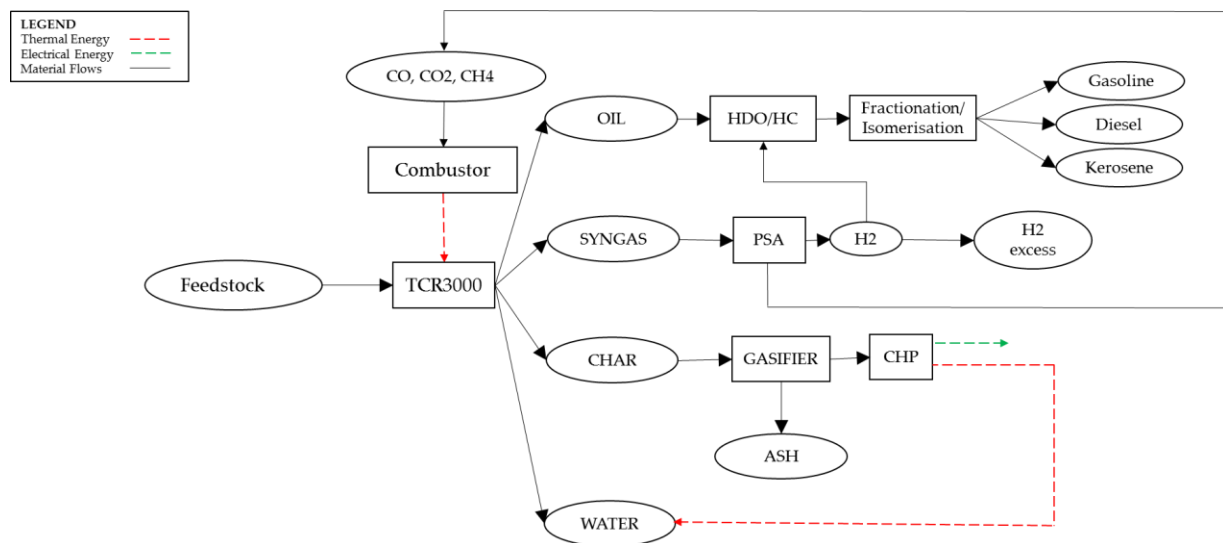


**Figure 7.2** Process Flow Diagram of Model 1

#### 7.3.2 Model 2

Model 2 is described in **Figure 7.3** and evidently it excludes the upgrading of oil. The pyrolysis oil is destined to a burner to produce heat for the combustor upstream of TCR. In this case, the hydrogen can be directly sold together with thermal energy and electricity from CHP.

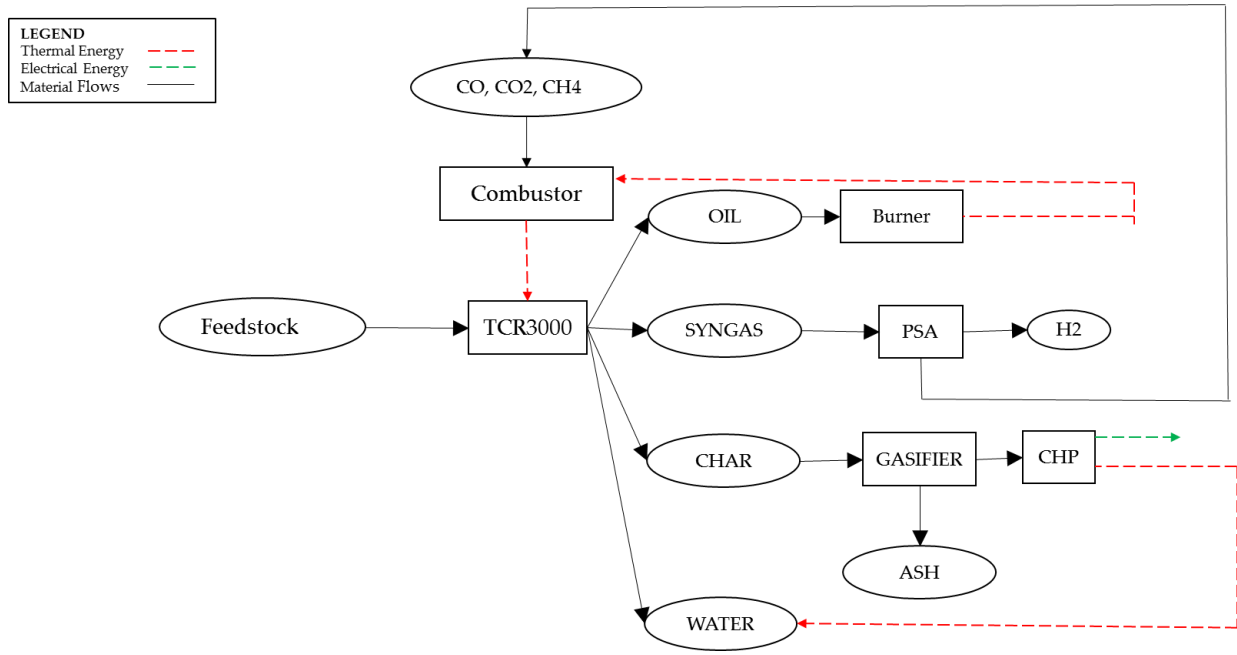


Figure 7.3 Process Flow Diagram of Model 2



## 7.4 Results

The results deriving from Model 1 and Model 2 are systematically reported in the APPENDICES at the end of the thesis and here commented for both feedstocks: solid grade laminate and carbon fibres. In terms of equipment required for Model 1 and Model 2, they differ for the cost of burner, which is only used in Model 2 and the HDO and fractionation plant, which is considered in Model 1. Furthermore, both models do not consider the cost of drier as feedstocks are already dried as mentioned previously. All the major plant items required for the process plant are listed in **Table 7.2** as follows, however only model 1 requires HDO plant as well as only model 2 requires a burner:

**Table 7.2** Complete list of the total equipment required

Feedstock Silo
Feedstock Tube Chain Conveyor
Feedstock Sluice system
Auger reactor
Post reactor
Flue gas distributor + High temperature valve
Combustion chamber + NOX AND SOX SCRUB
Syngas combustor
Burner
Gasifier
Induced Draft Blower + STACK Flue gas removal
Char Extraction Screw + Char Sluice + Char Chiller
Tube chain conveyor + silo
Air separator
Cyclone
Condensation Unit (Heat exchanger + ESP)
Table cooler
Oil water separator tank
Acid scrubber + ESP
Syngas compressor
PSA
H2 compressor
Flare
Propane tank
H2 storage
HDO plant and fractionation

## 7.4.1 Solid Grade Laminate

### 7.4.1.1 Total Capital Costs

#### Model 1

In Model 1, the Total Capital Costs are estimated as sum of fixed capital (FC) and working capital (WC). The FC include the total equipment purchase costs (PCE) referring to the items in **Table 7.2**, whose overall value is 7,635,000.00 €. The PCE is added to the incremental costs which are equipment installation (10% PCE), piping (5% PCE), instrumentation (15% PCE), electrical wiring (10% PCE), building and utilities infrastructures (10% PCE), storage (5% PCE) and site development (10% PCE) whose total value is 4,962,750.00 €. The total amount of is 12,597,750.00 € which represents the total physical plant cost (PPC). Finally, design and engineering, contracts and fee, contingency are computes as incrementals of PPC. These percentages are 5%, 5% and 20%, respectively, contributing by 3,779,325.00 €. Thus, the Fixed Capital is 16,377,075.00. By considering a working capital (WC) equal to 3% of FC, the total capital cost for model 1 is **16,704,616.00 €**.

#### Model 2

The PCE is equal to 5,695,000.00 € which is lower than that deriving from Model 1, as the HDO and fractionation plant is not present, even if the burner is here considered. The auxiliary equipment is 3,701,750.00 €, while other fees account for 2,819,025.00 €, contributing to a total fixed capital of 12,215,775.00 €. By summing fixed capital and working capital, the total capital cost is now **12,460,090.00 €**. In this scenario, the TCC is lower since the plant destined to HDO and fractionation contributes heavily.

### 7.4.1.2 Operating Costs

As already mentioned, the operating costs include labour costs, disposal costs, maintenance costs, administration and insurance, site rent and transport cost.

In order to estimate all these costs, the following assumptions for labour costs were considered in **Table 7.3** and they are the same for both models. Moreover, labour costs may vary in a large range according to cities, experiences and skills.

**Table 7.3** Labour costs assumptions

Labour costs			Ref.s
CEO	120,000	EUR/year	[7.8]
Sales director	60,000	EUR/year	[7.9]
Finance manager	60,000	EUR/year	[7.10]
HR manager	60,000	EUR/year	[7.11]
Technical manager	60,000	EUR/year	[7.12]

Technician on site	25	EUR/h	[7.13]
Labour workers on site	15	EUR/h	[7.14]

Both technician and labour workers are supposed to work shifts in such a way they are always on site at least during the first year (i.e. 8000 hours) of the plant in operation. Furthermore, new TCR plants are designed to be fully automated, thus requiring minimum labour force.

Regarding disposal costs, only ash was considered in the operating costs, since process water is totally evaporated in both models through heat coming from CHP plant. To dispose ashes, 85 €/ton was used in the computations based on landfill tax in UK, whereas the maintenance cost accounts for the 3% of the TCC. The cost of propane for the combustor can be considered negligible with respect to other costs as the process is self-reliant at the steady state regime. Finally, all other costs are estimated from values of a real demonstrator. According to these assumptions, the operating costs are reported in **Table 7.4**.

**Table 7.4** Operating costs for Model 1 and Model 2

Operating Costs	EUR/year
<i>Model 1</i>	1,685,378.50
<i>Model 2</i>	1,558,042.72

In this case, Model 1 has higher operating costs than Model 2 because of the higher maintenance costs related to the total capital cost including the HDO and fractionation plant in Model 1.

#### 7.4.1.3 Revenues

The TCR3000 plant receives revenues by selling its final products as well as the thermal and the electrical energy from the CHP plant. However, TCR products are different due to the amount of thermal energy required for the water evaporation. Indeed, these values depend on mass and energy balance coming from Model 1 and Model 2. Moreover, the production of electrical power is assumed to be completely sold even if it could be partly used as a source for lighting for the whole plant.

Furthermore, both models consider the feedstock gate fee corresponding to the amount paid to the plant to take waste feedstocks. The sale prices of products from TCR are reported in **Table 7.5**, although they may be subject to change:

**Table 7.5** Selling prices of products deriving from TCR3000

Revenues		Ref.s		
Electrical cost	€	75.00	EUR/MWh	[7.15]
Heat cost	€	35.00	EUR/MWh	[7.16]
Kerosene/Diesel/Petrol	€	1.20	EUR/L	[7.17]
Green H <sub>2</sub>	€	10.00	EUR/kg	[7.18]
Feedstock gate fee	€	20.00	EUR/ton	[7.19]

### *Model 1*

In Model 1, kerosene, petrol and diesel are sold together with the excess of hydrogen unused in the upgrading process and the energy from the CHP plant. The total revenues account for **5,335,206.49 €**.

### *Model 2*

In Model 2, only green hydrogen is sold, while the pyrolysis oil is directly burned to produce additional heat for the combustor. The remaining thermal energy is still high to be eventually sold with electricity from CHP. The total revenues are **4,930,513.07 €**.

The Model 1 got higher revenues than Model 2, thanks to the combined sales of biofuels and hydrogen, while all other revenues (**Table 7.5**) are similar. In particular, the production of hydrogen through PSA not only self-sustain the HDO process, but it is even more than the value required for that, leading to an excess of hydrogen that can be sold.

#### *7.4.1.4 Profits*

In order to evaluate the profitability of such investment, it is firstly necessary to evaluate the Gross Profit at first. The Gross Profit simply defines what you earn once you paid for all the items required for the operation of the plant, without taking into account taxes. The value of the Gross Profit is reported in **Table 7.6**.

**Table 7.6** Gross Profits for Model 1 and Model 2

Gross Profits	EUR
<i>Model 1</i>	3,649,828.00
<i>Model 2</i>	3,372,470.35

By assuming 30% taxes, the Net Profits become as illustrated in **Table 7.7**.

**Table 7.7** Net Profits for Model 1 and Model 2

<b>Net Profits</b>	<b>EUR</b>
<i>Model 1</i>	2,554,879.60
<i>Model 2</i>	2,360,729.25

Model 1 results more profitable than Model 2 by 194,150.35 €.

#### *7.4.1.5 Payback Period*

The payback period consists of the number of years the plant requires to repay the initial investment.

However, an additional year and 6 months are considered for the plant settlement in terms of building time and commissioning and optimization.

The final payback periods for Model 1 and Model 2 are shown in **Table 7.8**.

**Table 7.8** Payback period for Model 1 and Model 2

<b>Payback period</b>	<b>years</b>
<i>Model 1</i>	8.5
<i>Model 2</i>	7

Although Model 1 is more profitable in terms of net profits, it also requires more years to be ready to earn more profits after the initial investment is paid off. Hence, it is recommendable that equipment in Model 1 satisfies long life specifications so that the plant is competitive in the market even after 8 and a half years.

#### 7.4.1.6 ROI

The return on investment (ROI) is the ratio of after-tax operating income to the value of assets assuming there is not asset depreciation here. The ROI values for Model 1 and Model 2 are reported in **Table 7.9**:

**Table 7.9** ROI for Model 1 and Model 2

<b>ROI</b>	<b>%</b>
<i>Model 1</i>	15
<i>Model 2</i>	19

Both values are positive, meaning that the throughput of the investment is good because the profit from the investment is higher than the total capital cost. In this case Model 2 starts with a higher ROI, thus bringing more profit margin than Model 1. However, both ROI are expected to increase as the capital cost is supposed to decrease because of the assets' depreciation.

## 7.4.2 Carbon Fibres

As it was done for solid grade laminate, a similar procedure is now followed for carbon fibres under the same assumptions. By streamlining description of each sections, results from Model 1 and Model 2 are directly reported.

### 7.4.2.1 Total Capital Cost

Total Capital Costs for both Model 1 and Model 2 are reported in **Table 7.10**:

**Table 7.10** Total Capital Costs for Model 1 and Model 2

Total Capital Cost	EUR
<i>Model 1</i>	16,704,616.50
<i>Model 2</i>	12,460,090.50

Model 1 has higher TCC than model 2 due to the HDO and fractionation plant, whose cost is around EUR 2 million.

### 7.4.2.2 Operating Costs

The operating costs include labour costs, disposal costs, maintenance costs, administration and insurance, site rent and transport cost.

Under the same assumptions for labour costs (**Table 7.3**), ashes disposal costs (85 €/ton) and maintenance costs (~ 3% TCC), the operating costs of both model are reported in **Table 7.11**:

**Table 7.11** Operating costs for Model 1 and Model 2

Operating Costs	EUR/year
<i>Model 1</i>	1,817,611.30
<i>Model 2</i>	1,690,275.52

In this case Model 1 has higher operating costs than Model 2 because of the higher maintenance costs related to the total capital cost including the HDO and fractionation plant in Model 1. Their difference is equal to 127,335.78 EUR/year.

### 7.4.2.3 Revenues

The TCR3000 plant receives revenues by selling its final products and the thermal and electrical energy from the CHP plant. However, TCR products are different as well as the amount of thermal energy required for the water evaporation according to the

model. Similarly, both models consider the feedstock gate fee corresponding to the amount paid to the plant to take waste feedstocks. The sale prices of products from TCR are already reported in **Table 7.5**. Revenues deriving from Model 1 and Model 2 are shown in **Table 7.12**:

**Table 7.12** Revenues for Model 1 and Model 2

<b>Revenues</b>	<b>EUR</b>
<i>Model 1</i>	6,023,962.70
<i>Model 2</i>	5,862,085.33

The Model 1 got higher revenues than Model 2, thanks to the combined sales of biofuels and hydrogen, while all other revenues (**Table 7.5**) stay the same.

#### 7.4.2.4 Profits

In order to evaluate the profitability from TCR3000 investment, Gross Profit are computed and reported in **Table 7.13**:

**Table 7.13** Gross Profits for Model 1 and Model 2

<b>Gross Profits</b>	<b>EUR</b>
<i>Model 1</i>	4,206,351.41
<i>Model 2</i>	4,171,809.82

By assuming 30% taxes, the Net Profits become as illustrated in **Table 7.14**:

**Table 7.14** Net Profits for model 1 and model 2

<b>Net Profits</b>	<b>EUR</b>
<i>Model 1</i>	2,944,445.99
<i>Model 2</i>	2,920,266.87

Model 1 results more profitable than Model 2 and their difference account for 24,179.12 €. The sale of green hydrogen is more profitable than that of biofuels, even if it includes a high initial investment due to the HDO plant (about EUR 2 million).



#### 7.4.2.5 Payback Period

The final payback periods for model 1 and model 2 are shown in **Table 7.15** where an additional year and 6 months are considered for the plant settlement in terms of building time and commissioning and optimization:

**Table 7.15** Payback period for Model 1 and Model 2

<b>Payback period</b>	<b>years</b>
<i>Model 1</i>	7.5
<i>Model 2</i>	6

Model 2 is here more profitable in terms of payback period since it only requires 6 years to be ready to earn more profits once the initial investment is paid off.

#### 7.4.2.6 ROI

The return on investment (ROI) for both models is illustrated in **Table 7.16** and it measures the ratio of after-tax operating income to the value of assets assuming there is not asset depreciation here.

**Table 7.16** ROI for Model 1 and Model 2

<b>ROI</b>	<b>%</b>
<i>Model 1</i>	18
<i>Model 2</i>	23

Both values are positive meaning that throughput of the investment is good because the profit from the investment is higher than the total capital cost. In this case model 2 starts with a higher ROI, however both ROI are expected to increase as the capital cost is supposed to decrease because of the assets' depreciation.

## 7.5 Conclusions

In this chapter, the economic evaluations of TCR3000 plant processing solid grade laminate and carbon fibres were analysed. Such assessment was based on assumptions and estimation from a real demonstrator. Results suggested that Model 1 is more advantageous for solid grade laminate in terms of revenues, even its payback period is longer, whereas Model 1 is more profitable for carbon fibres.

By comparing solid grade laminate with carbon fibres (**Table 7.17**), TCC are identical since the equipment required for the technology is the same. The OC are almost comparable even if they differ only for the disposal costs of ashes. Indeed, the amount of ashes to be disposed from CF are greater than those from SGL in model 1. Revenues deriving from CF are higher and with Net Profits around EUR 400,000 more than SGL. Moreover, the initial investment is paid off in a shorter time and with a greater ROI which allows a larger margin to repay the TCC.

In conclusion, the investment on CF might be the most remunerative in terms of profit, payback period and ROI.

**Table 7.17** Comparison between Model 1 and Model 2 for different feedstocks

	<b>Model 1</b>	<b>Model 2</b>
<b>Solid Grade Laminate</b>		
Total Capital Costs [EUR]	€ 16,704,616.50	€ 12,460,090.50
Operating Costs [EUR/year]	€ 1,685,378.50	€ 1,558,042.72
Revenues [EUR]	€ 5,335,206.49	€ 4,930,513.07
Net Profits [EUR]	€ 2,554,879.60	€ 2,360,729.25
Payback period [years]	8.5	7
ROI [%]	15	19
<b>Carbon Fibres</b>		
Total Capital Costs [EUR]	€ 16,704,616.50	€ 12,460,090.50
Operating Costs [EUR/year]	€ 1,817,611.30	€ 1,690,275.52
Revenues [EUR]	€ 6,023,962.70	€ 5,862,085.33
Net Profits [EUR]	€ 2,944,445.99	€ 2,920,266.87
Payback period [years]	7.5	6
ROI [%]	18	23

## References

- [7.1]. M. Ouadi, N. Jaeger, C. Greenhalf, J. Santos, R. Conti, A. Hornung, Thermo-Catalytic Reforming of municipal solid waste, *Waste Management*, Volume 68, 2017, Pages 198-206;
- [7.2]. A. Hornung, H. Jahangiri, M. Ouadi, C. Kick, L. Deinert, B. Meyer, J. Grunwald, R. Daschner, A. Apfelbacher, M. Meiller, S. Eder, Thermo-Catalytic Reforming (TCR)–An important link between waste management and renewable fuels as part of the energy transition, *Applications in Energy and Combustion Science*, Volume 12, 2022, 100088;
- [7.3]. L. Starck, L. Pidol, N. Jeuland, T. Chapus, P. Bogers, J. Bauldrey, Production of Hydroprocessed Esters and Fatty Acids (HEFA) – Optimisation of Process Yield. *Oil & Gas Science and Technology - Revue d'IFP Energies nouvelles*, Institut Français du Pétrole (IFP), 2016, 71;
- [7.4]. Available online: [https://www.ieabioenergy.com/wp-content/uploads/2013/10/18\\_AR1999Task20colour.pdf](https://www.ieabioenergy.com/wp-content/uploads/2013/10/18_AR1999Task20colour.pdf) (accessed on 19/12/2022);
- [7.5]. Available online: <https://rentar.com/efficient-engines-thermodynamics-combustion-efficiency/> (accessed on 19/12/22);
- [7.6]. Available online: <https://energypedia.info/wiki/Cogeneration> (accessed on 19/12/2022);
- [7.7]. J. M. Coulson and J. F. Richardson, *Chemical Engineering*, Volume 6, Third Edition, Chemical Engineering Design, R. K. Sinnott;
- [7.8]. Available online: [https://www.payscale.com/research/DE/Job=Chief\\_Executive\\_Officer\\_\(CEO\)/Salary](https://www.payscale.com/research/DE/Job=Chief_Executive_Officer_(CEO)/Salary) (accessed on 29/10/2022);
- [7.9]. Available online: [https://www.payscale.com/research/IT/Job=Sales\\_Director/Salary](https://www.payscale.com/research/IT/Job=Sales_Director/Salary) (accessed on 29/10/2022);
- [7.10]. Available online: [https://www.payscale.com/research/DE/Job=Finance\\_Manager/Salary](https://www.payscale.com/research/DE/Job=Finance_Manager/Salary) (accessed on 29/10/2022);
- [7.11]. Available online: [https://www.payscale.com/research/IT/Job=Human\\_Resources\\_\(HR\)\\_Manager/Salary](https://www.payscale.com/research/IT/Job=Human_Resources_(HR)_Manager/Salary) (accessed on 29/10/2022);

- [7.12]. Available online: [https://www.payscale.com/research/DE/Job=Technical Project Manager/Salary](https://www.payscale.com/research/DE/Job=Technical_Project_Manager/Salary) (accessed on 29/10/2022);
- [7.13]. Available online: [https://www.payscale.com/research/DE/Job=Field Service Technician/Salary](https://www.payscale.com/research/DE/Job=Field_Service_Technician/Salary) (accessed on 29/10/2022);
- [7.14]. Available online: [https://ec.europa.eu/eurostat/statistics-explained/index.php?title=Wages and labour costs#Labour cost components](https://ec.europa.eu/eurostat/statistics-explained/index.php?title=Wages_and_labour_costs#Labour_cost_components) (accessed on 29/10/2022);
- [7.15]. Available online: [https://energy.ec.europa.eu/data-and-analysis/energy-prices-and-costs-europe/dashboard-energy-prices-eu-and-main-trading-partners\\_en](https://energy.ec.europa.eu/data-and-analysis/energy-prices-and-costs-europe/dashboard-energy-prices-eu-and-main-trading-partners_en) (accessed on 29/10/2022);
- [7.16]. P. Benalcazar, P. Kaszyński, J. Kamiński, Assessing the Effects of Uncertain Energy and Carbon Prices on the Operational Patterns and Economic Results of CHP Systems, *Energies* 2021, 14, 8216;
- [7.17]. Available online: [https://www.eea.europa.eu/data-and-maps/daviz/nominal-and-real-fuel-prices-6#tab-chart\\_1](https://www.eea.europa.eu/data-and-maps/daviz/nominal-and-real-fuel-prices-6#tab-chart_1) (accessed on 29/10/2022);
- [7.18]. Available online: <https://theicct.org/publication/fuels-eu-onsite-hydro-cost-feb22/> (accessed on 29/10/2022);
- [7.19]. Available online: [https://www.interregeurope.eu/sites/default/files/inline/Biogas\\_Potential-sizing-costs-risks\\_KKrell\\_150620.pdf](https://www.interregeurope.eu/sites/default/files/inline/Biogas_Potential-sizing-costs-risks_KKrell_150620.pdf) (accessed on 29/10/2022).

## Conclusions and future works

The objective of this final section is to review and summarize the results deriving from the analyses and the experimental tests over solid grade laminate (SGL) and carbon fibers (CF) through the thermo-catalytic reforming (TCR), discussing their benefits, implications, limitations and final recommendations for future works.

According to the research flow, the main goals of this work were accomplished by the following points:

- The potential advanced feedstocks availability in Europe by 2025;
- Assessment of the main thermochemical technologies;
- Description of the relatively recent Thermo-Catalytic Reforming technology;
- Characterization of novel feedstocks (SGL and CF) before TCR;
- Characterization of the final products after TCR.

From the estimate about availability, residues deriving from crops and forestry will be abundant in 2025, although wastes are the most promising despite the limiting European policies illustrated in **Chapter 2**.

This research involved two wastes that have never been processed before via TCR, thus contributing to increase the degree of novelty of the work.

The solid grade laminate, received from JCM Fine Joinery (UK), was the first material to be characterized and subjected to TCR in order to collect solid, liquid and gaseous products.

The SGL characterization was necessary to determine its feasibility to be processed in the thermo-catalytic reformer according to its physiochemical properties and the operating conditions; while the products characterizations was useful to understand how the mass and the energy of SGL were distributed between its final products. These results allowed evaluating if TCR can be used to produce value-added fuels.

According to the ultimate and proximate analyses, the solid grade laminate showed similar properties to wood in terms of oxygen, hydrogen and carbon content even if sulphur and nitrogen were found to be higher. The feedstock was already dried according to the low moisture content and its HHV was equal to 18.6 MJ/kg, thus showing a good quality to be used directly as a fuel in other thermal and thermochemical processes (e.g. incineration, combustion and gasification) beside TCR. Based on the mass and energy yields, TCR showed that half of SGL was converted to hydrogen-rich syngas with a high calorific value (20.11 MJ/kg), thus allowing to be involved either in further conversion processes or to be

stored as a chemical (e.g. hydrogenation of oil) or energy carrier for other applications (e.g. hydrogen fuel cells).

Furthermore, high production of char (equal to 28 wt%) was obtained from TCR. It was found to be rich in carbon and exhibited good catalytic effects as suggested by the high percentage of syngas and its low hydrogen and oxygen contents. This result also suggests that char from TCR could be used for combustion due to its HHV (25.94 MJ/kg) higher than the initial feedstock. Despite the lowest yields, pyrolysis oil showed good potentiality as a fuel. Therefore, a further upgrading (hydrotreatment) was achieved to remove nitrogen, oxygen, sulphur content as well as phenols and furans compounds. However, although the sulphur content was practically eliminated from raw oil, the oxygen content was still too high in both hydro-deoxygenated and hydrocracked oil, showing a poor selectivity of catalysts with oxygen compounds. This result suggests or catalyst was good for desulphurization but not for deoxygenation or the operating conditions (temperature and pressure) adopted for the hydrotreatment should be set differently.

After hydrocracking, the oil has a HHV of 37.05 MJ/kg, almost matching with heavy fuel oil (HFO), even if the hydrogen content decreased compared with the raw laminate oil, thus reducing the H/C ratio as illustrated in the Van Krevelen diagram in Figure 13.

The final HHV of the oil moved from 31.97 MJ/kg after TCR to 35.61 MJ/kg and 37.05 MJ/kg after HDO and HC, respectively.

The second material analyzed in this thesis was carbon fiber, received from Gen2Carbon (UK). As expected, CFs were rich in carbon showing a considerable stability in terms of char decomposition akin to coal. The higher values of carbon than other biomasses suggested their feasibility to be processed through thermal and thermo-chemical processes.

However, by using TCR, it turned out that only solid and gaseous products could be obtained. In fact, the pyrolysis oil was considered negligible as its mass yield was less than 2wt%. The most interesting result was found in the solid product, as virgin carbon fibers, looking fluffy and randomly structured, were partly recovered in the char and potentially reused in further manufacturing processes. The chaotic structure of these fibers sounded also beneficial to be used as adsorbent materials, meaning such fibers could work well like molecular sieves letting the gases with lower molecular sizes pass and separating them from the other gaseous species. For example, this type of material can find its application in the pollutants removal or hydrogen filtration from the gas mixture as happens in the pressure swing adsorption (PSA) method. However, at first glance, their pores diameter ranged from 20 to 100  $\mu\text{m}$  which are still too large to be used as molecular sieves having diameter in the range of 3-10 $\text{\AA}$  (e.g. 1  $\text{\AA}$  =10<sup>-4</sup>  $\mu\text{m}$ ).

An evident limitation of TCR is its incapacity to fully recovery virgin carbon fibers from resins in the char. Furthermore, these fibers were obtained through the partial oxidation of the feedstock under combustion conditions during the run, as highlighted by the loss of carbon and hydrogen and the increase in ash. This latter aspect together with the inconsistent production of oil point to the involvement of gasification as recovery process for fibers and production of syngas. As a matter of fact, products from gasification are mainly syngas and char. Finally, it was also found that disposal of char in landfill is harmful to the environment and not economical.

Regarding the gaseous product, it has been proven that TCR largely produces syngas with high calorific values (~34 MJ/kg), since hydrogen was found to be around 36% at a certain point during the test. However, the continuous blockages of the reactor, occurred during the experimental trial, could affect the final estimates, thus leading to the remark that new tests should be repeated in order to increase the reproducibility of the results.

In conclusion, final recommendations for future works can be resumed in the following points:

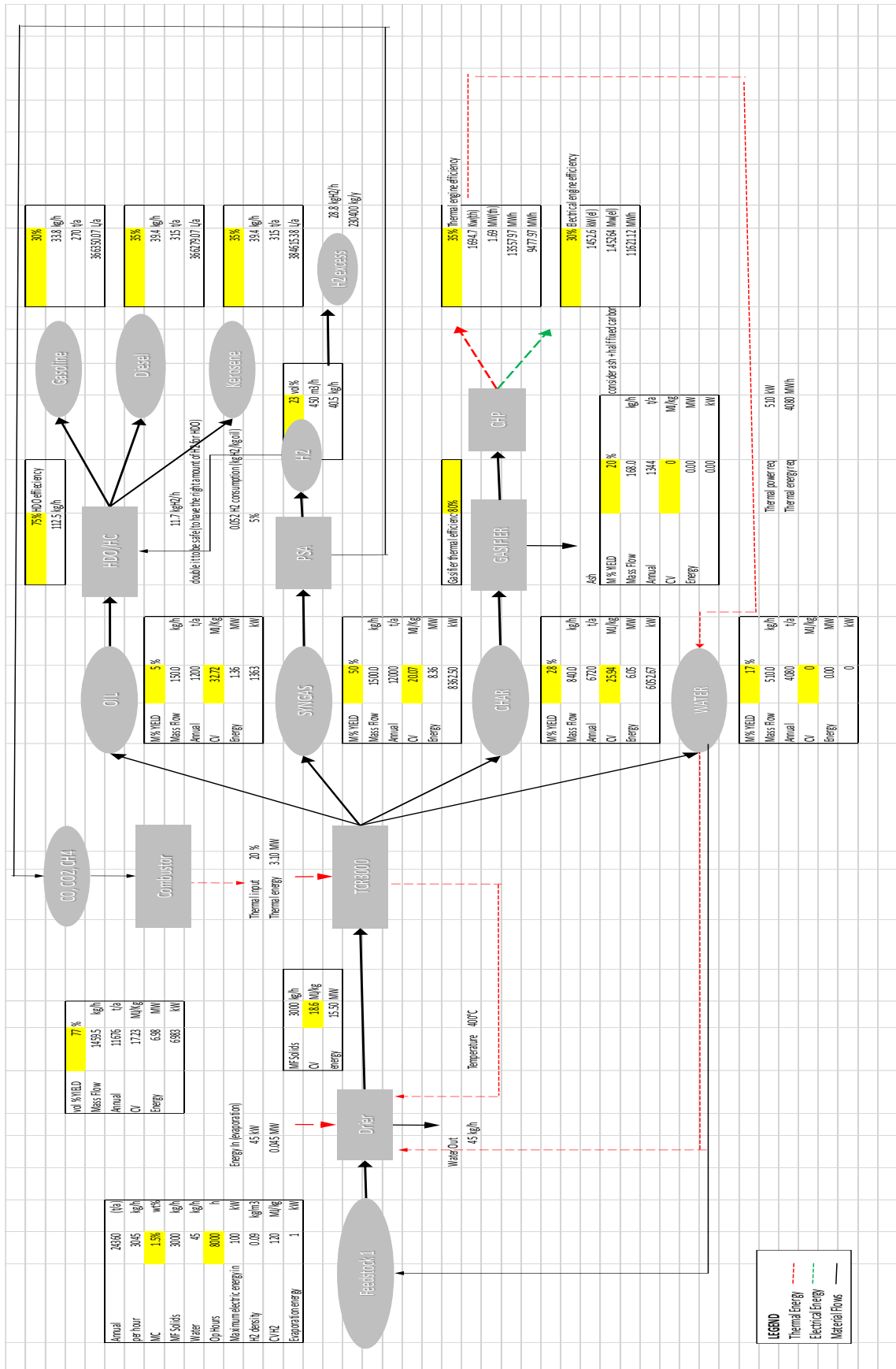
- The analysis of wastes availability is not complete, since other wastes should be considered like those deriving from different industrial sectors (e.g. kraft paper for SGL and CF). However, this is due to the lack of information that are limited to the open databases accessible online or literature review not yet available.
- SGL and CF are here considered as wastes, but both could not be named “advanced” since they are not explicitly specified in Annex IX of RED II. Hence, they would require a procedure to be certified as “advanced”;
- A more referential analysis of scale economy should be achieved for TCR plant, in order to have detailed information about CAPEX and OPEX;
- Regarding the hydrotreatment of SGL oil from TCR, new catalysts and new operating conditions should be tested in order to better remove heteroatoms from the oil. Moreover, other experimental trials should be required in order to study further properties (see Table 1, Chapter 1) in the oil. This will imply to process via TCR more and more SGL in order to get a sufficiently high amount of oil.





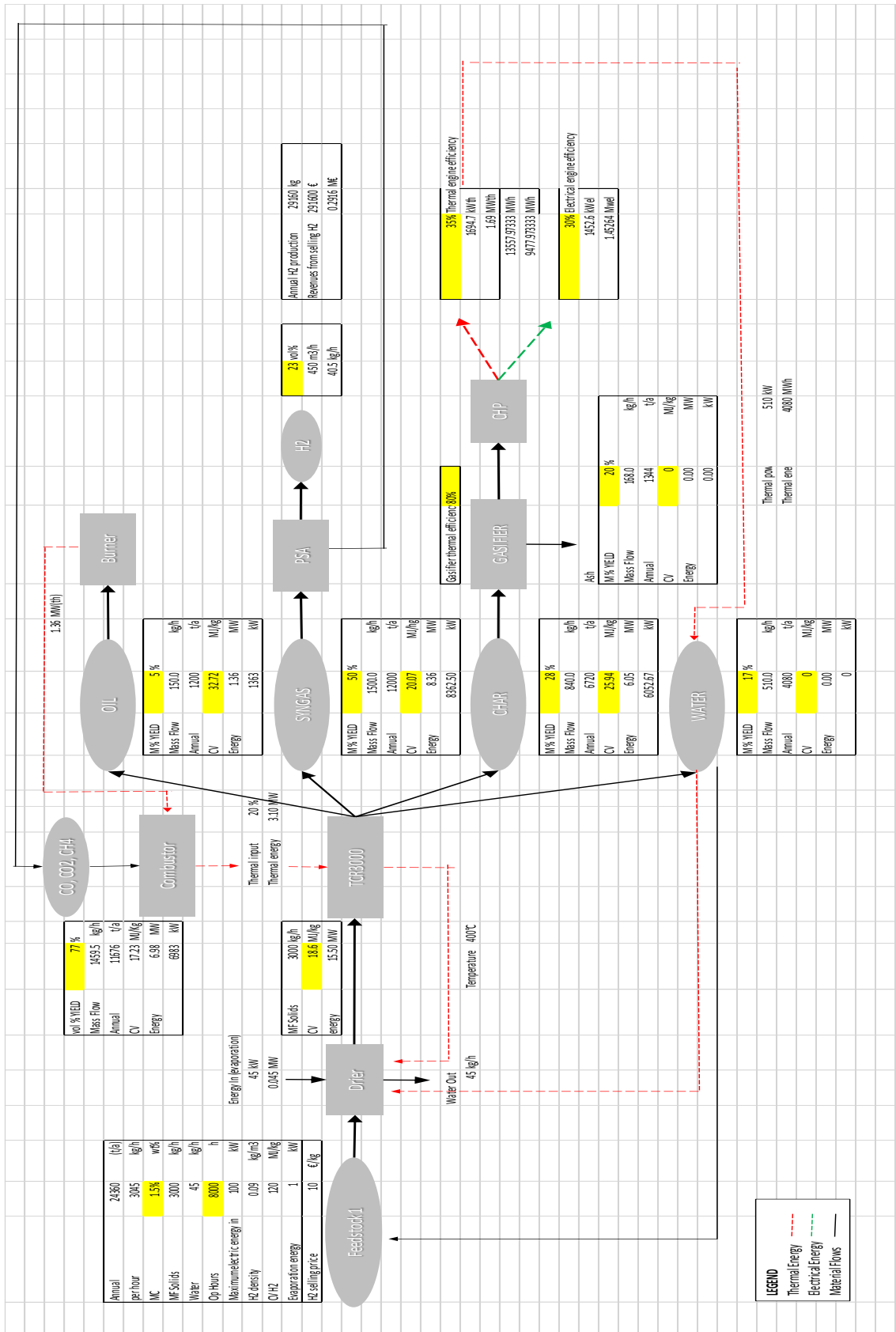
# APPENDIX A1

## (Mass and Energy balance for Solid Grade Laminate – Model 1)



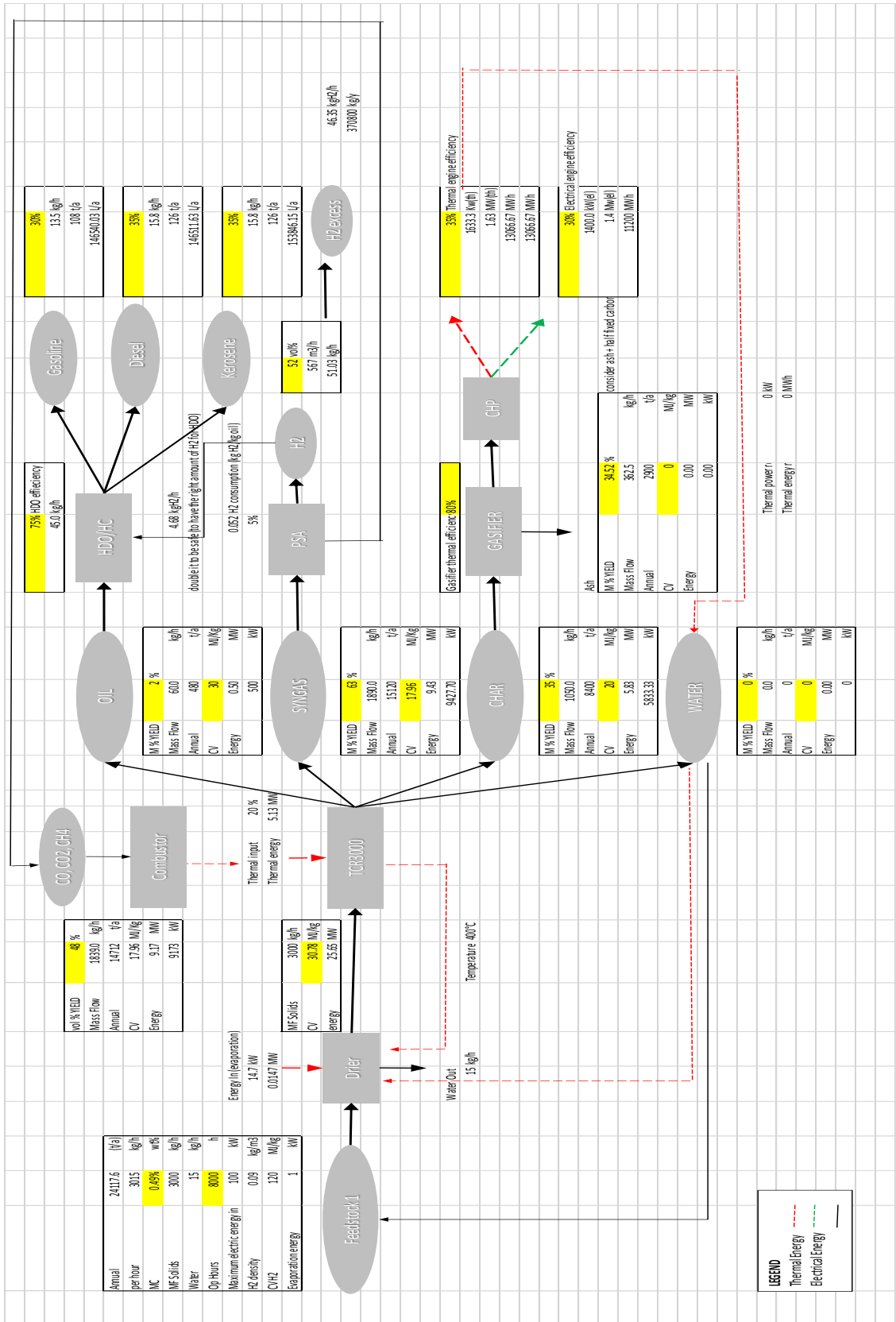
## APPENDIX A2

(Mass and Energy balance for Solid Grade Laminate – Model 2)



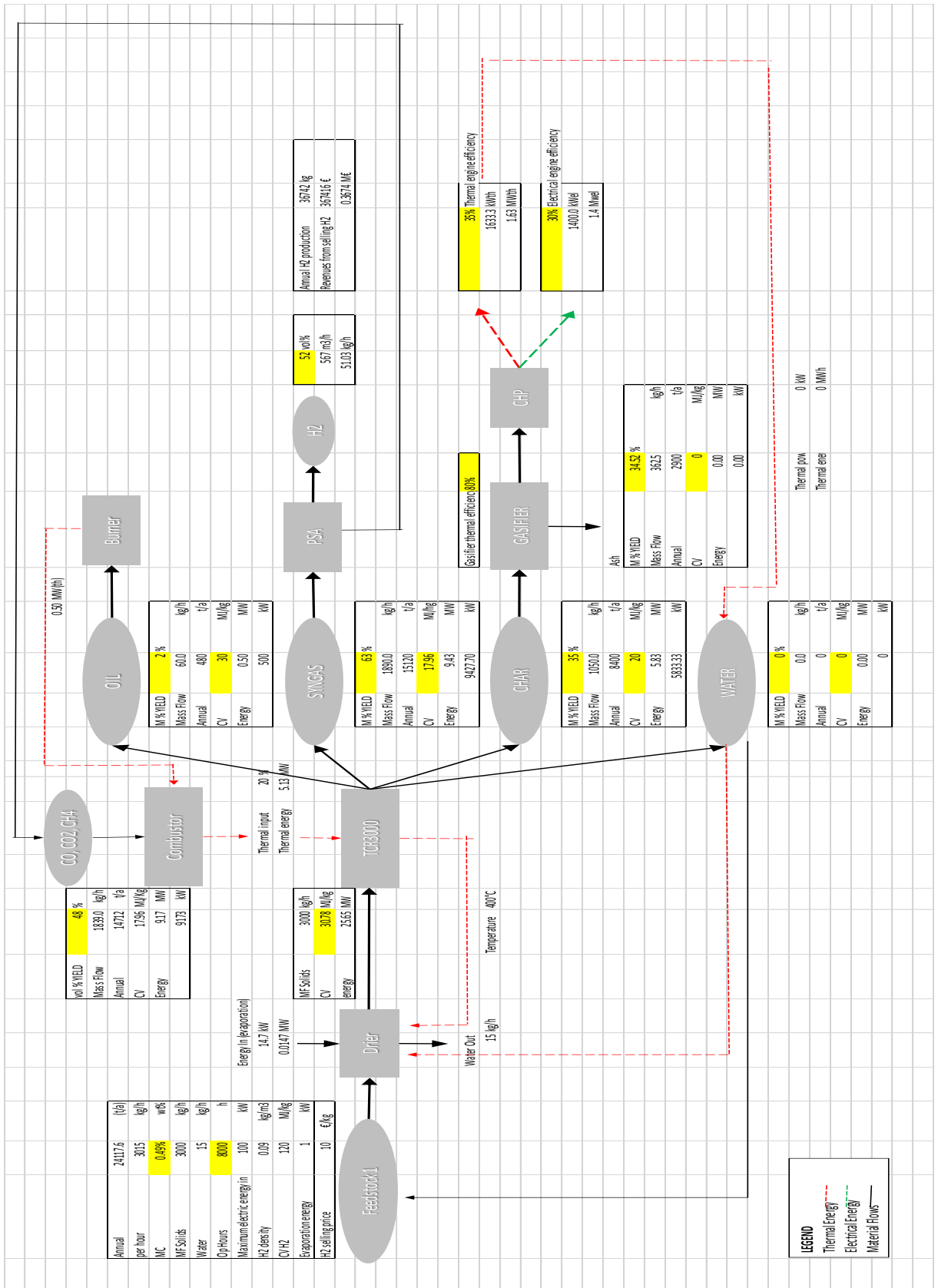
# APPENDIX B1

## (Mass and Energy balance for Carbon Fibers – Model 1)



## APPENDIX B2

(Mass and Energy balance for Carbon Fibers – Model 2)



## APPENDIX C1

(Economic evaluation for Solid Grade Laminate – Model 1)

Total equipment purchase (PCE)		EURO	
Feedstock/Silo	€	60,000.00	
Drier	€	50,000.00	
Feedstock Tube Chain Conveyor	€	40,000.00	
Feedstock/Sluice system	€	900,000.00	
Auger reactor	€	900,000.00	
Post reactor	€	40,000.00	
Flue gas distributor + High temperature valve	€	40,000.00	
Combustion chamber + NOx AND SOx Scrub	€	220,000.00	
Syngas combustor	€	120,000.00	
Burner	€	1,500,000.00	
Gasifier	€	20,000.00	
Induced Draft Blower + STACK Flue gas removal	€	30,000.00	
Char Extraction Screw + Char Sluice + Char Chiller	€	75,000.00	
Tube chain conveyor + silo	€	25,000.00	
Air separator	€	50,000.00	
Cyclone	€	75,000.00	
Condensation Unit (Heat exchanger + ESP)	€	50,000.00	
Table cooler	€	30,000.00	
Oil water separator tank	€	75,000.00	
Acid scrubber + ESP	€	150,000.00	
Syngas compressor	€	300,000.00	
PSA	€	700,000.00	
H2 compressor	€	60,000.00	
Flare	€	15,000.00	
Propane tank	€	150,000.00	
H2 Storage	€	2,000,000.00	
H2O plant and fractionation	€	7,635,000.00	
<b>Total PCE</b>	<b>€</b>	<b>7,635,000.00</b>	
Equipment erection	€	381,750.00	
Piping	€	1,145,250.00	
Instrumentation	€	763,500.00	
Electrical wiring	€	763,500.00	
Buildings & Utilities Infrastructure	€	381,750.00	
Storage	€	763,500.00	
Site development	€	4,962,750.00	
<b>Total</b>	<b>€</b>	<b>12,597,750.00</b>	
<b>Total physical plant cost (PPC)</b>	<b>€</b>	<b>629,887.50</b>	
Design and engineering	€	629,887.50	
Contract and fee	€	2,519,550.00	
Contingency	€	<b>3,779,315.00</b>	
<b>Total</b>	<b>€</b>	<b>46,377,075.00</b>	
Fixed capital	€	327,541.50	
Working capital	€	16,704,616.50	
<b>Total Capital Cost (TCC)</b>	<b>€</b>	<b>16,704,616.50</b>	

Operating Cost		EUR/y	
Labour costs	€	680,000.00	
Disposal cost	€	85.00	EUR/ton
Maintenance cost	€	501,138.50	EUR/y
Administration and Insurance	€	250,000.00	EUR/y
Site rent	€	70,000.00	EUR/y
Transport cost	€	70,000.00	EUR/y
<b>Total</b>	<b>€</b>	<b>1,685,378.50</b>	<b>EUR/y</b>

Revenues		EUR	
Electrical cost	€	75.00	EUR/MMwh
Heat cost	€	35.00	EUR/MMwh
Kerosene/Diesse/Petrol	€	1.20	EUR/l
Excess Green H2	€	10.00	EUR/kg
Feedstock gate fee	€	20.00	EUR/ton
<b>Total</b>	<b>€</b>	<b>3,649,828.00</b>	

Gross Profit - Model 1		EUR	
Tax @30% - Model 1	€	1,094,948.40	
<b>Net Profit - Model 1</b>	<b>€</b>	<b>2,554,879.60</b>	

Payback Period - Model 1		years	
6.54		1.5	(consider 1.5 year to let the plant settle)
<b>8.04</b>		<b>8.04</b>	

ROI		%	
<b>15%</b>			

CEO, sales director, finance manager, HR manager, technical manager		EUR/y	
Water disposal	€	-	EUR/y
Ash disposal	€	114,240.00	EUR/y

Electrical cost - Model 1		EUR	
Thermal cost - Model 1	€	331,729.07	EUR
Kerosene - Model 1	€	461,538.46	EUR
Diesel - Model 1	€	439,534.88	EUR
Petrol - Model 1	€	439,620.08	EUR
Model 2	€	2,304,000.00	EUR
<b>Total</b>	<b>€</b>	<b>487,200.00</b>	<b>EUR</b>
<b>Total</b>	<b>€</b>	<b>5,335,206.49</b>	<b>EUR</b>

(if I do not consider subsidies or incentives)

## APPENDIX C2

(Economic evaluation for Solid Grade Laminate – Model 2)

Total equipment purchase (PCE)		EURO	
Feedstock Silo	€	60,000.00	
Drier	€	-	
Feedstock Tube Chain Conveyor	€	50,000.00	
Feedstock Sluice system	€	40,000.00	
Auger reactor	€	900,000.00	
Post reactor	€	900,000.00	
Flue gas distributor + High Temperature valve	€	40,000.00	
Combustion chamber + NOX AND SOX SCRUB	€	220,000.00	
Syngas combustor	€	120,000.00	
Burner	€	60,000.00	
Gasifier	€	1,500,000.00	
Induced Draft Blower + STACK Flue gas removal	€	20,000.00	
Char Extraction Screw + Char Sluice + Char Chiller	€	30,000.00	
Tube chain conveyor + silo	€	75,000.00	
Air separator	€	25,000.00	
Cyclone	€	50,000.00	
Condensation Unit (Heat exchanger + ESP)	€	75,000.00	
Table cooler	€	50,000.00	
Oil water separator tank	€	30,000.00	
Acid scrubber + ESP	€	75,000.00	
Syngas compressor	€	150,000.00	
PSA	€	300,000.00	
H2 compressor	€	700,000.00	
Flare	€	60,000.00	
Propane tank	€	15,000.00	
H2 storage	€	150,000.00	
H2O plant and fractionation	€	-	
<b>Total PCE</b>	<b>€</b>	<b>5,695,000.00</b>	
Equipment erection	€	569,500.00	
Piping	€	284,750.00	
Instrumentation	€	894,250.00	
Electrical wiring	€	569,500.00	
Buildings & Utilities Infrastructure	€	569,500.00	
Storage	€	284,750.00	
Site development	€	569,500.00	
<b>Total</b>	<b>€</b>	<b>3,701,750.00</b>	
<b>Total physical plant cost (PPC)</b>	<b>€</b>	<b>9,396,750.00</b>	
Design and engineering	€	469,837.50	
Contract and fee	€	469,837.50	
Contingency	€	1,879,350.00	
<b>Total</b>	<b>€</b>	<b>2,819,025.00</b>	
<b>Fixed capital</b>	<b>€</b>	<b>12,215,775.00</b>	
<b>Working capital</b>	<b>€</b>	<b>244,315.50</b>	
<b>Total Capital Cost (TCC)</b>	<b>€</b>	<b>12,460,090.50</b>	

Operating Cost			
Labour costs	€	680,000.00	EUR/y
Disposal cost	€	85.00	EUR/ton
Maintenance cost	€	373,802.72	EUR/y
Administration and Insurance	€	250,000.00	EUR/y
Site rent	€	70,000.00	EUR/y
Transport cost	€	70,000.00	EUR/y
<b>Total</b>	<b>€</b>	<b>1,558,042.72</b>	<b>EUR/y</b>

Revenues			
Electrical cost	€	75.00	EUR/MWh
Heat cost	€	35.00	EUR/MWh
Selling Green H2	€	10.00	EUR/kg
Feedstock gate fee	€	20.00	EUR/ton
<b>Total</b>	<b>€</b>	<b>4,990,313.07</b>	<b>EUR</b>

<b>Gross Profit - Model 2</b>	<b>€</b>	<b>3,372,470.35</b>	
Tax @30% - Model 2	€	1,011,741.11	
<b>Net Profit - Model 2</b>	<b>€</b>	<b>2,360,729.25</b>	
<b>Payback Period - Model 2</b>		5.28	years
		1.50	years
<b>ROI</b>		19%	

## APPENDIX D1

### (Economic evaluation for Carbon Fibers – Model 1)

Total equipment purchase (PCE)		EURO	
Feedstock silo		€	60,000.00
Drier		€	50,000.00
Feedstock Tube Chain Conveyor		€	40,000.00
Feedstock Sluice system		€	900,000.00
Auger reactor		€	900,000.00
Post reactor		€	40,000.00
Flue gas distributor + High temperature valve		€	220,000.00
Combustion chamber + NOx AND SOx SCRUB		€	120,000.00
Syngas combustor		€	1,500,000.00
Burner		€	20,000.00
Gasifier		€	30,000.00
Induced Draft Blower + STACK Flue gas removal		€	75,000.00
Char Extraction Screw + Char Sluice + Char Chiller		€	25,000.00
Tube chain conveyor + silo		€	50,000.00
Air separator		€	75,000.00
Cyclone		€	30,000.00
Condensation Unit (Heat exchanger + ESP)		€	75,000.00
Table cooler		€	30,000.00
Oil water separator tank		€	150,000.00
Acid scrubber + ESP		€	300,000.00
Syngas compressor		€	700,000.00
PSA		€	60,000.00
H2 compressor		€	15,000.00
Flare		€	2,000,000.00
Propane tank		€	7,635,000.00
H2 storage		€	763,500.00
HDO plant and fractionation		€	1,145,250.00
<b>Total PCE</b>		<b>€</b>	<b>12,997,750.00</b>
Equipment erection		€	629,887.50
Piping		€	629,887.50
Instrumentation		€	629,887.50
Electrical wiring		€	2,519,550.00
Buildings & Utilities Infrastructure		€	3,779,325.00
Storage		€	763,500.00
Site development		€	4,962,750.00
<b>Total</b>		<b>€</b>	<b>12,997,750.00</b>
<b>Total physical plant cost (PPC)</b>		<b>€</b>	<b>12,997,750.00</b>
Design and engineering		€	629,887.50
Contract and fee		€	629,887.50
Contingency		€	2,519,550.00
<b>Total</b>		<b>€</b>	<b>3,779,325.00</b>
<b>Fixed capital</b>		<b>€</b>	<b>16,377,075.00</b>
<b>Working capital</b>		<b>€</b>	<b>327,541.50</b>
<b>Total Capital Cost (TCC)</b>		<b>€</b>	<b>16,704,616.50</b>

Operating Cost		EUR/y	
Labour costs		€	680,000.00
Disposal cost		€	85.00
Maintenance cost		€	501,138.50
Administration and Insurance		€	250,000.00
Site rent		€	70,000.00
Transport cost		€	70,000.00
<b>Total</b>		<b>€</b>	<b>1,817,611.30</b>

Revenues		EUR/ton	
Electrical cost		€	75.00
Heat cost		€	35.00
Kerosene/Diesel/Petrol		€	1.20
Excess Green H2		€	10.00
Feedstock gate fee		€	20.00
<b>Total</b>		<b>€</b>	<b>131.20</b>

Operating Cost		EUR/ton	
CEO, sales director, finance manager, HR manager, technical manager		€	246,472.80
Water disposal		€	-
Ash disposal		€	-

Revenues		EUR	
Electrical cost - Model 1		€	840,000.00
Thermal cost - Model 1		€	457,333.33
Kerosene - Model 1		€	184,615.38
Diesel - Model 1		€	175,813.95
Petrol - Model 1		€	175,848.03
Excess Green H2		€	3,708,000.00
Feedstock gate fee		€	482,352.00
<b>Total</b>		<b>€</b>	<b>6,023,962.70</b>

<b>Gross Profit - Model 1</b>	<b>€</b>	<b>4,206,351.41</b>
Tax @30% - Model 1	€	1,261,905.42
<b>Net Profit - Model 1</b>	<b>€</b>	<b>2,944,445.99</b>
<b>Payback Period - Model</b>	5.67	1 year to build and 6 months for commissioning and optimization
	1.5	(consider 1.5 year to let the plant settle)
	7.17	years
<b>ROI</b>	18%	

## APPENDIX D1

### (Economic evaluation for Carbon Fibers – Model 2)

Total equipment purchases (PCE)		EURO	
Feedstock Silo	€	60,000.00	
Drier	€	50,000.00	
Feedstock Tube Chain Conveyor	€	40,000.00	
Feedstock Sluice system	€	900,000.00	
Auger reactor	€	900,000.00	
Post reactor	€	40,000.00	
Flue gas distributor + High temperature valve	€	220,000.00	
Combustion chamber + NOX AND SOX SCRUB	€	120,000.00	
Syngas combustor	€	60,000.00	
Burner	€	1,500,000.00	
Gasifier	€	20,000.00	
Induced Draft Blower + STACK Flue gas removal	€	30,000.00	
Char Extraction Screw + Char Sluice + Char Chiller	€	75,000.00	
Tube chain conveyor + silo	€	25,000.00	
Air separator	€	50,000.00	
Cyclone	€	75,000.00	
Condensation Unit (Heat exchanger + ESP)	€	50,000.00	
Table cooler	€	30,000.00	
Oil water separator tank	€	75,000.00	
Acid scrubber + ESP	€	150,000.00	
Syngas compressor	€	300,000.00	
PSA	€	700,000.00	
H2 compressor	€	60,000.00	
Flare	€	15,000.00	
Propane tank	€	150,000.00	
H2 storage	€	-	
H2O plant and fractionation	€	569,500.00	
<b>Total PCE</b>	<b>€</b>	<b>5,695,000.00</b>	
Equipment erection	€	284,750.00	
Piping	€	854,250.00	
Instrumentation	€	569,500.00	
Electrical wiring	€	284,750.00	
Buildings & Utilities Infrastructure	€	569,500.00	
Storage	€	569,500.00	
Site development	€	3,701,750.00	
<b>Total</b>	<b>€</b>	<b>9,396,750.00</b>	
<b>Total physical plant cost (PPC)</b>	<b>€</b>	<b>469,837.50</b>	
Design and engineering	€	1,879,350.00	
Contract and fee	€	2,819,025.00	
Contingency	€	12,215,775.00	
<b>Total</b>	<b>€</b>	<b>244,315.50</b>	
<b>Working capital</b>	<b>€</b>	<b>12,460,090.50</b>	
<b>Total Capital Cost (TCC)</b>	<b>€</b>	<b>12,460,090.50</b>	

Operating Cost		EUR/y	
Labour costs	€	680,000.00	
Disposal cost	€	85.00	EUR/ton
Maintenance cost	€	373,802.72	EUR/y
Administration and Insurance	€	250,000.00	EUR/y
Site rent	€	70,000.00	EUR/y
Transport cost	€	70,000.00	EUR/y
<b>Total</b>	<b>€</b>	<b>1,690,275.52</b>	<b>EUR/y</b>

Revenues		EUR	
Electrical cost	€	75.00	EUR/MWh
Heat cost	€	35.00	EUR/MWh
Selling Green H2	€	10.00	EUR/kg
Feedstock gate fee	€	20.00	EUR/ton
<b>Total</b>	<b>€</b>	<b>5,862,085.33</b>	<b>EUR</b>

<b>Gross Profit - Model 2</b>	€	4,171,809.82	
Tax @30% - Model 2	€	1,251,542.95	
<b>Net Profit - Model 2</b>	€	2,920,266.87	
<b>Payback Period - Model 2</b>		4.27	years
<b>ROI</b>		1.50	years
		5.77	years
		23%	



## List of publications

### Papers 2020

F. Di Gruttola, G. Agati, P. Venturini, D. Borello, F. Rispoli, S. Gabriele, D. Simone, 2020, Numerical study of erosion due to online water washing in axial flow compressors, Proceedings of ASME Turbo Expo 2020, Turbomachinery Technical Conference and Exposition, September 21-25, 2020, London, England (virtual conference), paper no. GT2020-14767.

E. Cerruti, F. Di Gruttola, G. Lauro, T. D. Valentini, P. Fiaschi, R. Sorrenti, D. Borello, Assessment of Feedstocks and Technologies for Advanced Biofuel Production, presentato al 75° Congresso Nazionale ATI (conferenza virtuale), 15-16 settembre 2020.

G. Agati, F. Di Gruttola, S. Gabriele, D. Simone, P. Venturini, D. Borello, Water washing of axial flow compressors: numerical study on the fate of injected droplets, E3S Web Conf. Volume 197, 2020, 75th National ATI Congress – #7 Clean Energy for all (ATI 2020);

### Papers 2021

G. Agati, F. Di Gruttola, S. Gabriele, D. Simone, P. Venturini, D. Borello, Evaluation of water washing efficiency and erosion risk in an axial compressor for different water injection conditions, 76th National ATI Congress (*online conference*), 15-17 September 2021.

F. Di Gruttola, D. Borello, Analysis of the EU Secondary Biomass Availability and Conversion Processes to Produce Advanced Biofuels: Use of Existing Databases for Assessing a Metric Evaluation for the 2025 Perspective, Sustainability, pp.7882, vol. 13 (14). 2021.

G. Agati, F. Di Gruttola, D. Borello, F. Rispoli, P. Venturini, S. Gabriele, D. Simone, Numerical study of droplet erosion in the first-stage rotor of an axial flow compressor, Proceedings of ASME Turbo Expo 2021.

## Papers 2022

O. Palone, G. Barberi, F. Di Gruttola, G. G. Gagliardi, L. Cedola, D. Borello, Assessment of a multi-step revamping methodology for cleaner steel production, *Journal of Cleaner Production*, 2022 (under revision).

G. Agati, A. Castorrini, F. Di Gruttola, S. Gabriele, F. Rispoli, D. Simone, P. Venturini, D. Borello, Numerical prediction of long-term droplet erosion and washing efficiency of an axial compressors through the use of a discrete mesh morphing approach, *Proceedings of ASME Turbo Expo 2022 Turbomachinery Technical Conference and Exposition, GT2022*, June 13-17, 2022, Rotterdam, The Netherlands;

L. Mazzotta, F. Di Gruttola, O. Palone, D. Borello, Analysis of the nox emissions deriving from hydrogen/air combustion in a swirling non-premixed annular micro-combustor, *Proceedings of ASME Turbo Expo 2022 Turbomachinery Technical Conference and Exposition, GT2022*, June 13-17, 2022, Rotterdam, The Netherlands;

O. Palone, A. Hoxha, G. G. Gagliardi, F. Di Gruttola, D. Borello, Methanol Production by a Chemical Looping Cycle using a Blast Furnace Gases, *Proceedings of ASME Turbo Expo 2022 Turbomachinery Technical Conference and Exposition, GT2022*, June 13-17, 2022, Rotterdam, The Netherlands;

G. Agati, A. Castorrini, F. Di Gruttola, S. Gabriele, F. Rispoli, D. Simone, P. Venturini, D. Borello, Numerical prediction of long-term droplet erosion and washing efficiency of an axial compressors through the use of a discrete mesh morphing approach, *ASME. J. Turbomach.* (doi: <https://doi.org/10.1115/1.4055649>).